Behaviour of Horizontal Connections for Precast Concrete Load-bearing Shear Wall Panels Subjected to Reversed Cyclic Shear Loading

by

Jeffrey S. West

A Thesis
Submitted to the University of Manitoba
In Partial Fulfillment of the
Requirements for the Degree of

Master Of Science In Civil Engineering

Department of Civil Engineering
University of Manitoba
Winnipeg, Manitoba

(c) August, 1993

National Library
of Canada

Bibliothèque nationale
du Canada

Acquisitions and
Bibliographic Services Branch

Direction des acquisitions et
des services bibliographiques

395 Wellington Street
Ottawa, Ontario
K1A 0N4

395, rue Wellington
Ottawa (Ontario)
K1A 0N4

The author has granted an irrevocable non-exclusive licence allowing the National Library of Canada to reproduce, loan, distribute or sell copies of his/her thesis by any means and in any form or format, making this thesis available to interested persons.

L'auteur a accordé une licence irrévocable et non exclusive permettant à la Bibliothèque nationale du Canada de reproduire, prêter, distribuer ou vendre des copies de sa thèse de quelque manière et sous quelque forme que ce soit pour mettre des exemplaires de cette thèse à la disposition des personnes intéressées.

The author retains ownership of the copyright in his/her thesis. Neither the thesis nor substantial extracts from it may be printed or otherwise reproduced without his/her permission.

L'auteur conserve la propriété du droit d'auteur qui protège sa thèse. Ni la thèse ni des extraits substantiels de celle-ci ne doivent être imprimés ou autrement reproduits sans son autorisation.

Canada

Name __JEFFREY WEST__

Dissertation Abstracts International is arranged by broad, general subject categories. Please select the one subject which most nearly describes the content of your dissertation. Enter the corresponding four-digit code in the spaces provided.

CIVIL ENGINEERING

SUBJECT TERM

0 5 4 3 U·M·I

SUBJECT CODE

Subject Categories

THE HUMANITIES AND SOCIAL SCIENCES

COMMUNICATIONS AND THE ARTS
Architecture 0729
Art History 0377
Cinema 0900
Dance 0378
Fine Arts 0357
Information Science 0723
Journalism 0391
Library Science 0399
Mass Communications 0708
Music 0413
Speech Communication 0459
Theater 0465

EDUCATION
General 0515
Administration 0514
Adult and Continuing 0516
Agricultural 0517
Art 0273
Bilingual and Multicultural 0282
Business 0688
Community College 0275
Curriculum and Instruction 0727
Early Childhood 0518
Elementary 0524
Finance 0277
Guidance and Counseling 0519
Health 0680
Higher 0745
History of 0520
Home Economics 0278
Industrial 0521
Language and Literature 0279
Mathematics 0280
Music 0522
Philosophy of 0998
Physical 0523

Psychology 0525
Reading 0535
Religious 0527
Sciences 0714
Secondary 0533
Social Sciences 0534
Sociology of 0340
Special 0529
Teacher Training 0530
Technology 0710
Tests and Measurements 0288
Vocational 0747

LANGUAGE, LITERATURE AND LINGUISTICS
Language
  General 0679
  Ancient 0289
  Linguistics 0290
  Modern 0291
Literature
  General 0401
  Classical 0294
  Comparative 0295
  Medieval 0297
  Modern 0298
  African 0316
  American 0591
  Asian 0305
  Canadian (English) 0352
  Canadian (French) 0355
  English 0593
  Germanic 0311
  Latin American 0312
  Middle Eastern 0315
  Romance 0313
  Slavic and East European 0314

PHILOSOPHY, RELIGION AND THEOLOGY
Philosophy 0422
Religion
  General 0318
  Biblical Studies 0321
  Clergy 0319
  History of 0320
  Philosophy of 0322
Theology 0469

SOCIAL SCIENCES
American Studies 0323
Anthropology
  Archaeology 0324
  Cultural 0326
  Physical 0327
Business Administration
  General 0310
  Accounting 0272
  Banking 0770
  Management 0454
  Marketing 0338
Canadian Studies 0385
Economics
  General 0501
  Agricultural 0503
  Commerce-Business 0505
  Finance 0508
  History 0509
  Labor 0510
  Theory 0511
Folklore 0358
Geography 0366
Gerontology 0351
History
  General 0578

Ancient 0579
Medieval 0581
Modern 0582
Black 0328
African 0331
Asia, Australia and Oceania 0332
Canadian 0334
European 0335
Latin American 0336
Middle Eastern 0333
United States 0337
History of Science 0585
Law 0398
Political Science
  General 0615
  International Law and
    Relations 0616
  Public Administration 0617
Recreation 0814
Social Work 0452
Sociology
  General 0626
  Criminology and Penology ... 0627
  Demography 0938
  Ethnic and Racial Studies 0631
  Individual and Family
    Studies 0628
  Industrial and Labor
    Relations 0629
  Public and Social Welfare 0630
  Social Structure and
    Development 0700
  Theory and Methods 0344
Transportation 0709
Urban and Regional Planning 0999
Women's Studies 0453

THE SCIENCES AND ENGINEERING

BIOLOGICAL SCIENCES
Agriculture
  General 0473
  Agronomy 0285
  Animal Culture and
    Nutrition 0475
  Animal Pathology 0476
  Food Science and
    Technology 0359
  Forestry and Wildlife 0478
  Plant Culture 0479
  Plant Pathology 0480
  Plant Physiology 0817
  Range Management 0777
  Wood Technology 0746
Biology
  General 0306
  Anatomy 0287
  Biostatistics 0308
  Botany 0309
  Cell 0379
  Ecology 0329
  Entomology 0353
  Genetics 0369
  Limnology 0793
  Microbiology 0410
  Molecular 0307
  Neuroscience 0317
  Oceanography 0416
  Physiology 0433
  Radiation 0821
  Veterinary Science 0778
  Zoology 0472
Biophysics
  General 0786
  Medical 0760

EARTH SCIENCES
Biogeochemistry 0425
Geochemistry 0996

Geodesy 0370
Geology 0372
Geophysics 0373
Hydrology 0388
Mineralogy 0411
Paleobotany 0345
Paleoecology 0426
Paleontology 0418
Paleozoology 0985
Palynology 0427
Physical Geography 0368
Physical Oceanography 0415

HEALTH AND ENVIRONMENTAL SCIENCES
Environmental Sciences 0768
Health Sciences
  General 0566
  Audiology 0300
  Chemotherapy 0992
  Dentistry 0567
  Education 0350
  Hospital Management 0769
  Human Development 0758
  Immunology 0982
  Medicine and Surgery 0564
  Mental Health 0347
  Nursing 0569
  Nutrition 0570
  Obstetrics and Gynecology .. 0380
  Occupational Health and
    Therapy 0354
  Ophthalmology 0381
  Pathology 0571
  Pharmacology 0419
  Pharmacy 0572
  Physical Therapy 0382
  Public Health 0573
  Radiology 0574
  Recreation 0575

Speech Pathology 0460
Toxicology 0383
Home Economics 0386

PHYSICAL SCIENCES
Pure Sciences
Chemistry
  General 0485
  Agricultural 0749
  Analytical 0486
  Biochemistry 0487
  Inorganic 0488
  Nuclear 0738
  Organic 0490
  Pharmaceutical 0491
  Physical 0494
  Polymer 0495
  Radiation 0754
Mathematics 0405
Physics
  General 0605
  Acoustics 0986
  Astronomy and
    Astrophysics 0606
  Atmospheric Science 0608
  Atomic 0748
  Electronics and Electricity 0607
  Elementary Particles and
    High Energy 0798
  Fluid and Plasma 0759
  Molecular 0609
  Nuclear 0610
  Optics 0752
  Radiation 0756
  Solid State 0611
Statistics 0463

Applied Sciences
Applied Mechanics 0346
Computer Science 0984

Engineering
  General 0537
  Aerospace 0538
  Agricultural 0539
  Automotive 0540
  Biomedical 0541
  Chemical 0542
  Civil 0543
  Electronics and Electrical 0544
  Heat and Thermodynamics ... 0348
  Hydraulic 0545
  Industrial 0546
  Marine 0547
  Materials Science 0794
  Mechanical 0548
  Metallurgy 0743
  Mining 0551
  Nuclear 0552
  Packaging 0549
  Petroleum 0765
  Sanitary and Municipal 0554
  System Science 0790
Geotechnology 0428
Operations Research 0796
Plastics Technology 0795
Textile Technology 0994

PSYCHOLOGY
General 0621
Behavioral 0384
Clinical 0622
Developmental 0620
Experimental 0623
Industrial 0624
Personality 0625
Physiological 0989
Psychobiology 0349
Psychometrics 0632
Social 0451

Nom _____

Dissertation Abstracts International est organisé en catégories de sujets. Veuillez s.v.p. choisir le sujet qui décrit le mieux votre thèse et inscrivez le code numérique approprié dans l'espace réservé ci-dessous.

☐☐☐☐☐ U·M·I

SUJET CODE DE SUJET

Catégories par sujets

HUMANITÉS ET SCIENCES SOCIALES

COMMUNICATIONS ET LES ARTS
Architecture	0729
Beaux-arts	0357
Bibliothéconomie	0399
Cinéma	0900
Communication verbale	0459
Communications	0708
Danse	0378
Histoire de l'art	0377
Journalisme	0391
Musique	0413
Sciences de l'information	0723
Théâtre	0465

ÉDUCATION
Généralités	515
Administration	0514
Art	0273
Collèges communautaires	0275
Commerce	0688
Économie domestique	0278
Éducation permanente	0516
Éducation préscolaire	0518
Éducation sanitaire	0680
Enseignement agricole	0517
Enseignement bilingue et multiculturel	0282
Enseignement industriel	0521
Enseignement primaire.	0524
Enseignement professionnel	0747
Enseignement religieux	0527
Enseignement secondaire	0533
Enseignement spécial	0529
Enseignement supérieur	0745
Évaluation	0288
Finances	0277
Formation des enseignants	0530
Histoire de l'éducation	0520
Langues et littérature	0279

Lecture	0535
Mathématiques	0280
Musique	0522
Orientation et consultation	0519
Philosophie de l'éducation	0998
Physique	0523
Programmes d'études et enseignement	0727
Psychologie	0525
Sciences	0714
Sciences sociales	0534
Sociologie de l'éducation	0340
Technologie	0710

LANGUE, LITTÉRATURE ET LINGUISTIQUE
Langues
Généralités	0679
Anciennes	0289
Linguistique	0290
Modernes	0291

Littérature
Généralités	0401
Anciennes	0294
Comparée	0295
Médiévale	0297
Moderne	0298
Africaine	0316
Américaine	0591
Anglaise	0593
Asiatique	0305
Canadienne (Anglaise)	0352
Canadienne (Française)	0355
Germanique	0311
Latino-américaine	0312
Moyen-orientale	0315
Romane	0313
Slave et est-européenne	0314

PHILOSOPHIE, RELIGION ET THÉOLOGIE
Philosophie	0422

Religion
Généralités	0318
Clergé	0319
Études bibliques	0321
Histoire des religions	0320
Philosophie de la religion	0322
Théologie	0469

SCIENCES SOCIALES
Anthropologie
Archéologie	0324
Culturelle	0326
Physique	0327
Droit	0398

Économie
Généralités	0501
Commerce-Affaires	0505
Économie agricole	0503
Économie du travail	0510
Finances	0508
Histoire	0509
Théorie	0511
Études américaines	0323
Études canadiennes	0385
Études féministes	0453
Folklore	0358
Géographie	0366
Gérontologie	0351

Gestion des affaires
Généralités	0310
Administration	0454
Banques	0770
Comptabilité	0272
Marketing	0338

Histoire
Histoire générale	0578

Ancienne	0579
Médiévale	0581
Moderne	0582
Histoire des noirs	0328
Africaine	0331
Canadienne	0334
États-Unis	0337
Européenne	0335
Moyen-orientale	0333
Latino-américaine	0336
Asie, Australie et Océanie	0332
Histoire des sciences	0585
Loisirs	0814
Planification urbaine et régionale	0999

Science politique
Généralités	0615
Administration publique	0617
Droit et relations internationales	0616

Sociologie
Généralités	0626
Aide et bien-être social	0630
Criminologie et établissements pénitentiaires	0627
Démographie	0938
Études de l' individu et de la famille	0628
Études des relations interethniques et des relations raciales	0631
Structure et développement social	0700
Théorie et méthodes.	0344
Travail et relations industrielles	0629
Transports	0709
Travail social	0452

SCIENCES ET INGÉNIERIE

SCIENCES BIOLOGIQUES
Agriculture
Généralités	0473
Agronomie.	0285
Alimentation et technologie alimentaire	0359
Culture	0479
Élevage et alimentation	0475
Exploitation des péturages	0777
Pathologie animale	0476
Pathologie végétale	0480
Physiologie végétale	0817
Sylviculture et faune	0478
Technologie du bois	0746

Biologie
Généralités	0306
Anatomie	0287
Biologie (Statistiques)	0308
Biologie moléculaire	0307
Botanique	0309
Cellule	0379
Écologie	0329
Entomologie	0353
Génétique	0369
Limnologie	0793
Microbiologie	0410
Neurologie	0317
Océanographie	0416
Physiologie	0433
Radiation	0821
Science vétérinaire	0778
Zoologie	0472

Biophysique
Généralités	0786
Médicale	0760

SCIENCES DE LA TERRE
Biogéochimie	0425
Géochimie	0996
Géodésie	0370
Géographie physique	0368

Géologie	0372
Géophysique	0373
Hydrologie	0388
Minéralogie	0411
Océanographie physique	0415
Paléobotanique	0345
Paléoécologie	0426
Paléontologie	0418
Paléozoologie	0985
Palynologie	0427

SCIENCES DE LA SANTÉ ET DE L'ENVIRONNEMENT
Économie domestique	0386
Sciences de l'environnement	0768

Sciences de la santé
Généralités	0566
Administration des hipitaux	0769
Alimentation et nutrition	0570
Audiologie	0300
Chimiothérapie	0992
Dentisterie	0567
Développement humain	0758
Enseignement	0350
Immunologie	0982
Loisirs	0575
Médecine du travail et thérapie	0354
Médecine et chirurgie	0564
Obstétrique et gynécologie	0380
Ophtalmologie	0381
Orthophonie	0460
Pathologie	0571
Pharmacie	0572
Pharmacologie	0419
Physiothérapie	0382
Radiologie	0574
Santé mentale	0347
Santé publique	0573
Soins infirmiers	0569
Toxicologie	0383

SCIENCES PHYSIQUES
Sciences Pures
Chimie
Généralités	0485
Biochimie	487
Chimie agricole	0749
Chimie analytique	0486
Chimie minérale	0488
Chimie nucléaire	0738
Chimie organique	0490
Chimie pharmaceutique	0491
Physique	0494
PolymÇres	0495
Radiation	0754
Mathématiques	0405

Physique
Généralités	0605
Acoustique	0986
Astronomie et astrophysique	0606
Electronique et électricité	0607
Fluides et plasma	0759
Météorologie	0608
Optique	0752
Particules (Physique nucléaire)	0798
Physique atomique	0748
Physique de l'état solide	0611
Physique moléculaire	0609
Physique nucléaire	0610
Radiation	0756
Statistiques	0463

Sciences Appliqués Et Technologie
Informatique	0984

Ingénierie
Généralités	0537
Agricole	0539
Automobile	0540

Biomédicale	0541
Chaleur et ther modynamique	0348
Conditionnement (Emballage)	0549
Génie aérospatial	0538
Génie chimique	0542
Génie civil	0543
Génie électronique et électrique	0544
Génie industriel	0546
Génie mécanique	0548
Génie nucléaire	0552
Ingénierie des systèmes	0790
Mécanique navale	0547
Métallurgie	0743
Science des matériaux	0794
Technique du pétrole	0765
Technique minière	0551
Techniques sanitaires et municipales	0554
Technologie hydraulique	0545
Mécanique appliquée	0346
Géotechnologie	0428
Matières plastiques (Technologie)	0795
Recherche opérationnelle	0796
Textiles et tissus (Technologie)	0794

PSYCHOLOGIE
Généralités	0621
Personnalité	0625
Psychobiologie	0349
Psychologie clinique	0622
Psychologie du comportement	0384
Psychologie du développement	0620
Psychologie expérimentale	0623
Psychologie industrielle	0624
Psychologie physiologique	0989
Psychologie sociale	0451
Psychométrie	0632

✪

BEHAVIOUR OF HORIZONTAL CONNECTIONS FOR
PRECAST CONCRETE LOAD-BEARING SHEAR WALL PANELS
SUBJECTED TO REVERSED CYCLIC SHEAR LOADING

BY

JEFFREY S. WEST

A Thesis submitted to the Faculty of Graduate Studies of the University of Manitoba in partial fulfillment of the requirements for the degree of

MASTER OF SCIENCE

© 1993

ABSTRACT

The performance of precast concrete load bearing shear wall panel structures subjected to earthquakes relies on the behaviour and integrity of the connections between the panels. Design of these structures requires the ability to predict the behaviour of the connections. This thesis presents the results of an experimental program conducted to study the behaviour of horizontal connections for precast wall panels subjected to large reversed cyclic shear loading. The study considered some of the typical connection configurations currently used in practice. These included connections with mild steel continuity bars, multiple shear keys and post-tensioning using strands or bars. Prototype specimens were tested under reversed cyclic shear loading with constant load normal to the connection to simulate gravity loads. The results were compared with the behaviour of identical connection configurations tested under monotonic loading conditions in a previous research program (10,11,17,18,29,30). The test results were used to evaluate the effects of cyclic loading, to identify the contribution of each component of the connection and to determine the various limit states cyclic behaviour of the connection configurations.

All of the connection configurations tested in this program under reversed cyclic loading exhibited stable hysteretic behaviour following the initiation of slip at the connection. The mode of failure under cyclic loading was due to extensive crushing and spalling of the dry pack. The deterioration of the dry pack altered the shear resistance mechanisms and significantly reduced the shear resistance of the connection. This behaviour was not observed for the specimens tested under monotonic loading conditions.

The test results indicated that the behaviour of the connections with dry pack only, dry pack with post-tensioned strands and connections with multiple shear keys was not

significantly affected by the cyclic loading conditions. The strength of the connection with mild steel continuity bars was significantly reduced by the cyclic loading. The connection with post-tensioned bars experienced a gradual reduction of shear resistance over the duration of the cyclic loading due to a progressive loss of prestressing.

The applicability of the previously proposed shear resistance models for monotonic loading conditions was determined. Where required, modifications were proposed for the previous models to allow application to cyclic loading conditions. The use of the proposed models for cyclic shear behaviour was illustrated in detail and the predicted values were compared with the measured results. Lastly, design recommendations were made for horizontal connections for precast concrete load-bearing shear wall panels subjected to reversed cyclic shear loading.

ACKNOWLEDGMENTS

TABLE OF CONTENTS

LIST OF TABLES

LIST OF FIGURES

LIST OF SYMBOLS

A_c total cross-sectional area of the connection

A_{ck} cross-sectional area of the portion of the connection covered by shear keys

A_{cr} total cross-sectional area of the diagonal cracks through the shear keys

A_{cs} average area of the diagonal portion of the compressive strut

A_{cu} shear area of the hollow-core slab at ultimate

A_{c1} area of the hollow-core slab in contact with the dry pack

A_{c2} area of the concrete fill in contact with the dry pack

A_s cross-sectional area of the continuity bars crossing the connection

b initial thickness of the connection (gap between the precast panels)

d depth of shear key

f_{c2} compressive strength of the cracked dry pack

f'_c cylinder compressive strength of the panel concrete

f'_g equivalent standard cylinder compressive strength of the dry pack

f_t tensile strength of the dry pack

f_{t1} tensile strength of the hollow-core slab

f_{t2} tensile strength of the concrete fill

f_y nominal yield strength of the mild steel continuity bars

F_{bi} tensile force per post-tensioned bar at applied slip magnitude i

F_{bo} portion of the gravity load resisted by one continuity bar at the start of testing

F_{boi} portion of the gravity load resisted by one continuity bar or post-tensioned bar during cycle at slip magnitude i (measured at zero slip position)

F_{bxi} horizontal component of tensile force per post-tensioned bar at applied slip magnitude i

F_{byi} vertical component of tensile force per post-tensioned bar at applied slip magnitude i

F_{pe} effective post-tensioning force per bar

F_{pei} effective post-tensioning force per bar at applied slip magnitude i

F_{tu} magnified tensile capacity of the hollow-core slab at ultimate

F_{t1} magnified tensile capacity of the hollow-core slab

F_{t2} magnified tensile capacity of the concrete fill

ΔF_{bi} increase of axial bar force due to the kinking mechanism at applied slip magnitude i

ΔF_{bxi} horizontal component of the increase of axial bar force due to the kinking mechanism at applied slip magnitude i

ΔF_{byi} vertical component of the increase of axial bar force due to the kinking mechanism at applied slip magnitude i

h maximum length of shear key

L_1 deformed length of the continuity bar (flexural mechanism)

L_2 kink length of the continuity bar (kinking mechanism)

M fixed end moment in the continuity bar

M_p plastic moment capacity of the continuity bar

P_g gravity load

t thickness of precast concrete panel

V_a shear resistance of the connection with shear keys immediately after cracking under monotonic loading conditions

V_{cr} cracking shear resistance of the connection

V_f frictional resistance of the connection

V_{f1} shear resistance component provided by friction due to the net gravity load acting on the dry pack

V_{f2} shear resistance component provided by friction due to clamping action (kinking mechanism)

V_{f3} shear resistance component provided by friction due to post-tensioning of the connection using strands

V_{f4} shear resistance component provided by friction due to the tensile force in the post-tensioned bars

V_{hm} maximum shear resistance of the hollow-core slab

V_{hu} ultimate shear resistance of the hollow-core slab

V_{h1} shear resistance component provided by the flexural mechanism in the continuity bars

V_{h2} direct shear resistance component provided by the kinking mechanism

V_{h3} direct shear resistance component provided by the kinking mechanism in the post-tensioned bars

V_{r} shear resistance of the connection

$V_{r_{I}}$ shear resistance of the connection during Stage I of cyclic shear behaviour

$V_{r_{II}}$ shear resistance of the connection during Stage II of cyclic shear behaviour

$V_{r_{III}}$ shear resistance of the connection during Stage III of cyclic shear behaviour

V_{u} ultimate shear resistance of the connection

V_{w} weld shear strength of the mechanical shear connector

α inclination of the diagonal portion of the compressive strut to the horizontal

δ applied slip

ε_{pe} effective prestressing strain

ε_{1} average maximum principal strain in the dry pack at cracking

μ coefficient of friction

σ_{n} compressive stress normal to the connection

σ_{ng} compressive stress normal to the connection due to the gravity loads

σ_{np} compressive stress normal to the connection due to post-tensioning

σ_{n1} compressive stress acting on the dry pack due to the net gravity load

or

total compressive stress normal to the connection distributed to the hollow-core slab

σ'_{n1} total compressive stress normal to the connection distributed to the hollow-core slab at ultimate

σ_{n2} compressive stress acting on the dry pack due to clamping action (kinking mechanism)

or

total compressive stress normal to the connection distributed to the concrete fill

σ_{n3} compressive stress acting on the dry pack due to post-tensioning using strands

σ_{n4} compressive stress acting on the dry pack due to the tensile force in the post-tensioned bars

θ inclination of the shear key to the vertical

CHAPTER 1

INTRODUCTION

1.0   GENERAL

Precast shear walls are an economical construction system for low, medium and high rise construction due to the ease and speed of assembly at the erection site and the high quality of the precast elements. Typically, the precast concrete load bearing shear wall panel structural system carries both the vertical loads and the lateral loads on the structure. The wall panels of the structure are normally oriented longitudinally and transversely to resist the lateral loads in these directions and may also support the floor system of the structure. This form of construction is well suited to residential housing and hotels as the structural nature of the walls provides excellent fire resistance and noise suppression between units.

At present, the use of precast concrete panel systems is very limited in areas of low to moderate seismic risk and is virtually non-existent in active seismic zones. This exclusion from use is because the seismic behaviour of this type of structural system is not well known. The wall panels and floor panels of such systems are normally assumed to behave elastically under seismic loading and consequently, the seismic behaviour of the structure is strongly dependent on the horizontal and vertical connections for dissipation of energy. Since the horizontal connections of the structure must carry both vertical and lateral loads, they play a more critical role in sustaining the stability and integrity of the structure. Consequently, it is crucial to understand the behaviour of the horizontal connections between the precast structural members subjected to large reversed cyclic loading which could be induced during an earthquake. The

current design codes (1,4,19,28) provide very limited information about the design of connections for precast concrete in seismic zones.

Acceptance and competitiveness of precast concrete load bearing shear wall panel systems depends mainly on understanding the behaviour of the connections and development of design guidelines and recommendations for these types of connections. Therefore, this research program was undertaken to investigate the reversed cyclic shear behaviour of typical horizontal connection configurations for precast concrete load-bearing shear wall panels.

1.2   OBJECTIVE

The objective of this research program was to determine the behaviour of precast concrete load bearing shear wall panels under reversed cyclic loading equivalent to earthquake loading conditions. The behaviour of the connections was examined using prototype connection details typically used by the precast industry. In parallel, analytical models were developed to describe the behaviour at various limit states. The analytical models and test results, including the failure modes, were used to introduce design recommendations for the connections of precast concrete load bearing shear wall panel systems in seismic zones.

1.3   SCOPE

The scope of the research program included typical horizontal connections used for precast concrete load bearing shear wall buildings up to ten stories high (low to medium rise structures). The experimental portion of the research program involved a total of six specimens consisting of prototype shear wall panels and connection details. These specimens included the following five different connection configurations:

DP: Plain surface connection with dry pack only

RW: Plain surface connection with dry pack and mild steel continuity bars

PTS: Plain surface connection with dry pack and post-tensioned strands

SK: Dry packed multiple shear keys

PTB: Plain surface connection with dry pack and post-tensioned bars

The first four connection configurations were tested under monotonic loading conditions in a previous study at the University of Manitoba (10,11,17,18,29,30). The fifth configuration was tested under both monotonic and reversed cyclic loading conditions in this program. Therefore, using a database of experimental results for a total of ten specimens (five pairs) tested under both static and cyclic loading, the connection behaviour under earthquake loading conditions was evaluated in terms of:

- behaviour at various limit states
- modes of failure
- contribution of each component of the connection
- coefficient of friction depending on the condition of the dry pack

The various limit states of the connections include the initiation of slip or cracking, the shear resistance after the initiation of slip and the ultimate or residual shear resistance of the connection after failure.

The specimens tested under cyclic loading conditions were subjected to a loading history of fully reversed cycles, applied under both load control and displacement control to examine the behaviour of the connection in the elastic and inelastic ranges of behaviour respectively. All of the specimens were subjected to a constant stress perpendicular to the connection to simulate the effects of gravity loads on the connection.

CHAPTER 2

LITERATURE REVIEW

2.0   INTRODUCTION

Over the last several decades the demand for economical housing has fueled the development and use of precast concrete structural systems. The modular nature of apartment type housing units is ideally suited to precast concrete structures because the repetition between stories allows mass production of the precast units. The controlled environment of the precast manufacturing plant allows for excellent quality control, tight tolerances and preapplied architectural finishes. The repetitive nature of the system also allows rapid erection, even under severe weather conditions.

Precast shear wall panel systems are commonly used for residential housing and hotels. This system uses standardized wall and floor panels assembled to form a box type bearing wall structure, as shown in Figure 2.1. The walls of the structure carry both the gravity loads and the lateral loads on the structure and an intermediate frame is not required. The wall panels of the structure are oriented both longitudinally and transversely to resist the lateral loads in these directions and may also support the hollow-core slabs that make up the floor system of the structure. Typically, the competitive advantage of precast structural systems lies in the reduced erection time and cost. For precast shear wall panel structures, this is achieved by using large wall panels with minimal connections. Unfortunately, this approach exemplifies the inherent weakness of precast concrete; the connection between the elements. In general, the connections create a lack of continuity in the structure. Also, the connections have a lower strength and stiffness than the wall panels and therefore form planes of weakness and stress

concentration in the structure. In non-seismic regions, where wind is normally the controlling design criteria, large demands are not placed on the structure and only nominal reinforcement is required at the connections. This allows for quickly assembled and economical connections. For this reason, precast shear wall panel structures have flourished in the non-seismic areas of the world. In seismically active regions, the use of precast concrete structural systems has primarily been limited to low rise structures. The main reason for the exclusion from use in medium and high-rise applications is the lack of knowledge of how this type of construction will perform under seismic loading conditions. Coupled with this shortage of technical information, the current design codes of North America (1,4,19,28) do not specifically address the use of precast concrete in seismic zones. Rather, precast concrete is required to comply with code provisions developed for cast-in-place concrete that do not consider the unique behaviour of precast concrete and in most cases eliminate the competitive advantages of its use. Before precast concrete structures can be used with confidence in seismic regions and before specific code provisions for its use will be developed, the behaviour of precast concrete structures must be verified

The remainder of this chapter will discuss the seismic behaviour of precast concrete structures and will review the previous research into the static and dynamic (cyclic) behaviour of the connections for precast concrete shear walls. Also, experimental testing methods for studying the dynamic behaviour of structural subassemblies will be reviewed. Lastly, a summary of cyclic loading histories is made.

2.1   SEISMIC BEHAVIOUR OF PRECAST CONCRETE STRUCTURES

The behaviour of a structure subjected to an earthquake is defined by its response and its capacity, or in general terms, by the demands placed on the structure and by the ability of the structure to sustain those demands. For illustrative purposes, the seismic behaviour of the

structure can be described simply in terms of energy. An earthquake is a source of tremendous energy. Earthquakes are caused by differential movement in the Earth's crust, called plate tectonics. This movement produces a build up of strain energy in the Earth's crust until a fault ruptures or slips and the energy is suddenly released. The strain energy released during an earthquake propagates away from the rupture or slip location in waves, producing ground motions. When the ground motions encounter a structure, some of the energy is transferred to the structure. The response of the structure determines how much of the earthquake's energy is absorbed by the structure. The capacity of the structure is the amount of seismic energy that can be absorbed by the structure without collapse.

2.1.1   Response of Precast Concrete Shear Wall Panel Structures

The response of a structure, or the amount of energy absorbed by a structure, determines the magnitude and distribution of forces induced in a structure during an earthquake. The amount of absorbed energy can be considered as the net work done on a structure by the ground motions of an earthquake. By definition, work is the product of force and displacement. Therefore, the interaction of the base shear force induced in the structure with the ground motions at the base of the structure produces work and thus imparts energy to the structure. This concept is illustrated by the following equation.

$$E_{s(absorb)} = W(t_1) = \int_0^{t_1} V(t)\, x'(t)\, dt$$

where,

$E_{s(absorb)}$ = seismic energy absorbed by structure

$V(t)$ = base shear force (sum of lateral shear forces induced in the structure at each storey)

$x'(t)$ = ground velocity

$x'(t)dt$ = displacement

The base shear depends on the dynamic nature of the structure, specifically, the maximum displaced shape induced in the structure during a given earthquake. The displaced shape of a structure subjected to base vibration (i.e. an earthquake) is primarily a function of the structure's natural period of vibration and damping characteristics. The natural vibration period is dependent on the structural stiffness and mass. For monolithic structures with regular structural form, such as cast-in-place concrete, these parameters can be estimated with reasonable accuracy and therefore the response can be determined with confidence. Because of the jointed nature of precast concrete structures, estimation of the stiffness characteristics of the structure can be very difficult. As mentioned previously, the connections of a precast concrete structure constitute regions of low strength and stiffness and therefore become locations of concentrated stress and deformation. During an earthquake, the demands placed on the connection may exceed the elastic limit of the connection and dead load compressive stresses may be overcome by flexural tensile stresses at the connection. As a result, horizontal slip may occur along the connection and/or the connection may begin to open and close, referred to as rocking. These mechanisms result in softening of the lateral force-displacement relationship or stiffness of the structure and the response of the structure becomes non-linear. Structures with non-linear force-displacement characteristics typically do not have a unique natural vibration period since the stiffness of the structure is continuously varying. These factors make response prediction for precast concrete shear wall panel structures uncertain at best. The non-linear force-displacement characteristics of the structure must be well defined before the response of the structure can be estimated. This requires a thorough understanding of the behaviour of the connections, both in shear and flexure, since the connections are the controlling mechanism in the structural system.

2.1.2   Capacity of Precast Concrete Shear Wall Panel Structures

The capacity of a structure is the maximum amount of energy that can be absorbed during an earthquake without failure. To avoid collapse, the capacity of the structure must be greater than or equal to the amount of seismic energy absorbed by the structure, determined from the response of the structure. The capacity of the structure consists of two components, elastic strain energy and dissipated energy. Elastic strain energy represents energy that is temporarily stored by the structure through elastic deformation of the structural members. For a hypothetical structure with infinite strength, all of the seismic energy will be absorbed by internal strain energy. The force level associated with this behaviour could be quite considerable to sustain the input energy from a large earthquake and in most design applications this approach is not practical. To limit the design forces in the members, some of the absorbed energy must therefore be dissipated. The most common structural mechanism for energy dissipation is inelastic deformation or hysteresis. To utilize this mechanism safely and effectively, the behaviour of a structure is elastic at service load levels and becomes inelastic only during a large earthquake to allow energy dissipation. This is referred to as an elastoplastic response. This concept is illustrated in Figure 2.2, where the lateral force-displacement relationship for an elastic structure (A) and an elastoplastic structure (B) is shown. Both structures have equal capacity to sustain seismic energy represented by the area under the curves, but, Structure A behaves elastically and must resist considerably higher force than Structure B. The behaviour of Structure B is elastic until yielding ($_y$) and inelastic as the remainder of the input energy is absorbed. The ability of a structure to deform inelastically can be quantified as ductility, defined as the ratio of maximum deformation to the deformation at yield. From Figure 2.2 it is obvious that Structure B can be designed for a lower force level if adequate ductility is provided to sustain the inelastic behaviour and increased overall deformation (δ_t).

The amount of elastic and inelastic behaviour required to sustain a given earthquake is not unique. The choice of each is left to the designer and is highly dependent on the strength and ductility characteristics of the structural system selected. Due to the jointed nature of precast concrete, large demands are usually placed on the connections of the structure during an earthquake. As a result, the capacity of a precast concrete structure is generally defined by the connections. Therefore, the seismic design process, specifically the estimation of the capacity of a precast concrete structure, requires a detailed knowledge of the strength, deformation and ductility characteristics of the connections.

2.2 EVALUATING STRUCTURAL BEHAVIOUR (EXPERIMENTAL TESTING METHODS)

A common method for determining the behaviour of structures or structural components is through experimental testing methods. Full size or scale model tests have shown to be very effective in determining both the response and capacity characteristics of a structural system. In general, there are four main forms of experimental methods that can be used to investigate different aspects of structural behaviour. Each is described below.

2.2.1 Static Tests

Static or monotonic loading tests are commonly used to determine the capacity of members subjected to monotonic loading only, such as gravity and wind loads. In a static test, the load is applied slowly in unidirectional increments until failure. The strength, stiffness, failure modes and contributions of various structural components can be determined in this type of test. The results from static tests are often used as a basis for other forms of more advanced dynamic testing.

2.2.2 Quasistatic (Reversed Cyclic) Tests

This type of test is primarily used to determine the capacity of structures subjected to earthquakes because of the reversing nature of seismic loading. The strength, stiffness variation, ductility, energy dissipation, modes of failure, contribution of structural components and the ability to sustain repeated cycles of loading can be determined with the quasistatic testing method. The loading in quasistatic tests is applied in fully reversed cycles of force or displacement. The pattern of loading can be modeled after an assumed dynamic response, but most often a simple history of loading beginning with cycles in the elastic range and progressively increases the load or displacement level until failure occurs. Each load or displacement level is maintained for a certain number of cycles before proceeding to the next level. Many different loading histories have been proposed and used by different researchers to achieve different results. The evaluation of various loading histories is discussed in references 7, 16 and 23. The slow nature of the loading in a quasistatic test allows examination of the specimen behaviour and damage propagation under the effects of repeated loading. Although this form of testing is not truly representative of the actual conditions during an earthquake, an estimation of the capacity of the structure can be obtained. By comparing the characteristics of different design approaches tested in the same manner, the relative merits of each design can evaluated and possible design alternatives or improvements can be identified before proceeding to more complex and expensive dynamic testing methods.

2.2.3 Pseudodynamic Tests

Pseudodynamic tests are used to determine the ability of a structure to withstand a given earthquake motion. In this form of test, the structure or structural subassembly is fixed to a structural floor and time-varying loads are applied on the structure at selected locations. The load characteristics are predetermined using a computer analysis of the structure subjected

to the given earthquake. Because the loading is time-dependent and based on actual analysis results, the seismic behaviour of the structure can be determined more realistically than with quasistatic tests. In general, this method of testing is more expensive than quasistatic testing and may require larger laboratory facilities.

2.2.4   Shaking Table Tests (Earthquake Simulator)

Shaking table tests provide the most realistic method for determining the seismic behaviour of a structure. In this form of dynamic test, a structure or structural subassembly is fastened to a testing bed or table, and loading is induced in the specimen by rapidly moving the table with computer controlled actuators. The pattern of shaking is modeled after actual historical measured earthquake ground motions. Because the shaking induces an inertial response in the specimen, as in an actual earthquake, the strength and deformation demands placed on the structure can be realistically determined. Also, since a given earthquake does not have a particular strength, deformation or energy dissipation demand, the shaking table test is suitable for determining whether a specific design can withstand the given earthquake.

Although shaking table tests provide the best method for determining the seismic behaviour of a structure, it is not without limitations. For example, due to the rapid rate of loading, it is difficult to obtain a close observation of the progression of damage and behaviour during the test. Also, most shaking tables are not large enough to handle full size structures and therefore scale models or structural subassemblies must be tested. Lastly, compared to other forms of testing, shaking table tests can be very expensive.

2.2.5   Comparison of Quasistatic and Shaking Table Testing Methods

Each of the testing methods described above have relative merits and limitations for evaluating the seismic behaviour of structures. Oliva, Gavrilovic and Clough (25) performed an experimental testing program to compare and evaluate the usefulness of the quasistatic (pseudostatic) and shaking table testing methods for determining the behaviour of precast shear wall panel structures. The tests were performed on one-third (1/3) scale, 3 storey subassemblies of a precast concrete large panel shear wall system. The walls were precast reinforced concrete and supported precast floor panels at each storey. The horizontal connections were cast-in-place and used the "European" form of construction as shown in Figure 2.3. Vertical continuity between the panels was provided by mild steel reinforcement, connected at each horizontal joint with a coupler. The two testing methods were compared on the basis of visible damage, predominant damage mechanisms, strength and stiffness variation, deformability and energy dissipation.

The loading in the quasistatic tests was applied in displacement increments, each maintained for three fully reversed cycles, and progressively increased until failure. For the shaking table tests, additional weight was added to the specimen to simulate the gravity loads and to induce inertial behaviour in the model. The ground motion pattern used in the shaking table test was taken from the El Centro earthquake records (May, 1940). The comparison of the test results is briefly summarized below.

Damage to the subassemblies was very similar in both testing procedures: cracking occurred at the lowest horizontal joint and was followed by yielding, buckling and rupturing of the vertical continuity reinforcement. In the quasistatic test, the damage was symmetric due to the fully reversed loading pattern. The damage in the shaking table tests was generally non-

symmetric because once damage was initiated at a particular location, the localized loss of strength and stiffness tended to concentrate damage in that area.

Overall strength, stiffness variation and strength degradation were in good agreement between the two testing methods. This is illustrated by the comparison of the base moment versus top displacement relationship for specimens from the two different tests. This is shown in Figure 2.4, where the strength envelope from the quasistatic test is superimposed on the moment-displacement history from the shaking table test. The behaviour of the specimen from the shaking table test is not symmetric for reasons discussed previously, but the overall behaviour compares well between the two tests.

The most significant difference between the two testing methods was observed in the capacity for energy dissipation, indicated by the area under a full base moment-top displacement hysteresis loop. The quasistatic test results consistently indicated a higher capacity for energy dissipation than the shaking table tests. Oliva et al suggested that this was due to the slow rate of loading in the quasistatic test that would allow forces to redistribute and damage propagation to occur while loading. In the shaking table tests the damage was more concentrated which limited the volume of material able to deform inelastically, thus limiting the capacity for energy dissipation. Because the shaking table testing method is generally felt to more realistically represent actual seismic loading conditions in a structure, Oliva et al concluded that the capacity for energy dissipation determined from the shaking table tests would be closer to the actual capacity of the structure than the results from the quasistatic tests.

From the observed test results, Oliva et al concluded that the quasistatic testing method was ideal for determining the damage mechanisms and strength and deformation characteristics of wall panel systems. On the other hand, they suggested that quasistatic tests alone were not sufficient to define the actual demand or response developed in a structure during an

earthquake because the capacity for energy dissipation could be over-predicted. For this purpose, a shaking table test should ideally be used.

2.3 INVESTIGATION OF CONNECTION BEHAVIOUR USING COMPONENT TESTS

A considerable amount of research has been performed using component tests to evaluate the behaviour of connections for precast concrete shear wall panels. In the past, a large portion of this work has focused on the shear transfer at construction joints and at precast concrete connections under monotonic loading conditions. In recent years, this research has expanded to consider different connection configurations and the effects of cyclic loading. In the following sections, a brief summary of some of the more current research in these areas is provided. In addition, a detailed summary of the previous research at the University of Manitoba into the monotonic shear behaviour of the connections is provided. The applicability of the models proposed in the previous research for cyclic loading conditions will be evaluated in Chapter 5 of this thesis.

2.3.1 Monotonic Shear Behaviour - Previous Research at The University of Manitoba

An extensive four year research program was performed at the University of Manitoba to investigate the behaviour of horizontal connections for precast concrete load-bearing shear wall panels subjected to monotonic shear loading (10,11,17,18,29,30). The behaviour of nine connection configurations typically used in current practice was investigated. A total of twenty-two prototype precast concrete shear wall panel specimens were tested in three phases of research. The first phase (Foerster (10,11)) included four types of connections: a dry packed plain surface connection, a dry packed connection with continuity reinforcement and dry packed connections with two types of mechanical shear connectors, in addition to continuity bars. The second phase (Serrette (29,30)) included two different types of dry packed multiple

shear key configurations. The third phase (Hutchinson (17,18)) investigated the use of vertical post-tensioning tendons. The third phase also included connections which support hollow-core slabs with and without post-tensioning. All of the connections were subjected to a constant load perpendicular to the connection to simulate the effects of gravity loads on the connection. During the three phases of research, the effects of different load levels normal to the connection were investigated. The details of the different connection configurations examined in these three phases are shown in Figure 2.5. The configuration of the test specimens, shown in Figure 2.6, was selected to allow the application of direct shear loading on the connection.

Based on the results of the three phases of research, it was concluded that:

1. An increase in the level of load perpendicular to the connection increases the shear capacity of the connection.

2. If bond is present between the dry pack and the precast concrete panels, the initiation of slip at the connection will occur suddenly due to breaking of the bond. The shear resistance of the connection at cracking is independent of the type of shear reinforcement used in the connection.

3. The ultimate capacity of the connection is significantly increased by the presence of continuity bars and/or mechanical shear connectors, as shown in Figure 2.7

4. The presence of shear keys may increase the maximum shear resistance of the connection up to 60% greater than to the plain surface connection tested under the same level of load perpendicular to the connection, as shown in Figure 2.8.

5. The two different shear key configurations considered in Phase II did not affect the behaviour or capacity of the connection.

6. The shear resistance of connections with shear keys is primarily dependent on the strength of the weaker connection material and the level of load perpendicular to the connection. In this research, the dry pack was the controlling material.

7. Post-tensioning of the connection may be considered by including the effective post-tensioning stresses on the connection with the gravity loads normal to the connection.

8. The maximum shear capacity of the connections supporting hollow-core slabs is governed by the lower magnitude of the frictional resistance of the connection and the shear resistance of the hollow-core slab. At higher levels of load perpendicular to the connection, the frictional resistance of the connection may exceed the shear capacity of the hollow-core slab and therefore the strength and stiffness of the connection with hollow-core slab will be reduced, as shown in Figure 2.9.

9. At ultimate, it is assumed that a complete loss of bond occurs between the hollow-core slab and the concrete fill within the cores, reducing the shear resistance of the connection.

The test results from each phase were used to isolate the contribution of each connection component and to propose mathematical models to predict the shear resistance of the different connection configurations under monotonic loading conditions at various limit states. The proposed models are described by phase in the following sections.

Phase I: Connections with Continuity Bars and Mechanical Shear Connectors

The behaviour of the connections tested in the first phase of the previous research could be described by two limit states; the shear resistance prior to the initiation of slip (at cracking), and the ultimate shear resistance after the initiation of slip.

All of the connection configurations tested in this phase experienced a sudden initiation of slip due to breaking of the bond between the dry pack and the precast concrete panels. This was defined as cracking of the connection. The cracking shear resistance of the connection, V_{cr}, is predicted as:

$$V_{cr} = \sqrt{f_t \left(f_t + \sigma_n \right)} \, A_c \qquad\qquad (2.1)$$

where

f_t = tensile strength of the dry pack

$\quad = 0.5\sqrt{f'_g}$

f'_g = compressive strength of the dry pack

σ_n = compressive stress normal to the connection

A_c = connection area

After the initiation of slip, the ultimate shear resistance, V_u, of the dry packed connection with continuity bars and welded shear connectors is predicted as:

$$V_u = \mu \sigma_n A_c + \frac{A_s f_y}{\sqrt{3}} + V_w \qquad\qquad (2.2)$$

where

μ = coefficient of friction, 0.7 +/- 0.1 is proposed

σ_n = compressive stress perpendicular to the connection

A_c = connection area

A_s = total cross-sectional area of continuity bars

f_y = nominal yield strength of continuity bars

V_w = weld shear strength of the mechanical shear connector

The ultimate strength of the connection was considered to occur at a slip magnitude of 5 mm.

The experimental results indicated that the contribution of the various shear resistance components were independent, and therefore could be added or removed according to the particular connection configuration under consideration.

Phase II: Connections With Dry Packed Multiple Shear Keys

The behaviour of the connections tested in the second phase of the previous research could be described using three limit states; cracking of the connection, shear resistance immediately after cracking and the ultimate shear resistance.

Initially, the shear resistance of the connection with multiple shear keys is provided by a combination of frictional resistance and direct bearing on the dry pack within the shear keys. Cracking of the connection occurs suddenly when the bearing resistance of the dry pack within the shear keys is exceeded. The cracking shear resistance of the connection is predicted as:

$$V_{cr} = \mu \sigma_n \left(A_c - ndt \tan \theta \right) + \sqrt{f_t (f_t + \sigma_n)} \, A_{cr} \tag{2.3}$$

where

μ = coefficient of friction, 0.7 +/- 0.1 is proposed

σ_n = compressive stress perpendicular to the connection

A_c = connection area

n = number of shear keys

d = depth of shear key

t = precast concrete panel thickness

θ = inclination of shear key to the vertical

f_t = tensile strength of dry pack

$$= 0.6\sqrt{f'_g}$$

f'_g = compressive strength of dry pack

A_{cr} = total cross-sectional area of diagonal cracks through shear keys

$$= nt\sqrt{h^2 + b^2}$$

h = maximum length of the shear key

b = initial thickness of the connection (gap between the precast panels)

The first term of this expression represents the frictional resistance of the connection. The second term of the expression is the bearing resistance of the dry pack.

Immediately after cracking, the shear resistance of the connection is provided by the compressive strength of struts which form between the diagonal cracks in the shear keys and by frictional resistance along the slip surface, as shown in Figure 2.10. The shear resistance of the connection after cracking, V_a, is predicted as:

$$V_a = (n-1)f_{c2} A_{cs} \sin\alpha + \mu[\,\sigma_n A_c - (n-1)f_{c2} A_{cs} \cos\alpha\,] \tag{2.4}$$

where

f_{c2} = compressive strength of the cracked dry pack

$$= \frac{f'_g}{0.8 + 170\varepsilon_1}$$

f_g = compressive strength of the dry pack

ε_1 = average maximum principal strain in the dry pack at cracking, a value of 0.004 is proposed based on experimental results

A_{cs} = average area of diagonal portion of the strut

$$= \frac{0.5(b+d)t}{\cos \theta}$$

θ = inclination of the shear key to the vertical

α = inclination of diagonal portion of the strut to horizontal

      $= \tan^{-1}(h/b)$

After cracking of the connection, slip occurs and eventually the strut mechanism deteriorates. At this point, the shear resistance of the connection is provided only by friction along a newly formed sliding plane. This represents the ultimate strength of the connection, V_u, and may be predicted as:

$$V_u = 0.2\sqrt{f'g}\, A_{ck} + 0.5\sigma_n A_c \tag{2.5}$$

where

A_{ck} = cross-sectional area of the portion of the connection covered by the shear keys

The ultimate strength of the connection is considered to occur at a slip of 5 mm.

Phase III: Connections with Post-tensioning and Supporting Hollow-Core Slabs

Post-tensioning of the connection with strands was determined to increase the frictional resistance of the connection. The amount of increase was directly proportional to the level of stress perpendicular to the connection, produced by post-tensioning. The frictional resistance V_p of connections with post-tensioned strands is predicted as:

$$V_f = \mu (\sigma_{ng} + \sigma_{np}) A_c \qquad\qquad (2.6)$$

where

μ = coefficient of friction, a value of 0.7+/- 0.1 is proposed

σ_{ng} = compressive stress normal to the connection due to gravity loads

σ_{np} = compressive stress normal to the connection due to post-tensioning

A_c = cross-sectional area of the connection

At low levels of stress perpendicular to the connection, the presence of hollow-core slab did not affect the behaviour of the connection. At high stress levels, the presence of the hollow-core slab significantly reduced the maximum and ultimate strength of the connection compared to connections without hollow-core slabs. Therefore, the shear resistance of connections supporting hollow-core slab can be predicted as the lesser value of the frictional resistance of the connection, V_f (Equation 2.6), and the shear resistance of the hollow core slab, V_h. The maximum shear resistance of the hollow-core slab, V_{hm}, is predicted as:

$$V_{hm} = \tfrac{2}{3} (A_{c1}F_{t1} + A_{c2}F_{t2}) \qquad\qquad (2.7)$$

where

A_{c1} = area of the hollow-core slab in contact with the dry pack

A_{c2} = area of the concrete fill in contact with the dry pack

F_{ti} = magnified tensile capacity of the hollow-core (1) and concrete fill (2)

$\phantom{F_{ti}}= \sqrt{f_{ti}(f_{ti} + \sigma_{ni})}$

f_{ti} = tensile strength of the hollow-core (1) and concrete fill (2)

σ_{ni} = compressive normal stress including the effect of post-tensioning distributed to the hollow-core (1) and concrete fill (2). σ_{ni} is evaluated by determining the distribution of vertical stresses at the connection.

At ultimate, it is assumed that a complete loss of bond occurs between the hollow-core and the concrete fill within the cores. As a result, the applied shear load is transferred through only the web area of the hollow-core slab and the shear resistance of the connection at ultimate is determined as the lesser of the frictional resistance, V_f, (Equation 2.6) and the ultimate shear resistance of the hollow-core slab, V_{hu}. The ultimate shear resistance of the hollow-core slab is predicted as:

$$V_{hu} = \frac{2}{3} \ (A_{cu}F_{tu} + A_{c2}F_{t2})$$

(2.8)

where

A_{cu} = summation of the area of the webs at mid-height of the hollow-core slab beneath the contact area A_{c1}

= A_{c1} / 4 for the geometry of the hollow-core slabs used in this research

A_{c2} = area of the concrete fill in contact with the dry pack

F_{tu} = magnified tensile capacity of the hollow-core at ultimate

= $\sqrt{f_{t1}(f_{t1} + \sigma'_{n1})}$

σ'_{n1} = compressive normal stress including the effect of post-tensioning distributed to the hollow-core at ultimate

= $4\sigma_{n1}$ in this research due to the reduction of the contact area at ultimate

F_{t2} = magnified tensile capacity of the concrete fill at ultimate

The ultimate shear resistance is assumed to occur at a slip of 5 mm.

2.3.2   Cyclic Shear Behaviour

In the current literature, the information on the cyclic shear behaviour of horizontal connections for precast concrete shear wall panels is not abundant. To supplement this, similar research on shear transfer across construction joints and cracks in cast-in-place concrete can be considered. Although the shear interface is not identical to the connections between precast panels, the concepts and mechanisms of shear transfer are similar.

Aoyama, Noguchi, Ochiai and Horikawa (2) studied the effects of shear transfer across cracks in reinforced concrete shear walls. The shear failure plane was initiated by introducing notches in the sides of the specimen. Mild steel reinforcement was placed across the failure plane at a right angle. The reinforcement ratio across the shear plane was 1.0%. The specimens were tested under constant uniform stress of 0.981 MPa normal to the connection and were subjected to reversed cyclic shear loading. Some of the specimens were modified to allow isolation of the interface friction and the dowel action of the reinforcement. In one specimen, flexible vinyl sleeves were placed over the shear plane reinforcement to eliminate the dowel action of the reinforcement and to isolate interface shear transfer. In another specimen, a thin, greased copper plate was placed at the shear plane to eliminate interface shear transfer and allow isolation of the dowel action of the reinforcement. The following observations were made from the experimental results:

1. The stiffness of the unmodified specimens and the specimen where dowel action was eliminated was significantly higher than the stiffness of the specimen with dowel action only.

2. On each cycle of loading, after the load was returned to zero, the specimen with dowel action only had little or no residual slip at the connection, while the other specimens all measured a residual slip after unloading.

3. The superimposed behaviour of the specimen with dowel action only and the specimen with interface shear transfer only matched the behaviour of the unmodified specimens very closely. This suggests that the shear resistance components may be isolated and studied individually.

4. For the reinforcement ratio and level of stress normal to the failure plane considered in the research, the contribution of the interface shear transfer (interface friction) ranged from 75% to 83 % and the contribution from the dowel action ranged from 17% to 25%.

Paulay, Park and Phillips (26) studied the shear resistance of horizontal construction joints in cast-in-place concrete shear walls. The construction joint occurs when fresh concrete is placed against a hardened concrete surface. Thirty-six specimens were tested to study the effects of surface preparation and reinforcing content on the behaviour of the joints under monotonic and cyclic shear loading. Three different steel contents were considered; 0.31%, 0.69% and 1.23%. Six reinforcing bars were placed across the joint and the bar size was changed to provide the desired steel content. The cyclic loading pattern consisted of 5 cycles at an applied load of 75% of the maximum load measured from the monotonic tests, and 5 cycles at an applied slip displacement in the order of 2.3 mm to 3.8 mm. The specimens were not subjected to a compressive stress normal to the joint. The joint behaviour was defined in terms of interface shear transfer and dowel action. The shear friction theory was assumed by Paulay et al to provide the interface shear transfer. Dowel action was assumed to be provided by one or a combination of three mechanisms; flexure, shear and kinking, as shown in Figure 2.11. Based on the experimental results, the following observations were made:

1. The shear resistance provided by dowel action appeared to be proportional to the steel content. This suggests that the dowel action is likely due to the shear mechanism and/or the kinking mechanism, rather than the flexural mechanism in which the shear resistance is not proportional to the shear resistance.

2. A significant amount of slip may be required to initiate dowel action. Therefore, for service load design purposes, the effect of dowel action should be ignored.

3. Under the effects of cyclic loading, the most heavily reinforced specimens experienced a progressive loss of stiffness with each cycle. The specimens with the smaller two reinforcement ratios were able to sustain the design capacity predicted using the shear friction concept under the cyclic loading.

4. The relative loss of stiffness and reduced strength for the most heavily reinforced specimen compared to the other specimens could be attributed to the higher bearing stresses around the larger bars which could cause premature deterioration of the concrete around the bars.

Hanson (13) investigated the cyclic shear behaviour of horizontal connections for interior precast concrete shear walls that supported floor slabs. Five full scale specimens were tested under simulated seismic loading to determine the coefficient of friction for "extremely smooth joint surfaces". The joint surfaces were intentionally made very smooth by casting the joint surface of the panel against plastic coated plywood to test an extreme situation. The loading perpendicular to the connection was maintained at a constant level of 4.83 MPa for all of the specimens but one. In this specimen, the normal load on the connection was varied from 1.21 MPa to 7.24 MPa to determine the effects of different load levels on the coefficient of friction. Some of the connections were provided with vertical ties (continuity reinforcement). The loading history used to simulate seismic conditions was applied entirely in the inelastic range of behaviour and consisted of three cycles at a slip of 2.54 mm, followed by nine cycles to 5.1 mm and finally three or more cycles at a slip of at least 7.6 mm. For the specimen tested

under varying normal load levels, additional cycles were added during the loading history at each of the load levels. The typical behaviour of the connections consisted of an initial peak load at the initiation of slip, followed by stable hysteresis loops with no visible deterioration, as shown in Figure 2.12. The initial peak load was extremely variable and was attributed to breaking of bond between the connection and the panels. Because temperature affects and construction movements may damage the bond in actual shear wall structures, Hanson suggested that the initial peak load due to bond has no meaning in seismic applications and should be ignored. The stable hysteretic behaviour after the initiation of slip produced consistent friction coefficients in the range of 0.2 to 0.4. These values are very low in comparison with most other reported friction coefficients and Hanson attributed this to the extreme condition of the joint surfaces. In Figure 2.12, typical hysteresis loops are shown for connections with and without vertical ties. Specimen R3 did not have vertical ties and exhibited almost perfectly rectangular shear - slip loops. The addition of vertical ties for Specimen R2 produced skewed hysteresis loops with a parallelogram-like shape. The skewed shape of the shear - slip behaviour was attributed to the additional resistance provided by bending of the vertical ties (dowel action).

Harris and Abboud (14) studied the monotonic and cyclic behaviour of horizontal shear wall connections. 3/32 scale models were used to evaluate the seismic performance of interior horizontal connections supporting floor slabs. The main variables investigated in this research were:

1. Loading history: monotonic or reversed cyclic

2. The magnitude and distribution of the normal forces on the connection

3. The amount of connection reinforcement (vertical ties)

A total of sixteen specimens were tested, eight under monotonic loading and eight under reversed cyclic loading. Of the eight pairs of specimens, five pairs were tested under a constant uniform stress perpendicular to the connection, ranging from zero to 2 MPa. The remaining three pairs were subjected to a triangular stress distribution on the connection to simulate the effects of bending moment on the connection. The moment due to the stress gradient on the connection did not vary during the loading. The loading history for the specimens tested under reversed cyclic loading consisted of three cycles at each load level. The load levels were taken as a small percentage of the measured ultimate strength of the companion specimen tested under monotonic loading. The load increments were increased until failure of the connection.

For the specimens tested under monotonic loading, a sudden large slip occurred at approximately 95% of the ultimate shear strength. Failure of the connections was due to splitting and crushing of the floor slabs in the vicinity of the vertical ties. Under cyclic loading, the behaviour of the connection prior to failure exhibited pinched shear -slip loops, as shown in Figure 2.13(a). Note that the horizontal axis in this figure has a very small scale and the maximum measured slip is less than 0.05 mm. After failure of the connection, defined as a reduction of shear resistance, the behaviour of the connection became stable with almost perfectly rectangular hysteresis loops, as shown in Figure 2.13(b). This indicated a substantial increase of energy dissipation. Failure of the connection was characterized by splitting of the floor slabs adjacent to the vertical ties. Although the failure modes were similar, the ultimate strength of the connections tested under cyclic shear loading was approximately 5% to 33% less than the ultimate strength of the identical specimen tested under monotonic loading. In addition, the amount of slip at ultimate was larger for the cyclically loaded specimens. The behaviour and failure modes of the specimens tested under shear loading with an overturning moment were similar to the behaviour observed under pure shear loading. With an overturning

moment, the hysteresis loops became slightly less pinched prior to failure, but the ultimate strength of the connection was reduced.

No attempt was made by Harris and Abboud to identify the components of shear resistance for the connections. Based on the experimental data, the following observations were made:

1. The coefficients of friction were determined to range from 0.72 to 1.52 using the shear friction concept.
2. The strength of the connection was only increased slightly by doubling the area of the vertical ties across the connection.
3. The shear resistance of the connection was significantly increased by increasing the normal load level on the connection.

Fukuda and Kubota (12) performed an experimental study on the monotonic and reversed cyclic shear behaviour of horizontal connections in precast concrete panel structures. The test specimens were assumed to represent the flexural compression zone of a shear wall panel subjected to earthquake magnitude loading. The specimens consisted of two precast wall panels connected horizontally with a mortared joint. Two continuity bars were provided across the joint in all specimens. Two series of specimens were tested; the first with constant uniform compressive stress of 1.96 MPa on the connection to simulate gravity loads and the second series with a varying uniform stress on the connection to simulate the conditions of the zone at one end of a shear wall panel during reversed cyclic flexural loading. During the shear loading in the positive direction, a compressive stress of 7.85 MPa is applied on the specimen to simulate the flexural compressive stresses, and in the negative direction of shear loading, the continuity reinforcement was yielded in tension to simulate the flexural tensile forces on the

connection. Only the results under constant normal stress will discussed in this section since the second series of specimens are outside the scope of this thesis.

The typical experimental results of the specimens tested under monotonic and reversed cyclic loading are shown in Figure 2.14(a). Under monotonic loading, the shear resistance of the connection after the initiation of slip maintains constant until the slip reaches approximately 7 mm, at which point the resistance begins to increase linearly. The specimens tested under reversed cyclic loading displayed stable hysteresis loops with a parallelogram shape. Fukuda and Kubota proposed a model for predicting the shear resistance of the connection based on the assumption of interface friction and dowel action of the continuity reinforcement. The dowel action of the reinforcement is assumed to be dominated by the kinking mechanism. As the connection is deformed in shear, a tensile force is induced in the continuity bars at the connection level. The vertical component of the force in the bars will provide a clamping stress on the connection, increasing the frictional resistance of the connection. The horizontal component of the force will directly resist the applied shear loading. Once the reinforcement yields in tension, Fukuda and Kubota proposed that the plastic moment capacity of the bars should also be included in the shear resistance. The idealized form of this mechanism is shown in Figure 2.14(b). The dowel length, L, was determined to be 40 to 50 mm, based on the deformed shape of the continuity bars at the completion of the experiment. The coefficient of friction in this research was determined to be 0.5. This friction coefficient, when used in combination with the proposed mechanisms of the dowel action, provided very good results when compared to the measured behaviour.

Iso, Higashi, Endo and Numoto (20) investigated the behaviour of horizontal and vertical connections in a composite construction system of precast and cast-in-place concrete. The system consists of precast concrete wall panels, joined by a cast-in-place joint at each storey. The cast-in-place joint ties together the precast wall system and acts as a topping on the

precast floor system, as shown in Figure 2.15(a). The edges of the panels have shear keys or cotters to provide shear transfer between the precast panels and the cast-in-place joint. Curtain vertical reinforcement in the precast panels extends into the cast-in-place concrete to provide vertical continuity. The variables in this research program were the type of shear loading and the level of load normal to the connection. Five horizontal connection specimens were tested in this program, one under monotonic loading and the remainder under reversed cyclic loading. The configuration of the specimen is shown in Figure 2.15(b). The monotonic specimen and two of the cyclic shear specimens were tested with no load normal to the connection. The remaining two cyclic specimens were tested under a uniform normal stress of 0.33 MPa. The cyclic loading was applied using increments of slip, each maintained for three fully reversed cycles.

Typical experimental results for the specimens tested under monotonic and cyclic loading with no normal load are shown in Figure 2.15(c). The monotonic results are shown as a dashed line in this figure. Based on these results there is little or no effect on the cracking strength or the maximum strength of the connection due to cyclic loading. Initially, cracks developed along the interface between the precast and cast-in-place concrete. After the maximum shear strength was attained, significant cracks occurred at the base of the lugs of the shear keys (cotters) in the precast panels and the load carrying capacity of the connection was reduced suddenly. This failure mechanism was identical under both monotonic and cyclic loading conditions and at both levels of normal load. Increasing the normal load increased the cracking and maximum shear strengths but did not affect the failure mechanism. Iso et al proposed a model for strength prediction based on the interface friction, strength of the shear keys and dowel action of the reinforcement. A coefficient of friction of 0.7 was proposed for the interface friction. The dowel action of the reinforcement was assumed to be provided by the shear strength of the bars, given by $A_s f_y / \sqrt{3}$. Because failure occurred due to cracking through the lugs of the shear keys, the contribution from the shear keys (cotters) was based on

the cracking and ultimate shear strength of the precast panel concrete at the cotters, proposed as $0.1f'_c$ and $0.15f'_c$, respectively. Thus, the contribution from the shear keys would be calculated as the base area of the cotters multiplied by the cracking shear stress or ultimate shear stress, as desired. The predicted shear strengths compared very well to the measured values.

CHAPTER 3

EXPERIMENTAL PROGRAM

3.0   INTRODUCTION

This experimental program was designed to evaluate the effects of large reversed cyclic shear loading on the behaviour of typical horizontal connections for precast concrete load-bearing shear wall panels. A database of 26 specimens, tested under monotonic shear loading in three previous research programs at the University of Manitoba, was used as a basis of comparison for the behaviour of five different connection configurations tested under reversed cyclic loading.

This chapter describes the experimental parameters, test specimens, material specifications, instrumentation, loading frame and testing procedure used in this research program.

3.1   EXPERIMENTAL PARAMETERS

A total of six specimens were tested in this experimental program. Each specimen consisted of two precast concrete wall panels, joined by a horizontal connection, as shown in Figure 3.1. The principal experimental variable of this research was the configuration of the horizontal connection between the panels.

3.1.1   Connection Configurations

In this program, the cyclic shear behaviour of five different connection configurations, currently used in practice, was investigated. The connection configurations considered in this program were:

Type DP: Plain surface connection with dry pack only

Type RW: Plain surface connection with dry pack and mild steel continuity bars

Type PTS: Plain surface connection with dry pack and post-tensioned strands

Type PTB: Plain surface connection with dry pack and post-tensioned high strength bars

Type SK: Dry packed multiple shear keys

The five connection configurations are shown in Figure 3.2. Each of the connection configurations was tested under fully reversed cyclic shear loading. In addition, connection type PTB was also tested under monotonic shear loading because this configuration was not considered in the previous research at the University of Manitoba. Each specimen was denoted according the two or three letter specimen mark assigned above for the various connection types. The specimen with connection type PTB tested under monotonic (static) loading was denoted as Specimen PTB-S. The details of the experimental parameters are summarized in Table 3.1.

3.1.2   Gravity Loads (Vertical Loads)

All of the specimens in this experimental program were subjected to a constant vertical load to simulate the effects of gravity loads on the walls. The first specimen tested, Specimen DP, was subjected to a uniform vertical stress of 4 MPa. The remaining specimens were subjected to a simulated gravity load producing a uniform vertical stress of 2 MPa on the

connection. The stress level of 2 MPa is representative of the gravity load stresses at the base storey level of a typical ten storey precast concrete load-bearing shear wall structure. The simulated gravity load was maintained constant over the duration of shear loading.

3.1.3 Loading History

A quasi-static, reversed cyclic loading history was used in this program to simulate the effects of earthquake loading on the connection. The loading history utilized a combination of load control cycles and displacement control cycles to fully examine the elastic and inelastic ranges of connection behaviour. Initially, the loading history was applied using load control. The loading increments were taken as approximately 20% of the predicted strength of the connection at the initiation of slip or cracking under monotonic loading. Each load level was maintained for three fully reversed cycles. Once the initiation of slip, or cracking of the connection, was observed, the behaviour of the connection became inelastic and the loading history was applied using displacement control. The initiation of slip was defined as the point at which 0.1 mm of relative horizontal slip was measured between the panels in each direction of loading. The displacement increments were taken as 1.0 mm increments of relative horizontal slip measured between the panels at the connection. Each applied slip magnitude was maintained for three fully reversed cycles. The test was continued, under displacement control, until failure of the connection occurred. Failure was defined as a 20% reduction of the shear resistance of the connection due to an increase of applied slip. After failure of the connection, the test was concluded by applying several single cycles at increasing applied slip magnitudes to determine the residual strength of the connection. The general form of the loading history is shown in Figures 3.3(a) and 3.3(b).

3.2   DESCRIPTION OF TEST SPECIMENS

The overall shape and dimensions of the specimens in this program was identical. Some minor variations were required to make allowance for placement of the different connection configuration details. The details of the precast wall panels and the connections are discussed in the following sections.

3.2.1   Connection Details

The horizontal connections consisted of a space or gap between the precast concrete panels filled with dry pack, and where applicable, a form of continuity element. In actual structures, the gap between the panels is used for alignment purposes and is filled with dry pack, a zero slump mixture of sand, normal Portland Cement, and water. The dry consistency allows compaction of the dry pack into the gap between the panels to form the connection. The typical thickness of the gap is 20 mm. All specimens in this experimental program had a connection gap of 20 mm. The first specimen tested, Specimen DP, had a connection region 1000 mm long and 150 mm wide, for a connection area of 150,000 mm². The remaining five specimens had a connection region 1200 mm long and 150 mm wide, for a connection area of 180,000 mm². The details of the connection types are shown in Figure 3.2, and are described below.

Specimen DP: Plain surface connection with dry pack only. The connection of Specimen DP had a plain surface (no shear keys) and was filled with dry pack. No continuity elements were used to allow isolation of the contribution of the dry pack to the connection behaviour. Typically, some form of vertical continuity element is required across the connection and therefore this connection configuration is not used by itself in practice.

Specimen RW: <u>Plain surface connection with dry pack and mild steel continuity bars.</u> The connection of Specimen RW had a plain surface and was filled with dry pack. Two 25M, Grade 400W continuity bars were provided across the connection at 900 mm on centre. The continuity bars were connected by welding to a 75x75x10 mm steel angle, as shown in Figure 3.4. The configuration of the continuity bars and the location of the steel angles are shown in Figure 3.5. In the upper concrete panel, the continuity bars were straight and protrude from the panel. In the lower concrete panel, the angles were welded to the ends of a single continuity bar, bent to form a "U" shape. The shape of the continuity bar in the lower panel was required because sufficient development length could not be provided for a straight bar. Pockets were provided around the angle in the lower panel to facilitate welding of the bars from the upper panel during specimen assembly. A close-up of the weld location in the pocket is shown in Figure 3.6. After welding of the continuity bars, the connection was dry packed.

Specimen PTS: <u>Plain surface connection with dry pack and post-tensioned strands.</u> The connection of Specimen PTS had a plain surface and was filled with dry pack. The connection was post-tensioned using two 7-wire, 12.7 mm diameter prestressing strands, located at 900 mm on centre. The dry pack was allowed to cure for seven days prior to post-tensioning. The strands were tensioned to produce an effective prestressing force of 108 kN per strand at the time of testing. This produced an effective vertical stress of 1.2 MPa on the connection area. The strands were placed in galvanized steel ducts, cast in the panels. The ducts were coupled at the connection inside a small pocket cast into the top

surface of the lower concrete panel, as shown in Figure 3.7. After post-tensioning, the ducts were filled with an expansive grout.

Specimen PTB: Plain surface connection with dry pack and post-tensioned bars.   The connection of Specimen PTB had a plain surface and was filled with dry pack. The connection was post-tensioned using two 5/8" diameter threaded prestressing bars (Dywidag Bars), located at 900 mm on centre. Seven days after dry packing, the bars were tensioned to the same level as the strands, producing an effective vertical stress on the connection of 1.2 MPa. Using the same procedure as the strands, the bars were placed inside galvanized steel ducts and after post-tensioning, the ducts were filled with an expansive grout.

Specimen SK: Dry packed multiple shear keys.   The connection of Specimen SK consisted of five shear keys, as shown in Figure 3.8. The entire connection length including the shear keys was dry packed. The length of the shear key is 100 mm, the depth is 35 mm and the sides of the key are inclined at 23 degrees from the vertical. The dimensions of the lugs between the shear keys are identical to the dimensions of the shear keys, as shown in Figure 3.8.

3.2.2   Precast Concrete Wall Panels

All of the precast concrete panels used in this experimental program were fabricated by Con-Force Structures Limited of Winnipeg, Manitoba. Each specimen in this program consisted of a upper panel and a lower panel. During testing, the lower panel was fixed and the shear loading was applied on the upper panel. The "double corbel" configuration of the upper panel allowed the application of pure shear on the connection in both directions of loading. The connection area covered the length of the lower panel. The dimensions of the

lower panel were 1200 mm long and 1100 mm high. The upper panel was 3800 mm long, and the height of the panel was 1000 mm in the connection region and 1400 mm in the corbel regions. The thickness of both panels was 150 mm. This thickness is typical of an interior wall in a precast concrete load-bearing shear wall structure.

The overall configuration of the precast concrete wall panels, shown in Figure 3.1, was identical for all of the specimens. Some minor differences in the configuration and the reinforcement of the panels were required to accommodate the different connection types. Four sets of panel designs were required to account for the connection types. Separate design were used for Specimen DP, Specimen RW, the post-tensioned specimens (PTS, PTB and PTB-S) and for Specimen SK. The panel configuration and reinforcement details for Specimen DP are shown in Figure 3.9. The reinforcement for Specimen DP did not include any continuity elements or connection detailing. The panel configuration and reinforcement details for Specimen RW are shown in Figure 3.10. Pockets were left in the lower panel over half of the steel angle to facilitate welding of the continuity bars from the upper panel during assembly. The pocket detail is shown in Figure 3.5. The panel configuration and reinforcement details for the post-tensioned specimens are shown in Figure 3.11. The bottom corners of the lower panel were notched to accommodate the post-tensioning chuck or nut. The post-tensioning anchorage detail is shown in Figure 3.12. The galvanized steel ducts were elliptical in cross-section with radii of approximately 30 mm and 60 mm. The elliptical cross-section was required to provide clearance between the main flexural reinforcement of the panels. The panel configuration of Specimen SK is shown in Figure 3.13. The stirrup depth was reduced for this specimen to accommodate the shear keys. The bar details for all of the panels are shown in Figure 3.14. All reinforcement used in the panels was Grade 400W.

3.3   MATERIAL SPECIFICATIONS

3.3.1   Panel Concrete

The concrete mix for the precast panels fabricated by Con-Force Structures Limited had the following proportions:

Coarse Aggregate (3/4" stone)	1157 kg/m³
Sand	801 kg/m³
Type 30 Portland Cement (High Early)	332 kg/m³
Pozzolith 322N	0.75 l/m³
MB-AE 10 Air Entrainment Solution	50 ml/m³
Water	119 l/m³

For each specimen, the strength of the concrete was monitored using five (5) standard 150 mm x 300 mm cylinders cast according to CSA specifications. Two of the cylinders were tested after 28 days, and the remaining cylinders were tested at the time of testing of the specimen.

3.3.2   Dry Pack

The dry pack used in this experiment was prepared and placed by Con-Force Structures Limited personnel, using the same procedures as in practice. The mix proportions of the dry pack are as follows:

	by volume
Sand	2 parts
Normal Portland Cement (Type 10)	1 part
Water (approximate)	0.5 parts

The proportion of water added is approximate and can be best described as the amount required to achieve the desired consistency. The dry pack has a zero slump and is readily compactable.

The strength of the dry pack was monitored using 50 mm cubes, made using brass molds, and 75 mm cubes, made using concrete molds. No difference was observed between the strength results from the two types of molds. For the specimens with post-tensioning, cubes were tested for 7 day strength (prior to post-tensioning), 28 day strength and strength at the time of testing. For Specimens RW and SK, cubes were tested for 28 day strength and strength at the time of testing. For Specimen DP, the dry pack strength was determined at the time of testing only.

3.3.3   Post-tensioning Grout

The grout used for the post-tensioning ducts had a liquid consistency to allow pumping. The grout was prepared and placed by personnel from Supercrete Inc. of Winnipeg, Manitoba, using the same procedures as in practice. The mix proportions are as follows

	per bag cement	by mass
Type 30 Portland Cement (High Early)	1 bag	1 part
Water	17 litres	0.424 parts

Non-shrink Ad-mixture	340 ml	0.0086 parts
(CPD Part C Grout Ad-mixture)		

The strength of the grout at the time of testing of the specimen was monitored using 50mm cubes made using brass molds.

3.3.4   Mild Steel Reinforcing Bars

All of the reinforcing bars used in this program, including the continuity bars, were Grade 400W. The nominal yield strength of the bars is 400 MPa. The measured properties of the bars were tested using two samples of 25M size bars. A measured yield strength of 500 MPa, a measured maximum strength of 640 MPa and a measured elongation at failure of 10% were determined from testing of these bars. The average measured strain-strain relationship for the bars is shown in Figure 3.15. The nominal and measured material properties are compared in Table 3.2.

3.3.5   Post-tensioning Strands

Seven wire, 12.7 mm diameter post-tensioning strands were used in this experimental program. The strands had a nominal ultimate strength of 1860 MPa. The measured properties of the strands were determined by testing of two samples. The average ultimate strength of the test samples was 1926 MPa, and the average yield strength, measured at a strain of 1%, was 1746 MPa or 91% of the ultimate strength. The average measured stress-strain relationship for the strands is shown in Figure 3.16.

3.3.6   Post-tensioning Bars

High strength Dywidag threaded bars with a diameter of 5/8" were used for post-tensioning in this experimental program. The bars had a nominal ultimate strength of 1080 MPa. The measured material properties were determined by testing of three samples. The average measured ultimate strength of the bars was 1137 MPa and the average yield strength, measured at a 0.2% offset, was 897 MPa or 79% of the ultimate strength. The average measured stress-strain relationship for the three bars is shown in Figure 3.17.

3.4   SPECIMEN ASSEMBLY

The precast concrete wall panels fabricated by Con-Force Structures Limited were delivered to Structures Lab at the University of Manitoba. Assembly of the specimens, including dry packing, and where applicable, welding and post-tensioning, was performed in the Structures Lab.

3.4.1   General Assembly

The specimens were assembled in an upright position. Initially the lower panel was placed vertically and the upper panel was lowered into position. For the specimens with post-tensioning, the post-tensioning bars or strands were installed and the galvanized steel ducts were coupled as the upper panel was lowered. The 20 mm gap between the two panels at the connection was achieved using wooden shims. After ensuring that the alignment of the panels and the 20 mm gap at the connection were uniform, the panels were connected together by bolting steel angles across the connection at four locations. Bolting of the angles was facilitated using threaded inserts in the panels. The angles were left on the specimens until immediately prior to testing to ensure the integrity of the connection. After the connection was

secured with the steel angles, the wooden shims were removed. In the case of Specimen RW, the continuity bars from the upper panel were welded into the steel angle embedded in the lower panel at this time.

3.4.2   Dry Packing

After erection of the panels, the gap between the panels was packed with dry pack by Con-Force Structures Limited personnel, as shown in Figure 3.18. Initially, one side of the connection was formed closed with boards and packing proceeded from the opposite side. After completing dry packing from one side, the forming boards were removed and packing was finished from the other side of the connection. The cube specimens for strength testing were also made at this time. After dry packing, the dry pack was sprinkled with water occasionally for a period of one hour, and then the connection and the cubes were wrapped in wet burlap and polyethylene sheets for a period of 24 hours.

3.4.3   Post-tensioning

Post-tensioning of Specimens PTS, PTB and PTB-S occurred seven (7) days after dry packing. Prior to post-tensioning, the 7 day strength of the dry pack was determined by testing three cubes. The acceptance criteria used for post-tensioning in practice (22) was a dry pack equivalent cylinder strength of at least 30 MPa. The equivalent cylinder strength is taken as 0.85 times the cube strength of the dry pack (22).

The post-tensioning procedure was identical for the strands and the bars, with the exception of the type of jack. Post-tensioning of the strands was performed using a hydraulic jack for strands, as shown in Figure 3.19(a). Post-tensioning of the bars was performed using a hydraulic hollow jack, as shown in Figure 3.19(b). The jacking force was monitored using a

calibrated load cell, located between the anchorage chuck or nut and the panel, as shown in Figure 3.20. The load cells were made and calibrated in the Structures Lab at the University of Manitoba. The details of the load cell are shown in Figure 3.21. The post-tensioning force for Specimens PTB and PTB-S was also monitored using electrical resistance strain gauges located on the bars at the connection level. Each strand or bar was jacked separately. To avoid tensile stresses at the connection due to the post-tensioning process, the strands or bars were jacked in stages. The first strand (bar) was jacked to one third of the desired jacking force and released. The second strand (bar) was then jacked to two thirds of the desired jacking force and released. The post-tensioning process was completed by jacking the first strand (bar) to the full post-tensioning force and finally by jacking the second strand (bar) to the full post-tensioning force.

Immediately following post-tensioning, the ducts were grouted by Supercrete Inc. personnel. The grout was pumped through tubes at the bottom of the ducts while air escaped through tubes at the top of the ducts, as shown in Figure 3.22. Pumping was continued until grout exited the tube at the top of the ducts, at which point the tubes were clamped closed.

3.5   INSTRUMENTATION

The connections were instrumented to measure the overall displacement and deformation of the connection and the strains within the continuity reinforcement where applicable.

3.5.1   Displacements

The horizontal and vertical displacements at the connection were measured using both electrical linear variable differential transducers (LVDT's) and mechanical dial gauges. The

relative horizontal slip between the panels was measured using two LVDT's located at opposite ends and sides of the connection, and by one dial gauge located at the middle of the connection. The variation of the thickness of the dry pack, or the thickness of the connection, was measured using four LVDT's, one located at each corner of the connection, and by one dial gauge located at the middle of the connection. The locations of the measurement stations are shown in Figures 3.23 and 3.24. The instrument stations were mounted on the panels using screws and insert plugs, fitted into 5 mm diameter holes drilled in the panels.

3.5.2 Continuity and Post-tensioning Bar Strains

The behaviour of the mild steel continuity bars and the post-tensioning bars was monitored using electrical resistance strain gauges, located at the connection level. The strain gauges had a 5 mm gauge length and a resistance of 120 ohms. Two gauges, one per bar, were used for Specimen RW. The location of the gauges is shown in Figure 3.25. The gauges were oriented axially on the bar and were mounted following welding of the continuity bars. Access to only one "side" of the bar limited the number of gauges to one per bar for Specimen RW. Four gauges, two per bar, were used for Specimens PTB and PTB-S. The location of the gauges is shown in Figure 3.26. The gauges were mounted on the post-tensioning bars prior to assembly of the specimens. This allowed placement of two gauges per bar.

3.5.3 Data Acquisition System

All of the LVDT and strain gauge readings were monitored continuously by a computer data acquisition system. In addition, the data acquisition system was used to monitor the applied shear load from the actuator load cell and the actuator stroke. The system consisted of a Hewlett Packard 80286 computer and a Datascan 40 channel data acquisition board. All data was simultaneously recorded on file and displayed on screen in graphical form using the

data acquisition software "LabTech Notebook". The graphical display of data allowed the cyclic shear resistance - slip behaviour of the connection (hysteresis loops) to be observed during the course of the experiment. All recorded data was transferred to floppy disks for later analysis.

3.6   LOADING FRAME

The specimens were tested using a structural steel loading frame constructed for this experiment in the Structures Lab at the University of Manitoba, as shown in Figures 3.27(a) and (b) and Figure 3.28. The lower panel of the specimen was fixed rigidly to the structural floor by post-tensioning to reaction abutments on the floor, as shown in Figure 3.27(a) and Figure 3.29. At the connection level, the lower panel was also fixed with cross beams attached to longitudinal beams cantilevered from the reaction wall. The cross beams, shown in Figures 3.27(a) and (b), and 3.30, resisted overturning of the lower panel. The longitudinal beams cantilevered from the reaction wall have been omitted from Figure 3.27(a) for clarity. The upper panel was braced against out-of-plane movements by four point lateral bracing on each side. Contact between the lateral braces and the upper panel was through teflon sheets to allow movement in the direction of the applied loading. The entire loading frame was braced laterally by diagonal members, shown in Figures 3.27(b) and 3.28. The diagonal braces have been omitted from Figure 3.27(a) for clarity. The simulated gravity load (vertical preload), normal to the connection, was applied using an independent prestressing system designed to allow displacements in the direction of the applied shear loading, as shown in Figures 3.27(a) and 3.28. The system utilized two hydraulic jacks and maintained a constant vertical load on the specimen through use of a regulator valve on the hydraulic pump. A series of plates and rollers were used to allow horizontal displacement of the panels while still maintaining the constant vertical load. A close-up of the system is shown in Figure 3.31. The shear loading on the specimen was provided by a 1000 kN MTS closed loop cyclic actuator. The actuator was

fixed to the reaction wall and the shear loading was applied on the upper concrete panel by means of a push-pull loading yoke. The loading yoke consisted of 4 Dywidag bars, two on each side of the panel. The entire loading frame was bolted to the structural floor and/or the reaction wall.

3.7   TESTING PROCEDURE

The entire testing procedure, including installation of the specimen in the loading frame, testing of the specimen and finally removal of the specimen from the loading frame, took a minimum of three days for two people to complete. The preparation sequence and testing sequence are summarized below.

3.7.1   Preparation Sequence

Preparation for testing began with mounting of the instrument stations. Holes were drilled into the panels and fitted with insert plugs at the desired instrument locations. The instrument stations were mounted on the panels using wood screws into the inserts. The instruments themselves were not installed until immediately prior to testing to prevent damage. The overhead crane was used to move the specimen into position in the loading frame. A portion of the loading frame, including half of the top beam, the end column and the diagonal braces, had to be disassembled and removed to allow placement of the specimen. Once the specimen was inside the loading frame, the frame was reassembled. Next, the specimen was aligned to be perpendicular to the reaction wall and on centre with the actuator. The specimen was then set on a layer of plaster of paris to provide uniform contact with the floor of the structures lab and to allow leveling, both in-plane and out-of-plane. Once the specimen was aligned and leveled satisfactorily, the lateral braces were put in place against the upper panel. Next, the vertical preload system (gravity load simulator) was positioned on top of the

specimen. A layer of plaster of paris was used between the preload system and the specimen to provide uniform contact. After the preload system was in place, the loading yoke was attached to the specimen and the actuator. At this point, a small vertical load (approximately 30 to 50 kN) was applied on the connection and the steel angles used to brace the connection were removed. The last stage of preparation was the final mounting and calibration of the instrumentation (LVDT's). Once the instrumentation was connected to the data acquisition system and tested, the preparation sequence was complete.

3.7.2   Testing Sequence

Immediately prior to testing, all of the instrumentation readings were zeroed and the initial mechanical dial gauge readings were taken. The vertical preload was then applied up to its full level and mechanical readings were taken again. During the test, all of the instrumentation was monitored continually and recorded at approximately 1 to 2 second intervals by the data acquisition system. Mechanical dial gauge readings were recorded at each load level and during one cycle at each applied slip magnitude.

For the experiments performed under fully reversed cyclic loading, the test began under load control. Each load increment was maintained for three complete cycles. The load level was incremented until the initiation of slip was observed at the connection. The initiation of slip was defined as the point at which 0.1 mm of slip was measured in both directions of loading. After the initiation of slip, loading was switched to displacement control with increments of relative horizontal slip between the panels. Each applied slip magnitude was maintained for three complete cycles. Failure of the connection was declared when a 20% reduction of the maximum measured shear resistance was observed. Following failure of the connection, the test was continued by applying single cycles at increasing slip magnitudes to determine the residual strength of the connection.

The experiment performed under monotonic loading followed a similar procedure. The test began under load control. The load was increased in increments of 100 kN until the initiation of slip. At each load level, mechanical readings were taken. After the initiation of slip, loading was switched to displacement control. Relative slip increments of 1.0 mm were applied on the connection until failure was observed.

Over the duration of both the cyclic and the monotonic loading tests, the presence and propagation of cracks and spalling was recorded and sketched on data sheets. Significant cracking and/or spalling was also photographed during the experiment. The entire testing sequence for a cyclic loading experiment took approximately 10 to 12 hours.

CHAPTER 4

EXPERIMENTAL RESULTS

4.0   INTRODUCTION

This chapter presents the experimental results for the six specimens tested in this program. The measured material properties are presented in this chapter in addition to the measured experimental results. The experimental results include the overall shear resistance - slip behaviour, the relationship between the variation of the dry pack thickness and the applied slip magnitude, the relationship between the applied shear load and the reduction of the dry pack thickness and the envelope of cyclic shear behaviour.

4.1   MATERIAL PROPERTIES

4.1.1   Panel Concrete

The compressive strength of the panel concrete for each specimen is presented in Table 4.1. Values are reported for the strength at 28 days and the strength at the time of testing.

4.1.2   Dry Pack

The compressive strength of the dry pack is reported in Table 4.2. The specimens were dry packed on three separate occasions, and therefore the specimens are grouped according to dry pack date in Table 4.2. The equivalent cylinder strength is taken as 0.85 times the cube strength of the dry pack (22). Dry pack strengths are reported at the time of testing

for all specimens. In addition, the 28 day strength is reported for all specimens with the exception of Specimen DP. In the case of the specimens with post-tensioning, the 7 day strength of the dry pack was also determined prior to post-tensioning of the specimens.

4.1.3   Post-tensioning Duct Grout

The compressive strength of the post-tensioning duct grout was determined using 50 mm cubes. The average cube strength for the three post-tensioned specimens was 51.0 MPa.

4.2   OVERALL TEST RESULTS

4.2.1   Shear Resistance - Slip Behaviour

The shear resistance - slip behaviour over the duration of the experiment is shown in Figures 4.1 to 4.6 for each of the specimens. The data shown in these figures is the relationship between the applied slip magnitude, measured by two "slip" LVDT's, and the measured shear resistance. A summary of the measured shear resistance at different points during the experiment is presented in Table 4.3.

4.2.2   Applied Slip Magnitude - Variation of Dry Pack Thickness

The variation of the dry pack thickness was measured by four "gap" LVDT's mounted vertically across the connection, as shown previously in Figure 3.23. The variation of the dry pack thickness after the initiation of slip is shown in Figures 4.7 to 4.12 for each of the specimens. Due to an error in the data acquisition software, data was not recorded for Specimen SK during the last two cycles at 2 mm and during the cycles at 3 mm and 4 mm

applied slip. Therefore, manually recorded dial gauge readings have been included in Figure 4.11 for these cycles.

4.2.3   Applied Shear Load - Reduction of Dry Pack Thickness

The relationship between the applied shear load and the reduction of dry pack thickness is shown in Figures 4.13 to 4.16 for Specimens RW, PTS, PTB and SK. These figures illustrate the reduction of the dry pack thickness over the duration of the entire experiment. The reduction of the dry pack thickness is measured by the four "gap" LVDT's. The apparent correlation between crushing of the dry pack and failure of the connection is evident in these figures. In the case of Specimen SK, as described in Section 4.2.2, manual dial gauge readings have been substituted for the missing data for the cycles at 2 mm, 3 mm and 4 mm applied slip in Figure 4.16.

4.2.4   Envelope of Cyclic Shear Behaviour

The overall cyclic shear behaviour of the connection can be defined by considering the envelope of the measured shear resistance - slip behaviour. The cyclic shear envelopes for each of the specimens tested under cyclic loading are shown in Figures 4.17 to 4.21. The numerical values for the cyclic shear envelopes are presented in Tables 4.4 to 4.8.

CHAPTER 5

DISCUSSION OF EXPERIMENTAL RESULTS

5.0   INTRODUCTION

In this chapter, the behaviour of the connections used for each of the six specimens tested in this program is discussed. The observed experimental results, presented previously in Chapter 4, are described in detail for each specimen and are used to define various limit states including the failure modes of the connections subjected to cyclic shear loads. In addition, the experimental results are used to identify the effect of cyclic loading and the contribution of the continuity elements such as the mild steel reinforcement, post-tensioning and shear keys.

5.1   SPECIMEN BEHAVIOUR

In general, the overall behaviour of the different connection configurations used in this experiment was similar. Initially, the connection was elastic and very stiff. Upon initiation of relative slip between the panels at the connection, the behaviour of the connection became inelastic with stable hysteresis loops. This behaviour continued until sudden crushing of the dry pack occurred, producing a substantial reduction of the shear resistance and failure of the connection. A detailed description of the behaviour of each connection configuration is given in the following sections.

5.1.1 Specimen DP

Specimen DP consisted of two panels, connected horizontally with a plain surface dry packed connection. The cross-sectional area of the connection was 150,000 mm². All of the remaining connection configurations had a connection area of 180,000 mm². Specimen DP was subjected to a load normal to the connection of 600 kN, producing an average vertical stress of 4 MPa on the connection. Specimen DP was the only specimen tested under a vertical preload of 4 MPa. All of the other specimens were tested at a preload of 2 MPa. The shear resistance - slip behaviour of Specimen DP over the duration of the experiment is shown in Figure 4.1.

Prior to the initiation of slip, the behaviour of the connection was very stiff and perfectly elastic as shown in Figure 5.1. This behaviour was maintained for 30 cycles and a maximum applied shear load level of 500 kN. During the 31st cycle, while attempting to reach an applied load level of 550 kN, the initiation of slip occurred suddenly due to breaking of the bond between the dry pack and the upper concrete panel at a load of +533 kN. The breaking of the bond was followed by a instantaneous slip of approximately 1.5 mm.

After the initiation of slip, the behaviour of the connection was inelastic, as shown in Figure 5.2, and loading was switched to reversed cyclic displacement control conditions. Horizontal sliding occurred along the interface between the top surface of the dry pack and the upper concrete panel. The behaviour of the connection remained fairly consistent for the first 24 cycles (cycles 32 to 55) under slip control conditions and maximum applied slip magnitude of 5.0 mm. In general, increase of the applied displacement up to 5 mm was accompanied by a slight increase of the shear resistance from 450 kN to 480 kN. This behaviour resulted in an almost perfect rectangular shape for the shear resistance - slip hysteresis loops, as shown in

Figure 5.2. During this portion of the test, the dry pack remained intact with only minor vertical cracks occurring at the ends of the connection as shown in Figure 5.3.

As the applied slip magnitude was increased to 6.0 mm, extensive crushing of the dry pack occurred, accompanied by significant reduction of the connection resistance as shown in Figure 5.4. The maximum shear resistance during these cycles was approximately 420 kN, or 80% of the maximum shear resistance measured during the test. Failure of the connection, defined as a 20% reduction of the shear resistance of the connection, was declared at this point of the experiment. Crushing of the dry pack was monitored by measuring the thickness of the dry pack. Prior to the reduction of the shear resistance during the cycles at 6 mm, little or no crushing of the had occurred and the measured dry pack thickness was 19.2 mm (initial thickness = 20.0 mm). At the completion of the cycles at 6 mm, the measured dry pack thickness was 13.4 mm, a reduction of 33%. The variation of the dry pack thickness over the duration of the experiment is shown in Figure 4.7.

To collect complete information after failure, the test was continued by applying one cycle each at applied slip magnitudes of 7 mm, 8 mm and 9 mm. During the cycle at 7 mm, the shear resistance of the connection was maintained at the level measured during the last cycle at 6 mm, as shown in Figure 5.4. Extensive spalling of the dry pack continued and a reduction of 9 mm of the initial dry pack thickness was measured, as shown in Figure 4.7. At an applied slip magnitude of 8 mm, the dry pack continued to crush and spall away, and the shear resistance - slip behaviour remained consistent. During the cycle at an applied slip magnitude of 9 mm, the dry pack was literally ground into powder. The measured shear resistance was an average value of approximately 420 kN, as shown in Figure 5.4. The test was terminated after the completion of this cycle. The measured thickness of the dry pack at the end of the test was approximately 5 mm, only 25% of the initial thickness. The condition of the dry pack is shown in Figure 5.5.

5.1.2 Specimen RW

Specimen RW consists of two precast concrete wall panels, connected horizontally by a plain surface, dry packed connection. The connection was also reinforced with two 25M, 400W mild steel continuity bars, spaced at 900 mm on centre. The specimen was subjected to a simulated gravity load, normal to the connection, of 360 kN, producing an equivalent vertical stress of 2 MPa on the connection. The shear resistance - slip behaviour of Specimen RW over the duration of the experiment is shown in Figure 4.2.

The behaviour of the connection prior to the initiation of slip was very stiff and perfectly elastic. This behaviour was maintained for 6 complete cycles and a maximum load level of 200 kN. During these cycles, no measurable slip was observed, as shown in Figure 5.6.

On the 7th cycle of loading, while attempting to reach a load level of 300 kN, the onset of non-linear behaviour was observed at approximately +270 kN. The initiation of slip, defined as a measured slip of 0.1 mm, occurred gradually as the applied shear load was increased to approximately 290 kN. Unlike the behaviour of Specimen DP, a sudden initiation of slip due to breaking of the bond between the concrete and the dry pack was not observed for this specimen. The sliding plane was observed at the interface between the dry pack and the upper concrete panel. The applied load was increased to 300 kN and a slip of 0.31 mm was observed. Three cycles were completed at 300 kN and the measured slip reached a maximum of 0.4 mm at +300 kN and -0.18 mm at -300 kN. The behaviour during these cycles was inelastic.

Following the cycles at 300 kN, loading was switched to displacement control (relative horizontal slip between the panels), with increments of 1.0 mm. Relative slip between the

panels continued at the interface between the top surface of the dry pack and the upper concrete panel. The behaviour of the connection was very consistent for the first 24 cycles under slip control (cycles 10 to 33) and a maximum slip magnitude of 8.0 mm. During this portion of the test, the inelastic behaviour of the connection exhibited stable hysteresis loops with a parallelogram-like shape, as shown in Figure 5.7. The initiation of slip, upon reversal of loading direction during a given cycle, occurred at a very consistent measured load level of +185 kN in the "push" direction and -210 kN in the "pull" direction. On a typical cycle of loading, the shear resistance increased steadily from the initiation of slip in one loading direction up to a maximum at the applied slip magnitude. This typical behaviour is illustrated in Figure 5.8.

The dry pack remained largely intact during this portion of the test. Upon first initiation of slip and during the three cycles at 1.0 mm, there were no visible cracks in the dry pack. Minor surface spalling and formation of vertical cracks were observed at both ends of the connection during the cycles at 3.0 mm, 4.0 mm and 5.0 mm. As the slip magnitudes increased, crack formation and surface spalling progressed inward from the ends of the connection. At the completion of 3 cycles at 7.0 mm, considerable surface spalling had occurred up to the location of the continuity reinforcement, a distance of 150 mm from each end of the connection. Minor surface spalling was evident over the remainder of the length of the connection. During the 3 cycles at 8.0 mm, spalling of the dry pack progressed and an overall slight reduction of the shear resistance was measured, as shown in Figure 5.7.

As the applied slip magnitude was increased to 9.0 mm, spalling of the dry pack increased dramatically. On the second cycle at 9.0 mm, extensive crushing of the dry pack began and a 50 kN reduction of the shear resistance was measured. In this investigation, failure was defined as the point at which a 20% reduction of the shear resistance of the connection occurred. On the third cycle, a loss of shear resistance of approximately 40% was

observed, and accordingly, "failure" of the connection was declared. The shear resistance-slip behaviour for these cycles is shown in Figure 5.9. The reduction of shear resistance during these cycles was 165 kN or 41% in the push direction and 190 kN or 49% in the pull direction. Crushing of the dry pack was monitored by measuring the thickness of the dry pack. Prior to the first cycle at 9.0 mm, the average measured dry pack thickness was 19.4 mm (initial thickness = 20 mm). Upon completion of the third cycle at 9.0 mm, crushing and spalling reduced the average dry pack thickness by 3.4 mm, to 16.0 mm. The condition of the dry pack before and after significant crushing is shown in Figures 5.10 and 5.11, respectively.

To collect complete information after failure, the test was continued by applying one cycle each at 10.0 mm and 12.0 mm relative slip. During the cycle at 10.0 mm, there was an additional reduction of the shear resistance. The maximum shear resistance at a slip of 10 mm was 124 kN. During this cycle there was continued crushing and spalling of the dry pack and a further reduction of the thickness of the dry pack of 2.8 mm was measured. In addition, out-of-plane buckling of the east continuity bar, shown in Figure 5.12, occurred at the connection level during the reverse loading portion of the cycle. At a relative slip magnitude of 12.0 mm, the shear resistance-slip behaviour of the connection decreased to a stabilized level with a maximum shear resistance of 142 kN, as shown in Figure 5.13. At the completion of this cycle, the test was terminated. The average measured dry pack thickness was 10.8 mm, or 54% of the initial thickness.

The average variation of the dry pack thickness (connection thickness) during the test is shown in Figure 4.8. From this figure, it is clear that prior to the cycles at a slip magnitude of 9.0 mm, the reduction in dry pack was very small (less than 3%). The reduction of the dry pack thickness increased significantly during the cycles at +/- 9.0 mm, coupled with failure of the connection. The correlation between the failure of the connection and crushing of the grout (reduction in dry pack thickness) is illustrated in Figure 4.13, where the relationship between

the measured shear resistance and the reduction of the dry pack thickness is shown. The failure of the connection appears to be correlated to the crushing of the dry pack.

The behaviour of the mild steel continuity reinforcement was measured using strain gauges. The measured strain gauge data is available for the duration of cycles at relative slip magnitudes from 1.0 mm to 6.0 mm, inclusive. The initial strain gauge readings, prior to the cycles at 1.0 mm slip, were lost due to a corrupt data file. Beyond the cycles at 6.0 mm, the strain readings became unreliable.

The strain behaviour of the bars during the experiment is shown in Figure 5.14. Before application of either the preload or the shear loading, the strain readings were initialized to a zero value. Following application of the vertical preload (360 kN), compressive strains were measured in the bars. As mentioned above, unfortunately this initial data was lost. However, this data is available for identical connection configurations tested under a separate research program at the University of Manitoba (flexural specimens RW and RS). The initial compressive strain in the bars was measured to be in the order of 0.5 milli-strain (0.0005) for these specimens. This suggests that a value of this order could be assumed with confidence for this test since the average compressive strain reading at the start of the cycles at 1.0 mm slip was measured to be 0.0005. After the initiation of slip and during the cycles at 1.0 mm and 2.0 mm slip, a small tensile increase in strain was observed. During the following cycles at slip magnitudes larger than 2.0 mm, a larger tensile increase of strain was observed. At the start of a given cycle (the zero slip position) a compression strain was measured in the bars. As the applied slip was increased to the desired magnitude, a tensile increase of strain was observed. When returned to the zero slip position upon completion of the given cycle, the strain magnitude returned to a value very close to that at the beginning of the cycle. As mentioned above, the strain gauge readings became unreliable after the cycles at 6.0 mm. At this point,

neither bar had reached the yield strain of 0.0025 (Figure 3.15). Several specific areas of the strain behaviour are discussed below.

The general strain behaviour of the individual bars can be illustrated clearly by averaging the strain readings for the three cycles at each slip magnitude. The average maximum strain in each direction of loading and the average strain at the zero slip position are plotted together for each slip magnitude in Figures 5.15(a) and 5.15(b), for the west and east bars respectively. By isolating and averaging the strain behaviour of the two bars, two aspects of note become apparent. First, the compressive strain at the zero slip position remains fairly constant for the west bar, while the east bar experiences an increased compressive strain over the course of the experiment. This increase is particularly significant during the cycles at 1 mm, 2 mm, 3 mm and 4 mm. The variation of the compressive bar strain at the zero slip position for both bars is shown in Figure 5.16. The second item of note is that the change of strain during a given cycle is not equal in the two directions of loading. The west bar appears to experience a larger tensile increase of strain during the positive or push cycles than in the opposite direction of loading. Conversely, the east bar experiences a larger tensile increase of strain during the negative or pull cycles. The tensile increase of strain can be determined by subtracting the compressive strain at the start of the cycle from the maximum strain measured at the applied slip magnitude. In Figure 5.17, the change of bar strain at each applied slip magnitude is shown for both bars, in both directions of loading. The tensile increase of strain is clearly not the same in opposite directions of loading for either bar. Also, the tensile increase of strain is quite different for the two bars at a given slip magnitude.

Although the individual behaviour of the two bars appears to be quite different, the overall strain behaviour appears to be equal in magnitude and distribution in both directions of loading. This is illustrated by considering the average envelope of maximum bar strains as shown in Figure 5.18. The envelopes of maximum bar strains for both the west and east bars

are also plotted individually in the figure. The fact that the average strain behaviour of the two bars is consistent in both directions of loading suggests that the shear resistance mechanism provided by the continuity reinforcement is consistent throughout the test, despite the differences in individual bar behaviour.

5.1.3   Specimen PTS

Specimen PTS consists of two precast concrete wall panels, connected horizontally by a plain surface, dry packed connection. The connection was post-tensioned using two 12.7 mm diameter 7-wire prestressing strands, spaced at 900 mm on centre. The strands were post-tensioned to produce an equivalent stress on the connection of 1.2 MPa. The specimen was subjected to a simulated gravity load, applied normal to the connection, of 360 kN, producing an equivalent vertical stress of 2 MPa on the connection. The shear resistance - slip behaviour of Specimen PTS over the duration of the experiment is shown in Figure 4.3.

The behaviour of the connection prior to the initiation of slip was very stiff and perfectly elastic. This behaviour was maintained for 12 complete cycles and a maximum applied shear load level of 400 kN. During these cycles, no measurable slip was observed. During the following three cycles, at an applied shear load level of 500 kN, a very small slip of approximately 0.1 mm was measured. The behaviour of the connection remained stable for the duration of the cycles at 500 kN and the measured slip did not increase. For these reasons, this point was not defined as the initiation of slip, although a slip of 0.1 mm was measured. The behaviour of the connection prior to the initiation of slip is shown in Figure 5.19.

On the 16th cycle of loading, while attempting to reach an applied shear load level of 550 kN, the initiation of slip clearly occurred at a measured shear load of 530 kN. At this point, sustained slip was observed and the measured shear resistance of the connection did not

increase. Similar to Specimen RW, sudden breaking of the bond between the dry pack and the panels did not occur for Specimen PTS. Instead, a gradual onset of slip at the interface between the lower concrete panel and the bottom surface of the dry pack was observed. At this point, the behaviour of the connection became inelastic and the loading history was switched to displacement control (relative horizontal slip between the panels) with increments of 1.0 mm.

The inelastic behaviour of the connection after the initiation of slip was very consistent for the following 15 cycles of loading, up to and including an applied slip magnitude of 5 mm. This represents cycle 16 to cycle 30. The shear resistance - slip behaviour of the connection during these cycles is shown in Figure 5.20. The maximum measured shear resistance for these cycles remained very consistent at approximately 525 kN. Typically, the maximum shear resistance at a given applied slip magnitude was observed during the first cycle. During the second and third cycle at the same applied slip magnitude, a slight reduction of approximately 15 kN was measured. Overall, the inelastic behaviour of the connection remained consistent, producing stable hysteresis loops with a slightly skewed shape, as shown in Figure 5.20. On a typical cycle of loading, the shear resistance increased from the start of sliding (slip) in a given loading direction, to a maximum at the applied slip magnitude. The magnitude of the increase remained fairly constant at approximately 75 kN in both directions of loading for the duration of these cycles.

For the duration of cycles 15 to 30, the dry pack remained largely intact. During the third cycle at an applied slip magnitude of 2 mm, some vertical crack formation and surface spalling was observed in the dry pack at the ends of the connection. At the completion of the cycles at 3 mm, surface spalling of the dry pack had extended approximately 200 mm inward from both ends of the connection. Surface spalling continued to progress over the duration of loading and reached approximately 400 mm from the ends of the connection at the completion of the cycles at 5 mm slip. Initially, slip was observed at the interface between the lower

concrete panel and the bottom of the dry pack. During the cycles at 5 mm, slip was observed at both interfaces between the concrete panels and the dry pack.

On the 31st cycle of loading, at an applied slip magnitude of 6 mm, a reduction of approximately 35 kN was measured, as shown in Figure 5.21. In addition, rounding of the hysteresis loops was observed. On the second cycle at 6 mm, considerable spalling of the dry pack occurred along the length of the connection and a further reduction of the shear resistance was measured. On the third cycle crushing and spalling of the dry pack increased significantly and the shear resistance of the connection was reduced to 390 kN in the push direction of loading and 320 kN in the pull direction. This represented a 26% and 40% reduction of the maximum shear resistance and accordingly, failure of the connection was declared. The behaviour of the connection during these three cycles is shown in Figure 5.21. Prior to the cycles at 6 mm, crushing of the dry pack was not observed and the average measured dry pack thickness was 19.5 mm (initial thickness = 20.0 mm). At the completion of the three cycles at 6 mm, the average measured dry pack thickness was 17.3 mm, a reduction of 2.7 mm or 14% due to crushing and spalling. The variation of the thickness of the dry pack during the test is shown in Figure 4.9.

To determine the behaviour of the connection after failure, the test was continued by applying one cycle each at applied slip magnitudes of 7 mm, 8 mm, 9 mm and 10 mm. The shear resistance - slip behaviour of the connection during these cycles is shown in Figure 5.22. During these cycles, crushing and spalling of the connection continued and the shear resistance - slip behaviour of the connection appeared to stabilize. The maximum shear resistance measured during these cycles ranged from 200 kN to 240 kN. This represents an average loss of shear resistance of 60%. At the start of the cycle to 7 mm, the measured dry pack thickness was 17.3 mm. At the completion of the cycle at 10 mm, the dry pack thickness was measured

to be 9.0 mm, or 45% of the initial thickness. After the completion of a total of 37 cycles of loading and a maximum applied slip, magnitude of 10 mm, the test was terminated.

Similar to the behaviour observed for Specimen DP and RW, failure of the connection appears to correspond with sudden and significant crushing of the dry pack, illustrated in Figure 4.14. Prior to failure of the connection, the reduction of dry pack thickness was approximately 0.5 mm. Significant crushing of the dry pack, indicated by a large and continued reduction of the thickness of the dry pack, corresponds to a substantial loss of shear resistance of the connection. The condition of the dry pack before and after significant crushing is shown in Figures 5.23 and 5.24, respectively.

5.1.4   Specimen PTB

Specimen PTB consists of two precast concrete wall panels, connected horizontally by a plain surface, dry packed connection. The connection was post-tensioned using two 5/8" diameter Dywidag prestressing bars, spaced at 900 mm on centre. The bars were post-tensioned to produce an equivalent stress on the connection of 1.2 MPa. The specimen was subjected to a simulated gravity load, normal to the connection, of 360 kN, producing an equivalent stress of 2 MPa on the connection. The shear resistance - slip behaviour of Specimen PTB over the duration of the experiment is shown in Figure 4.4.

The behaviour of the connection prior to the initiation of slip was very stiff and perfectly elastic. This behaviour was maintained for 15 complete cycles and a maximum applied shear load level of 500 kN. During these cycles, no measurable slip was observed, as shown in Figure 5.25.

On the 16th cycle of loading, while attempting to reach an applied shear load level of 550 kN, the initiation of slip occurred at a measured shear load of 530 kN. As for Specimens RW and PTS, sudden breaking of the bond between the dry pack and the panels did not occur for Specimen PTB. Instead, a gradual onset of slip at the interface between the upper concrete panel and the top surface of the dry pack was observed. At this point, the behaviour of the connection became inelastic and the loading history was switched to displacement control (relative horizontal slip between the panels) with increments of 1.0 mm.

The inelastic behaviour of the connection after the initiation of slip was fairly consistent up to and including an applied slip magnitude of 9 mm. This represents 27 cycles of loading, from cycle 16 to cycle 42. The shear resistance - slip behaviour of the connection during these cycles is shown in Figure 5.26. During the cycles at 1 mm and 2 mm applied slip, the shear resistance of the connection increased slightly to reach a maximum of 545 kN at 2 mm slip. As the applied slip magnitude was increased beyond 2 mm, a progressive reduction of the measured shear resistance was observed. The measured reduction consistently ranged from 15 kN to 20 kN for each increased applied slip magnitude. However, the behaviour at a given slip magnitude remained consistent, producing stable hysteresis loops, as shown in Figure 5.26. At an applied slip magnitude of 9 mm, the maximum measured shear resistance was 440 kN, a reduction of approximately 18% from the maximum shear resistance measured at 2 mm. On a typical cycle of loading, the shear resistance increased from the start of sliding (slip) in a given loading direction, to a maximum at the applied slip magnitude, producing a parallelogram-like hysteresis loop.. The magnitude of the increase remained fairly constant at approximately 120 kN in both directions of loading for the duration of these cycles.

The dry pack remained largely intact during the cycles up to and including an applied slip of 9 mm. Some minor vertical crack formation was observed in the dry pack at the ends of the connection during the cycles at 2 mm slip. As the test progressed, vertical crack formation

and surface spalling were observed initially at the ends of the connection, and eventually begun to advance inwards. At an applied slip magnitude of 5 mm, some surface spalling had occurred along most of the length of the connection and the dry pack at the ends of the connection was significantly cracked for a length of approximately 200 mm. The deterioration of the dry pack lessened during the cycles at 6 mm, 7 mm and 8 mm, but began to increase again during the cycles at 9 mm applied slip. During this portion of the test, cracking or spalling was not observed in the precast concrete panels.

As the applied slip magnitude was increased to 10 mm, very significant crushing and spalling of the dry pack were observed. During the first cycle at 10 mm, the maximum shear resistance was 370 kN. This represents a reduction of 24% from the maximum measured shear resistance of the connection. Accordingly, failure of the connection was declared at this time. In addition, rounding of the hysteresis loops became pronounced, as shown in Figure 5.27. During the second cycle at 10 mm, crushing of the dry pack continued and the shear resistance was reduced to 300 kN in the "push direction, and 240 kN in the "pull" direction of loading. This is a decrease of 44% and 56% in the push and pull loading directions respectively. On the third cycle at 10 mm, the shear resistance of the connection was further decreased to 130 kN in the push direction and 100 kN in the pull direction. These values represent 24% and 18% of the maximum shear resistance measured for the connection. Prior to the cycles at 10 mm, crushing of the dry pack was not observed and the average measured dry pack thickness was 19.2 mm (initial thickness = 20.0 mm). At the completion of the three cycles at 10 mm, the average measured dry pack thickness was 12.9 mm, a reduction of 6.3 mm or 33% due to crushing and spalling. The variation of the thickness of the dry pack during the test is shown in Figure 4.10.

After failure of the connection, the test was continued by applying one cycle each at 12 mm, 14 mm and 16 mm to determine the residual capacity of the connection. The shear

resistance - slip behaviour of the connection during these cycles is shown in Figure 5.28. The connection behaviour during the last cycle at 10 mm is also shown in this figure. During the cycle at 12 mm, crushing and spalling of the dry pack continued, but the shear resistance of the connection remained consistent with the last cycle at 10 mm, as shown in Figure 5.28. The measured thickness of the dry pack was 10.5 mm at the completion of this cycle. During the cycles at an applied slip magnitude of 14 mm and 16 mm, the shear resistance of the connection began to increase as the applied slip increased beyond approximately 10 mm. Near the zero slip position of the cycle, the shear resistance was consistent with the magnitude measured during the last cycle at 10 mm and the cycle at 12 mm. This produced a "dog-bone" shape for the shear resistance - slip hysteresis loops during these cycles, as shown in Figure 5.28. The maximum shear resistance measured at an applied slip magnitude of 14 mm was 220 kN, in the pull direction of loading. At an applied slip magnitude of 16 mm, the maximum shear resistance was 275 kN, in the push direction of loading. At the completion of the cycle at 16 mm, the test was terminated. The average measured dry pack thickness at the completion of testing was 8.2 mm, or 41% of the initial thickness. The condition of the dry pack before and after significant crushing is shown in Figures 5.29 and 5.30, respectively.

Similar to the behaviour observed for cyclic shear Specimens DP, RW and PTS, failure of the connection appears to correspond with sudden and significant crushing of the dry pack, illustrated in Figure 4.15. Prior to failure of the connection, the reduction of dry pack thickness was less than 1 mm. Significant crushing of the dry pack, indicated by a large and continued reduction of the thickness of the dry pack, corresponds to a substantial loss of shear resistance of the connection.

The behaviour of the post-tensioned Dywidag bars was measured using electrical resistance strain gauges. The measured strain gauge data is available up to an applied slip

magnitude of 4 mm. However, two of the gauges were lost during the cycles at a slip magnitude of 2 mm, and one gauge was lost during the cycles 3 mm.

Immediately after post-tensioning, the average initial measured bar strain was 0.00323. The jacking force per bar was 114.2 kN. At the time of testing, the average measured strain was 0.00311. This represents a prestressing loss of approximately 3.5%. Upon application of the preload, a small prestressing loss of approximately 0.000060 was measured, resulting in an effective average strain of 0.00305. The total average prestressing loss was 5.5%. The measured strains for each gauge are shown in Table 5.1. The elastic modulus of the prestressing bars is 200,000 MPa, measured from tensile tests of three Dywidag bars (Figure 3.17). Using the measured elastic modulus and bar strains, the effective prestressing force per bar is calculated to be 107.9 kN. This will produce a vertical stress of 1.2 MPa on the connection, as designed.

The measured strain readings for each bar are shown in separate figures for clarity, due to the large amount of data. The variation of bar strain, prior to the initiation of slip, is shown in Figures 5.31(a) and 5.31(b), for the west bar and east bar respectively. In these figures, the relationship between the applied shear load and the measured bar strain prior to the initiation of slip is illustrated. Data is shown for the load control cycles up to and including the cycles at an applied shear load of 500 kN. Prior to the initiation of slip, little or no variation of strain occurs in either bar. The variation of strain after the initiation of slip is shown in Figures 5.32(a) and 5.32(b), for the west bar and east bar respectively. In these figures, the relationship between the applied slip magnitude and the measured bar strains after the initiation of slip is illustrated. Data is shown for the slip control cycles from the first initiation of slip up to the point at which the strain readings became unreliable. Following the initiation of slip, some variation of strain was measured in the bars. The outside gauge on the west bar appears to have measured a significant variation of strain during the cycles at 2 mm. Because the strain readings from the

gauges on the east bar and the inside gauge on the west bar did not measure a large variation of strain, it is possible that the readings from the outside gauge on the west bar are unreliable.

From the strain data shown in Figures 5.31 and 5.32, three items should be noted. First, it appears that prior to the initiation of slip, the bar strains are unaffected by the applied shear loading. Second, after the initiation of slip, a small strain gradient is developed between the gauges located on opposite sides of the bars. The magnitude of the variation of the measured strains, and thus the strain gradient, does not appear to be significant for the range of reliable strain readings. Therefore, the amount of flexural deformation within the bars will be negligible. The third item of note is the variation of strain at the zero slip position of the cycle. It is assumed that when the connection is at the zero slip position, the force within the prestressing bars represents the effective prestressing force on the connection. Figures 5.32(a) and 5.32(b) indicate that the strain at the zero slip position is gradually reduced during the test after the initiation of slip. The average strain at the zero slip position in each bar is shown per cycle in Figure 5.33. Although the data is somewhat limited, it does indicate a reduction of the effective prestressing strain over the duration of the experiment.

5.1.5   Specimen SK

Specimen SK consists of two precast concrete wall panels, connected horizontally by a dry packed connection with multiple shear keys. The specimen was subjected to a simulated gravity load, normal to the connection, of 360 kN, producing an equivalent stress of 2 MPa on the connection. The overall shear resistance - slip behaviour of the specimen is shown in Figure 4.5.

The behaviour of the connection prior to the initiation of slip was very stiff and perfectly elastic. This behaviour was maintained for 21 complete cycles and a maximum

applied shear load level of 400 kN. As the applied shear load was increased in the following cycles, a small amount of slip was measured, but the shear resistance continued to increase steadily. As mentioned previously, the initiation of slip is assumed to have occurred if a slip magnitude of 0.1 mm is measured in both directions of loading. On the 34 cycle of loading, a slip of 0.1 mm and 0.3 mm was measured in the push and pull directions of loading respectively, at an applied shear load level of 650 kN. This point was defined as the initiation of slip. The shear resistance - slip behaviour of the connection prior to the initiation of slip is shown in Figure 5.34. The behaviour after the initiation of slip is shown in Figure 5.35(a). The same data is shown with an enlarged scale in Figure 5.35(b). From this figure it is clear that the behaviour of the connection is inelastic. Although the initiation of slip had occurred and the behaviour of the connection was inelastic, the shear resistance of the connection continued to increase while the slip magnitude was limited to less than 1 mm. This behaviour continued up to and including an applied shear load level of 800 kN. During the three cycles at 800 kN, a maximum slip of 0.45 mm and 0.83 mm was measured in the push and pull directions of loading. On the 45th cycle of loading, the connection resisted an applied shear load of 850 kN in the push direction of loading. While attempting to reach the same load level in the pull direction, sudden and simultaneous diagonal cracking of the dry pack within each of the shear keys occurred, resulting in an instantaneous slip of approximately 10 mm and a substantial reduction of the shear resistance. The crack pattern of the dry pack within the shear keys is shown in Figure 5.36. The shear resistance - slip behaviour of the connection during cycle 45 is shown in Figure 5.37. At this point, the connection was returned to the zero slip position and the loading history was switched to displacement control (relative horizontal slip between the panels) with increments of 1.0 mm. As the connection was returned to the zero slip position after sudden cracking of the connection, the shear resistance of the connection stabilized at approximately 420 kN. This represents a reduction of 50% from the maximum measured shear resistance. Therefore, failure of the connection was declared.

For the duration of loading up to cycle 45, the dry pack remained largely intact. No cracking or spalling of the dry pack was observed until the cycles at an applied shear load level of 750 kN (cycles 40 to 42). During these cycles, some minor vertical cracks became evident in the dry pack at the ends of the connection and on the north side of one shear key. This was the only damage visible to the naked eye prior to sudden diagonal cracking through the dry pack in each shear key as described above.

The shear resistance - slip behaviour of the connection after cracking is shown in Figure 5.38. The data shown is from the first cycle under slip control up to the end of the test. The data for the cycles at 3 mm and 4 mm was not recorded due to an error in the data acquisition system. Measurements recorded manually for are plotted in Figure 5.38 for these cycles. During the first at an applied slip magnitude of 1 mm, the maximum shear resistance was 430 kN in the push direction and 285 kN in the pull direction. The shear resistance in the push direction of loading was significantly higher than in the pull direction because of the orientation of the diagonal cracks in the dry pack within the shear keys. Since the dry pack was cracked while in the pull direction of loading, upon reversal of loading the shear resistance will be higher until a new slip plane is formed in the push direction. As the applied slip magnitude was increased to 2 mm, the maximum shear resistance was 400 kN and 335 kN in the push and pull directions respectively. Considerable spalling of the dry pack along the length of the connection and within the shear keys was observed. At 3 mm, the shear resistance in the push direction continued to decrease and a maximum value of 350 kN was measured. In the pull direction, the shear resistance stabilized at 335 kN. Spalling of the dry pack continued. At the completion of the three cycles at 3 mm, a uniform slip interface had formed along the length of the connection. The sliding plane was observed at the interface between the upper concrete panel and the dry pack and continued through each of the shear keys at this level, as shown in Figure 5.39. The experiment was continued by applying three cycles each at applied slip magnitudes of 4 mm, 5 mm, 6 mm and 7 mm. During these cycles, the shear resistance of the

connection remained very consistent at approximately 300 kN in both directions of loading. This produced almost perfectly rectangular hysteresis loops, as shown in Figure 5.38. To complete the experiment, one cycle each was applied at slip magnitudes of 8 mm, 9 mm and 10 mm. The shear resistance of the connection continued to remain at approximately 300 kN in both directions of loading and the dry pack continued to spall and crush. The experiment was concluded at this point. The condition of the dry pack at the end of the experiment is shown in Figure 5.40. The sliding plane is clearly evident in this photo.

Similar to the other specimens, the thickness of the dry pack, also the thickness of the connection, was measured during the experiment. The variation of the thickness of the dry pack over the duration of the experiment is shown in Figure 4.11. Prior to the failure of the connection due to cracking of the dry pack within the shear keys, only a minor reduction of the dry pack thickness was measured. In addition, during the cycles at an applied shear load level of 750 kN and 800 kN, opening of the connection was measured as the upper concrete panel slid upwards on the dry pack within the shear keys when the full load level was applied. When unloaded, the connection closed again, returning to the same thickness measured prior to the cycle. This is shown in Figure 5.41, where the relationship between the applied shear load and the variation of connection thickness is shown with an enlarged scale. After cracking of the dry pack within the shear keys, the thickness of the dry pack continued to reduce gradually and consistently, as shown in Figures 4.11 and 4.16. At the start of the first cycle at 1 mm, the thickness of the dry pack was 19.9 mm. At the completion of the cycle at 10 mm, the dry pack had been gradually reduced to a thickness of 13.1 mm, or 65% of the initial thickness. This behaviour was unique for the shear key connection, unlike the plain surface connections of the other specimen configurations where a sudden reduction of the dry pack thickness corresponded to failure of the connection.

5.1.6   Specimen PTB-S (Static Loading)

This section provides a brief summary of the observed experimental results for the static (monotonic) shear test of Specimen PTB-S. Specimen PTB-S has an identical configuration to Specimen PTB. Specimen PTB-S consists of two precast concrete wall panels, connected horizontally by a plain surface, dry packed connection. The connection was post-tensioned using two 5/8" diameter Dywidag prestressing bars, spaced at 900 mm on centre. The bars were post-tensioned to produce an equivalent stress on the connection of 1.2 MPa. The specimen was subjected to a simulated gravity load, normal to the connection, of 360 kN, producing an equivalent stress of 2 MPa on the connection. The shear resistance - slip behaviour of the connection over the duration of the experiment is shown in Figure 4.6

The behaviour of the connection prior to the initiation of slip was very stiff and no measurable slip was observed. The initiation of slip occurred gradually at an applied shear load of 555 kN. Sudden breaking of the bond between the panels and the dry pack was not observed for this specimen. Relative horizontal slip was observed at the interface between the dry pack and the lower concrete panel. At this point, loading was switched to displacement (slip) control.

At an applied slip magnitude of 2 mm, the measured shear resistance of the connection was reduced to 550 kN. The shear resistance maintained constant at this value up to an applied slip of 10 mm. During this portion of the test, slip was observed at both the interfaces between the dry pack and the two concrete panels. Only minor vertical crack formation and surface spalling were observed in the dry pack.

As the slip was increased beyond 10 mm, an increase in the measured shear resistance was observed, as shown in Figure 4.6. The shear resistance increased steadily up to a

maximum value of 785 kN at an applied slip magnitude of approximately 35 mm. As the applied slip was further increased, the measured shear resistance maintained constant at this value. At an applied slip of 64 mm, rupture of the east post-tensioned bar occurred, resulting in a sudden slip to 67 mm and a significant drop in shear resistance to 340 kN. This represented a 57% reduction of the shear resistance and accordingly, failure of the connection was declared. During the portion of the test from an applied slip of 10 mm to 64 mm, the dry pack remained essentially intact. Some formation of vertical cracks in the dry pack was observed, concentrated mostly at the ends of the connection and at the location of the post-tensioning bars. Also, minor surface spalling of the dry pack occurred along most of the length of the connection. The precast concrete panels also experienced some damage during this portion of the test. Initially, from an applied slip of 10 mm to 30 mm, cracking and spalling of the south-east end of the lower concrete panel occurred in the bearing areas against the loading frame and abutments. In addition, some spalling occurred in the connection region on the south side of the upper concrete panel, at the location of the east post-tensioning bar. From an applied slip of 30 mm to 64 mm, the spalling at the south end of the lower panel became considerable. In addition, some cracking, and eventually spalling, occurred in the connection region on the south side of the upper concrete panel, in the vicinity of the west post-tensioning bar.

To collect complete information after failure, the applied slip was increased from 67 mm to approximately 75 mm and the measured shear resistance maintained constant at 340 kN. This represents the residual strength of the connection. The test was concluded at this point.

As mentioned previously, the dry pack remained intact over the duration of the experiment. In addition, the connection thickness, or the thickness of the dry pack, did not vary significantly. The average variation of the dry pack thickness during the test is shown in Figure

4.12. This data shows a slight increase in the thickness of the connection. At slip magnitudes larger than 30 mm, the readings are unreliable due to cracking and spalling of the panel concrete in the regions of the LVDT stations, and therefore are shown as a "dashed" line in Figure 4.12. At the end of the test, the thickness of the connection was measured manually to be 20 mm +/- 0.5 mm. The condition of the dry pack at the end of the test is shown in Figure 5.42.

After the specimen was removed from the loading frame, the east post-tensioning bar was exposed at the connection level by removing the surrounding cracked panel concrete and dry pack, as shown in Figure 5.43. This allowed the deformed shape and rupture location of the bar to be determined, as shown schematically in Figure 5.44.

The behaviour of the post-tensioned Dywidag bars was measured using electrical resistance strain gauges. The measured strain gauge data is available up to an applied slip of 11 mm. However, two of the gauges were lost at a slip of 3 mm, and one gauge was lost at a slip of 8 mm.

Immediately after post-tensioning, the initial average measured bar strain was 0.00322. At the time of testing, the average measured strain was 0.00309. This represents a prestressing loss of approximately 4%. Upon application of the preload, only a very small prestressing loss of approximately 0.00002, or 0.6%, was measured. Using an elastic modulus of 200,000 MPa, the effective prestressing strain of 0.00307 will produce a vertical stress of 1.21 MPa on the connection area. The measured initial post-tensioning strains are presented in Table 5.2. The variation of bar strains prior to the initiation of slip is shown in Figure 5.45. In this figure, the relationship between the applied shear load and the measured strains is shown. Prior to the initiation of slip at an applied shear load of 555 kN, there was little or no variation in strain. Following the initiation of slip, the data suggests the occurrence of a minor amount of flexural

deformation in the bars, indicated by a measured strain gradient in both of the bars. This is illustrated clearly by the strain behaviour after the initiation of slip, shown in Figure 5.46. In this figure, the relationship between the applied slip and the measured bar strains is shown. For both bars, one gauge indicated a strain increase and the opposite gauge indicated a strain decrease, producing a strain gradient within the bar. Up to an applied slip of 10 mm, it appears that only a minor variation of strain has occurred. The location of the strain gauges measures the extreme fiber strains in the bars. In addition, the average of the strain readings from the two gauges is the axial force in the bar. The measured data indicates that neither bar had reached the yield strain of 0.0045 (Figure 3.17) in flexure, or in tension, up to the point at which the strain readings became unreliable.

5.2   STAGES OF CYCLIC BEHAVIOUR

On the basis of the experimental results described in the preceding sections, the cyclic shear behaviour of the connections could be described in three distinct stages. In the first stage, the behaviour of the connection is elastic and very stiff. The connection behaves as a monolithic member and slip is not observed between the precast concrete panels. The second stage commences with the initiation of slip between the panels. During this stage, the behaviour of the connection is inelastic and the dry pack within the connection remains intact. Little or no reduction of the thickness of the dry pack is measured. The shear resistance of the connection may increase or decrease, depending on the connection configuration. For Specimen SK, with multiple shear keys, a significant increase of the shear resistance is measured during the second stage, while the relative slip between the panels is limited to less than 1 mm. The third stage of behaviour represents failure of the connection, defined as a 20% reduction of the shear resistance. The third stage is initiated by sudden and extensive crushing and spalling of the dry pack, accompanied by a significant reduction of the shear resistance. For Specimen SK, the third stage is initiated by sudden cracking of the dry pack within the

shear keys. After the initial reduction of shear resistance, typically the behaviour of the connection stabilized at a reduced level, signifying the residual strength of the connection. Over the duration of the third stage, the dry pack continued to crush and spall, producing a significant reduction of the thickness of the dry pack. The three stages of the connection behaviour are illustrated in Figure 5.47. This figure shows the envelope of cyclic shear resistance - slip behaviour for Specimen PTS and represents typical behaviour for all of the connection configurations. In the case of Specimen SK, Stage II will be shortened, as the presence of the shear keys limits the measured slip to less than 1 mm.

5.3   INITIATION OF SLIP

As discussed in the preceding sections, the initiation of slip occurred gradually for all of the connection configurations with the exception of Specimen DP. This suggests that bond between the dry pack and the precast concrete panels was either non-existent, or had been destroyed by some means, possibly the effects of the cyclic loading. In the previous studies of the monotonic behaviour of the plain surface connections (i.e. without multiple shear keys) performed at the University of Manitoba, sudden initiation of slip due to breaking of the bond was only reported by Foerster (10,11). Foerster reported sudden "cracking" behaviour at the initiation of slip for connections with dry pack only and for connections with dry pack and mild steel continuity bars. The cracking strength of the connections was observed to be significantly higher than the shear resistance of the connection after the initiation of slip. Foerster also tested a connection with dry pack and continuity bars which had been deliberately "pre-cracked" prior to testing. The initiation of slip for this specimen occurred gradually, while the shear resistance after the initiation of slip was identical to the similar specimens which had not been pre-cracked. The gradual onset of slip was similar to the results observed by Serrette (29,30) for one connection with dry pack only and by Hutchinson (17,18) for connections with dry pack only and connections with post-tensioning, with and without hollow-core slabs. These results

suggest that bond between the dry pack and the precast panels was non-existent at the initiation of slip. Because these specimens were tested under monotonic loading, the bond could not have been destroyed by the effects of cyclic loading and therefore must not have been present at all, or had been destroyed in some unknown manner.

Based on the overall results from the three previous studies and the current cyclic loading program, it does not appear to be possible to absolutely determine if bond is present at the interface between the dry pack and the precast concrete panels. Therefore, it is not possible to predict whether the initiation of slip will occur gradually or suddenly due to breaking of the bond between the dry pack and the panels. In the interest of predicting the initiation of slip for design purposes where conservative results are desired, the presence of bond between the dry pack and the precast concrete panels should be ignored under both monotonic and cyclic loading conditions. The initiation of slip should therefore be assumed to occur gradually when the applied shear loading exceeds the shear resistance of the connection, determined assuming bond is not present. This will be discussed in detail in Chapter 6.

5.4   FAILURE MECHANISM UNDER CYCLIC LOADING CONDITIONS

The failure mechanism for the specimens tested under cyclic shear loading conditions was identical for all of the connection configurations. As described in Section 5.1, failure of all of the connection configurations was accompanied by sudden crushing and/or cracking of the dry pack. The effect of sudden crushing of the dry pack on the behaviour of the connection, depends on the configuration of the particular connection. While Specimen DP experienced only a minor loss of shear resistance at failure, the other configurations displayed a strength reduction in the order of 50%, as shown in Figures 4.1 to 4.6. For Specimen DP, where the shear resistance is provided only by friction, crushing of the dry pack represents a reduction of the only variable, the coefficient of friction. For Specimens PTS and PTB, crushing of the dry

pack was accompanied by a considerable loss of shear resistance compared to Specimen DP. Similar to Specimen DP, the coefficient of friction will be reduced. In addition, crushing of the dry pack and subsequent reduction of the dry pack thickness will result in a substantial loss of the prestressing force. Therefore, both the coefficient of friction and the equivalent vertical stress on the connection due to post-tensioning are reduced. In the case of Specimen RW, crushing of the dry pack caused two continuity bars to carry a significant portion of the simulated gravity load normal to the connection. This behaviour was confirmed by the out-of-plane buckling of one of the bars at the connection level towards the end of the test, shown in Figure 5.12. Because the continuity bars were forced to resist most of the applied vertical load, the effective vertical stress acting on the connection area is reduced, thus substantially reducing the shear resistance provided by friction. For Specimen SK, the shear resistance mechanism before failure of the dry pack is largely due to direct bearing within the shear keys. As a result, failure of the dry pack destroys this resistance mechanism, resulting in a very large reduction of shear resistance, as shown in Figure 4.5.

5.5   EFFECT OF MILD STEEL CONTINUITY BARS

The effect of the continuity bars is illustrated in Figure 5.48 by comparing the envelopes of cyclic shear resistance - slip behaviour for Specimen DP and Specimen RW. In this figure, the results from Specimen DP, tested with an applied vertical stress of 4 MPa, have been "scaled" to allow direct comparison with Specimen RW, tested under an applied vertical stress of 2 MPa. In general, the continuity bars will increase the overall shear resistance of the connection compared to the plain connection of Specimen DP. The presence of continuity bars has two effects on the shear resistance of the connection. First, the bars will resist a portion of the normal load on the connection, thereby reducing the effective stress on the dry pack and the frictional resistance of the connection. Over the duration of the cyclic loading, the portion of the vertical load resisted by the continuity bars will increase, as discussed in Section 5.1.2 and

shown in Figure 5.16. This will tend to reduce the frictional resistance of the connection during the test, particularly during Stage III of behaviour. The second effect of the continuity reinforcement is to provide an additional component of shear resistance. Relative slip between the panels will tend to deform the continuity bars. The resistance of the bars to slip deformation will therefore increase the shear resistance of the connection. As the applied slip magnitude is increased, the deformation and therefore the resistance of the bars will become more significant, increasing the shear resistance as shown in Figure 5.48.

5.6   EFFECT OF POST-TENSIONING

The envelopes of shear resistance - slip behaviour for Specimens DP, PTS and PTB are shown in Figure 5.49. Once again, the results of Specimen DP have been scaled to allow direct comparison with Specimens PTS and PTB, tested with an applied vertical stress of 2 MPa. The effect of post-tensioning is to increase the shear resistance of the connection at the initiation of slip and during Stage II of behaviour. The increase of shear resistance observed for Specimens PTS and PTB over Specimen DP is approximately proportional to the increase of effective vertical stress on the connection due to post-tensioning. Similar to the results observed by Hutchinson (17,18), this suggests that the effect of post-tensioning enhances the frictional resistance of the connection.

During Stage III of behaviour, crushing of the dry pack could result in a total loss of prestressing force. As a result, the frictional resistance of the connection provided by post-tensioning will be eliminated and the total shear resistance will be similar to Specimen DP. In the case of Specimen PTS, the shear resistance during Stage III is very close to that measured for Specimen DP, as shown in Figure 5.49. For Specimen PTB, the shear resistance during Stage III is lower than Specimen PTS and DP. It is possible that crushing of the dry pack may cause the post-tensioning bars to resist a portion of the applied vertical load during Stage III.

This would further reduce the effective vertical stress on the dry pack, thus reducing the frictional resistance of the connection.

5.7   EFFECT OF SHEAR KEYS

The effect of multiple shear keys is clearly evident when comparing the cyclic shear resistance - slip envelopes for Specimen DP and Specimen SK, as shown in Figure 5.50. The results of Specimen DP have been scaled to allow direct comparison with Specimen SK, tested with an applied vertical stress of 2 MPa. The maximum shear resistance of Specimen SK was 850 kN, more than three times the maximum shear resistance of Specimen DP. The increased shear resistance for Specimen SK is due to direct bearing on the dry pack within the shear keys. At the higher load levels before failure of the connection (cycles at 750 kN and 800 kN), the upper concrete panel was actually observed to slide upward on the shear keys, overcoming the 360 kN normal load. During these cycles, the entire shear load on the connection would be transferred between the panels by direct bearing on the dry pack within the shear keys. Obviously, the performance of the connection can be very significantly increased through the use of multiple shear keys.

After failure of the connection due to cracking of the dry pack within the shear keys, a uniform slip interface formed along the length of the connection and the shear resistance of the connection is only provided by friction along this interface. At this point, the shear resistance stabilized to a constant value of approximately 300 kN in both directions of loading. The shear resistance of Specimen DP after failure due to crushing of the dry pack stabilized at a level of approximately 210 kN (scaled value). Thus, after failure, the shear resistance of the connection with multiple shear keys was 43% higher than the plain surface connection. The increased shear resistance of Specimen SK may be attributed to the different slip interfaces for the two specimens. Since the newly formed interface of Specimen SK consists of a combination of dry

pack-to-dry pack regions within the shear keys and smooth concrete-to-dry pack regions, it could produce a higher frictional resistance compared to the plain surface connection of Specimen DP.

5.8   EFFECTS OF CYCLIC LOADING

The effects of cyclic loading on the behaviour of the various connection configurations can be evaluated by comparing the experimental results from the cyclic loading tests to the results obtained from the previous studies of the monotonic (static) shear behaviour performed at the University of Manitoba (Foerster (10,11), Serrette (29,30) and Hutchinson (17,18)). The results of these three experimental programs, including the proposed models, were described prviously in detail in Section 2.3.1. The behaviour of the connection with post-tensioned bars was not considered in the previous research and therefore, a model for prediction of the static behaviour of this connection configuration does not exist. The effects of cyclic loading on the behaviour of this connection will be evaluated using the results of the static test of Specimen PTB-S and cyclic test of Specimen PTB in the current experimental program.

5.8.1   Deterioration of the Dry Pack

The most significant effect of the cyclic loading is deterioration the dry pack. The deterioration occurs in the form of a reduction of the thickness of the dry pack.

Initially, during Stage II of the connection behaviour, the thickness of the dry pack was gradually reduced due to the grinding action of the cyclic loading. This was observed for Specimen RW and Specimen PTB. In the case of Specimen RW, the gradual reduction of the dry pack thickness causes the continuity bars to resist a larger portion of the applied vertical load, thereby reducing the frictional resistance of the connection over the duration of loading.

In the monotonic shear tests of similar specimens with mild steel continuity reinforcement performed and reported by Foerster (10,11), a measurable reduction of the dry pack thickness was not observed. In addition, strain readings from the continuity bars did not indicate an increase of the amount of compression resisted by the bars over the duration of the loading. For Specimen PTB, the gradual reduction of the dry pack thickness produced a gradual loss of prestressing in the bars. As a result, the frictional resistance of the connection was reduced over the duration of loading. The monotonic shear test of Specimen PTB-S did not experience a measurable reduction of dry pack thickness and the strain readings from the bars did not indicate a loss of prestress. In addition, a loss of shear resistance was not observed for Specimen PTB-S over the same range of applied slip.

The cyclic shear tests of the configurations with plain surface connections all experienced failure due to sudden and extensive crushing of the dry pack. This was previously defined as Stage III of the cyclic shear connection behaviour. In the monotonic shear test of Specimen PTB-S and the previously reported monotonic shear tests, none of the plain surface connection configurations experienced extensive crushing of the dry pack and therefore did not reach Stage III. In the case of Specimen PTB-S, loading was continued up to a very significant applied slip of 75 mm and crushing of the dry pack was not observed. These results suggest that the grinding action of the cyclic loading will eventually cause crushing of the dry pack, thereby introducing an additional limit state of behaviour beyond that observed for identical specimens tested under monotonic loading conditions.

5.8.2 Comparison With Previously Proposed Models for Monotonic Loading

In this section, the applicability of the static strength models proposed in the previous research by Foerster, Serrette and Hutchinson (10,11,17,18,29,30) for predicting cyclic behaviour will be evaluated. The static strength models are summarized in Section 2.3.1. In

the previous studies, with the exception of the connections with multiple shear keys, the observed behaviour corresponded to Stages I and II observed for the specimens tested under cyclic loading in the current research. The proposed models for the ultimate strength under monotonic loading corresponds to Stage II of the cyclic connection behaviour. In the case of the specimens with multiple shear keys tested under monotonic loading, significant deterioration of the dry pack was observed after cracking. Thus, the proposed models for the ultimate strength of these connections under monotonic loading corresponds to Stage III of the cyclic connection behaviour. In the following sub-sections, the previously proposed monotonic loading models will be used with the measured material properties presented in Chapter 4 to determine the predicted static strength of each specimen in the current program. The predicted static strength is then compared with the measured cyclic behaviour of the specimen.

5.8.2.1 Connections with Dry Pack Only

The mechanism of shear transfer for a plain surface dry packed connection is provided by interface friction, as described in Section 2.3.1 (Foerster, Serrette, Hutchinson (10,11,17,18,29,30)). The predicted monotonic maximum shear strength of Specimen DP is determined using Equation 2.2 as follows (since no continuity bars or shear connectors are used in Specimen DP, the second and third terms of Equation 2.2 are omitted):

$$V_f = \mu \, \sigma_n \, A_c$$

where

μ = coefficient of friction

= 0.7 +/- 0.1

σ_n = vertical stress on the connection

= 4 MPa

A_c = connection area

$$= 150,000 \text{ mm}^2$$

$$V_f \quad = 0.7 \,(\, 4 \text{ MPa} \,) \,(\, 150,000 \text{ mm}^2 \,)$$
$$= 420 \text{ kN}$$

The measured maximum shear resistance of Specimen DP during Stage II of behaviour was 480 kN. On the basis of the measured shear resistance, a coefficient of friction of 0.8 is obtained. This value corresponds well with the recommendations of the previous research for the coefficient of friction. It appears that the previously proposed monotonic shear strength model could be used with a coefficient of friction of 0.7 to conservatively predict the behaviour of the connection during Stage II. These results suggest that cyclic loading had no effect on the strength of the connection prior to significant deterioration of the dry pack.

5.8.2.2 Connections with Mild Steel Continuity Bars

The shear resistance of dry packed connections with mild steel continuity bars under monotonic loading is provided by a combination of interface friction and the resistance of the bars to shear deformation, as described in Section 2.3.1 (Foerster (10,11)). The predicted static shear strength of Specimen RW using Equation 2.2 is as follows:

$$V_r = \mu \, \sigma_n \, A_c + \frac{A_s f_y}{\sqrt{3}}$$

where

$\mu \quad$ = coefficient of friction

$\quad = 0.7 \text{ +/- } 0.1$

$\sigma_n \quad$ = vertical stress on the connection

$A_c \quad$ = connection area

$$= 180{,}000 \text{ mm}^2$$

A_s = total cross-sectional area of bars

$$= 2 \ (\ 500 \text{ mm}^2)$$

f_y = nominal yield strength of bars

$$= 400 \text{ MPa}$$

In the previous research, consideration was not given to the portion of the vertical preload which may be resisted by the continuity bars. In the case of Specimen RW, initial compressive strains in the order of 0.0005 were measured in the continuity bars due to the application of the vertical preload. This will reduce the vertical stress acting on the connection area to 1.44 MPa, from 2 MPa. Considering this, the shear resistance of the connection is determined as:

$$V_r = 0.7 \ (\ 1.44 \text{ MPa} \ ) \ (\ 180{,}000 \text{ mm}^2 \ ) \ + \ \frac{(\ 1000 \text{mm}^2 \ ) \ (\ 400 \text{MPa} \ )}{\sqrt{3}}$$
$$= 413 \text{ kN}$$

The measured shear resistance of Specimen RW during Stage II of behaviour ranged from approximately 290 kN at the initiation of slip to a maximum of 400 kN, considerably lower than the predicted value. In addition, it is likely that the actual coefficient of friction will be 0.8, as this was the value determined from the cyclic shear test of Specimen DP. A higher coefficient of friction will further increase the static loading prediction, becoming more unconservative. Based on the measured results, it appears that the previously proposed model for static strength prediction of this type of connection is not applicable for cyclic loading conditions. In particular, it is likely that the second term of the equation, related to the resistance provided by the bars, is the source of difference since the interface friction term of the equation appears to be sufficient in the case of Specimen DP.

5.8.2.3 Connections with Post-tensioned Strands

The shear resistance of connections with post-tensioned strands is provided by interface friction, as described in Section 2.3.1 (Hutchinson (17,18)). The frictional resistance of the connection is provided by both the applied vertical preload and the effects of the post-tensioning. The predicted monotonic shear strength of Specimen PTS is determined using Equation 2.6 as follows:

$$V_f = \mu \, (\, \sigma_{ng} + \sigma_{np} \,) \, A_c$$

where

μ = coefficient of friction

     = 0.7 +/- 0.1

σ_{ng} = vertical stress on the connection due to normal load

     = 2 MPa

σ_{np} = vertical stress on the connection due to post-tensioning

     = 1.2 MPa

A_c = connection area

     = 180,000 mm^2

V_f = 0.7 (2.0 MPa + 1.2 MPa) (180,000 mm^2)

     = 403 kN

The measured maximum shear resistance of Specimen PTS during Stage II of behaviour was 525 kN. The value remained essentially constant over the duration of Stage II of behaviour. On the basis of the measured shear resistance, a coefficient of friction of 0.91 is obtained. This value is slightly higher than the recommendations of the previous research for the coefficient of friction, but is not unreasonable. It appears that the previously proposed monotonic shear

strength model could be used with a coefficient of friction of 0.7 to conservatively predict the behaviour of the connection during Stage II. These results suggest that cyclic loading had no effect on the strength of the connection prior to significant deterioration of the dry pack.

5.8.2.4 Connections with Multiple Shear Keys

The shear resistance of connections with multiple shear keys is provided by interface friction and bearing on the dry pack within the shear keys, as described in Section 2.3.1 (Serrette (29,30)). The behaviour of the connection under static loading was observed to have three limit states; cracking, maximum shear resistance and ultimate shear resistance. The maximum shear resistance under static loading occurs after cracking of the dry pack within the shear keys but prior to the formation of a uniform sliding plane, in the same direction of loading. In the case of Specimen SK, tested under reversed cyclic loading, the loading direction was reversed immediately after cracking, destroying the strut mechanism associated with the maximum shear resistance, as described in Section 2.3.1. Therefore, the cracking shear resistance of the Specimen SK corresponded to the maximum measured shear resistance of the connection, and the maximum shear resistance associated with static loading conditions was not observed. The predicted static loading cracking shear resistance of Specimen SK is determined using Equation 2.3 as follows:

$$V_{cr} = \mu \sigma_n (A_c - ndt \tan \theta) + \sqrt{f_t (\sigma_n + f_t)} \, A_{cr}$$

where

μ = coefficient of friction

= 0.7 +/- 0.1

σ_n = vertical stress on the connection

= 2 MPa

A_c = connection area

$$= 180{,}000 \text{ mm}^2$$

n   = number of shear keys

     = 5

d   = depth of shear key

     = 35 mm

t   = panel thickness

     = 150 mm

θ   = inclination of shear key

     = 23.3 deg.

f_t = tensile strength of dry pack

     $= 0.6\sqrt{f'_g}$

f_g = equivalent standard cylinder strength of the dry pack

     = 0.85 x cube strength of dry pack

     = 51 MPa

A_{cr} = total cross-sectional area of diagonal cracks through shear keys

     $= nt\sqrt{h^2 + b^2}$

h   = maximum length of the shear key

     = 100 mm

b   = initial thickness of the connection (gap between the precast panels)

     = 20 mm

$$f_t = 0.6\sqrt{51 \text{ MPa}}$$
$$= 4.28 \text{ MPa}$$
$$A_{cr} = (5)(150)\sqrt{100^2 + 20^2}$$
$$= 76485.3 \text{ mm}^2$$

$$V_{cr} = 0.7(2)(180,000 - (5)(35)(100)\tan 23.2) + \sqrt{4.28(2 + 4.28)}\,(76485.3)$$
$$= 241.5 \text{ kN} + 396.5 \text{ kN}$$
$$= 638 \text{ kN}$$

The shear resistance of Specimen SK at cracking was 833 kN, considerably higher than the static prediction of 638 kN. It is unlikely that the difference between the predicted static cracking strength and the measured cyclic cracking strength is due to the cyclic loading. The proposed cracking shear resistance model for static loading conditions was found to provide very good correlation with the experimental results in the previous research (Serrette (29,30)). Therefore, the source of the difference is most likely related to the strength of the dry pack. It is possible that the dry pack within the shear keys was compacted to a higher level during placing than the cube specimens. This would result in a higher tensile strength for the in situ dry pack than that measured for the cube specimens, and would significantly increase the bearing resistance of the shear keys prior to cracking. At this stage, it is not possible to determine the actual strength of the in situ dry pack. Based on the measured results, it appears that the proposed static loading models and the measured material properties could be used to conservatively predict the cracking strength of connections with multiple shear keys under cyclic loading.

The ultimate shear resistance of the connection after the formation of a uniform sliding plane under static loading conditions can be predicted using Equation 2.5 as follows:

$$V_u = 0.2\sqrt{f'_g}\, A_{ck} + 0.5\sigma_n A_c$$

where

A_{ck} = cross-sectional area of the portion of the connection covered by the shear keys

= (780)(150)

$$= 117{,}000 \text{ mm}^2$$

$$V_u = 0.2\sqrt{51}\,(117{,}000) + 0.5(2)(180{,}000)$$
$$= 348.4 \text{ kN}$$

After formation of a uniform sliding plane, during Stage III of behaviour, the measured shear resistance of Specimen SK was 335 kN. Under the conditions of both static loading and cyclic loading, after the formation of a sliding plane, the connection appears to behave in a similar manner. Based on the measured data, it appears that the previously proposed model for the ultimate strength under monotonic loading conditions can be used to predict the strength of the connection under cyclic loading conditions during Stage III of behaviour.

CHAPTER 6

MECHANISMS OF SHEAR TRANSFER

6.0   INTRODUCTION

In this chapter, the shear resistance mechanisms for each of the six specimens tested in this program are examined. Shear resistance mechanisms are defined for each stage of behaviour. Where possible, the experimental results are used to evaluate and refine the proposed mechanisms to allow prediction of the connection behaviour under cyclic shear loading conditions.

6.1   SPECIMEN DP

The initiation of slip for Specimen DP occurred suddenly. This suggests that during Stage I of behaviour, prior to the initiation of slip, the shear resistance of the connection is provided by bond between the dry pack and the precast concrete panels. This behaviour was unique for Specimen DP, as no evidence of bond between the dry pack and the panels was observed for the other specimens tested under cyclic loading conditions. After the initiation of slip, during Stage II of behaviour, the shear resistance of the connection is provided by interface friction. The ultimate shear resistance of the connection after crushing of the dry pack (Stage III of behaviour) is also provided by interface friction.

6.1.1 Stage I - Initiation of Slip

If complete bond is maintained at the interface between the dry pack and the precast concrete panels, the initiation of slip will occur suddenly when the bond is broken. Sudden initiation of slip due to breaking of the bond can be predicted using the monotonic loading "cracking" model (Equation 2.1) proposed by Foerster (10,11) in the previous study at the University of Manitoba. The procedure for estimating the cracking shear resistance, V_{cr}, is given as follows:

$$V_{cr} = \sqrt{f_t (f_t + \sigma_n)} \, A_c \qquad\qquad (6.1)$$

where

f_t = tensile strength of dry pack

     $= 0.5 \sqrt{f_g'}$

f_g = equivalent standard cylinder strength of the dry pack

     = 0.85 x cube strength of dry pack

     = 32.4 MPa   (for Specimen DP)

σ_n = vertical stress on the connection

     = 4 MPa

A_c = connection area

     = 150,000 mm²

Therefore,

$$f_t = 0.5\sqrt{32.4}$$
$$= 2.85 \text{ MPa}$$

$$V_{cr} = \sqrt{2.85(2.85+4)}\,(150000)$$
$$= 663 \text{ kN}$$

The measured shear resistance at cracking was 533 kN. The predicted cracking load of 663 kN is 25% higher than the measured value. The reduction of the cracking strength could be attributed to the effect of the reversed cyclic loading in comparison to the static nature of the load from which the proposed model was developed. Considering the variables in Equation 6.1, it is possible that the cyclic loading caused a reduction of the tensile strength of the dry pack. Using this assumption, the cracking strength of the connection could be predicted by considering a reduction of approximately 30% of the dry pack tensile strength. Thus, the predicted cracking strength under cyclic loading conditions is determined as follows:

$$f_t = 0.7\left(0.5\sqrt{f'_g}\right)$$
$$= 0.7\left(0.5\sqrt{32.4}\right)$$
$$= 1.99 \text{ MPa}$$

$$V_{cr} = \sqrt{1.99(1.99+4)}\,(150000)$$
$$= 518 \text{ kN}$$

The predicted cracking strength of the connection considering a reduced tensile strength of the dry pack corresponds well to the measured value of 533 kN.

6.1.2 Stage II - After the Initiation of Slip

After the initiation of slip, the upper precast concrete panel slid relative to the bottom panel along the interface of the upper surface of the dry pack. At this stage, there was no measurable reduction of the thickness of the dry pack and the shear resistance of the connection remained fairly constant.

The shear resistance of the connection during Stage II is provided only by friction, due to the absence of continuity reinforcement or shear keys in this specimen. The behaviour and the measured constant shear resistance suggests a constant friction coefficient. As described in Section 5.8.2.1, the previously proposed monotonic loading model for the shear resistance of the connection appears to apply to the cyclic behaviour of the connection. Based on the measured shear resistance, a friction coefficient of $\mu = 0.8$ is obtained which is within the range of measured friction coefficients in the previous research.

6.1.3 Stage III - After Crushing of the Dry Pack

In this investigation, failure of the connection was defined as a 20% reduction of the shear resistance of the connection due to an increase of the applied slip magnitude. This stage was accompanied by extensive crushing and spalling of the dry pack. After failure of the connection, the shear resistance of the connection during Stage III remained consistent at a reduced level in spite of continued crushing of the dry pack.

As discussed above, the shear resistance is provided by interface friction and therefore a loss of shear resistance reflects a reduction of the coefficient of friction. The measured shear resistance of Specimen DP during Stage III was 420 kN. This corresponds to a coefficient of

friction of $\mu = 0.7$. On the basis of the measured results, it appears that crushing of the dry pack produces a reduction of the coefficient of friction from $\mu = 0.8$ to 0.7.

6.2   SPECIMEN RW

During Stage I, prior to the initiation of slip, the behaviour of the connection is elastic and the shear resistance is provided by interface friction. The second stage describes inelastic behaviour after the initiation of slip. During this stage, the shear resistance increases as the applied slip magnitude is increased and the shear resistance is provided by a combination of interface friction and the resistance of the continuity bar to deformation. In the third and final stage, the dry pack crushes and spalls extensively and a significant reduction of the shear resistance occurs.

6.2.1   Stage I - Initiation of Slip

The initiation of slip for Specimen RW occurred gradually without sudden cracking. This behaviour suggests that the bond between the dry pack and the precast concrete panels was non-existent or had possibly deteriorated due to the cyclic loading. If bond is not present between the dry pack and the panels, the initiation of slip will occur when the applied shear force exceeds the frictional resistance of the connection. Although there is continuity reinforcement across the connection for this specimen, theoretically, the shear resistance mechanisms associated with the reinforcement do not become active until slip has occurred. Therefore, the shear resistance at the initiation of slip is provided only by friction, produced by the net gravity load (applied vertical load) acting on the cross-sectional area of the connection. The net gravity load is the portion of the simulated gravity load carried by the dry pack of the connection. The remainder of the gravity load is resisted by the continuity reinforcement.

The frictional resistance provided by the net gravity load, V_{fl}, may be determined as follows:

$$V_{fl} = \mu \, \sigma_{nl} \, A_c \qquad\qquad (6.2)$$

where:

μ = coefficient of friction

       = 0.8 (measured from cyclic shear Specimen DP)

σ_{nl} = vertical stress acting on dry pack due to net gravity load

$$= \frac{P_g - nF_{bo}}{A_c}$$

P_g = applied gravity load

n = number of continuity bars

F_{bo} = portion of applied gravity load resisted by one continuity bar (compression force)

A_c = cross-sectional area of the connection

In practical terms, the initiation of slip is difficult to define. As mentioned above, it is assumed that prior to the initiation of slip, the continuity reinforcement does not contribute to the shear resistance of the connection. In reality, the onset of slip is not observable until some magnitude of slip has occurred. At this point, it is possible that the continuity reinforcement will also provide some amount of shear resistance. For this reason, in this experimental program, the initiation of slip is defined as the point at which 0.1 mm of slip has been measured, and the contribution of the continuity reinforcement at this slip magnitude will be

considered when predicting the initiation of slip. The contribution of the continuity bars is discussed in detail in the following sections.

6.2.2   Stage II - After the Initiation of Slip

The initiation of slip occurred at the interface between the upper concrete panel and the dry pack. During Stage II, the behaviour of the connection was inelastic and exhibited stable hysteresis loops. As the slip magnitude was increased, an increase of the shear resistance was measured. As described in Section 5.5, the shear resistance of the connection during Stage II is assumed to be provided by a combination of interface friction and the resistance of the continuity reinforcement to deformation. On the basis of the discussion in Section 5.8.2.2, the previously proposed model for monotonic loading does not appear to correctly describe the behaviour of the connection under cyclic loading. From the observed experimental behaviour, the continuity reinforcement appears to contribute to the overall shear resistance of the connection in a progression of two separate mechanisms. Initially, the contribution of the continuity reinforcement may be attributed to flexural deformation of the bar due to the relative slip between the panels. The idealized form of this mechanism is shown in Figure 6.1(a). The flexural resistance mechanism is dominant until the formation of plastic hinges in the bars. At this point, a second mechanism forms in the continuity reinforcement. This mechanism, referred to as "kinking action", is shown in Figure 6.1(b). As horizontal slip between the panels occurs, a tensile force is induced within the kinked length of the bar. The vertical component of this force will exert a vertical stress on the dry pack, increasing the frictional resistance of the connection. This is referred to as clamping action. In addition, the horizontal component of the tensile force in the bar will directly resist applied shear loading.

The total shear resistance of the connection during Stage II, V_r, can be separated into four components:

$$V_r = V_{f1} + V_{h1} + V_{f2} + V_{h2} \qquad (6.3)$$

Each of the shear resistance components is described in detail below.

Component V_{f1}:

The component V_{f1} represents the frictional resistance provided by the net gravity load acting on the cross-sectional area of the connection, as shown in Figure 6.2. Similar to the procedure described in Stage I, V_{f1} is estimated as follows:

$$V_{f1} = \mu \, \sigma_{n1} \, A_c \qquad (6.2)$$

where:

μ = coefficient of friction

= 0.8 (measured from cyclic shear Specimen DP)

σ_{n1} = average vertical stress acting on dry pack due to net gravity load for a particular slip magnitude, i

$$= \frac{P_g - nF_{boi}}{A_c}$$

P_g = applied gravity load

n = number of continuity bars

F_{boi} = compression force in one continuity bar due to the applied gravity load when the connection is at the zero slip position at the start of a cycle to slip magnitude i

$$A_c \quad = \text{cross-sectional area of the connection}$$

The difference between the calculation of V_{fl} in Stage I and Stage II is the magnitude of the force in the continuity bars, F_{boi}. Over the duration of cyclic loading, a gradual reduction of the thickness of the dry pack will occur. As a result, the portion of the applied gravity load resisted by the continuity reinforcement, F_{boi}, increases. As F_{boi} increases, the vertical stress acting on the connection, σ_{n1}, is reduced. Therefore, as the number of cycles and applied slip magnitude increases, the contribution of V_{fl} will be reduced.

Component V_{h1}:

The component V_{h1} represents the end shear forces resulting from flexural deformation of the continuity reinforcement, as shown in Figure 6.3. The flexural mechanism associated with V_{h1} was discussed previously and is shown in Figure 6.1(a). The bar is assumed to have "fixed" end conditions and is deformed over a length L_1. V_{h1} can be estimated as follows:

$$V_{h1} = n \times \frac{[2M]}{L_1} \qquad (6.4)$$

where:

$n \quad = \text{number of continuity bars}$

$M \quad = \text{fixed end moment in the bar}$

$L_1 \quad = \text{effective deformed length}$

The fixed end moment, M, is determined based on the flexural moment/curvature relationship of the bar and is limited by the plastic moment capacity, M_p. The curvature at the ends of the bar can be determined from the deformed shape, defined by the slip magnitude, δ, and the deformed length, L_1, as illustrated in Figure 6.1(a). V_{h1} will increase as the slip magnitude is increased, until plastic hinge formation occurs. At this point, V_{h1} is limited to:

$$V_{h1} = n \times \frac{[2M_p]}{L_1}$$

After the formation of plastic hinges, the reversed cyclic loading may cause deterioration of the concrete around the bar, allowing a progression of the plasticized region and thus an increase of the deformed length, L_1. Because the end moment is limited to M_p, this will tend to reduce the contribution of component V_{h1}.

Component V_{f2}:

The component V_{f2} is the frictional resistance provided by clamping action as shown in Figure 6.4. As discussed previously, clamping action is produced by a tensile increase of the axial force in the bar. This increase is due to the relative horizontal displacement of the ends of the bar while the vertical position of the ends of the bar is kept constant. This mechanism, referred to as "kinking action", is illustrated in Figure 6.1(b). V_{f2} may be estimated as follows:

$$V_{f2} = \mu \, \sigma_{n2} \, A_c \tag{6.5}$$

where:

μ = coefficient of friction

     = 0.8 (measured from cyclic shear Specimen DP)

σ_{n2} = average vertical stress acting on dry pack due to clamping action

$$= n \times \frac{[\Delta F_{byi}]}{A_c}$$

n   = number of continuity bars

ΔF_{byi} = vertical component of the increase of axial bar force at an applied slip magnitude, i, due to the kinking mechanism (defined in Figure 6.4 and Figure 6.1(b))

A_c = cross-sectional area of the connection

The kinking mechanism does not become significant until flexural hinge formation associated with component V_{h1} occurs. Once kinking action develops, the tensile increase of bar force, ΔF_{byi}, will become larger as the applied slip increases. Correspondingly, V_{f2} will increase as the magnitude of the applied slip increases.

V_{f2} is limited by the tensile yield strength of the bar. Experimental results indicate that at slip magnitudes up to 6.0 mm, the axial bar strain is well below the yield strain for the bar.

Component V_{h2}:

The component V_{h2} is provided by the kinking mechanism, as described above for component V_{f2}. V_{h2} may be estimated as follows:

$$V_{h2} = n \times [\Delta F_{bxi}] \tag{6.6}$$

where:

n = number of continuity bars

ΔF_{bxi} = horizontal component of the increase of axial bar force at an applied slip magnitude, i, due to the kinking mechanism (defined in Figure 6.4 and Figure 6.1(b))

V_{h2} is illustrated in Figure 6.4. As discussed for component V_{f2}, because V_{h2} is a function of the kinking mechanism, it does not develop until plastic hinge formation occurs, and then increases with applied slip magnitude.

6.2.3 Stage III - After Crushing of the Dry Pack

Failure of Specimen RW was accompanied by extensive crushing and spalling of the dry pack. For Specimen RW, this behaviour was observed during the cycles at an applied slip magnitude of 9.0 mm. During these cycles, an average reduction of shear resistance of 45% was measured. As the applied slip was increased, a further 25% reduction of the shear resistance was observed and out-of-plane buckling of one of the continuity bars occurred. Following this, the behaviour of the connection stabilized.

During Stage III, the observed behaviour of Specimen RW is rather complex. In addition, the absence of reliable strain readings for the continuity bars during this portion of the experiment makes it quite difficult to evaluate the mechanisms of the shear resistance. As extensive crushing and spalling of the dry pack occurs, the majority of the applied gravity load is resisted by the continuity reinforcement and contact between the upper concrete panel and the dry pack is reduced. As a result, the contribution from shear resistance components V_{f1} and V_{f2} is severely limited, producing a significant loss of shear resistance. As the deterioration of

the dry pack continues, the continuity reinforcement continues to resist a larger portion of the vertical loads until buckling of one or both of the continuity bars occurs at the connection level. At this point, a vertical force redistribution occurs and the dry pack carries an increased portion of the applied gravity load. Because the dry pack is once again resisting a portion of the applied gravity load, some amount of frictional resistance will be present and the behaviour of the connection becomes stabilized. Once buckling of the continuity reinforcement has occurred, it is likely that the shear resistance components associated with the flexural mechanism, V_{h1}, and the kinking mechanism, V_{f2} and V_{h2}, are no longer effective. Therefore, it could be assumed that the shear resistance of the connection is provided largely by the friction component V_{f1}. Quantification of the component V_{f1} during Stage III is very difficult for this specimen. Because the force in the continuity bars, F_{boi}, is unknown, it is not possible to determine the vertical stress acting on the dry pack due to the applied gravity load, σ_{n1}. Also, it is not clear if the continuity reinforcement will provide an additional contribution to the shear resistance through some other form of mechanism.

Because of the complex observed behaviour and the difficulty associated with quantifying the contribution of the continuity reinforcement during Stage III, a complete evaluation of the shear resistance mechanisms for this specimen is not possible using the experimental results.

6.2.4 Evaluation of the Proposed Mechanisms Using Experimental Results

The overall cyclic shear behaviour of the connection is defined by the envelope of the measured shear resistance - slip relationship, as shown in Figure 4.18. The measured experimental data, including the shear resistance envelope, can be utilized to examine the shear resistance mechanisms proposed in the preceding discussion. In addition, the experimental results can be used to define and calibrate the variables of the mechanisms to allow prediction

of the connection behaviour. In order to simplify the analysis and evaluation of the mechanisms while still considering all aspects of the cyclic behaviour, an average of the measured data at each applied slip magnitude was used. In addition, each applied slip magnitude was addressed separately to consider the effects of the cyclic loading during the previous cycles. In this section, the proposed shear resistance mechanisms are evaluated and the variables within the mechanisms are defined.

The proposed shear resistance mechanisms are primarily a function of the force within the continuity bars. As mentioned in the discussion of the experimental results, electrical resistance strain gauges were used to measure axial strains in the continuity reinforcement during the experiment. Using the strains, the axial force in the bars can be estimated. The average measured bar strains for the three cycles at each applied slip magnitude are presented in Table 6.1. The strain values for the zero slip position at the start of each slip magnitude, reported in Table 6.1, are the average of the east and west bar readings. The total bar strain measured at the applied slip magnitude is the average of the push direction and pull direction readings for both bars. The measured variation of axial bar force obtained using these strains is shown in Figure 6.5. The measured data was extrapolated to consider applied slip magnitudes at 7.0 mm and 8.0 mm. Figure 6.5 confirms that as the slip magnitude was increased, the amount of compression carried by the bars at the zero slip position also increased. This represents the increased portion of the applied gravity load resisted by the continuity reinforcement over the duration of the experiment. Figure 6.5 also illustrates the significant tensile increase of the axial force in the bars as the slip magnitude was increased.

6.2.4.1 Evaluation of Component V_{f1} (F_{boi})

The frictional resistance provided by the net gravity load acting on the connection is primarily a function of the portion of the gravity load resisted by the continuity bars. During

Stage I of behaviour, prediction of the first initiation of slip requires calculation of an initial value of V_{fl}. The force in the continuity reinforcement prior to the initiation of slip, F_{bo}, can be estimated by determining the distribution of vertical forces at the connection level using a transformed section analysis. In addition, shrinkage strains in the dry pack must be considered. A possible procedure for this is shown by the sample calculations in the Appendix. The initial strain in the bars is the sum of the shrinkage strain in the dry pack and the strain due to the applied gravity load. The calculated value of 0.00053 is of the same order of magnitude but slightly larger than the strain measured for this specimen and similar flexural specimens (refer to discussion of experimental results, Section 5.1.2). It is possible that the calculation of the shrinkage strain may be overestimated by the standard approach for determining shrinkage strains (CPCI Handbook p. 2-7 (3)). This method was developed for normal concrete and may not directly apply to dry pack. For design purposes, an initial strain of 0.00045 could reasonably be assumed for an applied gravity load of 360 kN.

During Stage II of behaviour, as discussed previously, the grinding action of the cyclic loading will tend to gradually reduce the thickness of the dry pack, increasing the portion of the applied gravity load resisted by the continuity bars, F_{boi} as shown in Figure 6.5. The relationship between the dry pack reduction and the increase of compressive bar strain can not be rationally determined from the limited experimental results. The results suggest that a length of the bars have become unbonded from the concrete and therefore the strains can not be determined simply by assuming a gauge length based on the initial connection thickness (20 mm). Further testing is required to define this relationship completely.

6.2.4.2 Evaluation of Components V_{h1}, V_{f2} and V_{h2} (L_1 and L_2)

Since the mechanisms proposed for the components V_{fl}, V_{f2} and V_{h2} are a function of the force in the bar, these three components can be determined directly from the experimental

results using the measured bar strains. With three of the four components known, the contribution due to V_{h1} can be determined by subtracting the known components from the total measured shear resistance, as shown below.

$$V_{h1} = V_r - (V_{f1} + V_{f2} + V_{h2})$$
(6.7)

The calculations for all four of the components are summarized in Table 6.2. In this table, the calculations for components V_{f1}, V_{f2} and V_{h2} are based entirely on measured data and the component V_{h1} is determined as shown in Equation 6.7. The kink length, L_2, is calculated according to the relationships defined in Figure 6.1(b), using the measured bar strains. The deformed length, L_1, is assumed as necessary to provide the required value of V_{h1} based on the assumed flexural mechanism shown in Figure 6.1(a). From the calculations for component V_{h1}, it appears that plastic hinge formation will occur at an applied slip magnitude between 2.0 mm and 3.0 mm. After the formation of plastic hinges, a progression of the plastified region must occur, due to the cyclic loading, to produce a decreasing contribution from component V_{h1}. The formation of plastic hinges at a slip magnitude between 2.0 mm and 3.0 mm corresponds very well with the assumed progression of the two mechanisms. As described previously, initially the flexural mechanism and component V_{h1} are assumed to dominate the shear resistance contribution from the continuity reinforcement. After the formation of plastic hinges due to flexural deformation, the kinking mechanism is assumed to develop and the shear resistance contribution from component V_{f2} becomes significant. In Figure 6.5, it is clear that the increase of bar force is not significant until a slip magnitude of 3.0 mm. This suggests that the kinking mechanism begins at a slip magnitude of 3.0 mm, which corresponds to the formation of plastic hinges due to the flexural mechanism.

Prediction of the components V_{h1}, V_{f2} and V_{h2} requires prediction of the forces within the continuity bars. From Figure 6.1(a) and (b), it is evident that this task requires the

deformed length, L_1, for component V_{h1}, and the kink length, L_2, for components V_{f2} and V_{h2}. The variation of the deformed length and the kink length, determined from the experimental results as described in the preceding paragraph, is shown in Figure 6.6. The two lengths appear to be unrelated. Because both the flexural mechanism and the kinking mechanism are assumed idealizations or approximations of the actual behaviour, it is not suprising that the two lengths are quite different. With only limited data from one specimen, it is difficult to fully evaluate the deformed length and the kink length based on experimental results. A database of several specimens could be used to determine a relationship for the two lengths, but lacking this, the deformed length and kink length can not be determined with confidence.

6.2.5   Variation of the Components of Shear Resistance

The variation of the four shear resistance components based on the assumed shear resistance mechanisms is shown in Figure 6.7, up to an applied slip magnitude of 8.0 mm. In this figure, only the positive loading direction of the shear resistance - slip envelope is shown for clarity. The components V_{f1}, V_{f2} and V_{h2} are determined using measured experimental data, and component V_{h1} is determined by subtracting the known components from the total measured shear resistance, as described in Section 6.2.4.2. The contribution and significance of the four components over the duration of the experiment are illustrated clearly in this figure. It appears that the assumed shear resistance mechanisms proposed in the previous section can be used to reasonably describe the behaviour of this type of connection under cyclic shear loading conditions, based on the measured data.

6.3   SPECIMEN PTS

The shear resistance of plain surface connections with post-tensioning is provided by interface friction. Stage I describes elastic behaviour prior to the initiation of slip. Interface

friction is provided by the applied vertical load and the prestressing. During Stage II, the behaviour is inelastic and the shear resistance remains constant. The applied vertical load and the prestressing of the connection continues to provide interface friction. In the third stage, the dry pack crushes and spalls extensively and a significant reduction of the shear resistance occurs. Crushing of the dry pack results in a complete loss of prestressing and interface friction is provided by the applied vertical load only.

6.3.1   Stage I - Initiation of Slip

Similar to the behaviour of Specimen RW, the initiation of slip occurred gradually without sudden cracking. This suggests that the bond between the dry pack and the concrete panels was negligible. If bond is not present, the initiation of slip will occur when the applied shear force exceeds the frictional resistance of the connection, provided by the applied vertical load and the post-tensioning force on the connection. The frictional resistance of the connection can be determined as described in Section 2.3.1 (Hutchinson (17,18)) and Section 5.8.2.3, using Equation 2.6. On the basis of the interface friction mechanism and the measured shear resistance at the initiation of slip of 530 kN, a coefficient of friction of $\mu = 0.92$ is obtained.

6.3.2   Stage II - After the Initiation of Slip

The initiation of slip was observed at the interface between the lower precast concrete panel and the bottom surface of the dry pack. The behaviour of the connection during this stage was inelastic and the measured shear resistance remained constant at approximately 525 kN in both directions of loading. The shear resistance of the connection is provided only by interface friction due to the absence of rigid continuity reinforcement or shear keys. Because the measured shear resistance of the connection remained consistent during Stage II of behaviour, it is likely that the coefficient of friction remains constant. In addition, the constant

shear resistance suggests that the effective prestressing force on the connection remained unchanged.   As described in Section 5.8.2.3, the shear resistance of this connection configuration during Stage II of cyclic behaviour can be described by the monotonic loading model proposed by Hutchinson (17,18). The measured shear resistance of 525 kN during Stage II results in a coefficient of friction of $\mu = 0.91$. The interface friction can be separated into two components to illustrate the contribution of the applied vertical load and the contribution of the post-tensioned strands.

$$V_r = V_{f1} + V_{f3} \tag{6.8}$$

Component V_{f1} is the frictional resistance provided by the simulated gravity load, and is estimated as:

$$V_{f1} = \mu \, \sigma_{n1} \, A_c \tag{6.2}$$

where

μ = coefficient of friction

= 0.91 (determined above)

σ_{n1} = average vertical stress acting on dry pack due to applied vertical load

= P_g / A_c (F_{boi} is zero)

A_c = cross-sectional area of the connection

Component V_{f1} was illustrated previously in Figure 6.2. In the case of Specimen PTS, F_{boi} is zero and V_{f1} does not vary over the duration of Stage II.

Component V_{f3} is the frictional resistance provided by post-tensioning of the connection, and is estimated as:

$$V_{f3} = \mu \sigma_{n3} A_c \qquad\qquad (6.9)$$

where

μ = coefficient of friction

    = 0.91 (determined above)

σ_{n3} = average vertical stress acting on dry pack due to post-tensioning

$$= \frac{n[F_{pe}]}{A_c}$$

n   = number of strands

F_{pe} = effective prestressing force per strand

A_c = cross-sectional area of the connection

Component V_{f3} is illustrated in Figure 6.8. For Specimen PTS, component V_{f3} does not vary during Stage II of behaviour.

6.3.3   Stage III - After Crushing of the Dry Pack

Failure of the connection was initiated by extensive crushing of the dry pack. After failure, crushing and spalling of the dry pack continued but the shear resistance of the connection remained consistent at a reduced level of approximately 220 kN. The crushing of the dry pack at failure produced a complete loss of prestressing. As a result, the contribution from component V_{f3} is reduced to zero and the shear resistance of the connection during Stage

III is provided by component V_{f1} only. In addition, similar to the behaviour observed for Specimen DP during Stage III, the coefficient of friction will be reduced. Considering the loss of prestressing and the measured shear resistance of 220 kN, a friction coefficient of $\mu = 0.62$ is obtained for Stage III of behaviour.

6.3.4 Variation of the Components of Shear Resistance

The overall cyclic shear behaviour of the connection is defined by the envelope of the shear resistance - slip behaviour, as shown in Figure 4.19. By separating the interface friction provided by the applied vertical load and the post-tensioning force on the connection into two components, the contribution of the two components over the duration of loading can be illustrated. The variation of the two components, V_{f1} and V_{f3}, is shown in Figure 6.9 with the envelope of shear resistance - slip behaviour. Similar to Figure 6.7 for Specimen RW, only the positive loading direction of the envelope is shown for clarity. During Stage II of behaviour, both components contribute to the shear resistance of the connection. After failure, in Stage III of behaviour, the interface friction due to post-tensioning, V_{f3}, is reduced to zero and the contribution from the applied vertical load is diminished due to the reduction of the friction coefficient, μ. It appears that the shear resistance mechanisms proposed in the previous research by Hutchinson can be modified as described in the preceding sections to reasonably describe the behaviour of this type of connection under cyclic loading conditions.

6.4 SPECIMEN PTB-S

Specimen PTB-S was tested under monotonic loading to determine the static behaviour of the connection, since this configuration was not considered in the previous research at the University of Manitoba (10,11,17,18,29,30). During Stage I of behaviour, prior to the initiation of slip, the shear resistance of the connection is provided by interface friction.

Interface friction is produced by the simulated gravity load normal to the connection and the post-tensioning of the connection. After the initiation of slip, during Stage II of behaviour, the shear resistance remained constant until the applied slip reached 10 mm and the shear resistance is provided by interface friction. As the applied slip is increased beyond 10 mm, the shear resistance of the connection increases. The shear resistance of the connection during this portion of the experiment is provided by a combination of interface friction and the resistance of the post-tensioning bars to deformation. The dry pack remained intact over the duration of the experiment, and therefore, Specimen PTB-S did not experience the equivalent of Stage III of behaviour.

6.4.1   Stage I - Initiation of Slip

The initiation of slip for Specimen PTB-S occurred gradually, indicating that bond was not present at the interface between the dry pack and the precast concrete panels. Therefore, the initiation of slip will occur when the applied shear loading exceeds the frictional resistance of the connection. The measured shear resistance of the connection at the initiation of slip was 555 kN. Similar to Specimen PTS, the interface friction is provided by the simulated gravity load and by post-tensioning of the connection. Using the same procedure described for Specimen PTS in Section 5.8.2.3, a slightly higher friction coefficient of $\mu = 0.96$ is obtained at the initiation of slip for Specimen PTB-S.

6.4.2   Stage II - After the Initiation of Slip

The initiation of slip occurred at the interface between the dry pack and the lower precast concrete panel. As described in Section 5.1.6, from the initiation of slip up to an applied slip of 10 mm, the measured shear resistance remained constant at approximately 550 kN. This value is very close to the shear resistance at the initiation of slip and the

measured shear resistance of Specimen PTS during Stage II of behaviour. This suggests that initially, the shear resistance of Specimen PTB-S is provided by interface friction due to the applied vertical preload and the prestressing of the connection. Also, because the shear resistance remains very consistent, the friction coefficient, μ, and the effective prestressing force on the connection must be constant during this portion of loading. On the basis of the measured shear resistance and the assumption of interface friction, a coefficient of friction of $\mu = 0.95$ is obtained. This value is close to the friction coefficient measured for Specimen PTS. It should be noted that Specimen PTS and Specimen PTB-S have an identical panel design and were dry packed at the same time, therefore it is not surprising that the friction coefficients are similar.

As described previously, the shear resistance of the connection began to increase when the applied slip exceeded 10 mm. It is assumed that the increase of the shear resistance is provided by the resistance of the post-tensioned bars to deformation, similar to the contribution of the mild steel continuity bar to the shear resistance of Specimen RW (Section 6.2.2). Unfortunately, the strain gauge readings had become unreliable at this point of the experiment, and therefore it is not possible to determine the shear resistance mechanisms provided by the post-tensioning bars based on the experimental results. Considering the shear resistance mechanisms proposed for Specimen RW, it is possible to suggest a similar approach to describe the mechanisms associated with the post-tensioning bars. In the case of Specimen PTB-S, it is not likely that the flexural mechanism, illustrated in Figure 6.1(a), will be significant due to the small flexural rigidity of the post-tensioning bars. Therefore, it can be reasonably assumed that the increase of the shear resistance is provided mainly by the kinking mechanism, illustrated in Figure 6.1(b). As the horizontal slip between the panels increases beyond 10 mm, a tensile force increase is induced within the bars, increasing the vertical stress on the dry pack. This will increase the frictional resistance of the connection. In addition, the horizontal component of the tensile force increase in the bar will directly resist the applied

shear loading. Because the experimental results did not measure an increase of the shear resistance until the applied slip exceeded 10 mm, this indicates that the kinking mechanism did not develop until this point. The delayed onset of the kinking mechanism may be attributed to the placement of the post-tensioning bars within ducts in the concrete panels. The ducts were filled with grout after post-tensioning. The grout, essentially a mixture of cement and water, has a very low stiffness and therefore a larger amount of slip deformation is required to initiate the kinking mechanism than if the bars were cast within concrete, as in the case of the mild steel continuity bars in Specimen RW.

The shear resistance of the connection can be separated into three components to illustrate the contribution of the applied vertical preload and the contribution of the post-tensioned bars. The contribution of the bars may be treated in a manner similar to the shear resistance components associated with the kinking mechanism, V_{f2} and V_{h2}, proposed for Specimen RW. The differences for Specimen PTB-S are that there is an initial tensile strain in the bars, and that the tensile force increase due to kinking action does not initiate until an applied slip of approximately 10 mm has been reached. On the basis of these observations, the total shear resistance, V_r, of Specimen PTB-S can be described in three components:

$$V_r = V_{f1} + V_{f4} + V_{h3} \qquad (6.10)$$

Each of the shear resistance components are described in detail below.

Component V_{f1}:

The component V_{f1} represents the frictional resistance provided by the simulated gravity load acting on the cross-sectional area of the connection. Component V_{f1} was illustrated previously in Figure 6.2. In the case of Specimen PTB-S, the entire gravity load in

resisted by the dry pack and therefore F_{boi} is zero. For Specimen PTB-S, V_{f1} is estimated as follows:

$$V_{f1} = \mu \sigma_{n1} A_c \qquad (6.2)$$

where

μ = coefficient of friction

= 0.95 (determined above)

σ_{n1} = average vertical stress acting on dry pack due to simulated gravity load

= P_g / A_c (F_{boi} is zero)

P_g = simulated gravity load (vertical preload)

A_c = cross-sectional area of the connection

For Specimen PTB-S, the component V_{f1} will not vary over the duration of the monotonic loading.

Component V_{f4}:

The component V_{f4} represents the frictional resistance provided by the tensile force in the post-tensioning bars, as shown in Figure 6.10. Initially, the force in the bars is due to prestressing only. If the applied slip exceeds 10 mm, the kinking mechanism is initiated, further increasing the tensile force in the bars and thus increasing the frictional resistance of the connection. Component V_{f4} can be estimated as follows:

$$V_{f4} = \mu \sigma_{n4} A_c \qquad (6.11)$$

where

μ = coefficient of friction

= 0.95 (determined above)

σ_{n4} = average vertical stress due to tensile force in post-tensioning bars

$$= \frac{n[F_{pe}]}{A_c}$$ if the applied slip is less than or equal to 10 mm

$$= \frac{n[F_{byi}]}{A_c}$$ if the applied slip exceeds 10 mm

n = number of bars

F_{pe} = effective prestressing force per bar

F_{byi} = vertical component of tensile force per bar, F_b, at applied slip i

F_{bi} = tensile force per bar at applied slip i

$$= F_{pe} + \Delta F_{bi}$$

ΔF_{bi} = tensile increase of bar force due to the kinking mechanism (defined in Figure 6.1(b) and Figure 6.10)

A_c = cross-sectional area of the connection

The tensile increase of the bar force due to the kinking mechanism is initiated if the applied slip exceeds 10 mm. This will increase the total tensile force in the bars and thus the vertical stress on the dry pack. As a result, the frictional resistance of the connection is increased.

Component V_{h3}:

The component V_{h3} is the horizontal component of the tensile force in the post-tensioning bars, as shown in Figure 6.10. The component V_{h3} does not develop until the applied slip exceeds 10 mm and the bars are deformed. V_{h3} may be estimated as follows:

$$V_{h3} = n\, [\, F_{bxi}\ ]$$
(6.12)

where

n   = number of bars

F_{bxi} = horizontal component of the tensile force per bar, F_b, at applied slip i

F_{bi} = tensile force per bar at applied slip i

     $= F_{pe} + \Delta F_{bi}$

F_{pe} = effective prestressing force per bar

ΔF_{bi} = tensile increase of bar force due to the kinking mechanism (defined in Figure 6.1(b) and Figure 6.10)

As mentioned above, component V_{h3} does not develop unless the applied slip exceeds 10 mm, and then increases as the applied slip is increased.

6.4.3   Evaluation of the Proposed Mechanisms Using Experimental Results

The overall shear resistance - slip behaviour of Specimen PTB-S was shown previously in Figure 4.6. Similar to the method used for Specimen RW, the experimental results can be utilized to examine the shear resistance mechanisms proposed for Specimen PTB-S in the previous sections. The interface friction resistance mechanism is well defined and may be used

with confidence in situations where the vertical force on the dry pack is due to the simulated gravity load and the post-tensioning force. If the applied slip exceeds approximately 10 mm, an increase of the shear resistance may occur. It is difficult to define the shear resistance mechanisms responsible for the increase lacking reliable strain gauge readings. In the previous section, it is proposed that the increase of the shear resistance is provided by the kinking mechanism. Although this can not be confirmed by experimental results, it is a reasonable assumption and may be used to describe the behaviour.

Prediction of the components V_{f4} and V_{h3} requires prediction of the tensile increase of force in the bars. Using the proposed kinking mechanism, illustrated in Figure 6.1(b), the tensile force increase at a given applied slip magnitude can be determined of the kink length, L_2, is known. Unfortunately, reliable strain gauge readings are not available for this portion of the experiment. With data from only one specimen, it is difficult to fully evaluate the kink length, and without an indication of the force within the bars, the kink length can not be determined with any level of confidence.

In practical terms, it would be extremely rare to reach a relative horizontal slip of 10 mm between the panels. A slip of this magnitude would certainly contribute to other forms of distress, such as instability, in the structure. Therefore, for design purposes, the shear resistance of the connection may be determined using simply the interface friction provided by the vertical gravity loads and the post-tensioning force on the connection.

6.4.4   Variation of the Components of Shear Resistance

The variation of the proposed components of shear resistance is shown in Figure 6.11. The measured shear resistance - slip behaviour is also shown in the figure. At applied slip values larger than 10 mm, the assumed variation of components V_{f4} and V_{h3} is shown since the

actual magnitudes of these components can not be determined with confidence from the experimental results.

6.5   SPECIMEN PTB

The shear resistance of a plain surface connection, post-tensioned with high strength bars, is provided primarily by interface friction. Interface friction is produced by the simulated gravity load and the effective post-tensioning force on the connection. Stage I describes elastic behaviour prior to the initiation of slip with the shear resistance of the connection provided entirely by interface friction. Stage II of behaviour describes the inelastic behaviour after the initiation of slip. Over the duration of loading, the shear resistance, provided by interface friction, decreases. Stage III of behaviour is initiated by extensive crushing and spalling of the dry pack and a significant loss of shear resistance. A loss of prestressing occurs and the shear resistance of the connection is provided by interface friction due to the simulated gravity load and by the resistance of the bars to deformation.

6.5.1   Stage I - Initiation of Slip

The initiation of slip for Specimen PTB occurred gradually. The observed behaviour was almost identical to that of Specimen PTB-S. This suggests that similarly, bond was not present at the interface between the dry pack and the precast concrete panels and therefore, the initiation of slip will occur when the applied shear loading exceeds the frictional resistance of the connection. The measured shear resistance at the initiation of slip was 530 kN. On the basis of this value, a friction coefficient of 0.92 is obtained. This friction coefficient is identical to the value obtained for Specimen PTS, suggesting that at the initiation of slip, the form of post-tensioning does not affect the shear resistance of the connection.

6.5.2 Stage II - After the initiation of Slip

The initiation of slip was observed at the interface between the top surface of the dry pack and the upper precast concrete panel. The behaviour of this connection configuration under monotonic loading, observed for Specimen PTB-S, indicated that following the initiation of slip, the shear resistance of the connection is provided by interface friction only and remains constant for an applied slip less than 10 mm. Under the effects of cyclic loading, Specimen PTB experienced a gradual loss of shear resistance during Stage II of behaviour and did not reach an applied slip magnitude of 10 mm due to failure as a result of crushing of the dry pack. Therefore, it is reasonable to assume that the shear resistance mechanism for Specimen PTB during Stage II of behaviour is provided by interface friction only. The gradual loss of shear resistance during Stage II may be attributed to a loss of prestressing, indicated by strain gauge readings from the post-tensioning bars during Stage II (Section 5.1.4). The coefficient of friction during Stage II is assumed to remain constant, based on the observed behaviour of Specimen PTS. The magnitude of the friction coefficient, μ, for Specimen PTB is determined to be 0.94. This is based on the measured shear resistance after the initiation of slip during the first cycle to an applied slip magnitude of 1.0 mm.

The shear resistance of Specimen PTB can be described using the same approach proposed for Specimen PTB-S, with some minor modifications to account for the effects of the cyclic loading. The shear resistance is as follows:

$$V_r = V_{f1} + V_{f4} + V_{h3} \qquad (6.10)$$

Because an applied slip of 10 mm was not attained during Stage II by Specimen PTB under cyclic loading, component V_{h3} does not develop and the shear resistance of the connection may be simply given as:

$$V_r = V_{f1} + V_{f4} \qquad (6.13)$$

Each of the shear resistance components are described in detail below.

Component V_{f1}:

The component V_{f1} represents the frictional resistance provided by the simulated gravity load acting on the cross-sectional area of the connection. Component V_{f1} was illustrated previously in Figure 6.2. In the case of Specimen PTB during Stage II, the entire gravity load in resisted by the dry pack and therefore F_{boi} is zero. V_{f1} is estimated as follows:

$$V_{f1} = \mu \, \sigma_{n1} \, A_c \qquad (6.2)$$

where

μ = coefficient of friction

= 0.94 (determined above)

σ_{n1} = average vertical stress acting on dry pack due to simulated gravity load

= P_g / A_c (F_{boi} is zero)

P_g = simulated gravity load (vertical preload)

A_c = cross-sectional area of the connection

For Specimen PTB, the component V_{f1} will not vary over the duration of Stage II.

Component V_{f4}:

The component V_{f4} represents the frictional resistance provided by the tensile force in the post-tensioning bars, as shown in Figure 6.10. Because the applied slip magnitude during Stage II does not exceed 10 mm, it is assumed that the kinking mechanism does not develop. The effect of the gradual loss of prestressing is considered by using the effective prestressing force at the start of the cycles to a given applied slip magnitude. This will account for the loss of prestressing during the preceding cycles. Component V_{f4} can be estimated as follows:

$$V_{f4} = \mu \sigma_{n4} A_c \tag{6.11}$$

where

μ = coefficient of friction

    = 0.94 (determined above)

σ_{n4} = average vertical stress acting on dry pack due to effective prestressing force

$$= \frac{n[F_{pei}]}{A_c}$$

n   = number of bars

F_{pei} = effective prestressing force per bar at applied slip magnitude i

A_c = cross-sectional area of the connection

Since the effective prestressing force per bar decreases as the applied slip magnitude increases, component V_{h4} will decrease over the duration of loading.

6.5.3   Stage III - After Crushing of the Dry Pack

Stage III was initiated by failure of the connection, caused by extensive crushing and spalling of the dry pack. Failure of the connection occurred during the three cycles at an applied slip magnitude of 10 mm. At the beginning of Stage III, the shear resistance was reduced significantly, to approximately 115 kN. As the applied slip magnitude was increased, the maximum measured shear resistance during each cycle began to increase.

Crushing of the dry pack during this stage results in a complete loss of prestressing. Similar to the behaviour observed for Specimen DP and Specimen PTS, the coefficient of friction will also be reduced during Stage III. The measured shear resistance of Specimen PTS during Stage III was 220 kN, approximately 100 kN greater than the shear resistance of Specimen PTB. Specimen PTS and Specimen PTB have an identical panel design and were dry packed at the same time. Therefore, it is likely that the coefficients of friction will be similar for these two specimens. If the friction coefficients are equal, the lower shear resistance of Specimen PTB suggests that the reduction of the connection thickness due to crushing of the dry pack has caused the bars to resist a portion of the simulated gravity load. This will reduce the vertical stress on the dry pack due to the simulated gravity load, and therefore will reduce the shear resistance of the connection.

As described in Section 5.1.4, the maximum shear resistance of the connection increased during the cycles at 14 mm and 16 mm. Similar to the behaviour of Specimen PTB-S at an applied slip greater than 10 mm and the behaviour of Specimen RW, it is possible that the increase of shear resistance is provided by the resistance of the bars to lateral deformation. In fact, because the post-tensioning of the connection is no longer effective and the force within the bars is compressive, the shear resistance mechanisms of Specimen PTB during Stage III are very similar to the mechanism of Specimen RW during Stage II. From Section 6.2.2:

$$V_r = V_{f1} + V_{h1} + V_{f2} + V_{h2} \qquad (6.3)$$

Because the flexural resistance of the post-tensioning bars is very small, the contribution from component V_{h1} will be minimal and may be neglected. Therefore, the shear resistance of Specimen PTB during Stage III of behaviour can be described as:

$$V_r = V_{f1} + V_{f2} + V_{h2} \qquad (6.14)$$

where

V_{f1} is the frictional resistance due to the net gravity load acting on the connection
(Equation 6.2)

V_{f2} is the frictional resistance due to clamping action (Equation 6.5)

V_{h2} is the direct shear resistance due to the kinking mechanism (Equation 6.6)

These shear resistance components were described previously in detail in Section 6.2.2. For Specimen PTB during Stage III of behaviour, the coefficient of friction will be $\mu = 0.62$, as described above.

6.5.4   Evaluation of the Proposed Mechanisms Using Experimental Results

The overall cyclic shear behaviour of the connection is defined by the envelope of the shear resistance - slip behaviour, as shown in Figure 4.20. The measured experimental data can be utilized to examine the shear resistance mechanisms proposed in the previous sections. Similar to the method used for Specimen RW, an average of the measured data at each applied

slip magnitude was addressed separately to consider the effects of the cyclic loading during the previous cycles.

6.5.4.1 Evaluation of Component V_{fl} (F_{boi})

Component V_{fl} represents the interface friction provided by the simulated gravity load acting on the dry pack. During Stages I and II, the coefficient of friction does not change and the entire gravity load acts on the dry pack. Therefore, component V_{fl} remains constant during the first two stages of behaviour. During Stage III, the contribution from component V_{fl} is reduced due to a lower friction coefficient and the redistribution of vertical forces at the connection due to crushing of the dry pack. Upon crushing, a portion of the applied vertical load is resisted by the bars, reducing the vertical stress on the dry pack. As mentioned previously, the forces within the bars are unknown during this stage of the experiment due to the lack of reliable strain gauge readings. However, the force distribution at the connection level may be estimated by considering the shear resistance of the connection at the zero slip position. When the connection is at the zero slip position during a given cycle, it is assumed that the bars are in a vertical position and therefore there is no contribution from the kinking mechanism. On the basis of this assumption, the shear resistance of the connection at this position must be provided by interface friction only, and the vertical stress on the dry pack can be determined using the assumed friction coefficient of $\mu = 0.62$. The calculations for the last cycle at 10 mm and the cycles at 12 mm, 14 mm and 16 mm are shown in Table 6.3. From these values, it appears that for design purposes, it could be assumed that 50% of the simulated gravity load is resisted by the bars during Stage III.

6.5.4.2 Evaluation of Component V_{f4} (F_{pei})

During Stages I and II, evaluation of component V_{f4} requires the effective prestressing force on the connection, F_{pei}. As described previously, a gradual reduction of the effective prestressing force occurs over the duration of Stage II. This is indicated by the variation of prestressing strain at the zero slip position, shown previously in Figure 5.33, and confirmed by the gradual loss of shear resistance. Unfortunately, the strain gauge data is only available up to an applied slip magnitude of 4 mm and thus the data must be extrapolated to consider larger slip magnitudes. This task is simplified by considering the overall measured shear resistance and the contribution of component V_{f1} during Stage II. The contribution from component V_{h4} can be determined by subtracting component V_{f1} from the measured shear resistance as shown below.

$$V_{f4} = V_r - V_{f1}$$

Based on the computed contribution from component V_{f4}, the effective prestressing force can be determined. The calculations for the effective prestressing strains are shown in Table 6.4. The loss of prestressing may be attributed to the gradual reduction of the thickness of the dry pack. Similar to Specimen RW, the relationship between the loss of prestressing and the reduction of the dry pack suggests that a length of the bars has become unbonded, allowing the change of strain at the connection to distribute over a longer "gauge length". Additional testing is necessary to define this relationship in general terms.

For practical purposes, the worst case scenario should be assumed until the relationship between the loss of prestressing and reduction of the dry pack thickness is defined. Therefore, a complete loss of prestressing should be assumed during Stage II of behaviour.

6.5.4.3 Evaluation of Components V_{f2} and V_{h2} (L_2)

During Stage III of behaviour, the components V_{f2} and V_{h2} are a function of the tensile force increase in the bars due to the kinking mechanism illustrated in Figure 6.1(b). The kink length, L_2, is required to evaluate the tensile force increase in the bars. Similar to Specimen PTB-S, reliable strain gauge readings are not available and therefore the kink length can not be evaluated with confidence without additional data. For design purposes, the shear resistance of the connection may be determined using simply the interface friction provided by the simulated gravity load.

6.5.5 Variation of the Components of Shear Resistance

The variation of the components V_{f1} and V_{f4} based on the assumed mechanisms is shown in Figure 6.12. Once again, only the positive loading direction of the shear resistance - slip envelope is shown for clarity. Components V_{f1} and V_{f4} are determined using measured data. After failure of the connection, during Stage III of behaviour, the assumed variation of components V_{f2} and V_{h2} is shown since the actual magnitude of these components can not be determined with confidence from the experimental results.

6.6 SPECIMEN SK

The observed behaviour of Specimen SK was somewhat different than the plain surface connections. Stage I describes elastic behaviour prior to the initiation of slip and the shear resistance is provided by interface friction. During Stage II, the behaviour of the connection is inelastic. A significant increase of the shear resistance is measured and slip is limited to less than 1 mm. The shear resistance of the connection is provided by a combination of interface friction and direct bearing on the dry pack within the shear keys. Failure occurs

due to simultaneous cracking of the dry pack within all five of the shear keys. During Stage III, extensive crushing and spalling of the dry pack occurs and a uniform sliding plane develops. The shear resistance of the connection is constant at a reduced level and is provided by interface friction along the newly formed uniform sliding plane.

6.6.1   Stage I - Initiation of Slip

The initiation of slip for Specimen SK is difficult to detect. Up to and including an applied shear load level of 400 kN, no measurable slip was observed and the behaviour of the connection was elastic. As the applied shear load was increased, a very small amount of slip was measured but it was not until an applied shear load level of 650 kN that 0.1 mm of slip was measured in both directions of loading (in this experimental program, the initiation of slip was defined as the point at which 0.1 mm slip was measured in both directions of loading). In the case of Specimen SK, the initiation of slip has clearly occurred prior to this point. The initiation of slip will occur when the applied shear loading exceeds the frictional resistance of the connection. For Specimen SK, when the frictional resistance is exceeded, bearing on the shear keys occurs immediately and therefore, the slip is limited and the shear resistance continues to increase. For this reason, the initiation of slip is not a significant limit state for connection configurations with multiple shear keys.

6.6.2   Stage II - After the Initiation of Slip

After the initiation of slip, the behaviour of the connection is inelastic. During Stage II, the slip was limited to less than 1 mm, and the shear resistance increased to a maximum of 850 kN. During this stage, the shear resistance of the connection is provided by a combination of interface friction and direct bearing on the dry pack within the shear keys. The shear resistance of the connection during Stage II is limited by the cracking strength of the dry pack

within the shear keys. Once cracking of the dry pack occurs, the bearing mechanism is destroyed and a significant reduction of the shear resistance occurs. The cracking shear resistance of the connection was proposed in the previous research at the University of Manitoba by Serrette (29,30) and is described in Section 2.3.1 and Section 5.8.2.4. As described in Section 5.8.2.4, it appears that cyclic loading did not have an effect on the cracking strength of the connection, and the previously proposed model for the cracking strength under monotonic loading (Equation 2.3) can be used directly for cyclic loading conditions.

6.6.3   Stage III - After Cracking of the Dry Pack Within the Shear Keys

Failure of the connection was initiated by sudden and simultaneous cracking of the dry pack within each of the shear keys. Cracking of the connection was accompanied by approximately a 50% reduction of the shear resistance. Following cracking of the connection, the loading direction was reversed, destroying the strut mechanism proposed by Serrette (29,30) (described in Section 2.3.1 and shown in Figure 2.10). After several additional cycles of loading, a uniform sliding plane developed along the length of the connection and the shear resistance was stabilized at a consistent level of approximately 335 kN. At this point, the shear resistance of the connection is provided by interface friction along the newly formed uniform sliding plane. Because the sliding plane consists of both panel-to-dry pack regions and dry pack-to-dry pack regions within the shear keys, the frictional resistance of the connection is not as simple as the plain surface connection of Specimen DP after crushing of the dry pack. The observed behaviour of Specimen SK during Stage III corresponds to the ultimate behaviour of the specimens tested under monotonic loading conditions by Serrette. As described in Section 5.8.2.4, it appears that cyclic loading did not have an effect on the shear resistance of the connection after the formation of a uniform sliding plane. Therefore, the ultimate strength

model proposed by Serrette (Equation 2.5) appears to be applicable to the cyclic loading conditions during Stage III of behaviour.

CHAPTER 7

PROPOSED MODELS (PREDICTION OF BEHAVIOUR)

7.0 INTRODUCTION

Behaviour of the connections under cyclic lading conditions can be predicted by evaluating the envelope of the shear resistance - slip relationship, using the proposed shear resistance mechanisms. The experimental results were used to simplify and calibrate the mechanisms as described in the preceding chapter. In this chapter, a methodology for using the proposed mechanisms and design assumptions to approximate the behaviour of the connection during each stage of behaviour is presented. The calculations for the shear resistance - slip envelope are described by stage in the following sections.

7.1 SPECIMEN DP

For plain surface connections with dry pack only, the behaviour of the connection does not vary significantly during each stage. Therefore, the cyclic connection behaviour can be predicted by simply determining the shear resistance of the connection at three limit states; the initiation of slip (at the end of Stage I), after the initiation of slip (during Stage II) and after crushing of the dry pack (during Stage III).

7.1.1 Stage I

Although the procedure described in section 6.1.1 for predicting the cracking strength of the connection appears to be satisfactory, as discussed in section 5.3, in general, it is not

possible to predict whether bond is present at the interface between the dry pack and the precast concrete panels prior to loading. Therefore, it may be unconservative to assume that bond is present and to use this approach to predict the initiation of slip. For design purposes, the initiation of slip should be assumed occur when the applied shear loading exceeds the frictional resistance of the connection. The frictional resistance of the connection was discussed previously in section 5.8.2.1 and in Chapter 6 for the other connection configurations. Using the apparent coefficient of friction of $\mu = 0.8$, determined in Section 5.8.2.1, the shear resistance of the connection is calculated as follows:

$$
\begin{aligned}
V_{r_1} &= \mu \, \sigma_n \, A_c \\
&= 0.8 \, (4\,\text{MPa}) \, (150{,}000\text{mm}^2) \\
&= 480 \text{ kN}
\end{aligned}
$$

The variables in the above expression have been defined previously. The predicted shear resistance of 480 kN is 10% less than the measured shear resistance of 533 kN. For design purposes, this approach may be used to conservatively predict the shear resistance of the connection at the initiation of slip.

7.1.2 Stage II

After the initiation of slip but prior to significant deterioration of the dry pack, the behaviour of the connection is inelastic and the shear resistance is provided by interface friction. During this stage, the apparent coefficient of friction is $\mu = 0.8$. The frictional resistance of the connection is determined using the same procedure shown above for Stage I of behaviour. Therefore, the shear resistance of the connection during Stage II is:

$$
V_{r_{II}} = 480 \text{ kN}
$$

The predicted shear resistance is equal to the measured value of 480 kN. In the previous research of the monotonic shear behaviour of the connections, the coefficient of friction was proposed as $\mu = 0.7$. Therefore, the value proposed for static loading could be used to conservatively predict the shear resistance of the connection during Stage II of cyclic behaviour.

7.1.3 Stage III

After failure of the connection, the shear resistance decreases and can be predicted using the same approach described for Stages I and II, but with a reduced friction coefficient of $\mu = 0.7$ due to extensive deterioration of the dry pack. The shear resistance of the connection during Stage III is calculated using the friction model as:

$$V_{r_{III}} = 420 \text{ kN}$$

The predicted shear resistance is equal to the measured value of 420 kN. A friction coefficient of $\mu = 0.6$ could be used for design purposes to conservatively predict the shear resistance of the connection during Stage III of cyclic behaviour.

7.1.4 Summary of Predicted Shear Resistance for Design Purposes

The calculations described above for each stage of behaviour were repeated using the friction coefficients proposed for design purposes. The values are presented in Table 7.1. The predicted design values are consistently conservative.

7.2 SPECIMEN RW

Under cyclic shear loading conditions, the behaviour of plain surface connections with dry pack and mild steel continuity reinforcement is rather complex. On the basis of the discussion in Chapter 6, there is insufficient experimental data to refine the proposed mechanism into a general design procedure at this time. In view of this, the cyclic connection behaviour must be approximated.

7.2.1 Stage I

During Stage I, the behaviour of the connection is elastic and very stiff. Prior to the initiation of slip between the panels, no measurable deformations occur at the connection. For design purposes, the initiation of slip may be assumed to occur when the frictional resistance of the connection is exceeded. The procedure proposed in the previous research by Foerster (10,11) may be used, ignoring the contribution of the continuity bars. Therefore, using Equation 2.2, the shear resistance at the initiation of slip may be approximated as:

$$V_{r_1} = \mu \, \sigma_n \, A_c$$

where

$\mu \quad = 0.7$

$\sigma_n \quad = 2 \, \text{MPa}$

$A_c \quad = 180,000 \, \text{mm}^2$

Thus

$$V_{r_I} = 252 \text{ kN}$$

This approach may be used to conservatively predict the initiation of slip under cyclic loading conditions.

7.2.2   Stage II

During Stage II, the behaviour of the connection is inelastic and the shear resistance of the connection is provided by all four of the shear resistance components, as described in Section 6.2.2 and shown by Equation 6.3 below.

$$V_{r_{II}} = V_{f1} + V_{h1} + V_{f2} + V_{h2}$$

Because the variation of the compressive bar force (F_{boi}) and the deformed and kink lengths (L_1 and L_2) can not rationally be predicted, this approach is not complete and can not be used for design purposes at this point. Therefore, the shear resistance may be predicted using the model proposed by Foerster (10,11), neglecting the contribution from the continuity bars. The shear resistance is determined using Equation 2.2 as follows:

$$V_{r_{II}} = (0.7)(2 \text{ MPa})(180,000 \text{ mm}^2)$$
$$= 252 \text{ kN}$$

7.2.3   Stage III

During Stage III, extensive crushing of the dry pack occurs and a significant reduction of the shear resistance results in failure of the connection. As discussed in Section 6.2.3, the behaviour of the connection during this stage is can not be fully defined from the limited

experimental results of this specimen. Therefore, a rational prediction of the shear resistance of the connection during this stage of behaviour can not be made.

7.2.4 Summary of Predicted Shear Resistance for Design Purposes

The predicted shear resistance of the connection at each stage using the proposed method for design purposes are presented in Table 7.2. The predicted values may seem excessively conservative, but until the behaviour of the connection can be fully defined based on a rational prediction of the mechanisms, this approach should consistently provide a lower bound of behaviour. The predicted shear resistance of Specimen RW using the proposed design recommendations is shown in Figure 7.1 with the measured shear resistance -slip behaviour of the connection

7.3 SPECIMEN PTS

For plain surface connections with dry pack and post-tensioned strands, the behaviour of the connection does not vary significantly during each stage. Therefore, similar to the procedure used for Specimen DP, the cyclic connection behaviour can be predicted by simply determining the shear resistance of the connection at three limit states; the initiation of slip (at the end of Stage I), after the initiation of slip (during Stage II) and after crushing of the dry pack (during Stage III).

7.3.1 Stage I

Prior to the initiation of slip, the behaviour of the connection is elastic. The initiation of slip occurs when the frictional resistance of the connection is exceeded. The initiation of slip

can be predicted using Equation 6.8 with the measured coefficient of friction of $\mu = 0.92$. The shear resistance is determined as follows:

$$
\begin{aligned}
V_{r_I} &= V_{f1} + V_{f3} \\
&= 0.92\,(2\,\text{MPa})\,(180{,}000\,\text{mm}^2) + 0.92(1.2\,\text{MPa})\,(180{,}000\,\text{mm}^2) \\
&= 530 \text{ kN}
\end{aligned}
$$

Components V_{f1} and V_{f3} are given by Equations 6.2 and 6.9. The predicted shear resistance is equal to the measured value of 530 kN. In the previous research, a friction coefficient of $\mu = 0.7$ was proposed for monotonic loading conditions. For design purposes, this value could be used to provide a conservative prediction of the shear resistance at the initiation of slip under cyclic loading.

7.3.2   Stage II

After the initiation of slip, the behaviour of the connection is inelastic and the shear resistance remains constant. The shear resistance during Stage II, provided by interface friction, is determined using the same procedure described above for Stage I with a friction coefficient of $\mu = 0.91$. The shear resistance of the connection is:

$$
V_{r_{II}} = 524 \text{ kN}
$$

The predicted value is equal to the measured shear resistance of 525 kN during Stage II. Once again, the shear resistance of the connection under cyclic loading conditions could be conservatively predicted for design purposes using the previously recommended friction coefficient for monotonic loading of $\mu = 0.7$.

7.3.3 Stage III

During Stage III, excessive crushing of the dry pack causes failure of the connection. The shear resistance of the connection is reduced by a complete loss of prestressing and by a reduced coefficient of friction. The loss of prestressing eliminates the contribution from component V_{f3} and the shear is provided by component V_{f1} only, with a friction coefficient of $\mu = 0.62$. The shear resistance of the connection is:

$$V_{r_{III}} = 0.62\,(2\,\text{MPa})\,(180,000\,\text{mm}^2)$$
$$= 223\ \text{kN}$$

The predicted value agrees very well with the measured shear resistance of 220 kN. Similar to Specimen DP, for design purposes, a friction coefficient of $\mu = 0.6$ could be used for Stage III of behaviour.

7.3.4 Summary of Predicted Shear Resistance for Design Purposes

The predicted shear resistance of the connection at each stage using the friction coefficients proposed for design purposes are presented in Table 7.3. The predicted values are up to 25% less than the measured shear resistance of the connections. Although this may be considered excessive, due to the observed variation of the measured friction coefficients, the proposed values should consistently provide a lower bound of results.

7.4 SPECIMEN PTB-S

Under monotonic loading conditions, the behaviour of plain surface connections with dry pack and post-tensioned bars appears to be similar to the behaviour of connections with

post-tensioned strands. This is true for slip magnitudes less than 10 mm. At larger slip magnitudes, the behaviour of the connection with post-tensioned bars becomes more complex, and as described in Section 6.4.2, can not be explained completely with the limited data from only one experimental specimen. Since a slip of 10 mm would rarely be attained in practical situations, the increase of shear resistance will be ignored for design purposes. Therefore, the monotonic behaviour of the connection can be predicted by considering the shear resistance at two limit states; the initiation of slip and after the initiation of slip. These limit states are equivalent to Stages I and II of behaviour, respectively.

7.4.1 Stage I

Similar to the other plain surface connection configurations, the initiation of slip occurs when the frictional resistance of the connection is exceeded. The frictional resistance of the connection can be determined using Equation 6.10, with a measured friction coefficient of $\mu = 0.96$. Since the applied slip is obviously less than 10 mm, component V_{h3} (Equation 6.12) is zero and component V_{f4} (Equation 6.11) is provided by the initial effective prestressing force on the connection. The shear resistance is determined as:

$$
\begin{aligned}
V_{r_1} &= V_{f1} + V_{f4} \\
&= 0.96\,(2\,\text{MPa})\,(180{,}000\,\text{mm}^2) + 0.96\,(1.2\,\text{MPa})\,(180{,}000\,\text{mm}^2) \\
&= 553\ \text{kN}
\end{aligned}
$$

The predicted shear resistance agrees with the measured value of 555 kN.

7.4.2 Stage II

After the initiation of slip, the shear resistance of the connection continues to be provided by interface friction. For slip magnitudes less than 10 mm, the shear resistance does not increase and interface friction is produced by the simulated gravity load and the effective post-tensioning force on the connection. The shear resistance of the connection is given by Equation 6.10, as shown below.

$$V_{r_{II}} = V_{f1} + V_{f4} + V_{h3}$$

As discussed above, the increase of shear resistance due to the kinking mechanism can not be defined confidently from the experimental results and should be ignored for design purposes. Therefore, the contribution from component V_{h3} should be taken as zero, and the contribution from component V_{f4} will remain constant. Thus for design purposes, the shear resistance of the connection after the initiation of slip can be determined using the same procedure described in Stage I for prediction of the initiation of slip, only with a slightly lower friction coefficient of $\mu = 0.95$. The shear resistance of the connection is:

$$V_{r_{II}} = 547 \text{ kN}$$

The measured shear resistance of 550 kN agrees with the predicted value of 547 kN. Similar to the recommendations for the other connection types, a lower coefficient of friction of $\mu = 0.7$ could be used to provide a conservative prediction of the shear resistance during Stage II of behaviour.

7.4.3   Summary of Predicted Shear Resistance for Design Purposes

The predicted shear resistance of Specimen PTB-S determined using the measured friction coefficients is shown in Figure 7.2 with the measured shear resistance - slip behaviour of the connection. At slip magnitudes larger than 10 mm, the increase of shear resistance has been ignored. The predicted shear resistance of the connection determined using the proposed friction coefficients for design purposes is also shown in Figure 7.2.   The predicted design values are consistently lower than the measured shear resistance.   The calculated shear resistance is also shown in Table 7.4.

7.5   SPECIMEN PTB

Under cyclic shear loading conditions, the behaviour of plain surface connections with dry pack and post-tensioned bars becomes more complicated than the monotonic behaviour of the connection. During Stage II of behaviour, a gradual loss of prestressing occurs due to the cyclic loading.   As described in Section 6.5.4.2, the variation of prestressing can not be rationally predicted.   In the third and final stage of behaviour, it appears that the kinking mechanism may develop in the bars.   Similar to the results of Specimen PTB-S, the contribution from the kinking mechanism can not be evaluated completely and should therefore be ignored for design purposes.

7.5.1   Stage I

Cyclic loading did not have a significant effect on the behaviour of Specimen PTB at the initiation of slip. At the initiation of slip, the full post-tensioning force may be assumed. The shear resistance of the connection can be determined using the same procedure described

for Specimen PTB-S at the initiation of slip. The friction coefficient under cyclic loading is $\mu =$ 0.92. The shear resistance of the connection is:

$$\begin{aligned} \mathrm{V}_{r_I} &= V_{f1} + V_{f4} \\ &= 0.92\,(2\,\mathrm{MPa})\,(180{,}000\,\mathrm{mm}^2) + 0.92\,(1.2\,\mathrm{MPa})\,(180{,}000\,\mathrm{mm}^2) \\ &= 530\ \mathrm{kN} \end{aligned}$$

Components V_{f1} and V_{f4} are determined by Equations 6.2 and 6.11. At the initiation of slip, the component V_{f4} is calculated using the initial effective prestressing strain in the bars. The predicted and measured values for the shear resistance are identical. Similar to the recommendations for Specimen PTS, a friction coefficient of $\mu = 0.7$ could be used to conservatively predict the shear resistance at the initiation of slip.

7.5.2   Stage II

During Stage II, the behaviour of the connection is inelastic and the shear resistance decreases as the applied slip and number of cycles increases. As described in Section 6.5.2, the shear resistance during this stage is provided by interface friction due to the simulated gravity load and the post-tensioning force on the connection. The shear resistance can be determined using Equation 6.13, shown below, with a friction coefficient of $\mu = 0.94$.

$$\mathrm{V}_{r_{II}} = V_{f1} + V_{f4}$$

Because the gradual loss of post-tensioning can not be rationally predicted at this time, for design purposes, the contribution of component V_{f4} should be taken as zero. The shear resistance during Stage II is determined as follows:

$$V_{r_{II}} = V_{f1}$$
$$= (0.94)(2 \text{ MPa})(180,000 \text{ mm}^2)$$
$$= 338 \text{ kN}$$

Component V_{f1} is defined by Equation 6.2. Although this approach may seem excessively conservative, it is necessary considering the lack of a rational model. For consistency, a friction coefficient of $\mu = 0.7$ is recommended for design purposes.

7.5.3 Stage III

In Stage III, extensive crushing of the dry pack causes a complete loss of prestressing and changes the vertical force distribution at the connection level. Initially, the shear resistance of the connection is reduced significantly, but as the applied slip magnitude increases, the shear resistance begins to increase due to the formation of the kinking mechanism and the shear resistance is given by Equation 6.14, shown below.

$$V_{r_{III}} = V_{f1} + V_{f2} + V_{h2}$$

As discussed in Section 6.5.4.3, the kinking mechanism can not be evaluated based on the limited experimental data. Therefore, for design purposes, the contributions from the kinking mechanism, components V_{f2} and V_{h2}, should be neglected. The shear resistance of the connection during Stage III can therefore be determined simply as:

$$V_{r_{III}} = V_{f1}$$

Component V_{f1} is defined by Equation 6.2. Since a vertical force redistribution has occurred at the connection level, the vertical stress acting on the dry pack must be determined as the net

gravity load acting on the connection. The portion of the simulated gravity load resisted by the bars was determined empirically in Section 6.5.4.1 to be on average, 90 kN per bar, or 180 kN in total. This will reduce the vertical stress on the dry pack by approximately 50%. The shear resistance of the connection during Stage III can be determined using Equation 6.2 as described in Section 6.2.2. The proposed coefficient of friction for Specimen PTB during Stage III is $\mu = 0.62$. The vertical stress on the dry pack is determined as follows:

$$\sigma_{n1} = \frac{P_g - 2F_{boi}}{A_c}$$
$$= \frac{(360\text{kN}) - 2(90\text{kN})}{(180,000\text{mm}^2)}$$
$$= 1 \text{ MPa}$$

Therefore,

$$V_{r_{III}} = (0.62)(1\text{MPa})(180,000\text{mm}^2)$$
$$= 112 \text{ kN}$$

The shear resistance of the connection during Stage III can be assumed constant for design purposes. Once again, using the same recommendations as for Specimen PTS, a coefficient of friction of $\mu = 0.6$ should be used for design purposes in Stage III.

7.5.4   Summary of Predicted Shear Resistance for Design Purposes

The predicted shear resistance of the connection at each stage using the proposed method for design purposes are presented in Table 7.5. The predicted shear resistance of Specimen PTB using the proposed design recommendations is shown in Figure 7.3 with the measured shear resistance -slip behaviour of the connection.

7.6   SPECIMEN SK

The observed behaviour of Specimen SK under cyclic loading conditions suggests that cyclic loading had little or no affect on the behaviour of the connection. The results indicate that the previously proposed models for the prediction of the connection behaviour under monotonic loading can be applied directly to cyclic loading conditions. The only observable difference of behaviour was that the strut mechanism associated with the shear resistance after cracking under monotonic loading (Figure 2.10 and Equation 2.4) was destroyed immediately due to the reversed cyclic pattern of loading on Specimen SK. Therefore, the cyclic behaviour of the connection can be determined by evaluating the shear resistance of the connection at two limit states: cracking of the connection (at the end of Stage II) and after development of a uniform slip interface (during Stage III). For Specimen SK, the initiation of slip is not a significant limit state because prior to cracking of the connection, the slip is limited by bearing on the shear keys.

7.6.1   Stage II

During Stage II, the behaviour of the connection is inelastic and the shear resistance of the connection is provided by a combination of interface friction and bearing on the dry pack within the shear keys. The shear resistance of the connection during Stage II continues to increase until cracking of the dry pack within the shear keys occurs, causing failure of the connection. The cracking shear resistance of the connection can be conservatively predicted using Equation 2.3 proposed in the previous research by Serrette (29,30) and summarized in Section 2.3.1 and Section 5.8.2.4. The predicted shear resistance at cracking is compared with the measured value in Table 7.6.

7.6.2   Stage III

After cracking of the connection, a significant reduction of the shear resistance occurs. After formation of a uniform sliding surface, the shear resistance of the connection is provided by interface friction. The frictional resistance can be predicted using the previously proposed "ultimate strength" model (Equation 2.5) summarized in Section 2.3.1 and Section 5.8.2.4 (Serrette (29,30)). The predicted shear resistance during Stage III of behaviour is compared with the measured value in Table 7.6.

CHAPTER 8

SUMMARY AND DESIGN RECOMMENDATIONS

8.1   SUMMARY

The objective of this research program was to investigate the effects of reversed cyclic loading on the behaviour of typical horizontal connections for precast concrete load-bearing shear wall panels. The behaviour of five different connection configurations was investigated. The connection configurations were:

DP: Plain surface connection with dry pack only

RW: Plain surface connection with dry pack and mild steel continuity bars

PTS: Plain surface connection with dry pack and post-tensioned with strands

PTB   Plain surface connection with dry pack and post-tensioned with bars

SK: Dry packed multiple shear keys

A total of six specimens were tested in this program, five under reversed cyclic loading and one under monotonic shear loading. The cyclic test results were compared with monotonic loading results of identical connection types from a previous research program at the University of Manitoba. One connection configuration, PTB, was not considered in the previous research and therefore was tested under both monotonic and cyclic loading in this research program. All of the specimens tested in this program were subjected to a constant uniform stress perpendicular to the connection to simulate the effects of gravity loads.

The effects of the reversed cyclic loading were evaluated on the basis of the observed failure modes and the shear resistance of the connection at the initiation of slip, after the initiation of slip and at failure.

8.2   DESIGN RECOMMENDATIONS

On the basis of the test results and observations from the six specimens tested in this program and the results from the previous studies of monotonic behaviour (10,11,17,18,29,30), the following design recommendations can be made:

1.)   The cyclic shear behaviour of the connections can be described in three general stages:

    I.   Elastic behaviour prior to the initiation of slip at the connection.

    II.   Inelastic behaviour after the initiation of slip but prior to significant deterioration of the dry pack.

    III.   Inelastic behaviour after significant deterioration of the dry pack and reduction of the shear resistance (failure of the connection).

2.)   The mode of failure under reversed cyclic loading conditions for all of the connection configurations was due to significant crushing and spalling of the dry pack. Crushing of the dry pack alters the shear resistance mechanisms and may dramatically reduce the shear resistance of the connection, depending on the specific mechanisms involved.

3.)   Failure due to crushing of the dry pack under cyclic loading conditions introduces an additional limit state beyond what was observed for identical specimens tested under monotonic loading conditions.

4.) The presence of shear keys significantly enhanced the shear resistance of the connection and limited slip prior to cracking of the dry pack within the shear keys. In practical seismic applications, accumulated slip over several stories is highly undesirable due to the resulting structural instability. The use of shear keys for limiting slip in seismic applications could enhance the overall behaviour of the structure.

5.) It is not possible to predict whether bond between the dry pack and the precast concrete panels exists prior to the initiation of slip. Bond is either not significant, or may be destroyed by handling of the specimens, shrinkage or by cyclic loading. Therefore, for design purposes, the presence of bond should be ignored when determining the shear resistance of the connection at the initiation of slip.

6.) Under cyclic loading conditions, the coefficient of friction for the plain surface connections (no shear keys) may be taken as 0.7 during Stages I and II of behaviour. After crushing of the dry pack, during Stage III of behaviour, a reduced coefficient of friction of 0.6 should be used to predict the residual strength of the connection.

7.) For plain surface connections with dry pack only (DP), cyclic loading does not appear to have any affect on the strength of the connection prior to failure due to crushing of the dry pack (prior to Stage III). The previously proposed model for the connection behaviour under monotonic loading conditions can be used to conservatively predict the behaviour of this connection during Stages I and II of cyclic behaviour without modification. After significant deterioration of the dry pack and failure of the connection (during Stage III), the cyclic behaviour may be predicted using the previously proposed model with a reduced friction coefficient.

8.) For plain surface connections with dry pack and post-tensioned strands (PTS), cyclic loading does not appear to have any affect of the strength of the connection prior to failure due to crushing of the dry pack (prior to Stage III). The previously proposed model for the connection behaviour under monotonic loading conditions can be used to conservatively predict the connection behaviour during Stages I and II. During Stage III, crushing of the dry pack may result in a complete loss of prestressing. The cyclic behaviour in this stage may be predicted using the previously proposed model with a reduced friction coefficient and without the effect of the normal stress due to post-tensioning.

9.) For connections with multiple shear keys (SK), cyclic loading does not appear to have any affect on the cracking strength or ultimate strength of the connection. The strut mechanism associated with the maximum shear strength of the connection after cracking under monotonic loading was destroyed by the reversed cyclic loading conditions. Therefore, under cyclic loading, the behaviour of the connection at cracking (transition between Stage II and III) and after failure (Stage III) may be predicted using the previously proposed models for the cracking strength and ultimate strength of connections with multiple shear keys under monotonic loading conditions.

10.) For connections with dry pack and mild steel continuity bars (RW), cyclic loading significantly reduced the strength of the connection. The previously proposed models for monotonic loading conditions are not applicable to cyclic loading conditions. The apparent effect of cyclic loading is to change the dowel action of the continuity bars from a shear mechanism to a combination of flexural and kinking mechanisms. This may be attributed to the deterioration of the concrete around the bars due to cyclic loading. The experimental data is not sufficient to allow a rational prediction of the cyclic behaviour using the proposed mechanisms. Therefore, the behaviour during

Stages I and II may be predicted using the previously proposed model for monotonic loading conditions, ignoring the contribution of the continuity bars.

11.) Under monotonic loading conditions, the behaviour of the connection with dry pack and post-tensioned bars (PTB) is identical to the behaviour of the connection with post-tensioned strands. Therefore, the previously proposed model for connections with post-tensioned strands may be used for connections with post-tensioned bars without modification.

12.) Under reversed cyclic loading conditions, the shear resistance of the connection with dry pack and post-tensioned bars (PTB) is gradually reduced over the duration of loading in comparison to the connection with post-tensioned strands. This may be attributed to a gradual loss of prestressing during Stage II of behaviour. After failure of the connection due to crushing of the dry pack, a complete loss of prestressing may occur. In addition, a vertical force redistribution occurs at the connection level and the normal stress on the dry pack due to gravity loads is reduced for connections with post-tensioned bars.

13.) During Stage I, the cyclic behaviour of connections with dry pack and post-tensioned bars may be predicted using the proposed method for connections with post-tensioned strands. During Stage II, the behaviour may be predicted assuming a complete loss of post-tensioning due to cyclic loading effects. During Stage III, the cyclic behaviour may be predicted using the proposed model for connections with post-tensioned strands with a reduced friction coefficient. In addition, the effect of post-tensioning is assumed to be zero and the normal stress on the dry pack due to gravity loads is reduced by up to one half.

8.3   SUGGESTIONS FOR FUTURE RESEARCH

On the basis of the results and conclusions of this research program, the following are some suggestions for further research in this area:

1. Additional specimens with mild steel continuity bars (Specimen RW) should be tested under reversed cyclic shear loading to fully evaluate the deformed length and kink length of the reinforcement related to the shear resistance mechanisms of the continuity bars. The effects of different bar sizes and number of bars should be investigated. The additional results should also be used to evaluate the relationship between the gradual reduction of the dry pack thickness and the increased compression force in the continuity loads from the applied normal loads.

2. Additional specimens post-tensioned with bars should be tested under reversed cyclic shear loading to evaluate the relationship between the gradual reduction of the dry pack thickness and the loss of post-tensioning.

3. The use of multiple shear keys in combination with mild steel continuity bars or post-tensioning should be investigated.

4. Research is needed to investigate the combined effect of cyclic flexural and shear loading on the behaviour of typical horizontal connection for precast concrete load-bearing shear walls.

REFERENCES

1. **ACI Committee 318**, "Building Code Requirements for Reinforced Concrete (ACI 318M-89)", American Concrete Institute, Detroit, Michigan, 1989.

2. **Aoyama, H., Noguchi, H., Ochiai, M. and Horikawa, K.,** "Shear Transfer Across Cracks in Reinforced Concrete Shear Walls", *Transactions of the Japan Concrete Institute*, Vol. 3, 1981, pp. 289-296.

3. **Canadian Prestressed Concrete Institute (CPCI)**, Metric Design Manual - Precast and Prestressed Concrete, 2nd Edition, Ottawa, Ontario, 1987.

4. **Canadian Standards Association (CSA)**, "Design of Concrete Structures for Buildings (CAN-A23.3-M84)", Rexdale, Ontario, 1984.

5. **Clough, D.P.** "Design of Connections for Precast Concrete Buildings for the Effects of Earthquakes", Final Report, No. NSF-85-004, March 1985.

6. **Collins, M.P. and Mitchell, D.,** Prestressed Concrete Basics, Canadian Prestressed Concrete Institute, Ottawa, Ontario, 1987.

7. **Derecho, A.T., Iqbal, M., Fintel, M. and Corley, W.G.** "Loading History for use in Quasistatic Simulated Earthquake Loading Tests", ACI Special Publication, SP 63-14, Reinforced Concrete Structures Subjected to Wind and Earthquake Forces, Detroit, 1980, pp. 329-356.

8. **Dowrick, D.J.,** Earthquake Resistant Design for Architects and Engineers, 2nd Edition, John Wiley and Sons, 1987.

9. **Englekirk, R.E.,** "Seismic Design Considerations for Precast Concrete Multistorey Buildings", *PCI Journal*, Vol. 35, No. 3, May-June 1990, p. 40.

10. **Foerster, H.R.** "Behaviour of the Connections Typically Used in Precast Concrete Load-Bearing Shear Wall Panels", Master of Science Thesis, University of Manitoba, 1987.

11. **Foerster, H.R., Rizkalla, S.H. and Huevel, J.S.** "Behaviour and Design of Shear Connections for Load-bearing Wall Panels", *PCI Journal*, Vol. 34, January-February 1989, pp. 102-119.

12. **Fukuda, M. and Kubota, T.,** "Experimental Study on Slip Behaviour at the Horizontal Joints of Precast Concrete Panel Structures", *Transactions of the Japan Concrete Institute*, Vol. 13, 1991, pp. 449-456.

13. **Hanson, N.W.,** "Design and Construction of Large-Panel Concrete Structures - Supplemental Report C: Seismic Tests of Horizontal Joints", Department of Housing and Urban Development, Washington, D.C., 1979.

14. **Harris, H.G., and Abboud, B.E.,** "Cyclic Shear Behaviour of Horizontal Joints in Precast Concrete Large Panel Buildings", Design of Prefabricated Buildings for Earthquake Loads, Applied Technology Council Publication ATC-8, 1981, pp. 403-438.

15. **Hicks, T.** "Connections Between Precast Concrete Members for Use in Seismic Zones", Master of Science Thesis, University of Washington, 1991.

16. **Huang, T. and Scribner, C.F.** "R/C Member Cyclic Response During Various Loadings", *Journal of Structural Engineering (ASCE)*, Vol. 110, No. 3, March 1984, pp. 477-489.

17. **Hutchinson, R.L.,** "Post-tensioned Horizontal Connections Typically Used for Precast Concrete Load-bearing Shear Wall Panels", Master of Science Thesis, University of Manitoba, 1990.

18. **Hutchinson, R.L., Rizkalla, S.H., Lau, M. and Huevel, J.S.** "Horizontal Post-Tensioned Connections for Precast Concrete Load-Bearing Shear Wall Panels", *PCI Journal*, Vol. 36, November-December 1991, pp. 64-76.

19. **International Conference of Building Officials,** Uniform Building Code, Pasadena, California, 1985.

20. **Iso, K., Higashi, Y., Endo, T. and Numoto, M.,** "The Behaviour of the Joint of R-PC Shear Wall Panels", *Transactions of the Japan Concrete Institute*, Vol. 3, 1981, pp. 297-304.

21. **Jaques, F.J. and Aswad, A.** "Seismic Design of Panel Wall Systems Using Vertical Post-Tensioning", Seminar on Precast Concrete Construction in Seismic Zones (JCI), Vol. 1, 1986, pp. 225-245.

22. **Lau, M.,** Con-Force Structures Ltd., Personal Correspondence, May and June 1992.

23. **Lefas, I.D. and Kotsovos, M.D.** "Strength and Deformation Characteristics of Reinforced Concrete Walls Under Load Reversals", *ACI Structural Journal*, Vol. 87, No. 6, November-December 1990, pp. 716-726.

24. **Naeim, F., Editor,** Seismic Design Handbook, Structural Engineering Series, VanNostrand Reinhold, New York, 1989.

25. **Oliva, M., Gavrilovic, P., and Clough, R.W.,** "Seismic Testing of Large Panel Precast Walls: Comparison of Pseudostatic and Shaking Table Tests", *Earthquake Engineering and Structural Dynamics*, Vol. 19, 1990, pp. 859-875.

26. **Paulay, T., Park, R. and Phillips, M.H.,** "Horizontal Construction Joints in Cast-In-Place Reinforced Concrete", ACI Special Publication SP-42: <u>Shear in Reinforced Concrete</u>, Vol. 2, 1974, pp 599-616.

27. **Prestressed Concrete Institute (PCI),** <u>PCI Design Handbook,</u> Chicago, Illinois, 1983.

28. **SEAOC,** <u>Recommended Lateral Force Requirements and Commentary</u>, Seismology Committee of the Structural Engineers Association of California, Sacramento, California, 1990.

29. **Serrette, R.L.,** "Multiple Shear Key Connections for Load-bearing Shear Wall Panels", Master of Science Thesis, University of Manitoba, 1988.

30. **Serrette, R.L., Rizkalla, S.H., Attiogbe, E.K. and Huevel, J.S.** "Multiple Shear Key Connections for Precast Shear Wall Panels", *PCI Journal*, Vol. 34, March-April 1989, pp. 104-120.

31. **Stanton, J.** "Connections in Precast Concrete Structures", *Concrete International: Design and Construction*, Vol. 9, No. 11, Nov. 1987, pp. 49-53.

Table 3.1: Experimental Program and Parameters

Specimen	Connection Configuration	Loading Type	Simulated Gravity Load (MPa)
DP	Plain Surface Connection with Dry Pack Only	Reversed Cyclic	4 MPa
RW	Plain Surface Connection with Dry Pack and Mild Steel Continuity Reinforcement	Reversed Cyclic	2 MPa
PTS	Plain Surface Connection with Dry Pack and Post-tensioned Strands	Reversed Cyclic	2 MPa
PTB	Plain Surface Connection with Dry Pack and Post-tensioned Bars	Reversed Cyclic	2 MPa
PTB-S	Plain Surface Connection with Dry Pack and Post-tensioned Bars	Monotonic	2 MPa
SK	Dry Packed Multiple Shear Keys	Reversed Cyclic	2 MPa

Table 3.2: Material Properties for Continuity Bars - 25M, Grade 400W

	Nominal Properties	Measured Properties
Elastic Modulus	200000 MPa	200000 MPa
Yield Stress	400 MPa	500 MPa
Yield Stain	0.002	0.0025
Maximum Stress	400 MPa	640 MPa
Rupture Strain	0.080 (minimum)	0.100

Table 4.1: Panel Concrete Compressive Strength

Specimen	Compressive Strength at 28 Days (MPa)	Compressive Strength at Time of Testing (MPa)
DP	N.A.	38.4
RW	44.4	51.1
PTS	42.6	48.4
PTB	46.8	56.4
PTB-S	45.0	50.6
SK	44.0	48.8

Table 4.2: Dry Pack Compressive Strength

Specimen DP:

	Cube Strength (MPa)	Equivalent Cylinder Strength (MPa)
Time of Testing	38.2	32.4

Specimens PTS, PTB and PTB-S:

	Cube Strength (MPa)	Equivalent Cylinder Strength (MPa)
7 Day Strength	49.9	42.4
28 Day Strength	58.4	49.6
Time of Testing	56.0	47.6

Specimens RW and SK:

	Cube Strength (MPa)	Equivalent Cylinder Strength (MPa)
28 Day Strength	57.0	48.5
Time of Testing	56.2	47.8

NOTE: Specimens are grouped according to dry pack date. Specimen DP was dry packed alone, Specimens PTS, PTB and PTB-S were dry packed together and Specimens RW and SK were dry packed together.

Table 4.3: Summary of Measured Shear Resistance During Loading

Specimen	Shear Resistance At Initiation of Slip or Cracking (kN)	Maximum Shear Resistance (kN)	Shear Resistance At Failure (kN)	Residual Shear Resistance After Failure * (kN)
DP	533	533	480	420
RW	290	400	400	100
PTS	530	530	500	220
PTB	530	545	370	120
PTB-S	555	785	785	340
SK	650	833 **	833	335

*   Average shear resistance measured at the zero slip position of the cycle after failure.

** Maximum shear resistance for Specimen SK was measured at failure due to cracking of the dry pack within the shear keys. The initiation of slip had occurred previously.

Table 4.4: Specimen DP - Cyclic Shear Envelope Values

Positive Direction		Negative Direction	
Slip Magnitude (mm)	Shear Resistance (kN)	Slip Magnitude (mm)	Shear Resistance (kN)
0.00	0.0	0.00	0.0
0.02	300.0	-0.02	-200.0
0.04	400.0	-0.07	-400.0
0.10	533.0	-0.10	-500.0
1.50	487.0	-1.50	-471.0
2.00	492.0	-2.00	-471.0
2.50	484.0	-2.50	-477.0
3.00	486.0	-3.00	-475.0
3.50	488.0	-3.50	-478.0
4.00	488.0	-4.00	-482.0
4.50	490.0	-4.50	-479.0
5.00	486.0	-5.00	-481.0
6.00	473.0	-6.00	-472.0
7.00	423.0	-7.00	-425.0
8.00	426.0	-8.00	-423.0
9.00	425.0	-9.00	-426.0

NOTE: The positive loading direction is the "push" direction. The negative loading direction is the "pull" loading direction.

Table 4.5: Specimen RW - Cyclic Shear Envelope Values

Positive Direction		Negative Direction	
Slip Magnitude (mm)	Shear Resistance (kN)	Slip Magnitude (mm)	Shear Resistance (kN)
0.00	0.0	0.00	0.0
0.00	100.0	0.00	-100.0
0.01	200.0	-0.01	-200.0
0.31	300.0	-0.18	-300.0
1.06	314.6	-1.00	-339.1
2.00	354.6	-1.98	-356.4
3.06	357.3	-2.98	-358.1
4.06	375.4	-3.98	-366.1
5.00	392.6	-5.07	-386.5
5.99	402.1	-5.99	-391.8
7.03	401.2	-7.06	-389.4
8.10	395.4	-8.06	-377.1
8.97	358.3	-8.98	-324.9
8.99	318.3	-9.09	-245.9
9.09	131.0	-9.00	-134.6
10.10	124.4	-10.05	-115.8
12.05	129.0	-12.00	-142.6

Table 4.6: Specimen PTS - Cyclic Shear Envelope Values

Positive Direction		Negative Direction	
Slip Magnitude (mm)	Shear Resistance (kN)	Slip Magnitude (mm)	Shear Resistance (kN)
0.00	0.0	0.00	0.0
0.01	101.8	0.00	-100.8
0.03	201.4	0.01	-202.6
0.05	303.3	0.02	-303.0
0.10	398.9	0.01	-405.5
0.26	507.4	0.01	-500.5
0.93	526.0	-1.06	-500.7
2.03	521.1	-1.98	-506.6
3.03	531.3	-3.01	-516.4
3.96	532.9	-3.96	-525.0
5.09	522.7	-4.99	-523.6
5.94	499.8	-5.98	-481.5
5.97	458.6	-6.02	-419.5
5.99	388.8	-6.07	-318.8
6.00	250.0	-6.00	-210.0
6.98	243.0	-7.08	-214.1
7.90	209.5	-7.99	-196.3
8.93	208.4	-9.02	-226.5
10.08	238.3	-9.99	-235.9

Table 4.7: Specimen PTB - Cyclic Shear Envelope Values

Positive Direction		Negative Direction	
Slip Magnitude (mm)	Shear Resistance (kN)	Slip Magnitude (mm)	Shear Resistance (kN)
0.00	0.0	0.00	0.0
0.00	101.0	0.00	-100.7
0.00	201.5	-0.01	-200.5
0.01	303.9	-0.01	-302.5
0.04	401.5	0.00	-399.8
0.10	502.6	0.00	-498.4
1.12	536.7	-0.99	-546.8
1.95	532.7	-2.03	-533.2
3.09	517.8	-3.01	-518.3
4.04	505.3	-4.05	-503.4
4.99	476.3	-5.02	-486.5
6.05	464.2	-6.03	-470.9
7.08	451.1	-6.98	-458.7
8.13	438.4	-7.97	-455.2
9.41	437.5	-9.00	-442.4
9.72	391.0	-10.08	-361.5
10.37	365.5	-10.18	-235.5
10.40	117.1	-10.01	-126.7
11.94	133.5	-12.07	-177.9
14.12	204.9	-13.97	-220.1
16.04	266.2	-16.12	-258.8

Table 4.8: Specimen SK - Cyclic Shear Envelope Values

Positive Direction		Negative Direction	
Slip Magnitude (mm)	Shear Resistance (kN)	Slip Magnitude (mm)	Shear Resistance (kN)
0.00	0.0	0.00	0.0
0.01	100.7	0.01	-100.0
0.01	151.0	0.00	-151.1
0.00	200.2	-0.01	-199.3
0.01	249.0	-0.02	-249.7
0.02	300.0	-0.03	-299.7
0.03	354.7	-0.04	-350.4
0.04	402.5	-0.05	-397.1
0.06	452.9	-0.08	-448.1
0.08	520.6	-0.14	-497.5
0.09	547.9	-0.19	-550.4
0.12	598.2	-0.26	-596.2
0.18	653.9	-0.32	-645.7
0.21	696.3	-0.41	-698.1
0.27	746.5	-0.55	-747.3
0.40	802.5	-0.74	-798.8
0.62	855.3	-1.07	-833.0
1.00	430.2	-1.05	-282.0
2.03	400.7	-2.00	-335.0
3.00	355.0	-3.00	-335.0
4.00	315.0	-4.00	-300.0
5.05	302.4	-5.01	-284.6
6.05	299.0	-6.00	-289.5
7.01	310.3	-7.01	-311.1
8.00	315.0	-8.15	-322.1
9.00	310.1	-9.00	-330.4
10.00	317.5	-10.09	-332.6

Table 5.1: Specimen PTB - Post-tensioning Bar Strains Prior to the Application of Shear Loading

	West Bar:		East Bar:		Average
	Outside	Inside	Outside	Inside	
At Jacking	0.00325	0.00317	0.00314	0.00335	0.00323
At Time of Test	0.00316	0.00302	0.00306	0.00322	0.00311
% Loss	2.77%	4.73%	2.55%	4.00%	3.51%
After Preload	0.00309	0.00295	0.00299	0.00318	0.00305
% Loss (total)	4.92%	6.94%	4.78%	5.19%	5.46%

Table 5.2: Specimen PTB-S - Post-tensioning Bar Strains Prior to the Application of Shear Loading

	West Bar:		East Bar:		Average
	Outside	Inside	Outside	Inside	
At Jacking	0.00321	0.00321	0.00312	0.00335	0.00322
At Time of Test	0.00308	0.00314	0.00300	0.00315	0.00309
% Loss	4.05%	2.18%	3.85%	5.97%	4.01%
After Preload	0.00307	0.00311	0.00300	0.00311	0.00307
% Loss (total)	4.36%	3.12%	3.85%	7.16%	4.62%

Table 6.1: Specimen RW - Average Measured Axial Bar Strains

Applied Slip Magnitude (mm)	Measured Bar Strain at Zero Slip	Measured Total Bar Strain	Measured Tensile Increase
0.0	-0.00045	-0.00045	0.00000
0.3	-0.00047	-0.00047	0.00000
1.0	-0.00050	-0.00048	0.00003
2.0	-0.00062	-0.00057	0.00005
3.0	-0.00078	-0.00067	0.00011
4.0	-0.00083	-0.00057	0.00026
5.0	-0.00085	-0.00039	0.00046
6.0	-0.00085	-0.00017	0.00068

Table 6.2: Specimen RW - Calculation of Shear Resistance Components Using Measured Data

Vf1: / Vh1:

Applied Slip (mm)	Measured V_r (kN)	Measured Bar Strain at Zero Slip	F_{boi} at Zero Slip (kN)	Vertical Stress σ_{n1} (MPa)	Component V_{f1} (kN)	Required Component V_{h1} (kN)	Required Deformed Length, L_1 (mm)	End Moment (kN-m)	Curvature
0.3	300.0	-0.00047	-94.0	1.48	212.8	87.2	41.6	0.91	0.00107
1.0	315.0	-0.00050	-100.2	1.44	207.9	103.1	45.1	1.16	0.00295
2.0	350.0	-0.00062	-124.0	1.31	188.8	153.0	43.1	1.65	0.00648
3.0	360.0	-0.00078	-155.7	1.14	163.5	178.2	42.0	1.85	Plastic
4.0	375.0	-0.00083	-166.8	1.07	154.5	177.2	41.8	1.85	Plastic
5.0	390.0	-0.00085	-169.7	1.06	152.3	161.3	45.9	1.85	Plastic
6.0	400.0	-0.00085	-169.5	1.06	152.4	134.6	55.0	1.85	Plastic
7.0	400.0	-0.00087	-174.0	1.03	148.8	100.4	73.7	1.85	Plastic
8.0	400.0	-0.00089	-178.0	1.01	145.6	61.2	121.0	1.85	Plastic

Vf2: / Vh2:

Applied Slip (mm)	Measured V_r (kN)	Measured Total Bar Strain	Tensile Strain Increase	"Kink" Length, L_2 (mm)	F_{bi} (kN)	F_{byi} (kN)	Vertical Stress σ_{n2} (MPa)	Component V_{f2} (kN)	Component V_{h2} (kN)
0.3	300.0	-0.00047	0.00000	N/A	-94.0	-94.0	0.00	0.0	0.0
1.0	315.0	-0.00048	0.00003	141.4	-95.2	-95.2	0.03	4.0	0.0
2.0	350.0	-0.00057	0.00005	198.4	-113.8	-113.8	0.06	8.1	0.1
3.0	360.0	-0.00067	0.00011	200.0	-133.2	-133.2	0.13	18.0	0.3
4.0	375.0	-0.00057	0.00026	174.6	-114.3	-114.3	0.29	42.0	1.2
5.0	390.0	-0.00039	0.00046	164.8	-77.7	-77.6	0.51	73.6	2.8
6.0	400.0	-0.00017	0.00068	163.3	-34.5	-34.5	0.75	108.0	5.0
7.0	400.0	0.00003	0.00090	165.4	5.0	5.0	0.99	143.2	7.6
8.0	400.0	0.00025	0.00114	167.5	50.0	49.9	1.27	182.4	10.9

Table 6.3: Specimen PTB - Computed Vertical Force Distribution at the
Connection Level During Stage III of Behaviour

Applied Slip Magnitude	Measured Shear Resistance At Zero Slip (kN)	Computed Vertical Stress Acting On Dry Pack (MPa)	Computed Force In P/T Bars, F_{boi} (kN)
10 mm (3rd)	115.0	1.03	174.5
12 mm	100.0	0.90	198.7
14 mm	112.0	1.00	179.4
16 mm	120.0	1.08	166.5

Table 6.4: Specimen PTB - Computed Effective Prestressing Strains During Stage II of Behaviour

Applied Slip Magnitude (mm)	Measured Maximum Shear Resistance V_r (kN)	Shear Resistance Component V_{f1} (kN)	Computed Shear Resistance Component V_{f4} (kN)	Computed Force per P/T Bar, F_{pci} (kN)	Computed Effective Prestressing Strain
1.0	535.0	338.4	196.6	104.6	0.00291
2.0	525.0	338.4	186.6	99.3	0.00276
3.0	515.0	338.4	176.6	93.9	0.00261
4.0	495.0	338.4	156.6	83.3	0.00232
5.0	475.0	338.4	136.6	72.7	0.00202
6.0	460.0	338.4	121.6	64.7	0.00180
7.0	450.0	338.4	111.6	59.4	0.00165
8.0	440.0	338.4	101.6	54.0	0.00150
9.0	420.0	338.4	81.6	43.4	0.00121

Table 7.1: Specimen DP - Summary of predicted shear resistance using proposed mechansims and design recommendations

Limit State	Predicted Shear Resistance	Measured Shear Resistance	$\dfrac{\text{Predicted}}{\text{Measured}}$
Stage I - Initiation of Slip ($\mu = 0.8$)	480 kN	533 kN	0.901
Stage II - After Initiation of Slip ($\mu = 0.7$)	420 kN	480 kN	0.875
Stage III - After Failure ($\mu = 0.6$)	360 kN	420 kN	0.857

Table 7.2: Specimen RW - Summary of predicted shear resistance using proposed mechansims and design recommendations

Limit State	Predicted Shear Resistance	Measured Shear Resistance	Predicted / Measured
Stage I - Initiation of Slip ($\mu = 0.7$)	252 kN	290 kN	0.869
Stage II - After Initiation of Slip ($\mu = 0.7$)	252 kN	400 kN (max.)	0.630

Table 7.3: Specimen PTS - Summary of predicted shear resistance using proposed
mechansims and design recommendations

Limit State	Predicted Shear Resistance	Measured Shear Resistance	$\dfrac{\text{Predicted}}{\text{Measured}}$
Stage I - Initiation of Slip ($\mu = 0.7$)	403 kN	530 kN	0.760
Stage II - After Initiation of Slip ($\mu = 0.7$)	403 kN	524 kN	0.768
Stage III - After Failure ($\mu = 0.6$)	216 kN	220 kN	0.982

Table 7.4: Specimen PTB-S - Summary of predicted shear resistance using proposed
mechansims and design recommendations

Limit State	Predicted Shear Resistance	Measured Shear Resistance	Predicted / Measured
Stage I - Initiation of Slip ($\mu = 0.7$)	403 kN	555 kN	0.726
Stage II - After Initiation of Slip ($\mu = 0.7$)	403 kN	550 kN	0.733

Table 7.5: Specimen PTB - Summary of predicted shear resistance using proposed mechansims and design recommendations

Limit State	Predicted Shear Resistance	Measured Shear Resistance	$\dfrac{\text{Predicted}}{\text{Measured}}$
Stage I - Initiation of Slip ($\mu = 0.7$)	403 kN	530 kN	0.760
Stage II - After Initiation of Slip ($\mu = 0.7$)	252 kN	423 kN (at failure)	0.597
Stage III - After Failure ($\mu = 0.6$)	108 kN	112 kN	0.964

Table 7.6: Specimen SK - Summary of predicted shear resistance using proposed mechansims and design recommendations

Limit State	Predicted Shear Resistance	Measured Shear Resistance	Predicted / Measured
Stage II - After Cracking of Shear Keys	638 kN	833 kN	0.766
Stage III - After Formation of Uniform Slip Plane	348 kN	335 kN	1.04
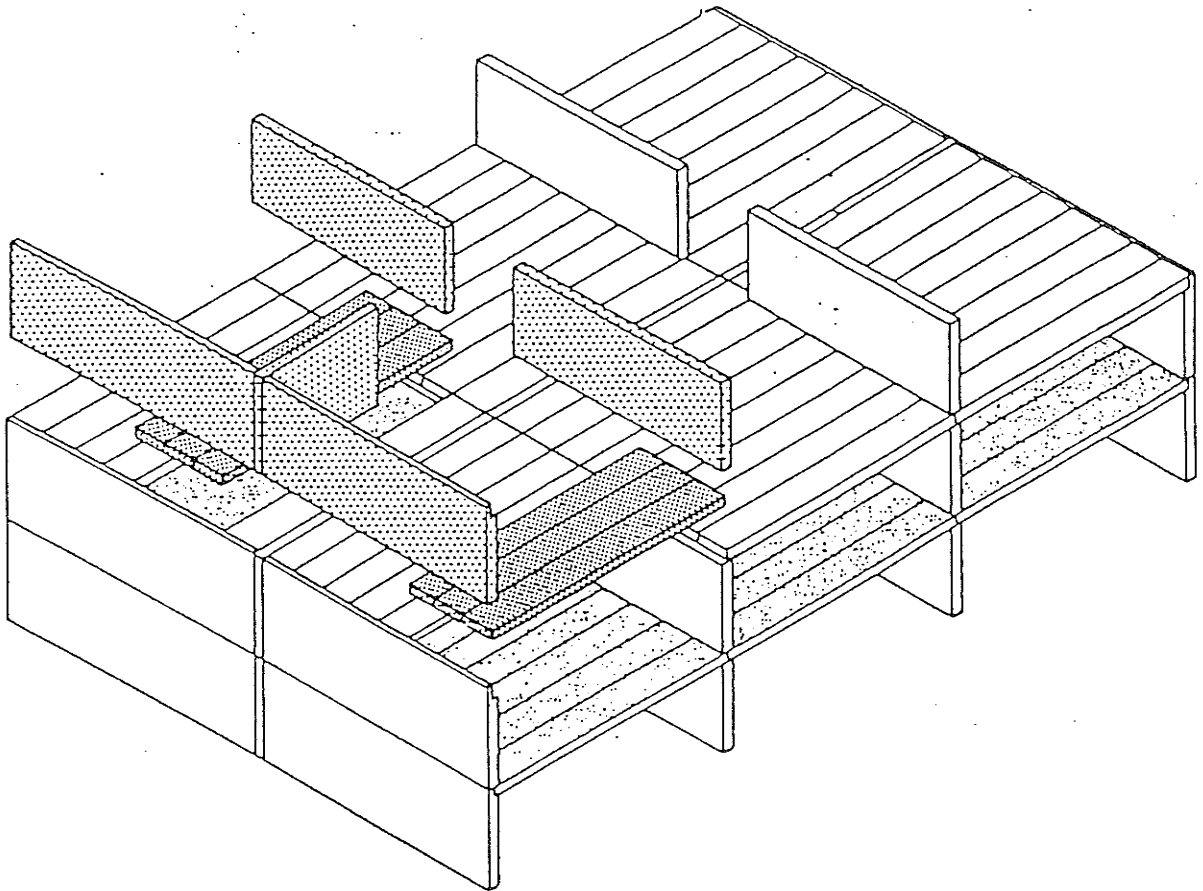
Figure 2.1   Load-bearing Shear Wall Panel System (Hanson (13))

Area A = Area B
(i.e. both structures
have equal capacity
to absorb energy)
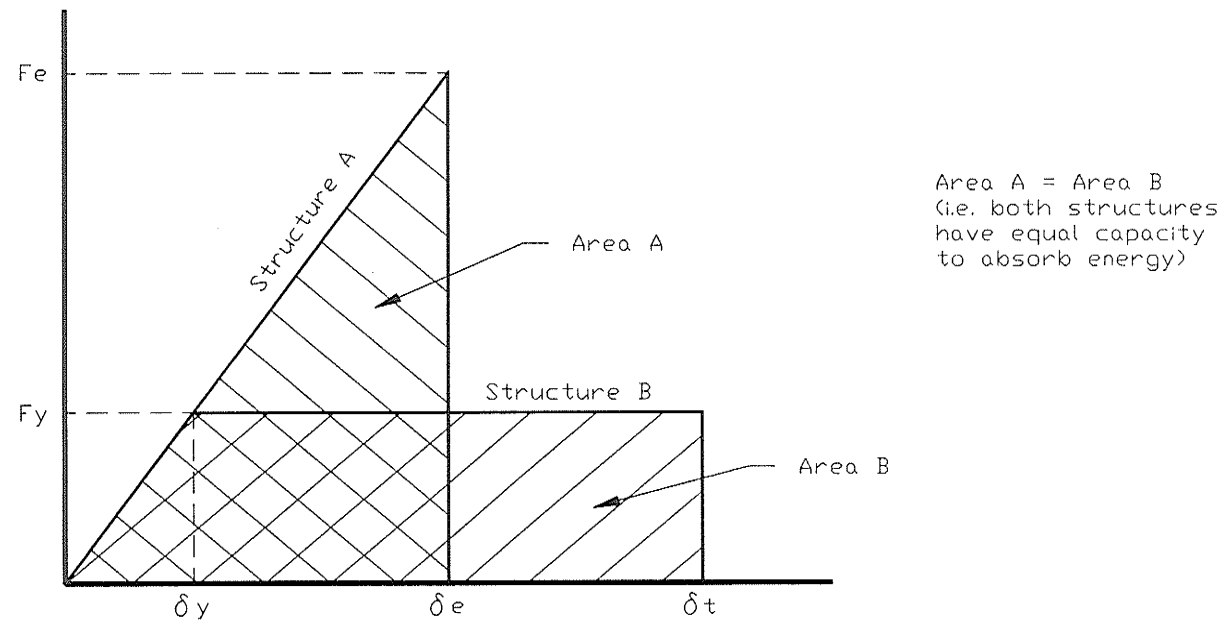
Figure 2.2   Equal Energy Response for Elastic and Elastoplastic Structures
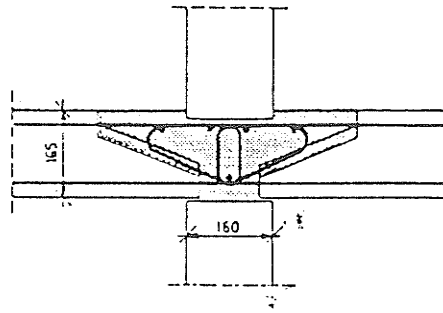
Figure 2.3   Connection Cross-section for the European Form of Construction (Oliva et al (25))
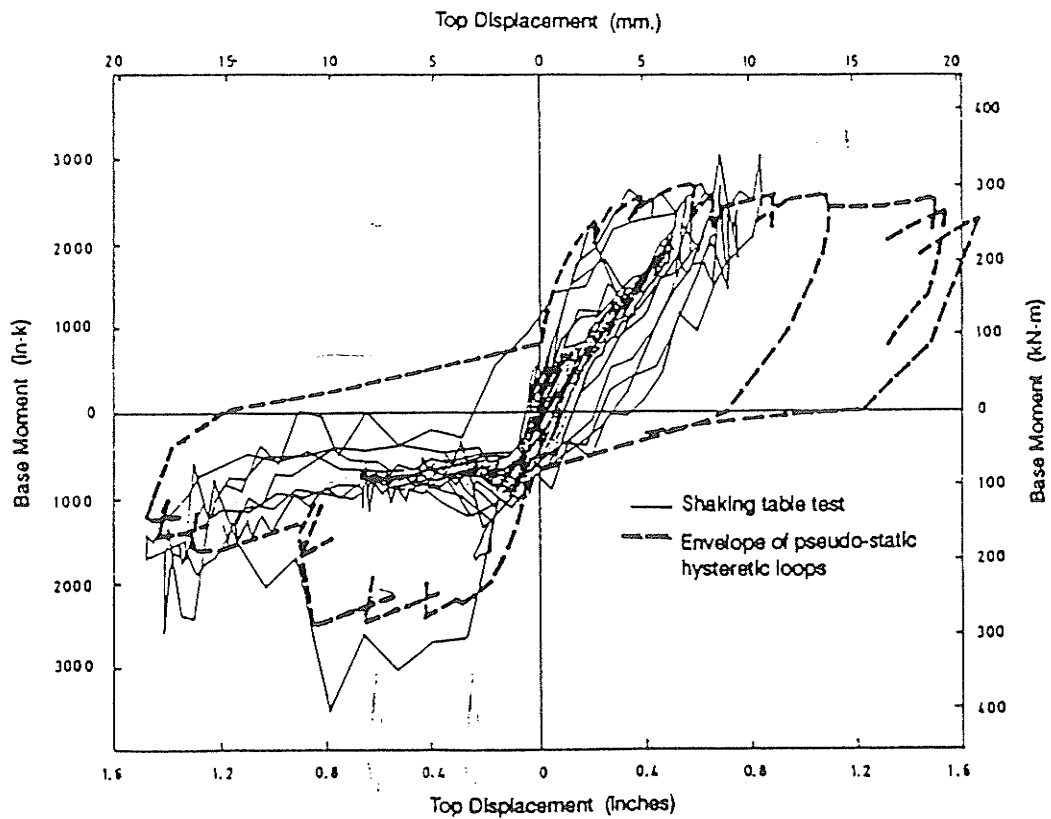
Figure 2.4   Comparison of Behaviour Between Shaking Table Tests and Pseudostatic Tests (Oliva et al (25))
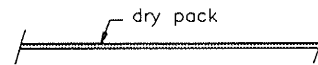
Dry packed plain surface connection
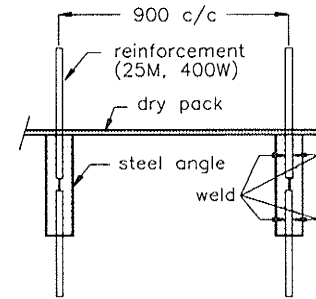
Continuity bars with welded connection
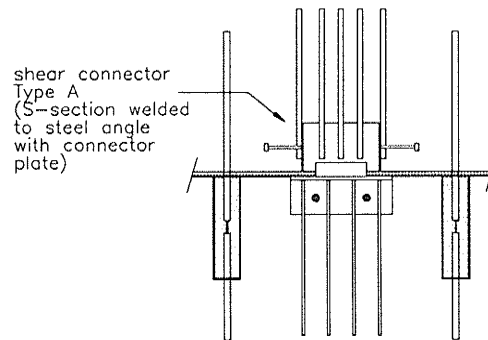
Continuity bars and shear connector A
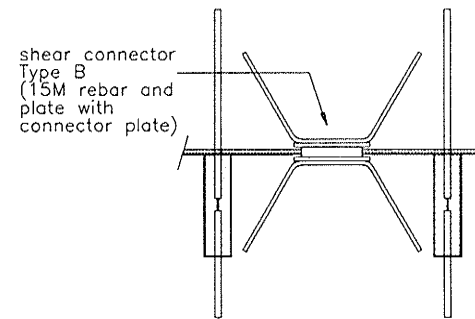
Continuity bars and shear connector B

Figure 2.5(a) Connection Configurations - Previous Research at the University of Manitoba Phase I

182

Dry Pack

Dry packed plain surface connection
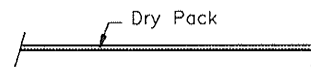
dry packed
shear keys (5)
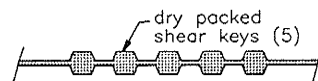
Large-size dry packed shear keys

dry packed
shear keys (8)
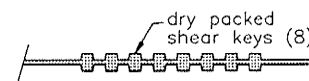
Small-size dry packed shear keys

Figure 2.5(b)   Connection Configurations - Previous Research at the University of Manitoba Phase II

dry pack

Hollow—core slab
(1200 x 200 mm)
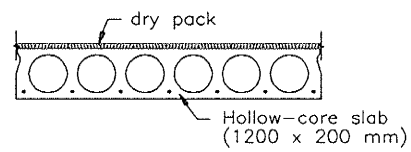
Dry pack and hollow—core slab

900 c/c

duct

dry pack

strand

Dry pack and post—tensioned strands

900 c/c

duct
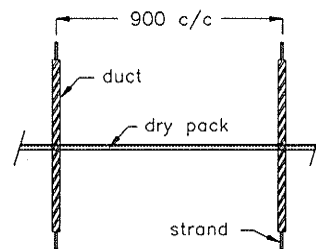
dry pack

Hollow—core slab
(1200 x 200 mm)
strand
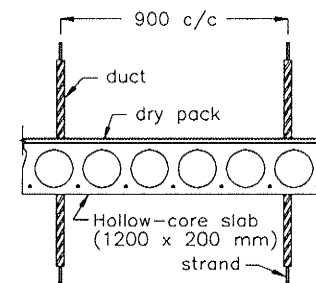
Dry pack, postensioned strands
and hollow core slab

Figure 2.5(c)   Connection Configurations - Previous Research at the University of Manitoba Phase III
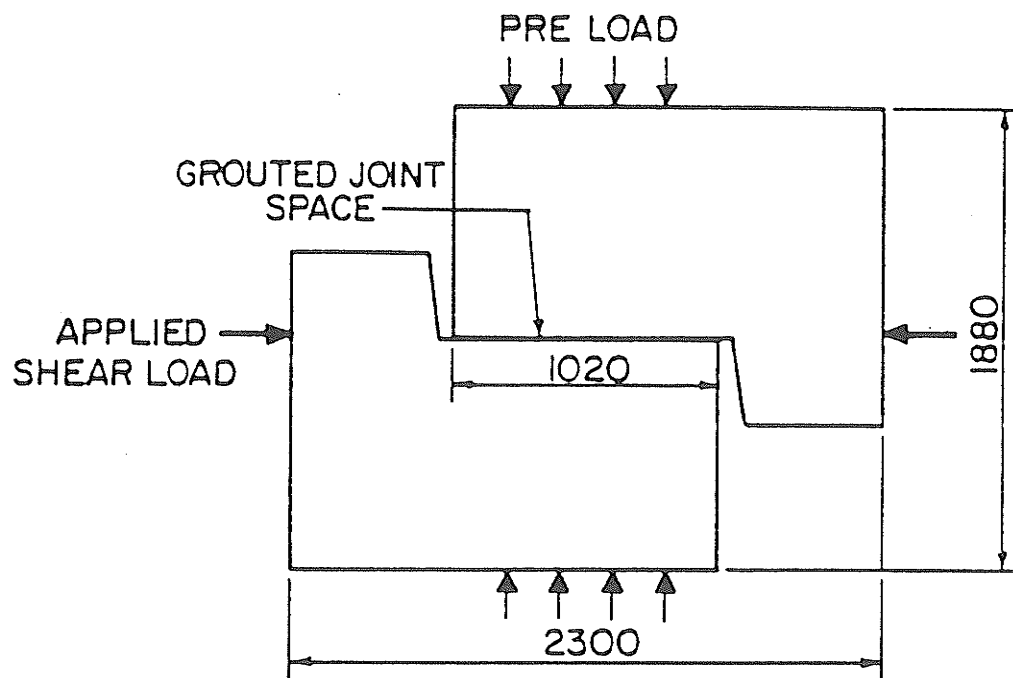
Figure 2.6   Test Specimen Configuration - Previous Research at the University of
Manitoba
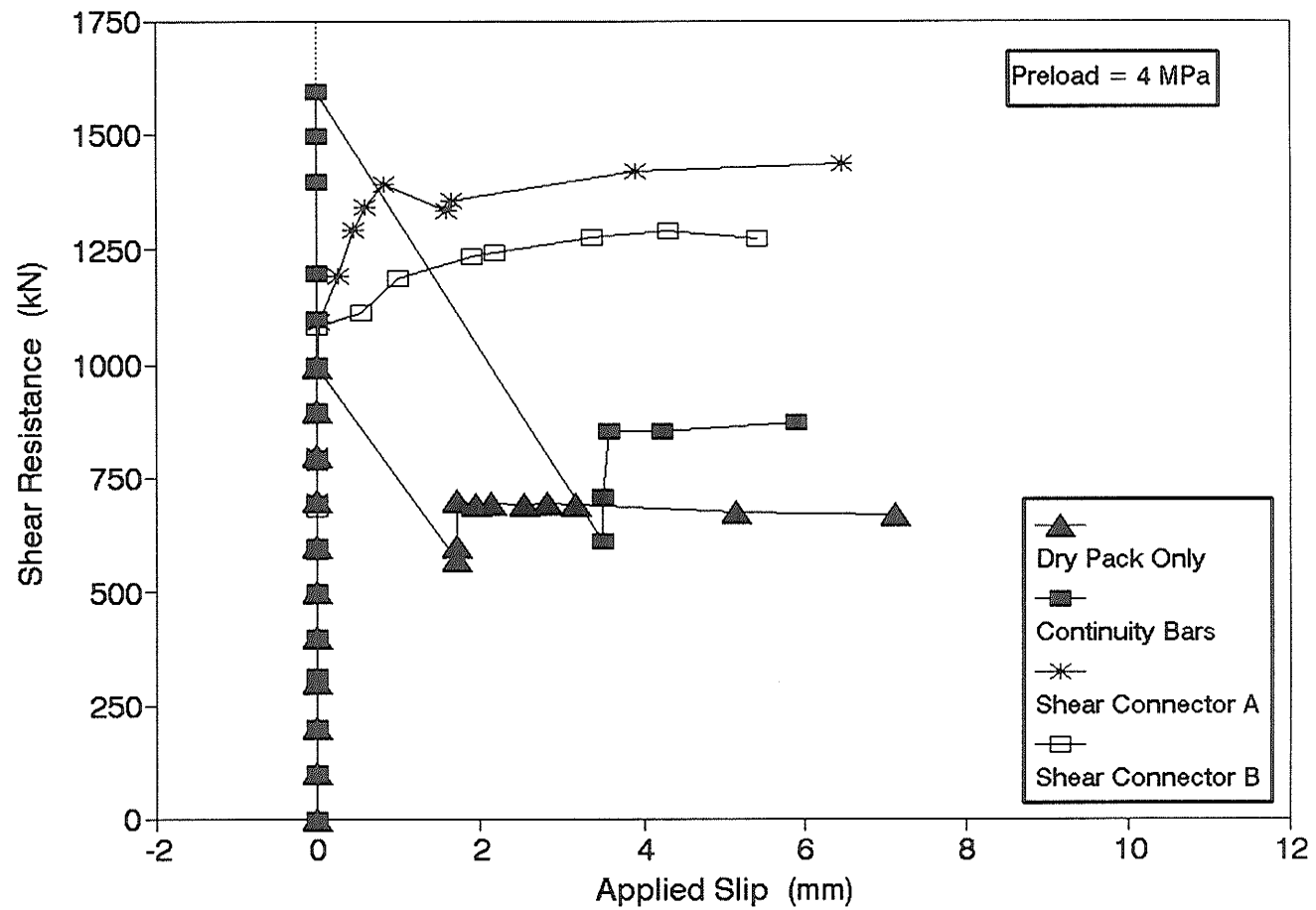
Figure 2.7   Typical Monotonic Shear Behaviour - Phase I of Previous Research
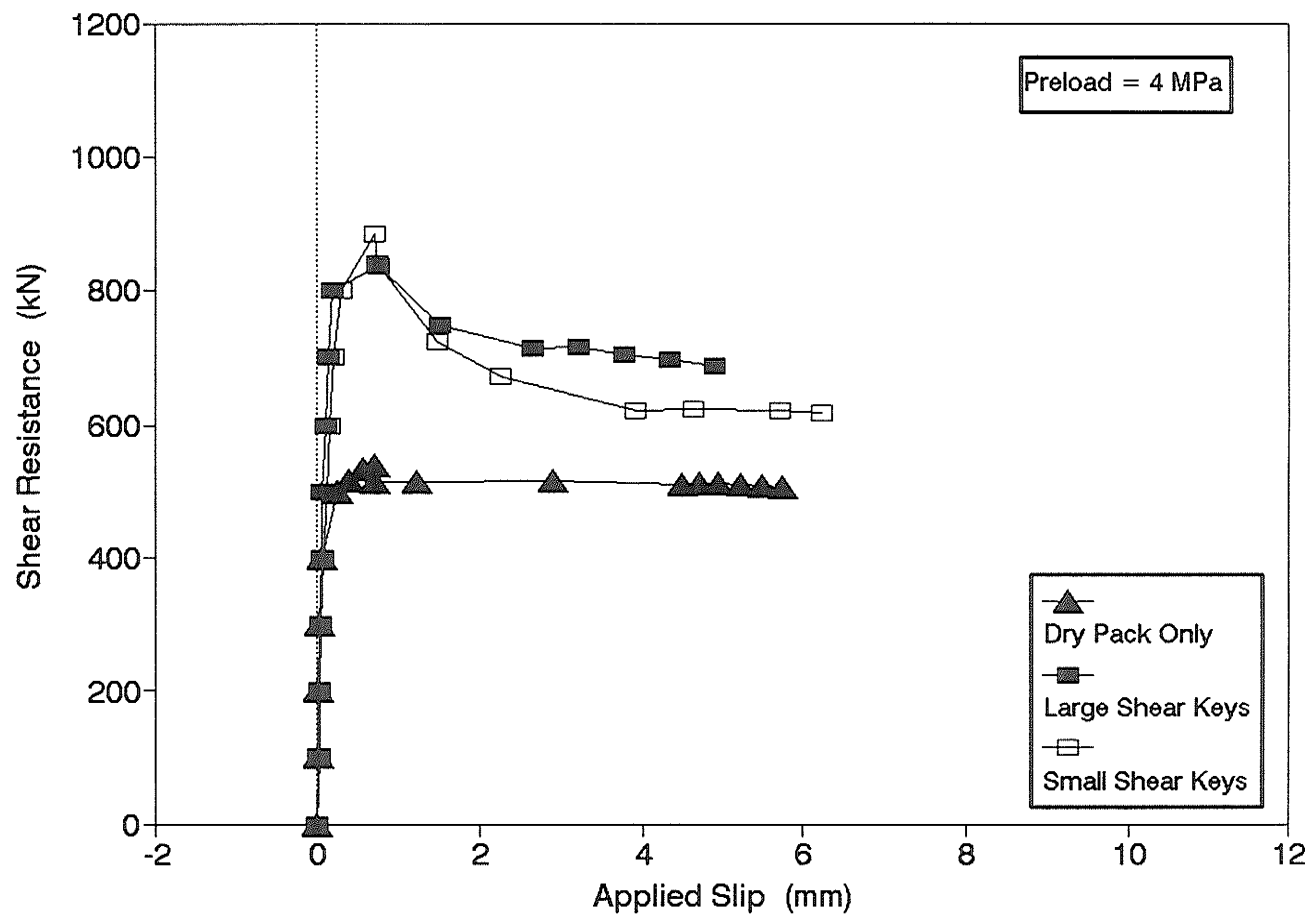
Figure 2.8   Typical Monotonic Shear Behaviour - Phase II of Previous Research
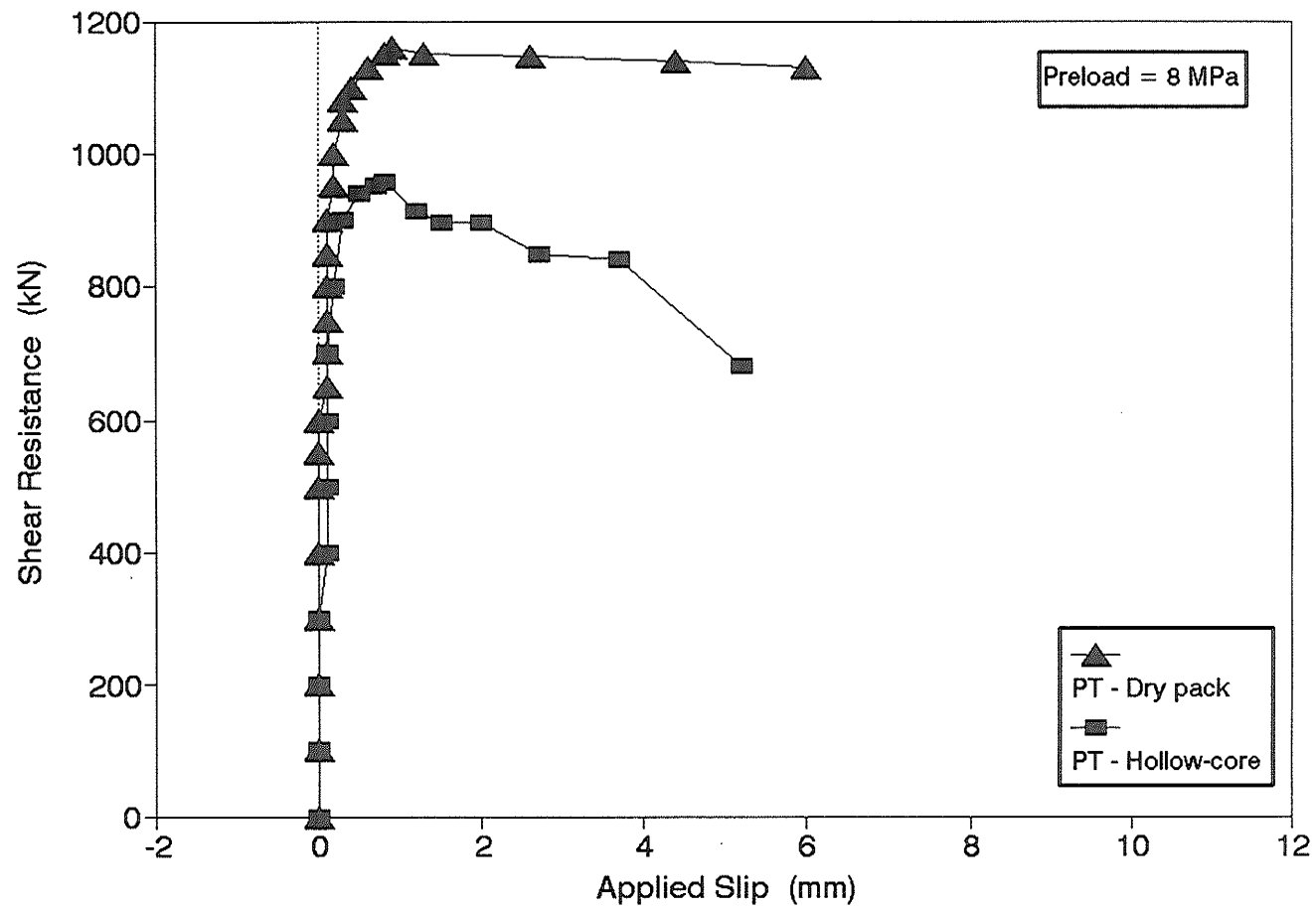
Figure 2.9   Typical Monotonic Shear Behaviour - Phase III of Previous Research
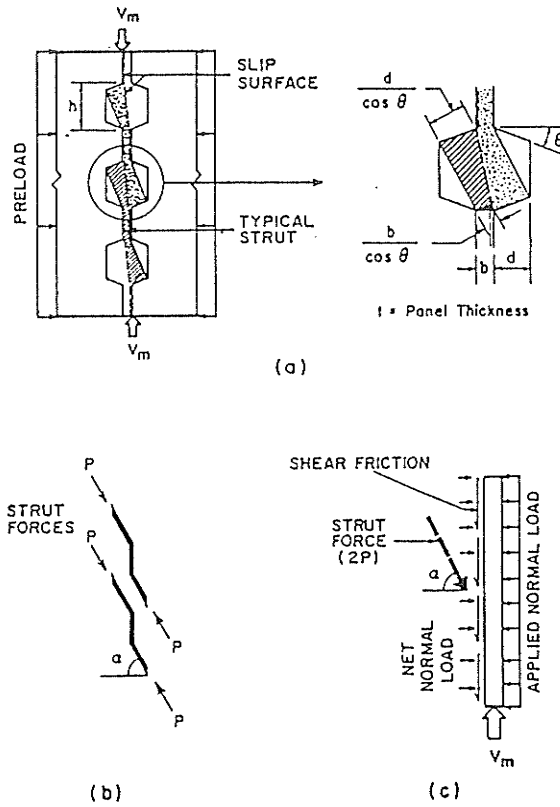
Figure 2.10   Strut Mechanism for Multiple Shear Key Connections (Serrette (30))
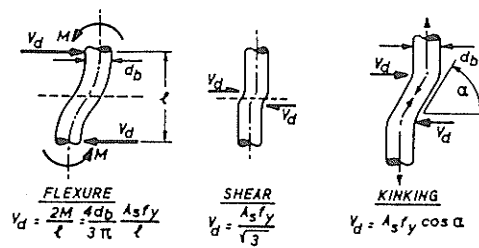
Figure 2.11   Mechanisms of Dowel Action (Paulay et al (26))
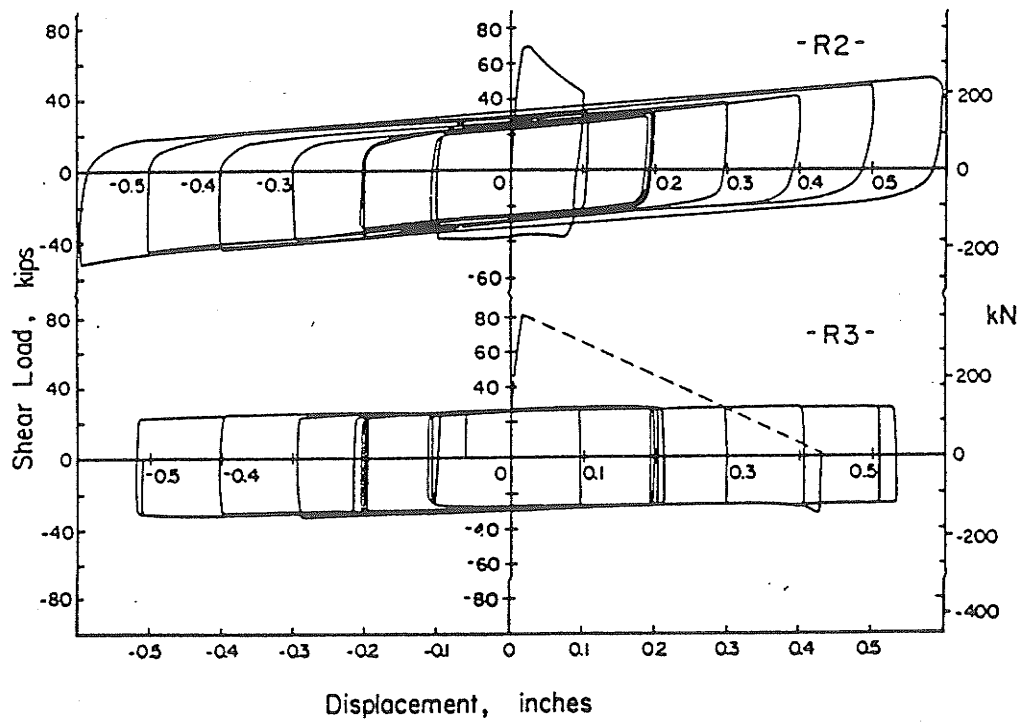
Figure 2.12   Typical Shear - Displacement Cycles - Connections With (R2) and Without (R3) Vertical Ties (Hanson (13))
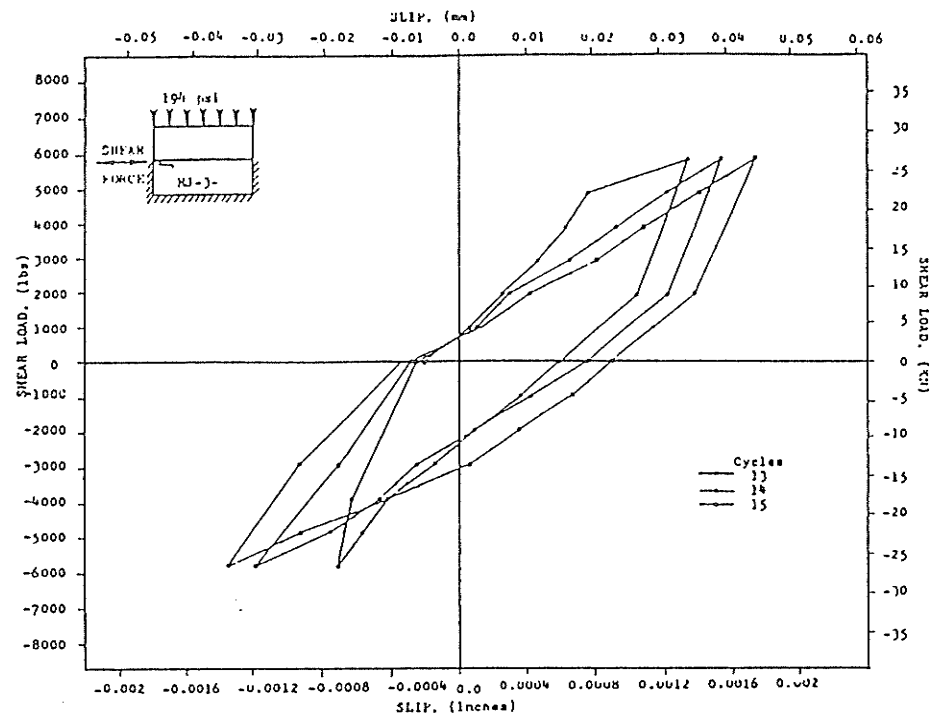
(a)
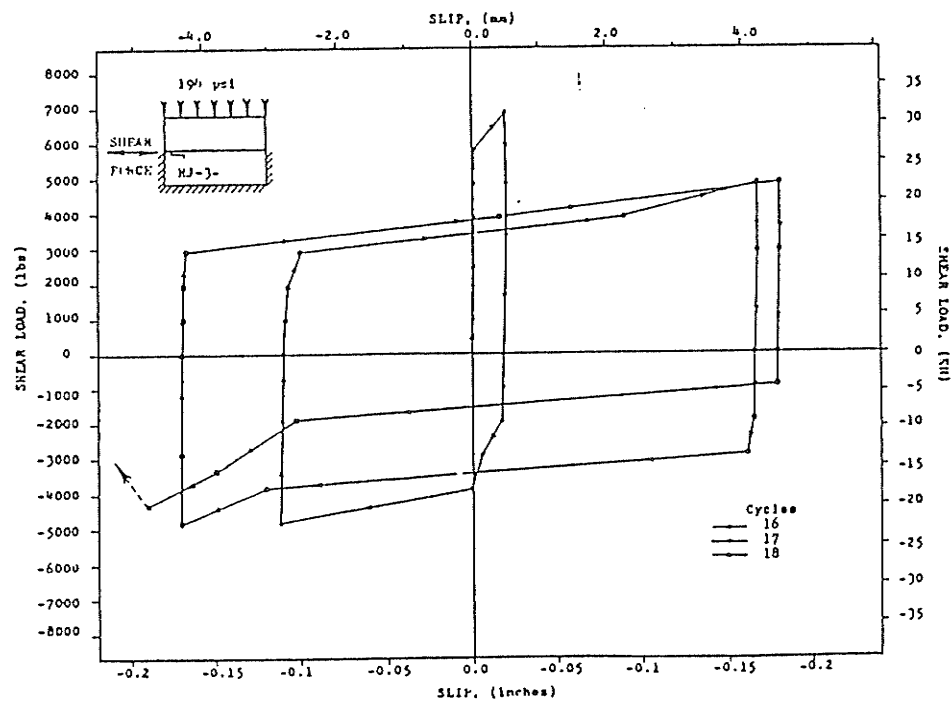
(b)

Figure 2.13 Typical Shear - Slip Cycles: a) prior to failure, and b) after failure (Harris and Abboud (14))
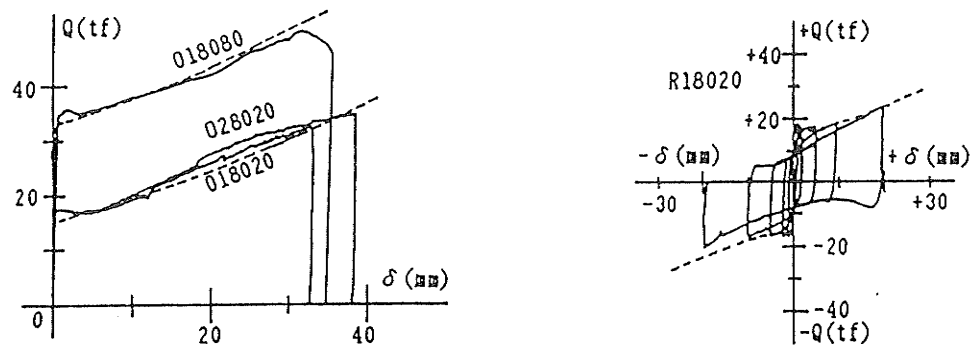
Figure 2.14(a) Typical Shear - Slip Behaviour Under Monotonic and Reversed Cyclic Shear Loading (Fukuda and Kubota (12))
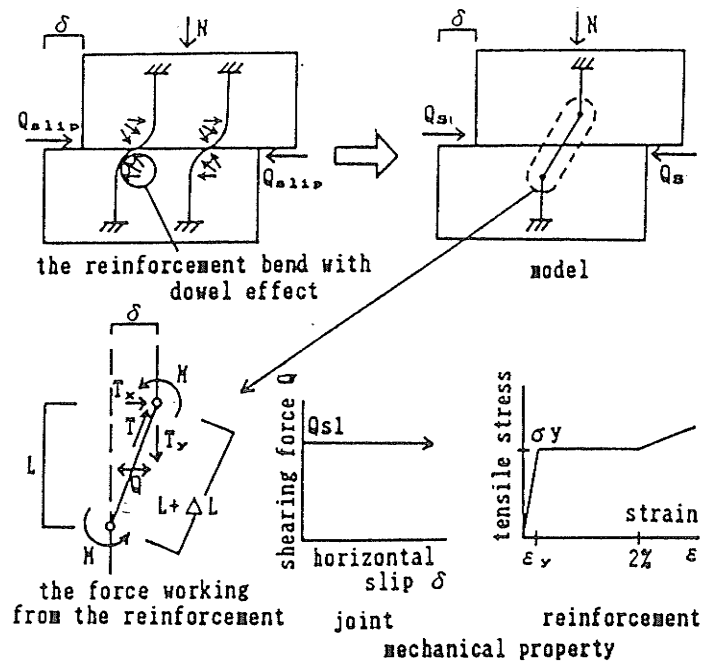
Figure 2.14(b) Shear Resistance Mechanism Provided by Continuity Reinforcement (Fukuda and Kubota (12))
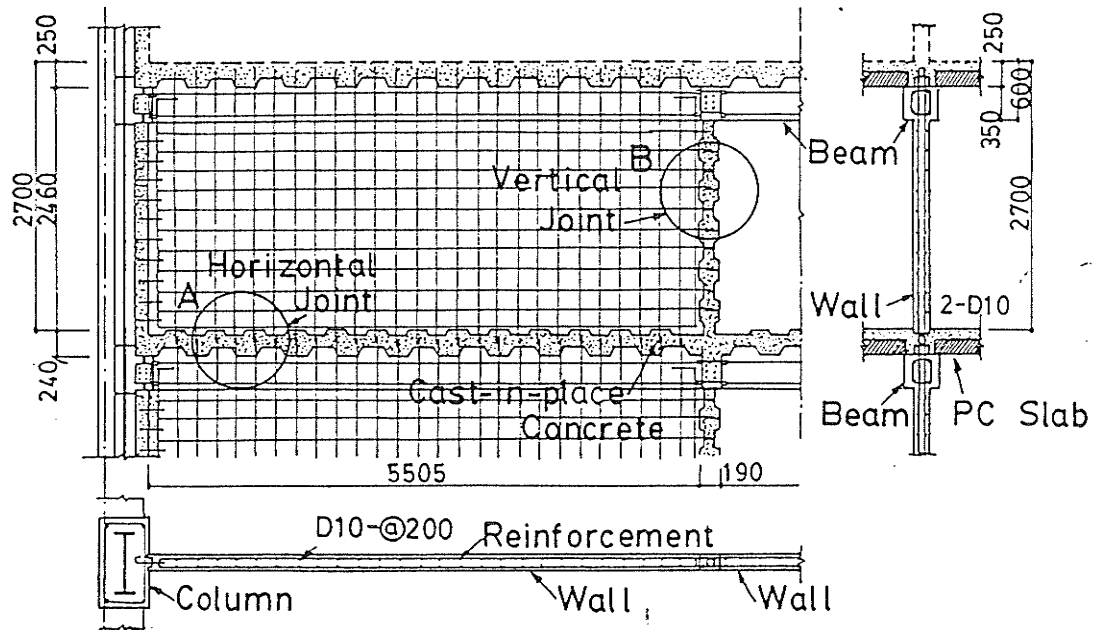
Figure 2.15(a) Composite Construction System for Large Panel Structures (Iso et al (20))
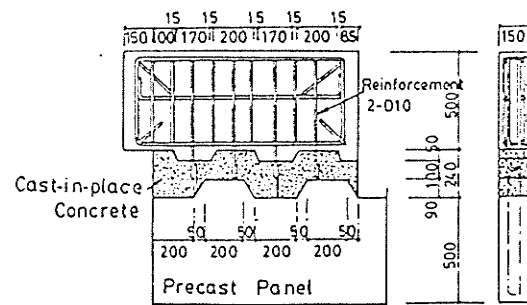
Figure 2.15(b) Specimen Configuration with Cotters (Shear Keys) (Iso et al (20))
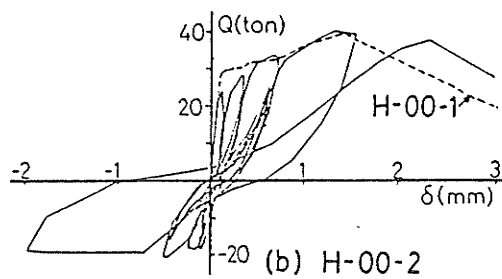
Figure 2.15(c) Typical Shear - Slip Behaviour Under Monotonic and Reversed Cyclic
Shear Loading (Iso et al (20))
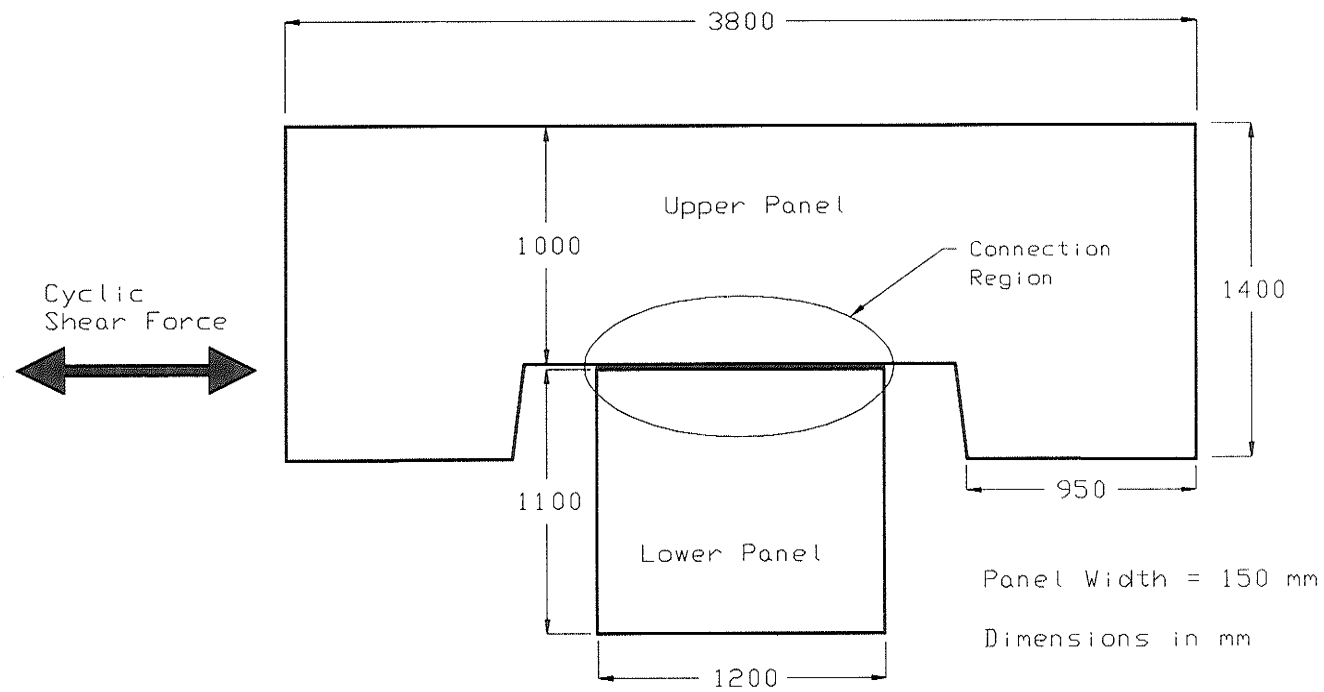
Figure 3.1   Test Specimen Configuration

dry pack

DP — Dry Pack Grout

900 c/c

reinforcement
(25M, 400W)

dry pack

weld

steel
angle
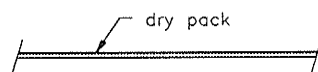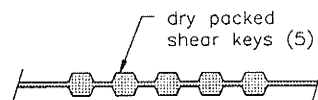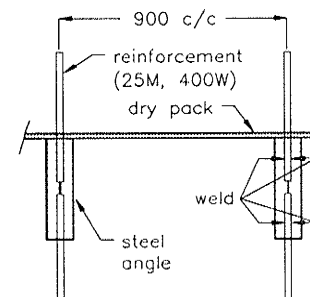
RW — Reinforcement, Welded
Connection

dry packed
shear keys (5)

SK — Shear Keys

900 c/c

duct

dry pack
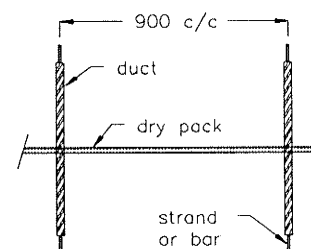
strand
or bar

PTS — Post-tensioned Strands
PTB — Post-tensioned Bars

Figure 3.2   Connection Configurations
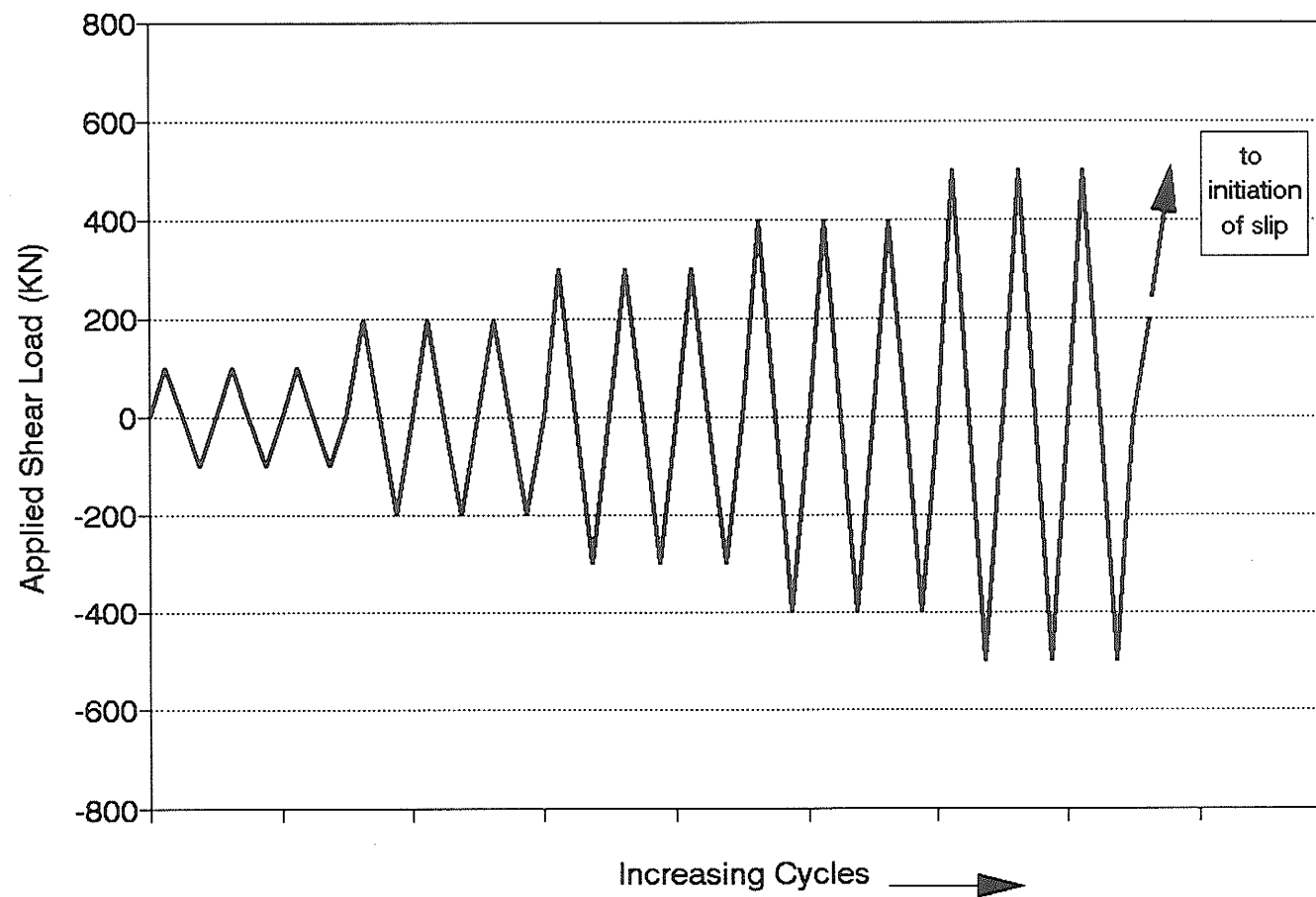
Figure 3.3(a)   Reversed Cyclic Loading History - Load Control Cycles

Figure 3.3(b)   Reversed Cyclic Loading History - Displacement Control Cycles

L 75x75x10 mm
(G40.21 - 300W)

240 mm

210 mm

660 mm

Section A

25M Rebar
Gr. 400W

925 mm

6 ⌐ 180   E480XX
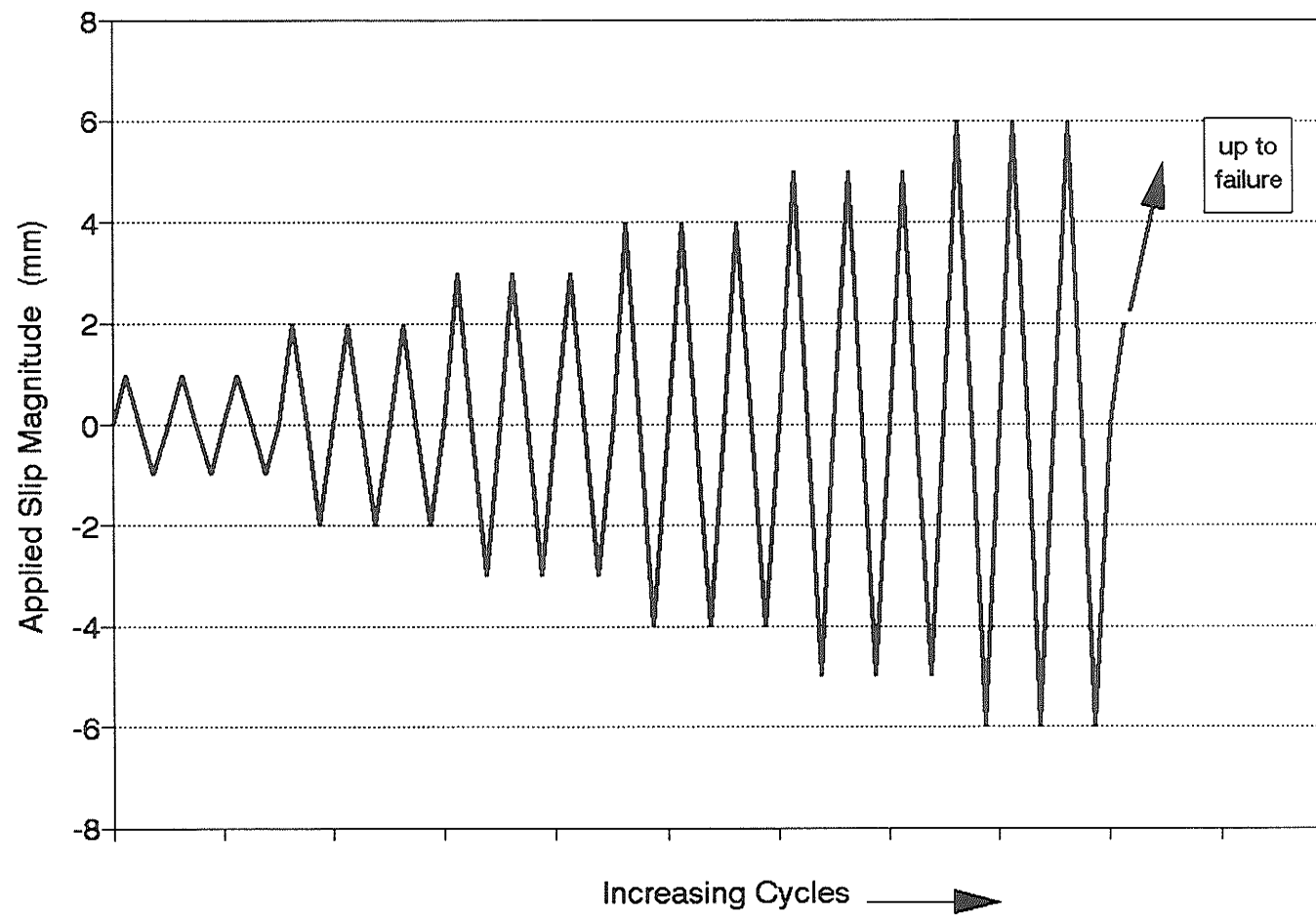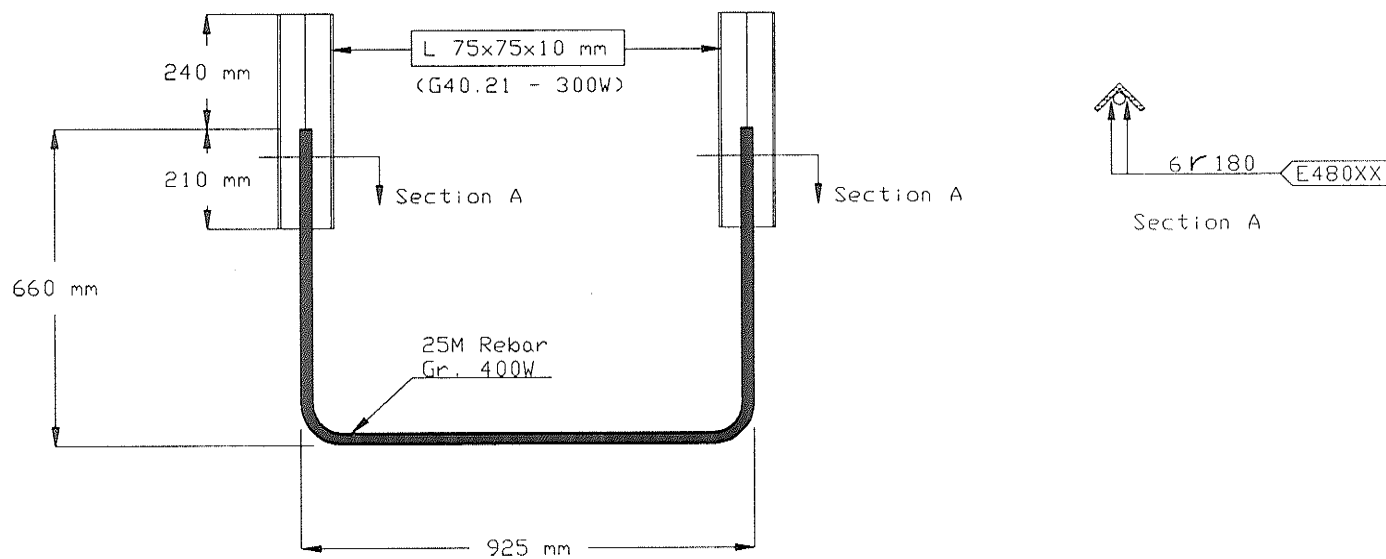
Section A

Figure 3.4   Continuity Bar Welding Details

900 mm o/c

Continuity Bar

Upper Panel

extension of cont.
bar to be welded
to steel angle
inside the pocket
when the connection
is assembled

Steel Angle

240 mm

A   A

Pocket

70 mm

Lower Panel

150 mm   140 mm

Section A-A   Pocket
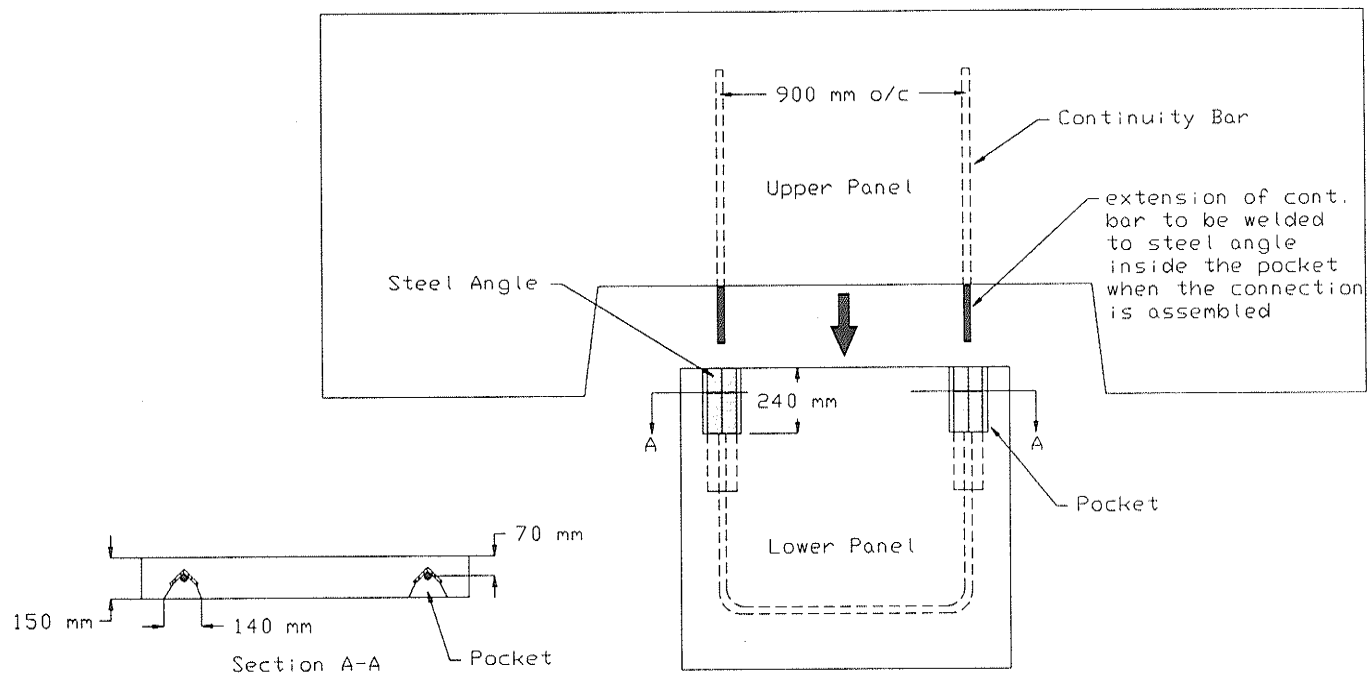
Figure 3.5   Specimen RW Configuration and Connection Assembly Details
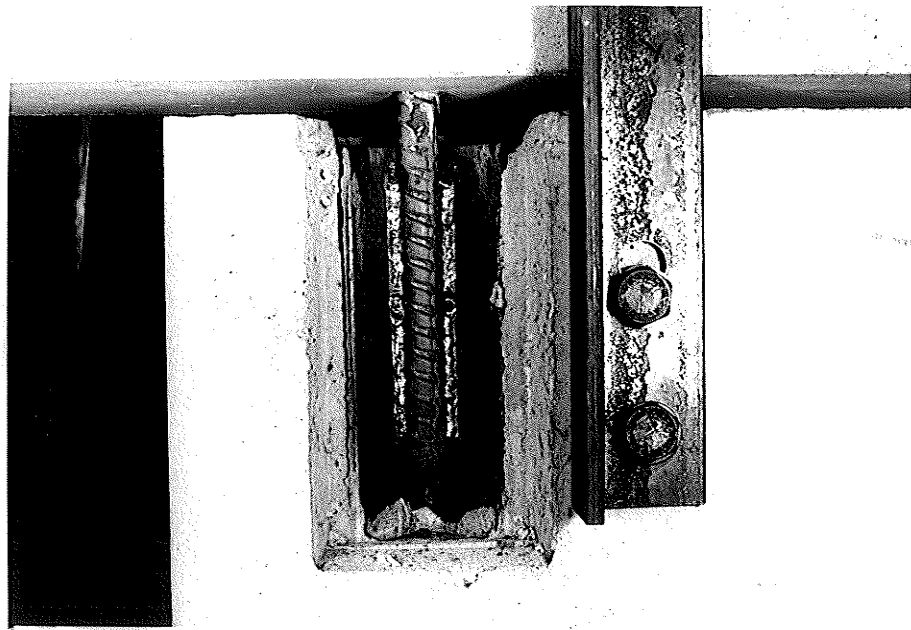
Figure 3.6   Continuity Bar Connection By Welding
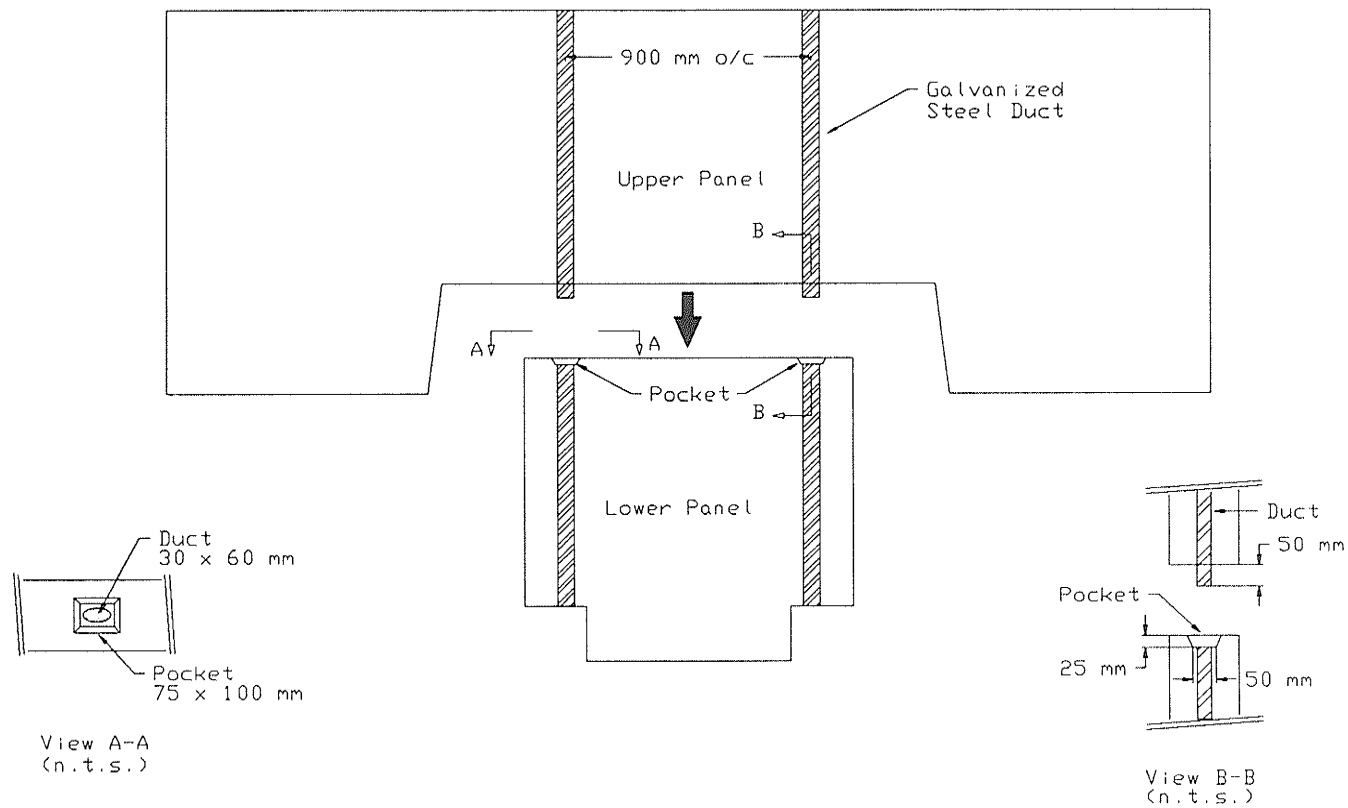
Figure 3.7   Post-tensioned Specimen Configuration and Connection Assembly Details
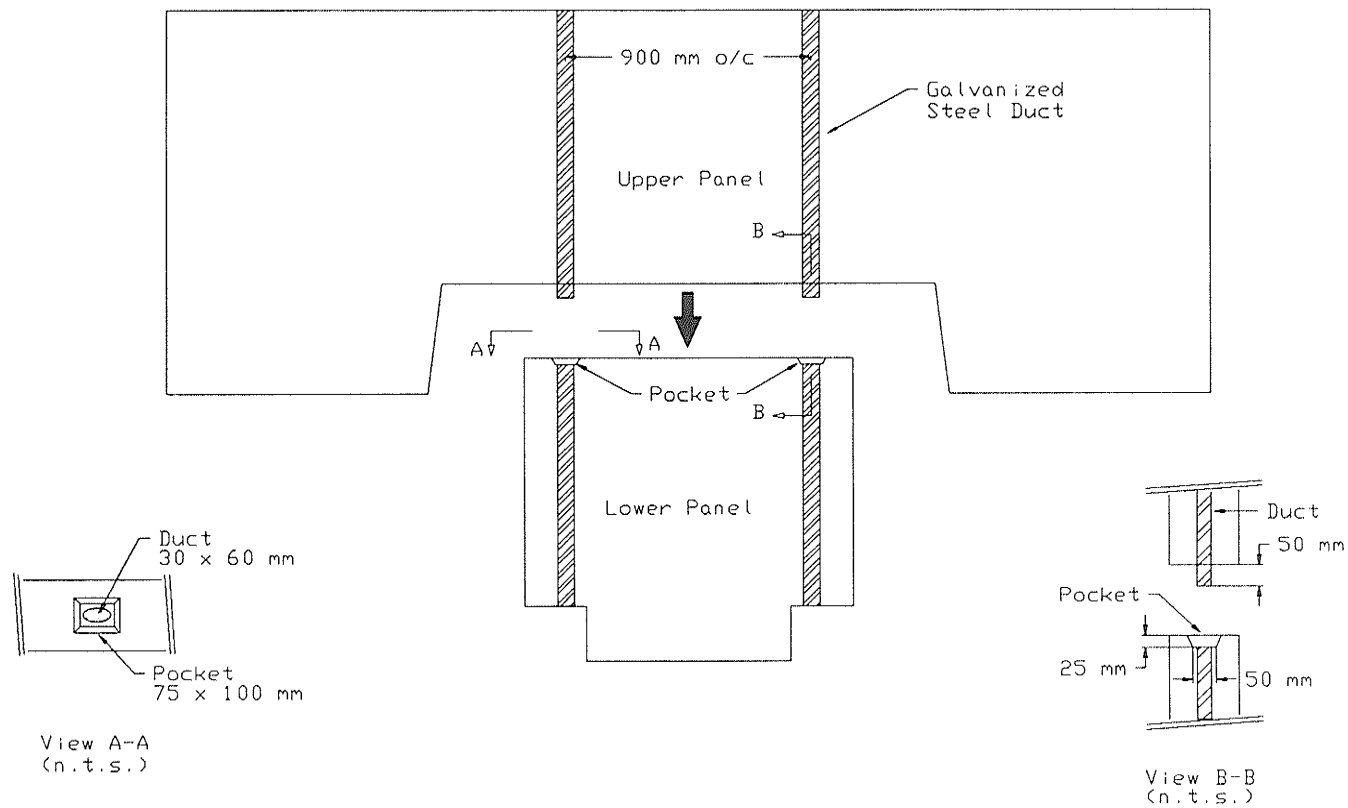
Figure 3.7   Post-tensioned Specimen Configuration and Connection Assembly Details
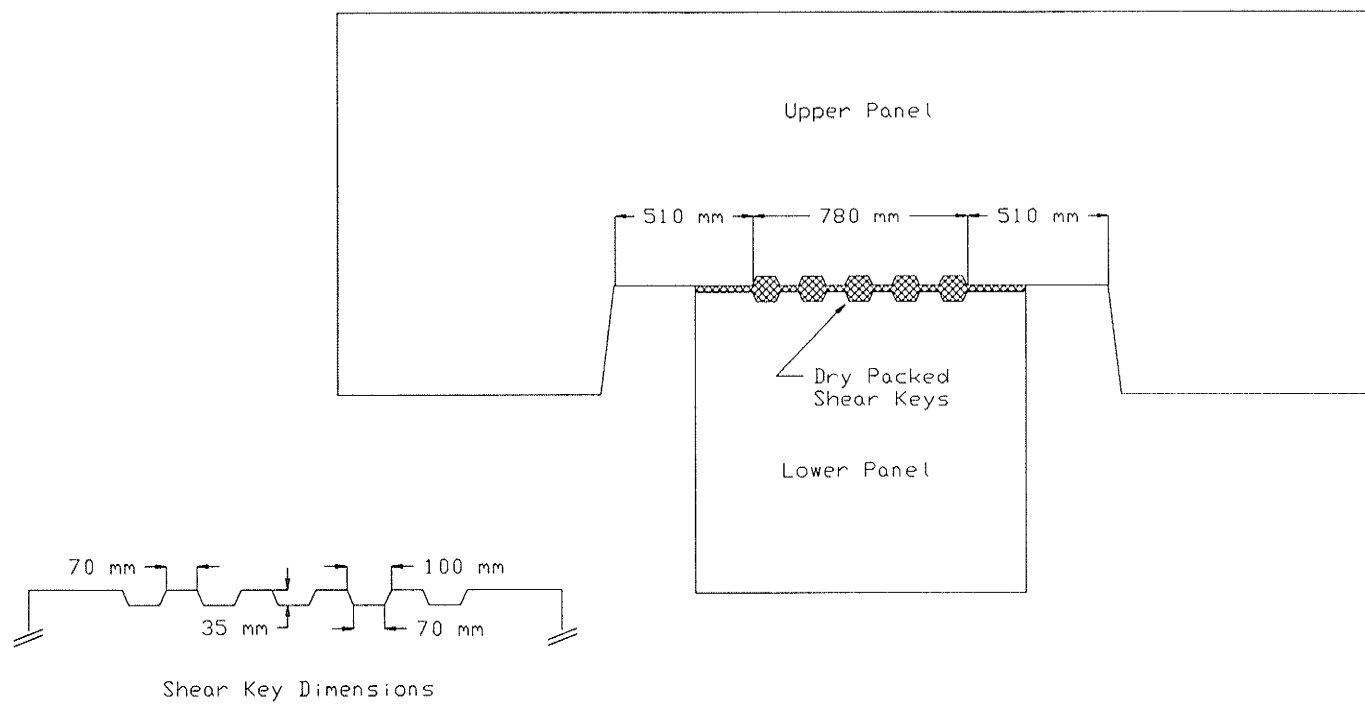
Figure 3.8   Specimen SK Configuration and Shear Key Dimensions
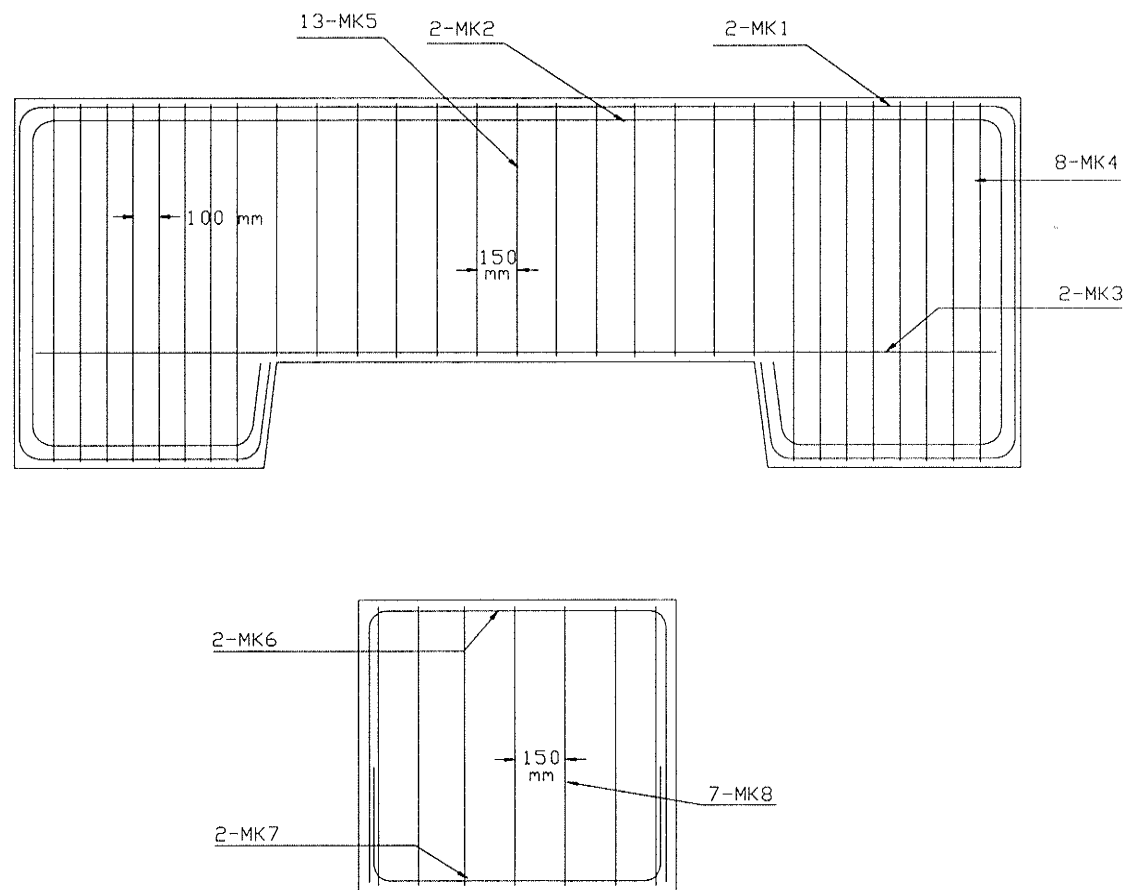
Figure 3.9   Specimen DP Reinforcement Details

Continuity Bar

15-MK5   2-MK2   2-MK1

8-MK4

100 mm

150 mm

2-MK3

210 mm

450 mm ── 900 mm c/c ── 450 mm

150 mm ── 900 mm c/c ── 150 mm

1-MK6 F.F
1-MK9 N.F.

Steel Angle

Continuity Bar

max. 190 mm

2-MK7

7-MK8
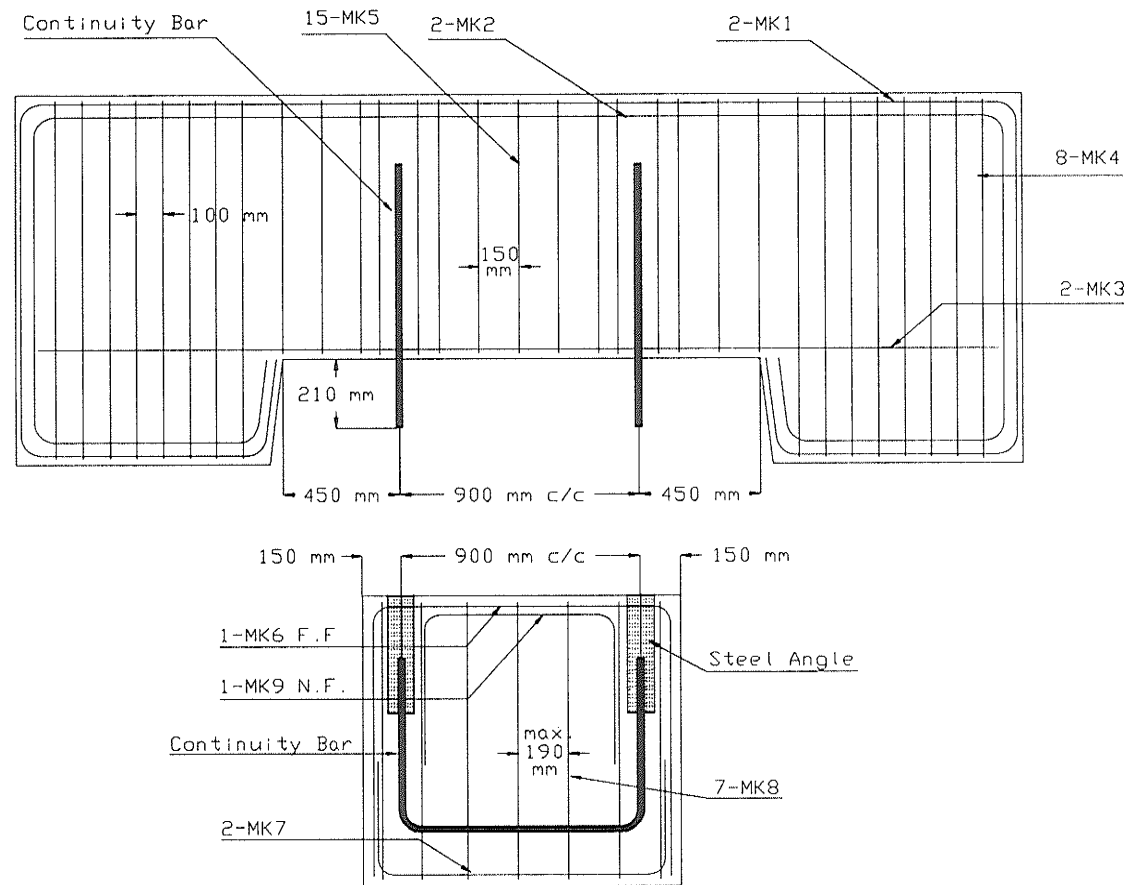
Figure 3.10   Specimen RW Reinforcement Details
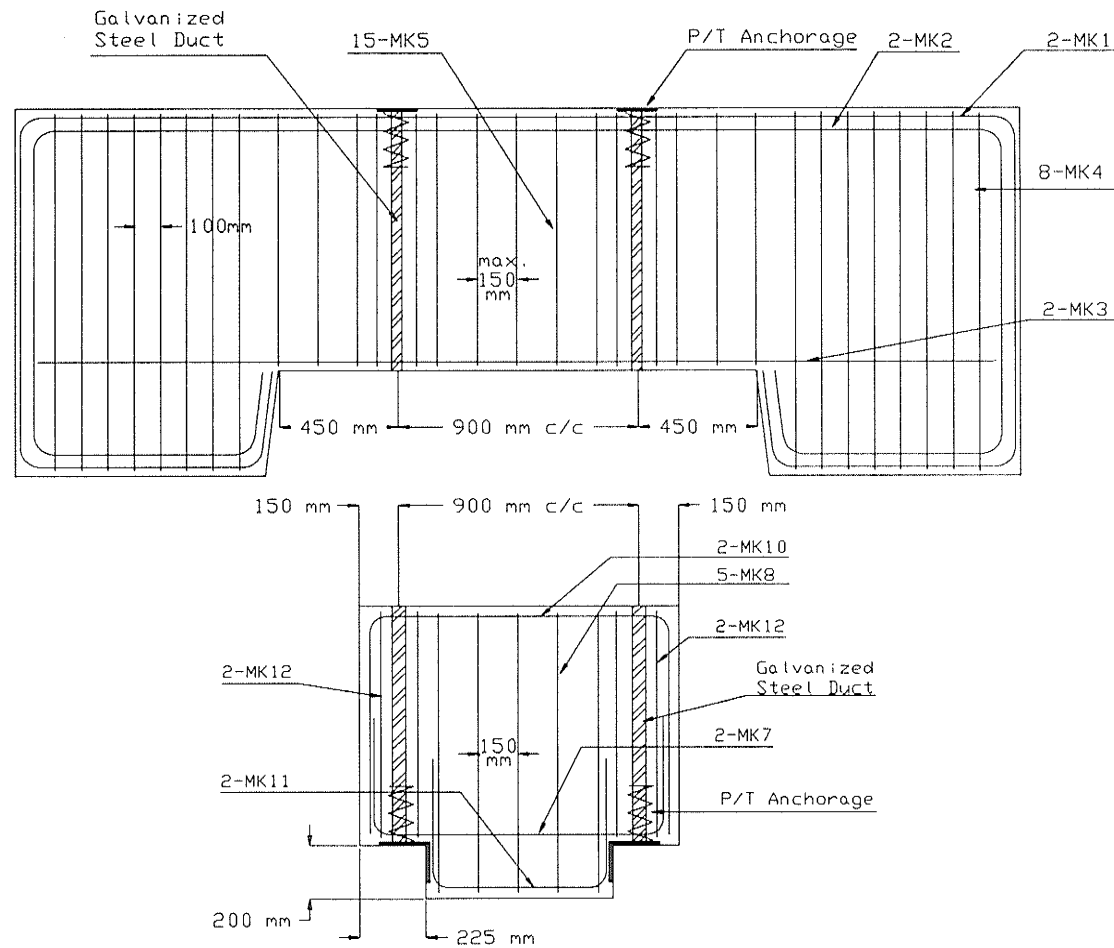
Figure 3.11   Specimen PTS, PTB and PTB-S Reinforcement Details

NOTE: Bearing plate width is 150 mm.

20 mm dia.

150 mm

15 mm

10M Spiral
(6 turns)

Steel Plate
Grade 300W

Nelson Stud
300 mm long
(15.9 mm dia.)

P/T Duct

Upper Panel Anchorage Detail

P/T Duct

Nelson Stud
300 mm long
(15.9 mm dia.)

10M Spiral
6 turns

Steel Plate
Grade 300W

15 mm (typ.)

115 mm

20 mm dia.

215 mm

6 Δ 150   E480XX
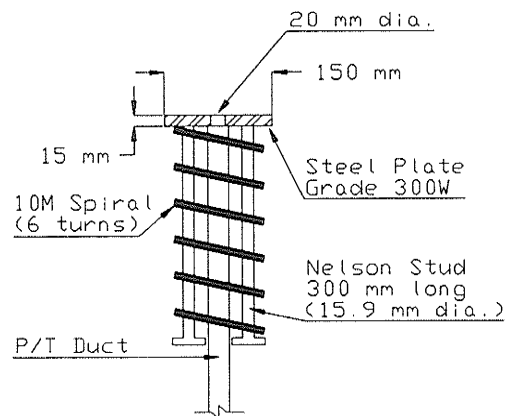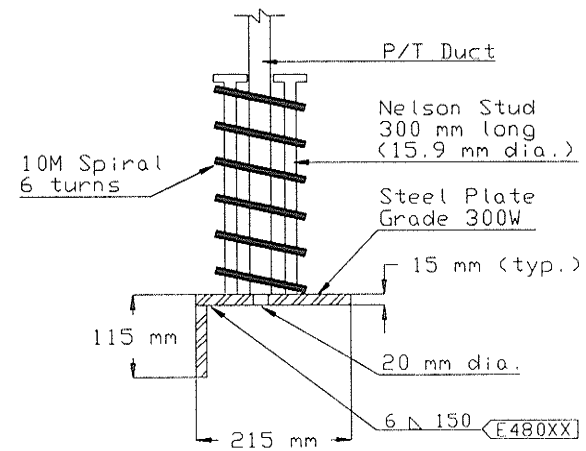
Lower Panel Anchorage Detail

Figure 3.12   Post-tensioning Anchorage Detail
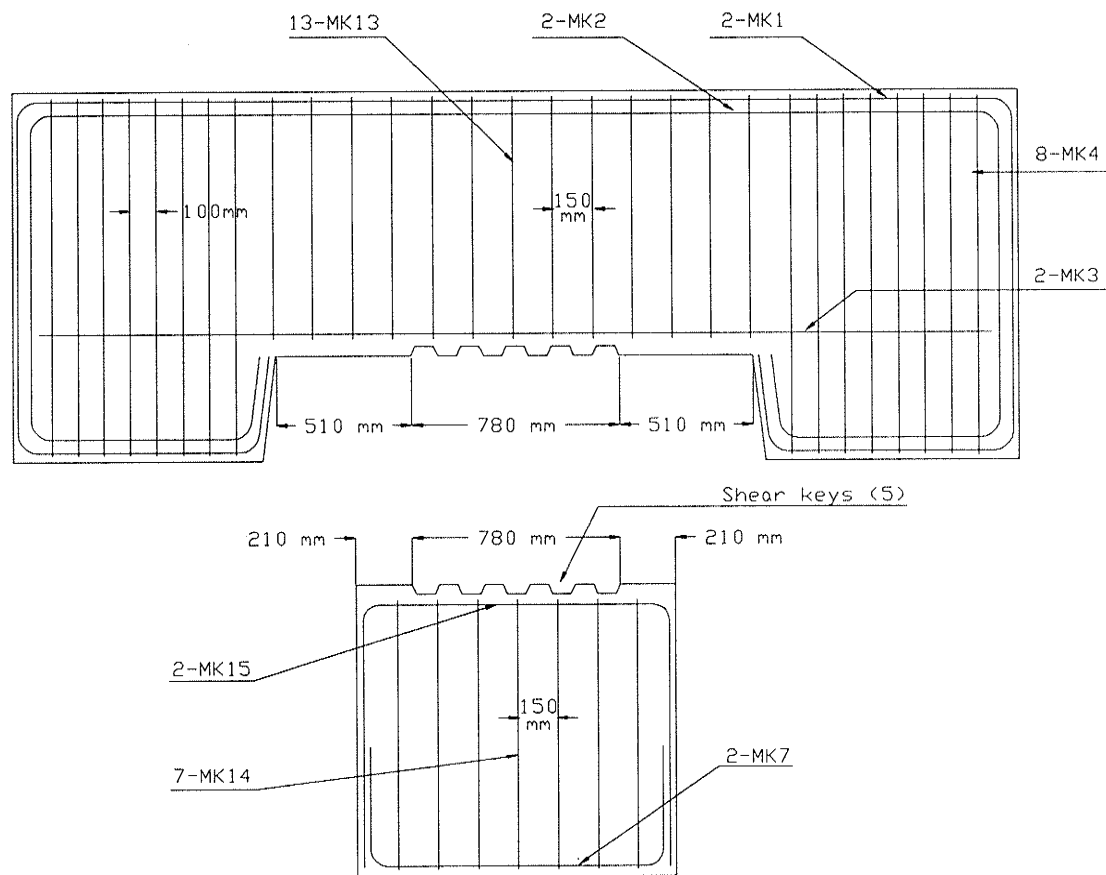
Figure 3.13   Specimen SK Reinforcement Details
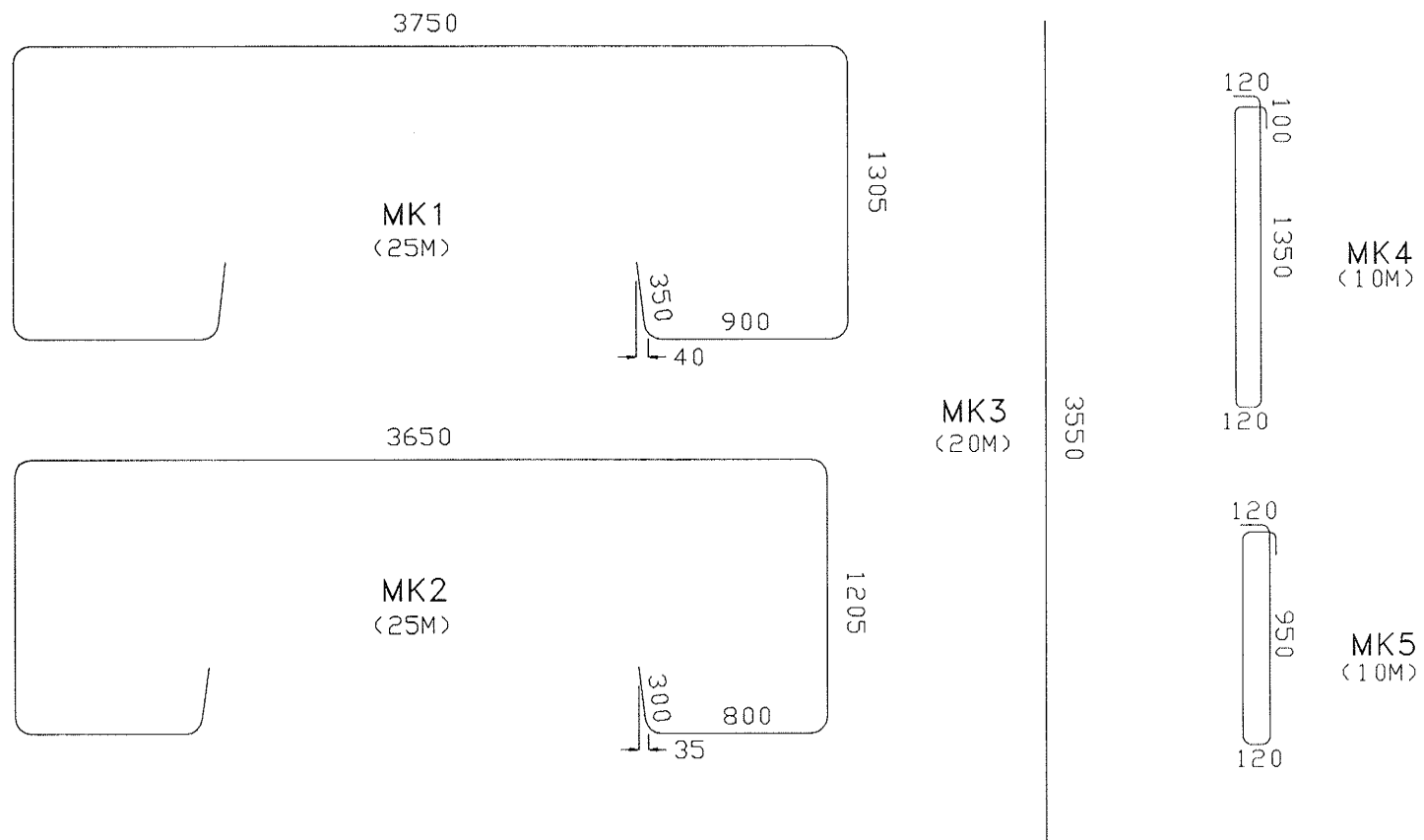
Figure 3.14(a) Reinforcing Bar Details
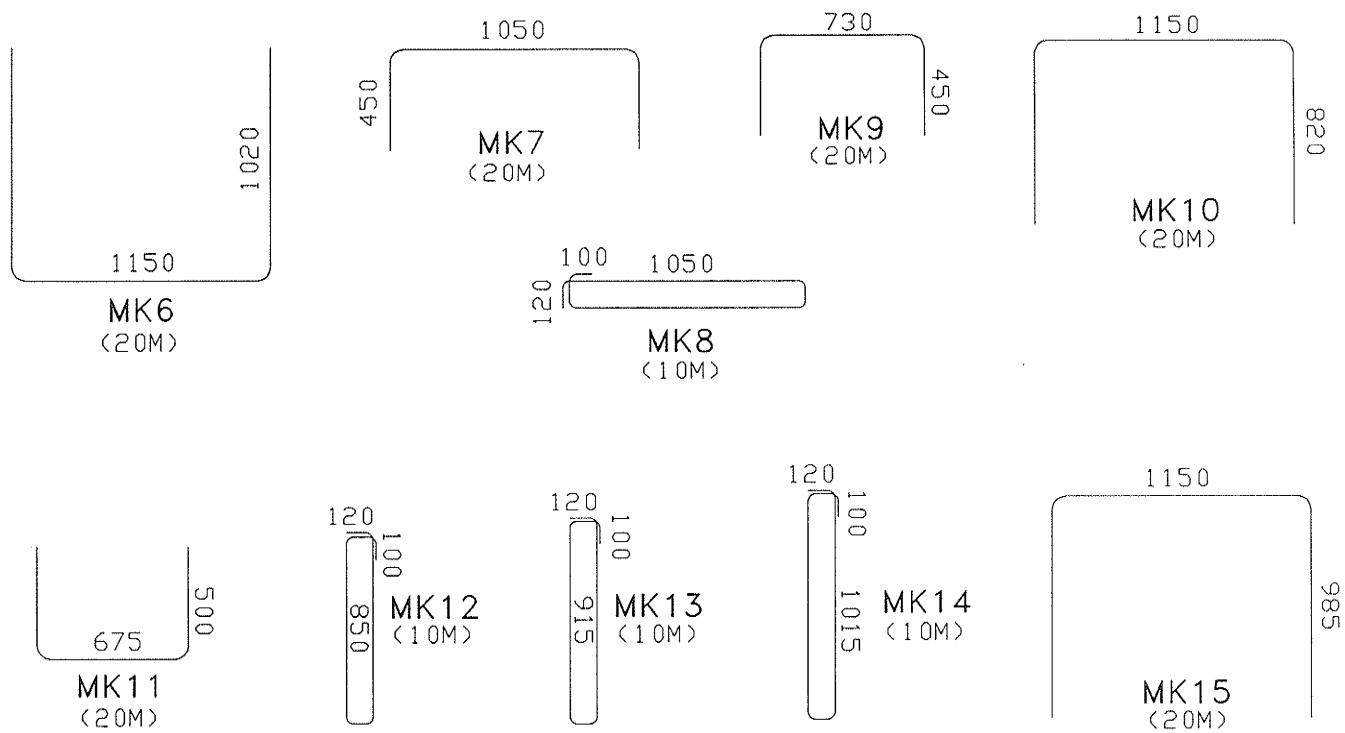
Figure 3.14(b) Reinforcing Bar Details
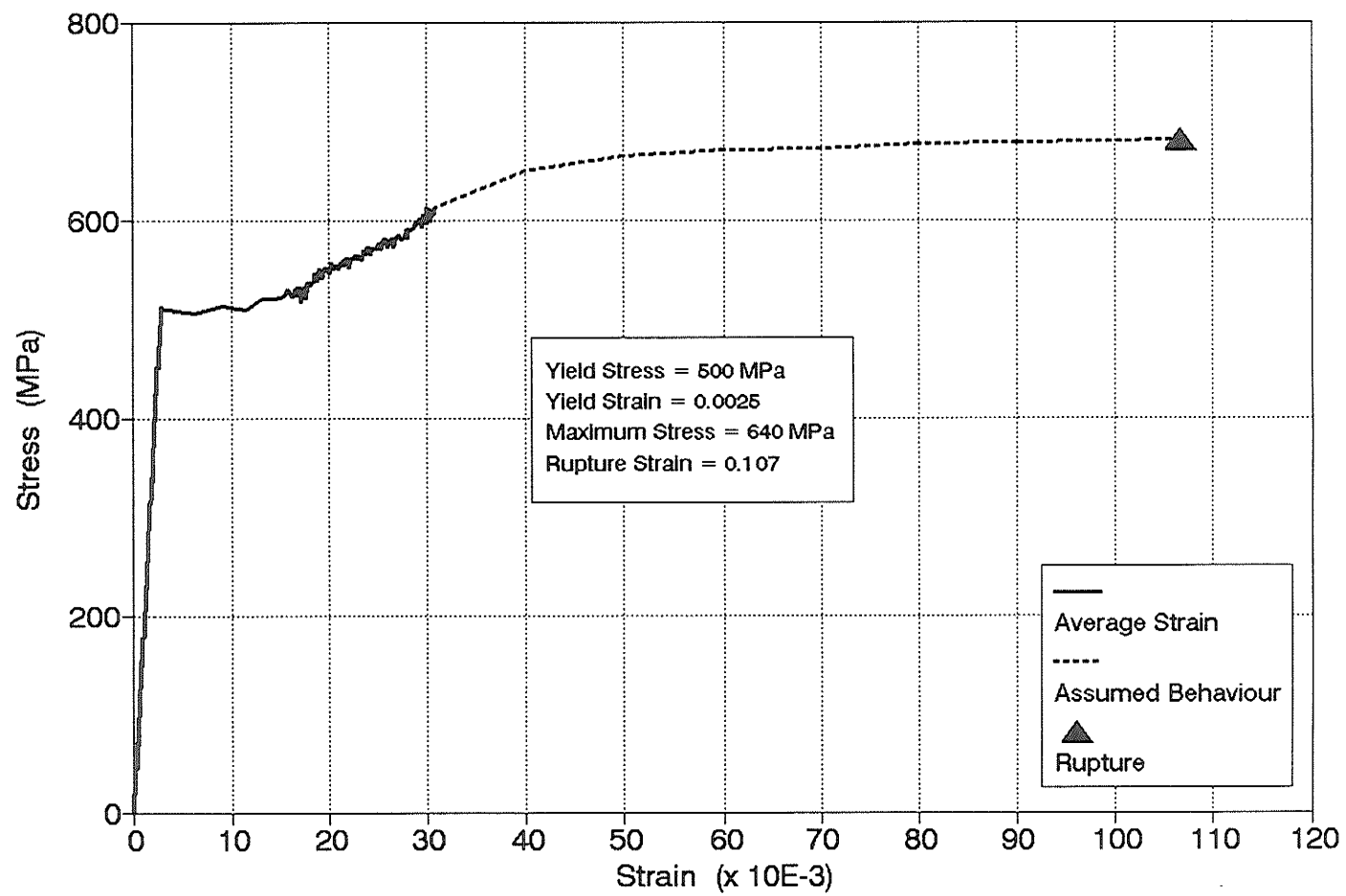
Figure 3.15   Stress - Strain Characteristics of Mild Steel Reinforcement
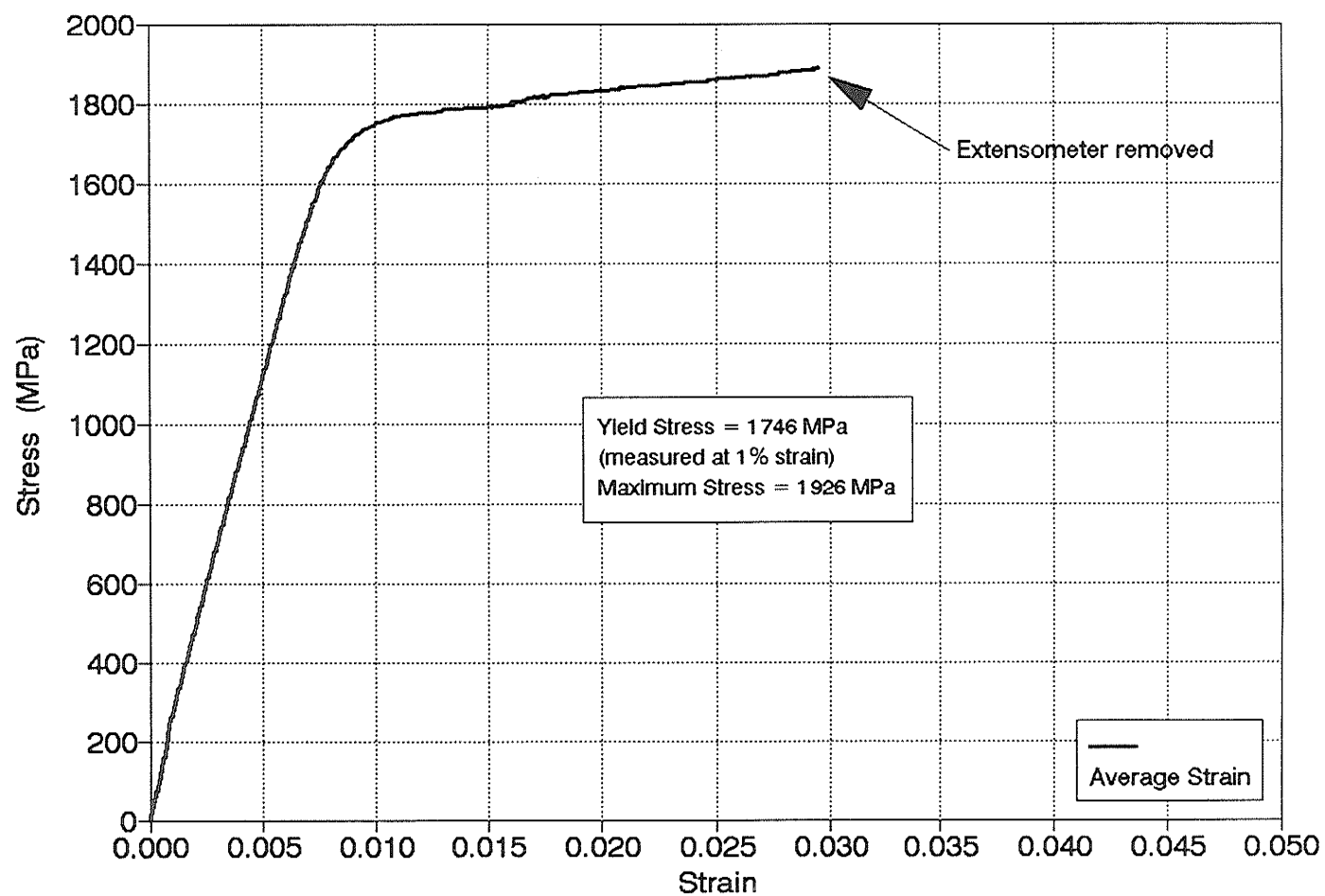
Figure 3.16   Stress - Strain Characteristics of Post-tensioning Strand
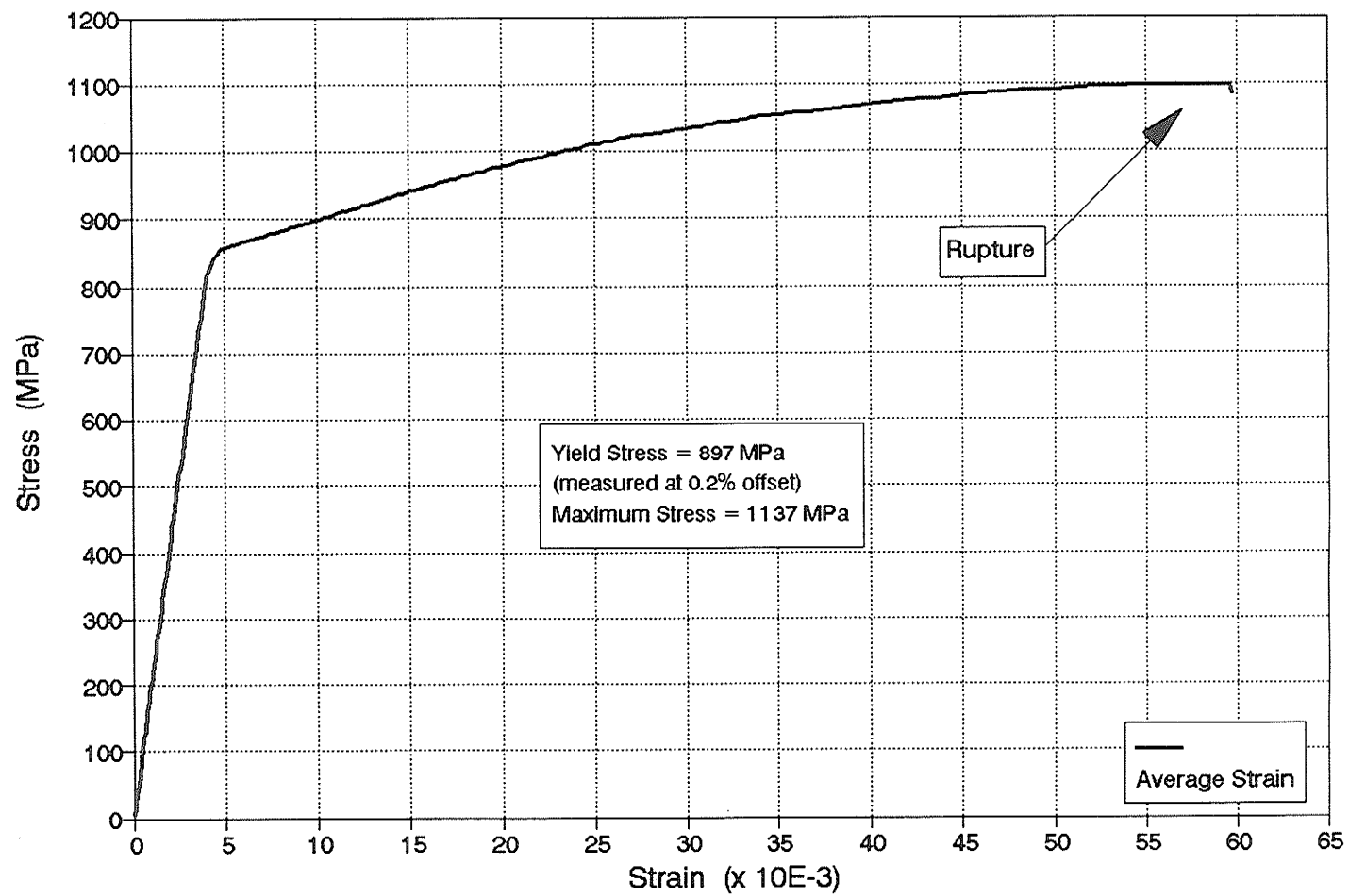
Figure 3.17   Stress - Strain Characteristics of Post-tensioning Bars
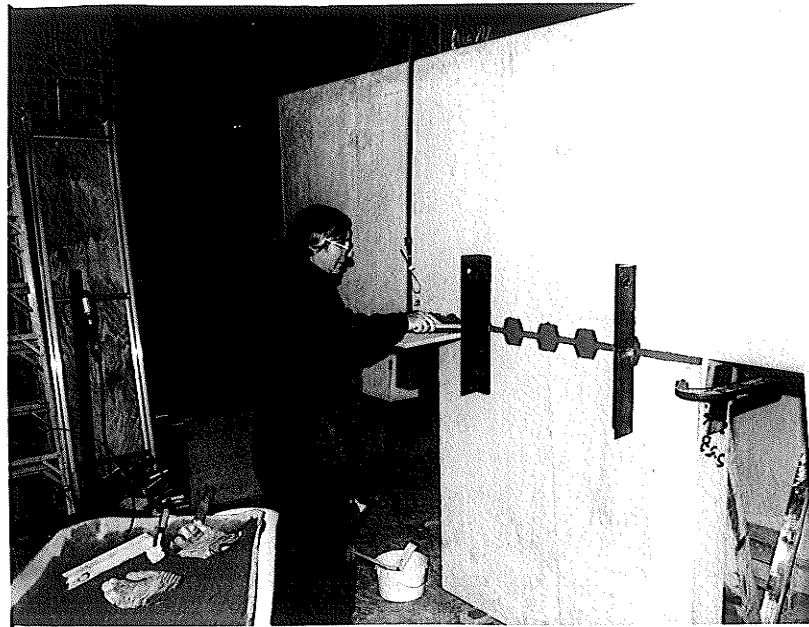
Figure 3.18   Dry Packing Process
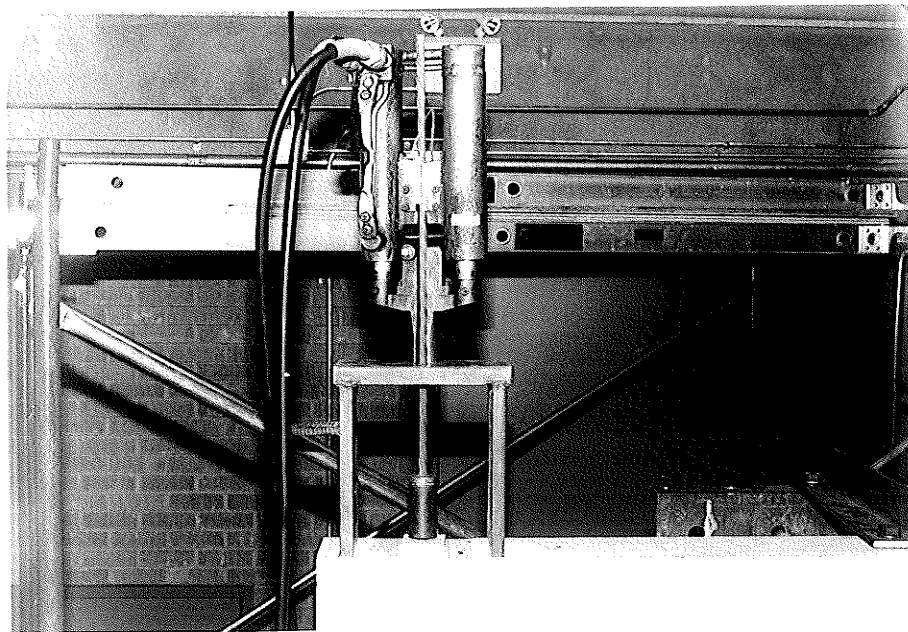
Figure 3.19(a) Jacking of Post-tensioning Strands
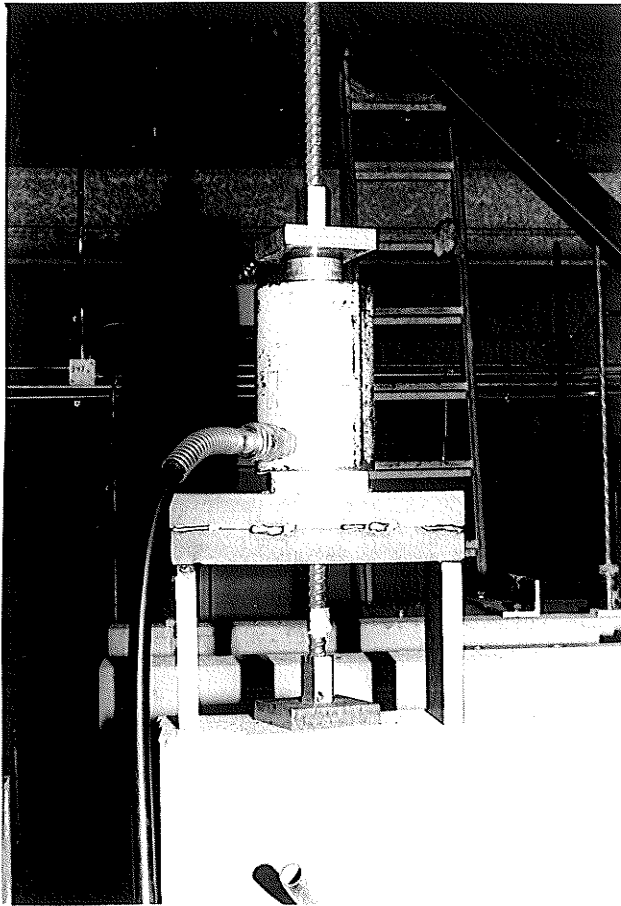
Figure 3.19(b) Jacking of Post-tensioning Bars
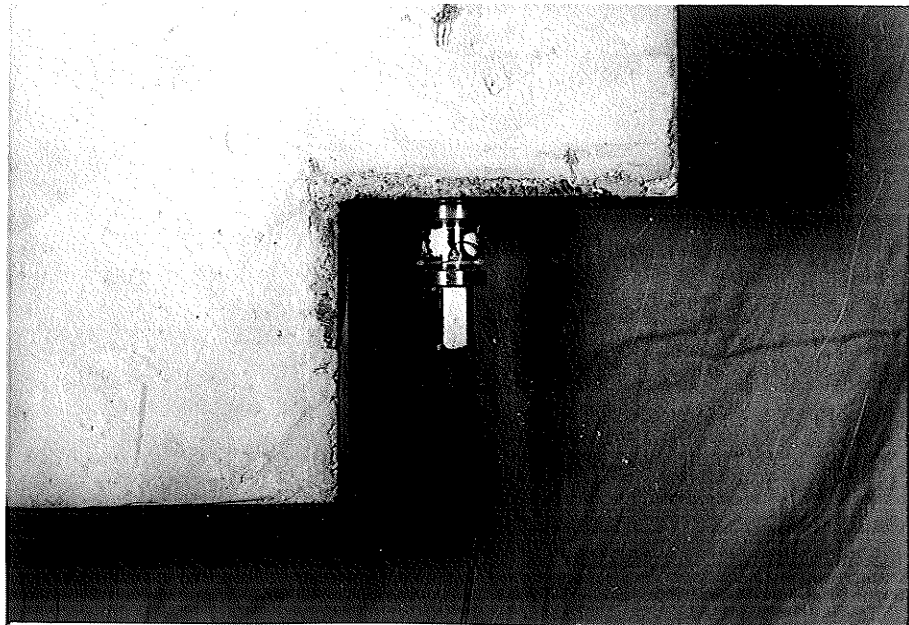
Figure 3.20   Post-tensioning Load Cell

19 mm dia.

Plan View

Load Cell uses four strain gauges around its circumference, two longitudinally and two transversely, wired in a full Wheatstone Bridge.

50 mm

10 mm

25 mm

38 mm dia.

Strain Gauge

Side View
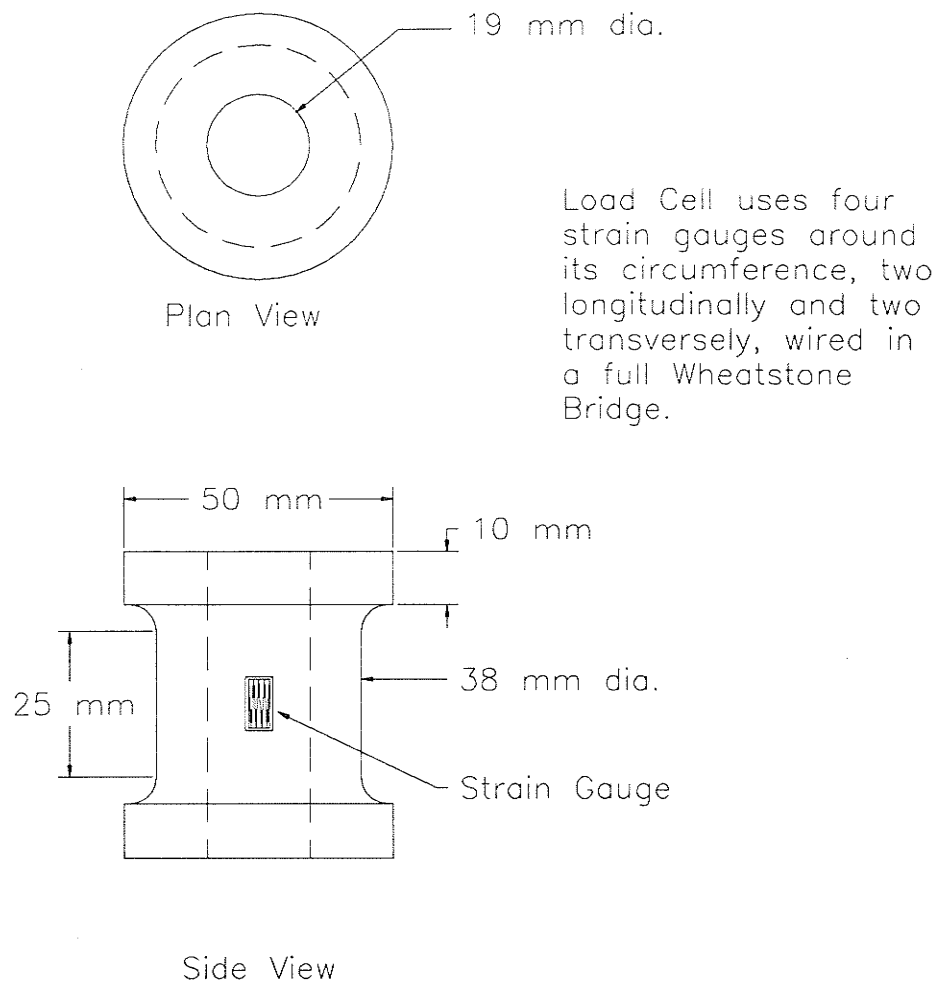
Figure 3.21   Post-tensioning Load Cell Details
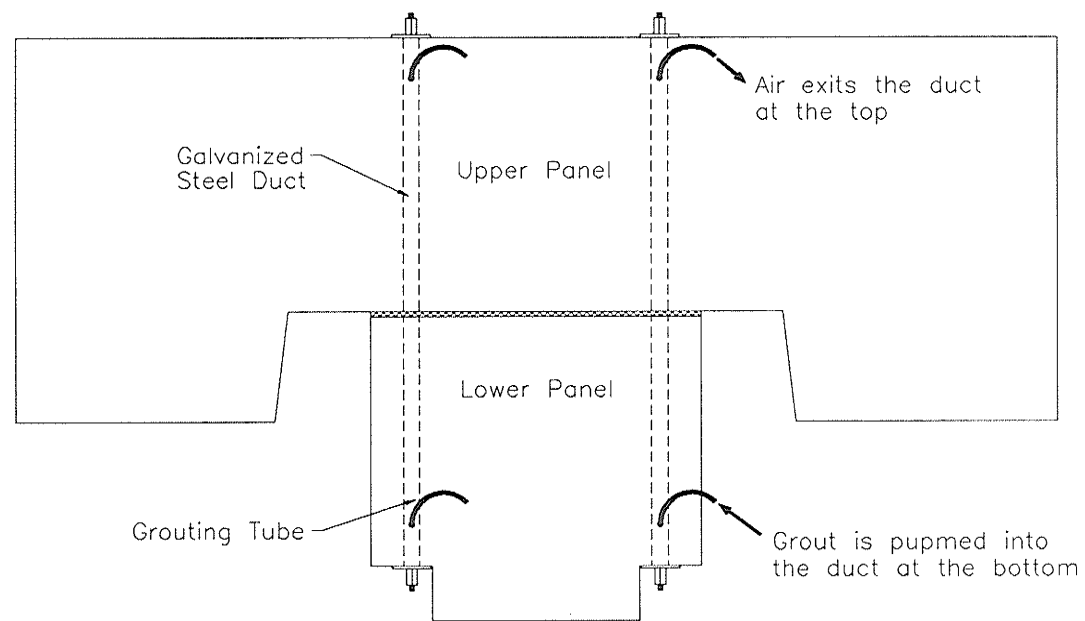
Figure 3.22   Grouting Procedure for Post-tensioning Ducts
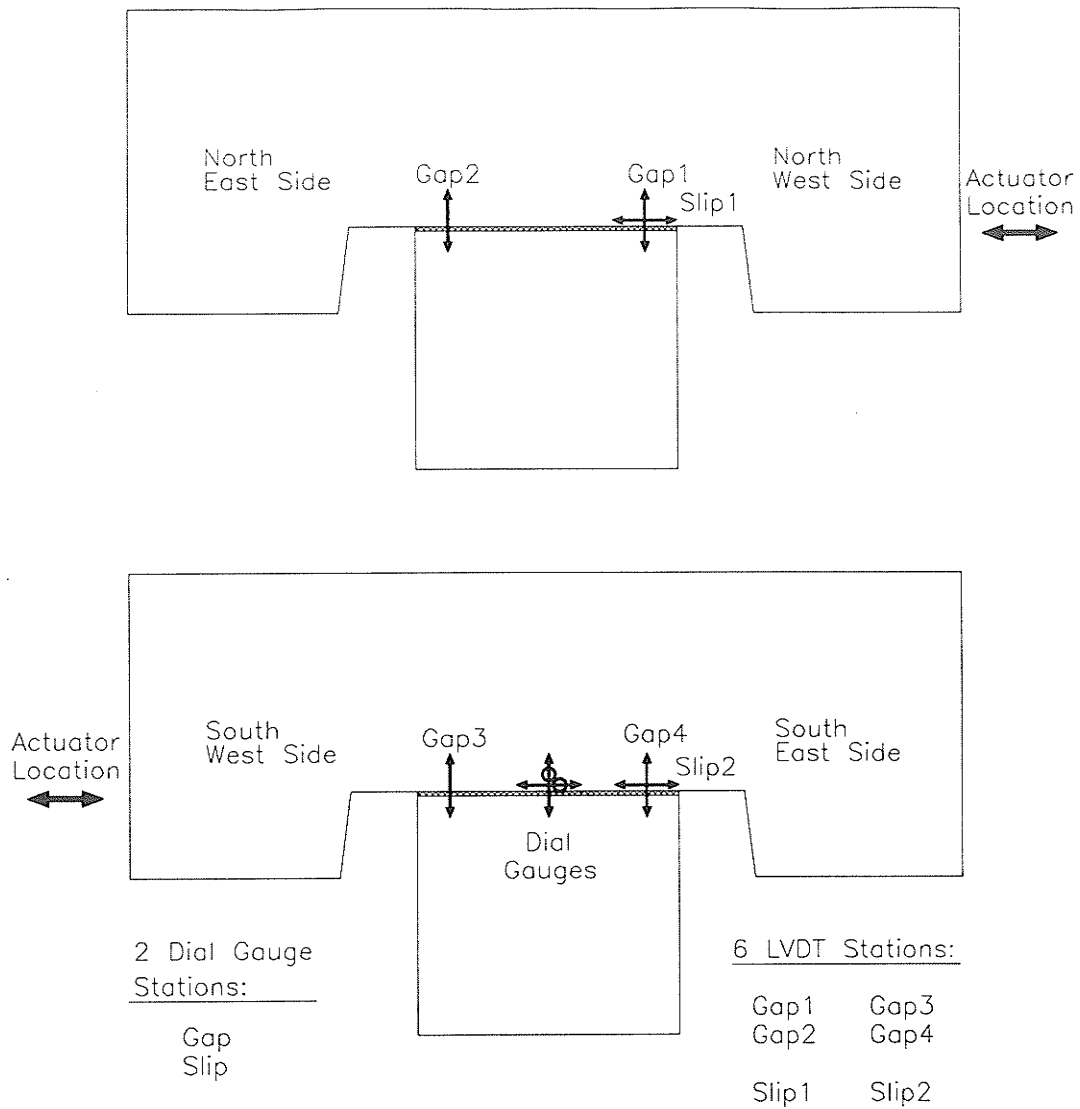
Figure 3.23   Specimen Instrumentation for Horizontal and Vertical Connection Displacements
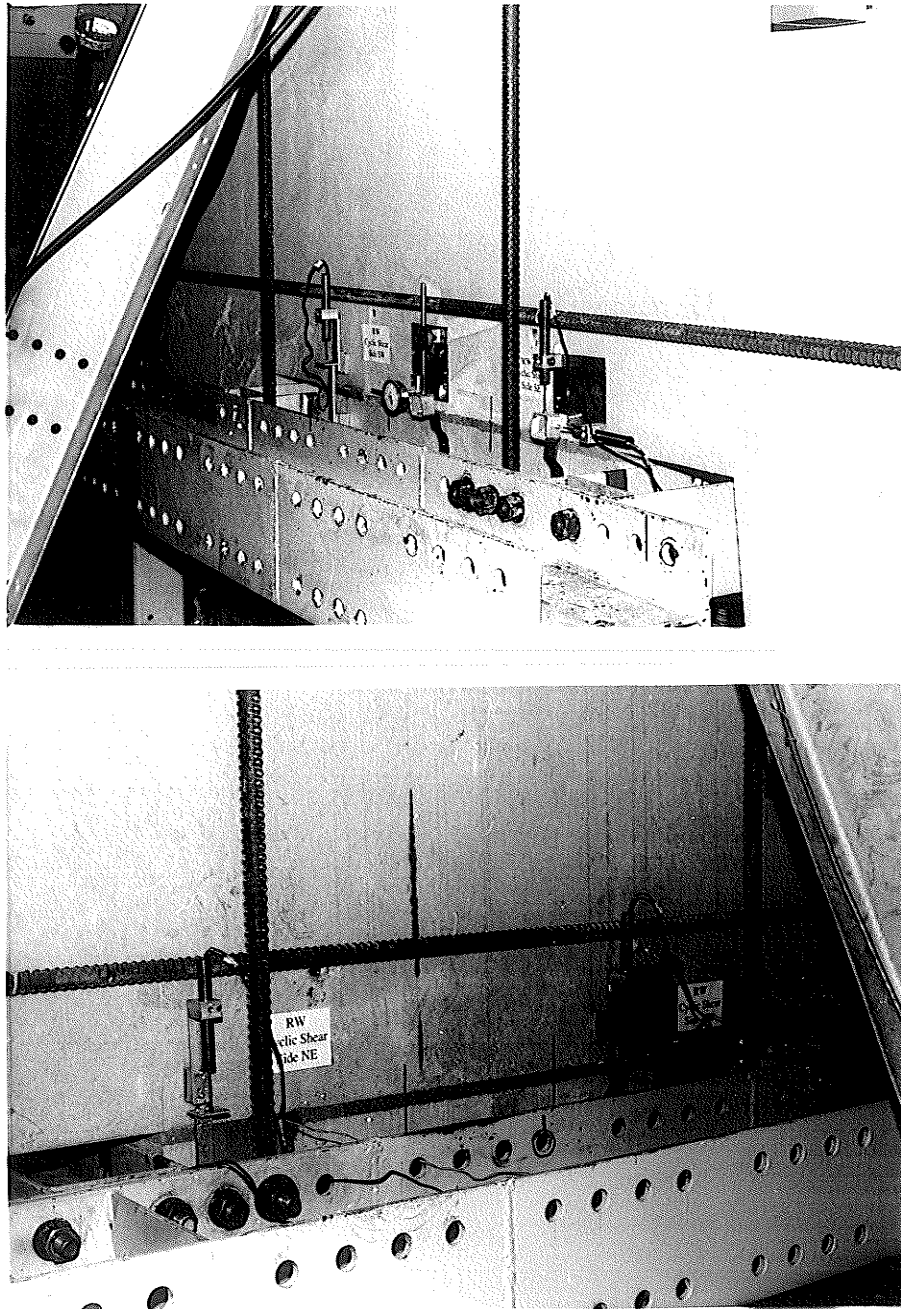
Figure 3.24   Specimen Instrumentation

Continuity
Reinforcement
(25M, 400W)

Strain Gauge

Strain Gauge

Actuator
Location

North
East Side

North
West Side

Strain Gauge

NOTE:
One 10 mm strain gauge was
placed on each bar. The gauge
was oriented axially on the bar.

222
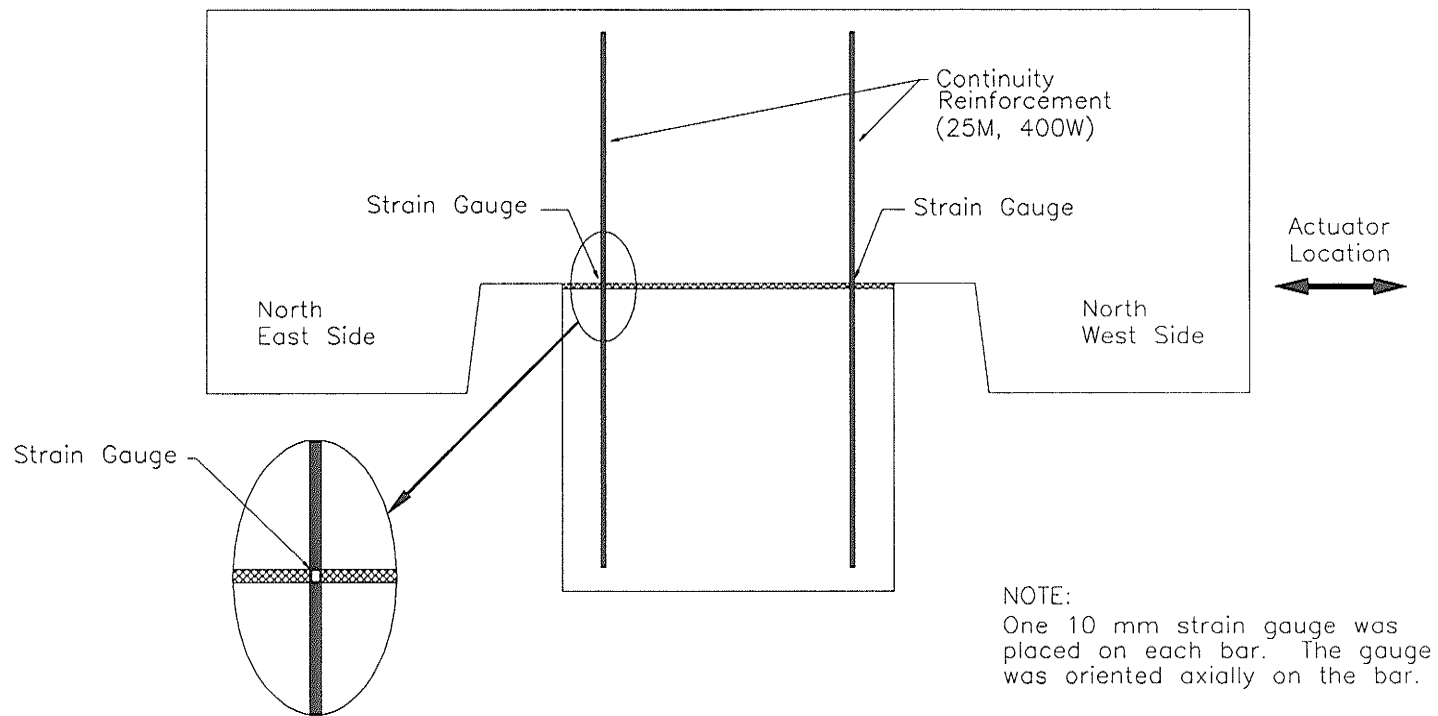
Figure 3.25   Strain Gauge Locations for Specimen RW
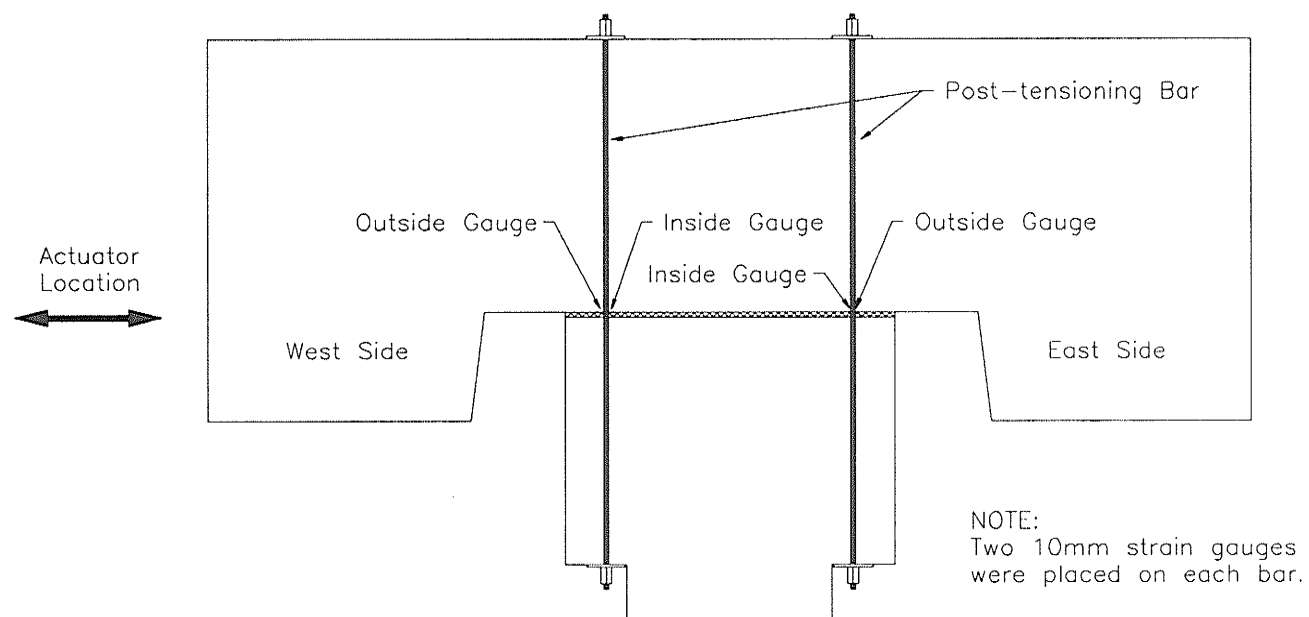
Figure 3.26   Strain Gauge Locations for Specimens PTB and PTB-S

Reaction Wall

Gravity Load Simulator

Lateral Brace

Loading Yoke

Cross Beam

Actuator

Lateral Brace

Reaction Abutment

Structural Floor

224
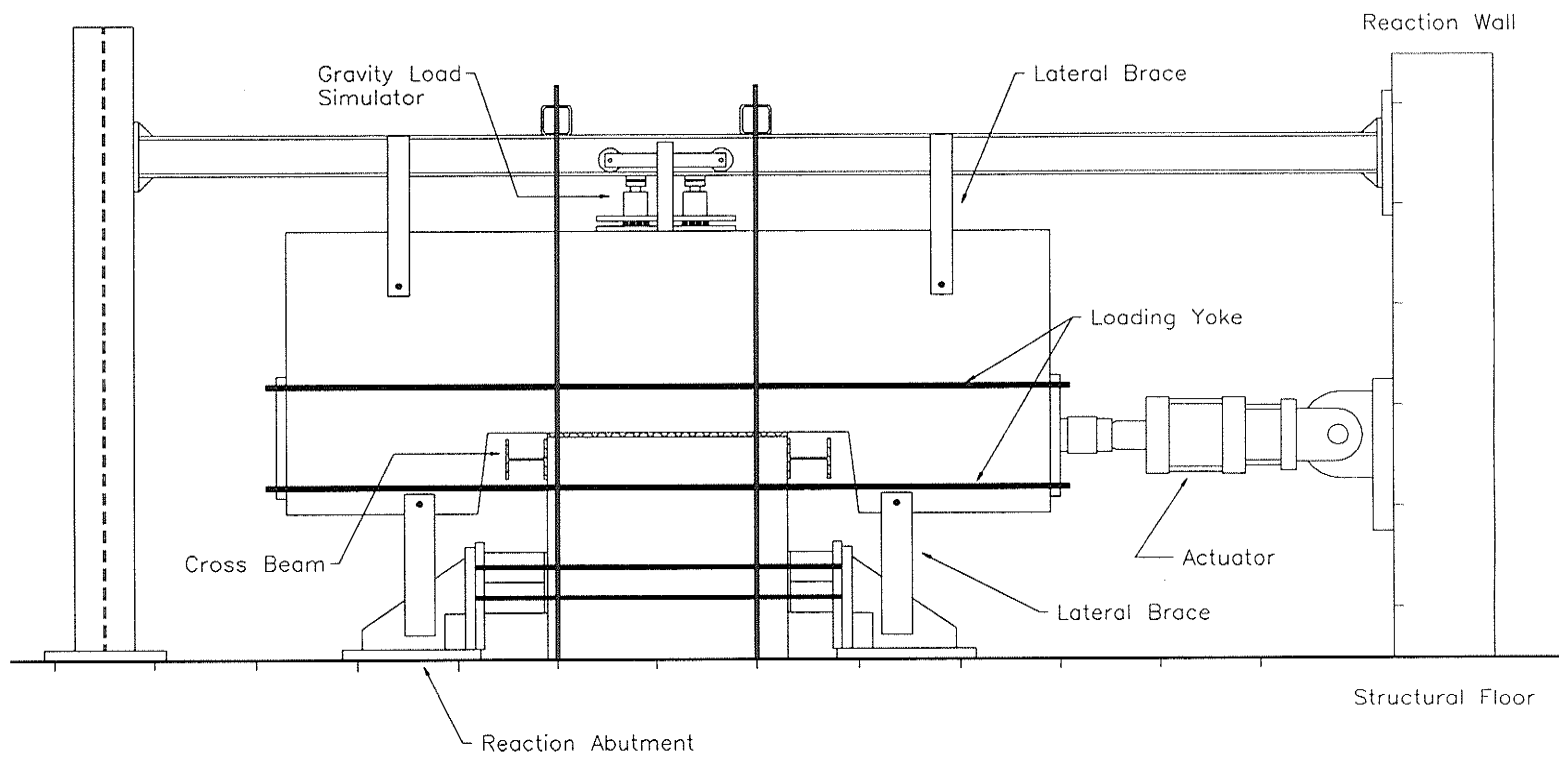
Figure 3.27(a) Loading Frame - Elevation

Reaction Wall

Gravity Load
Simulator

Lateral Bracing
for Loading Frame

Specimen

Longitudinal Beam
Cantilevered from
Reaction Wall

Structural Floor
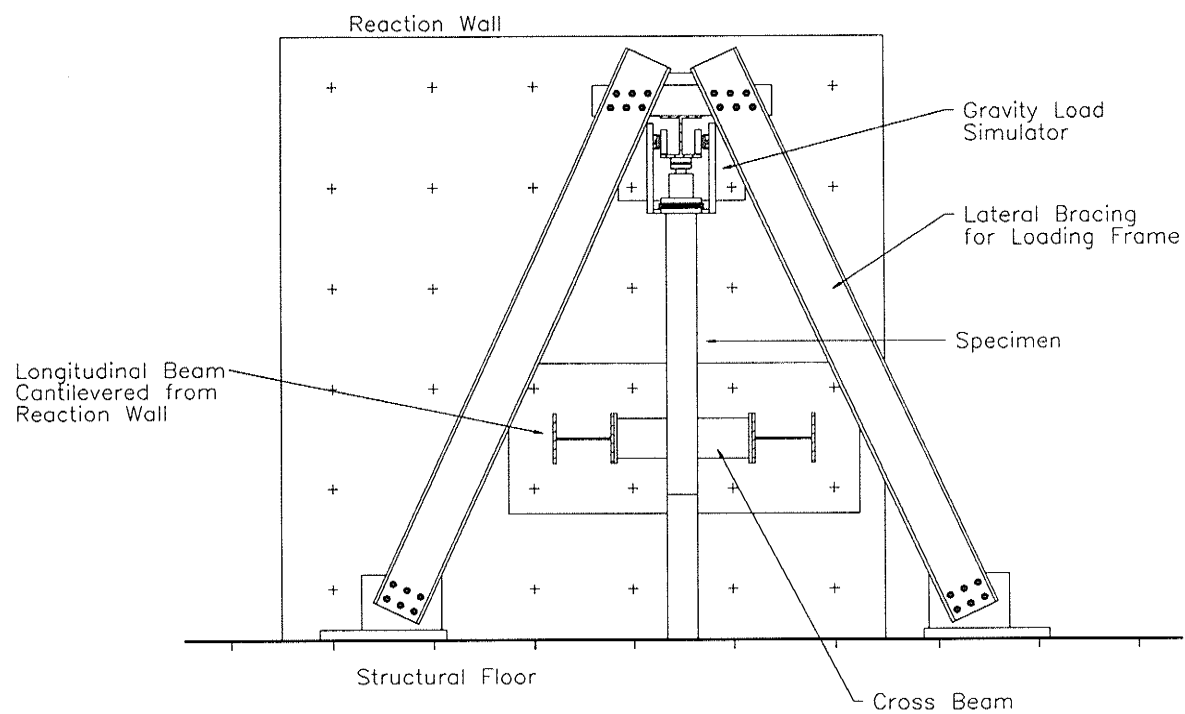
Cross Beam

Figure 3.27(b) Loading Frame - End View
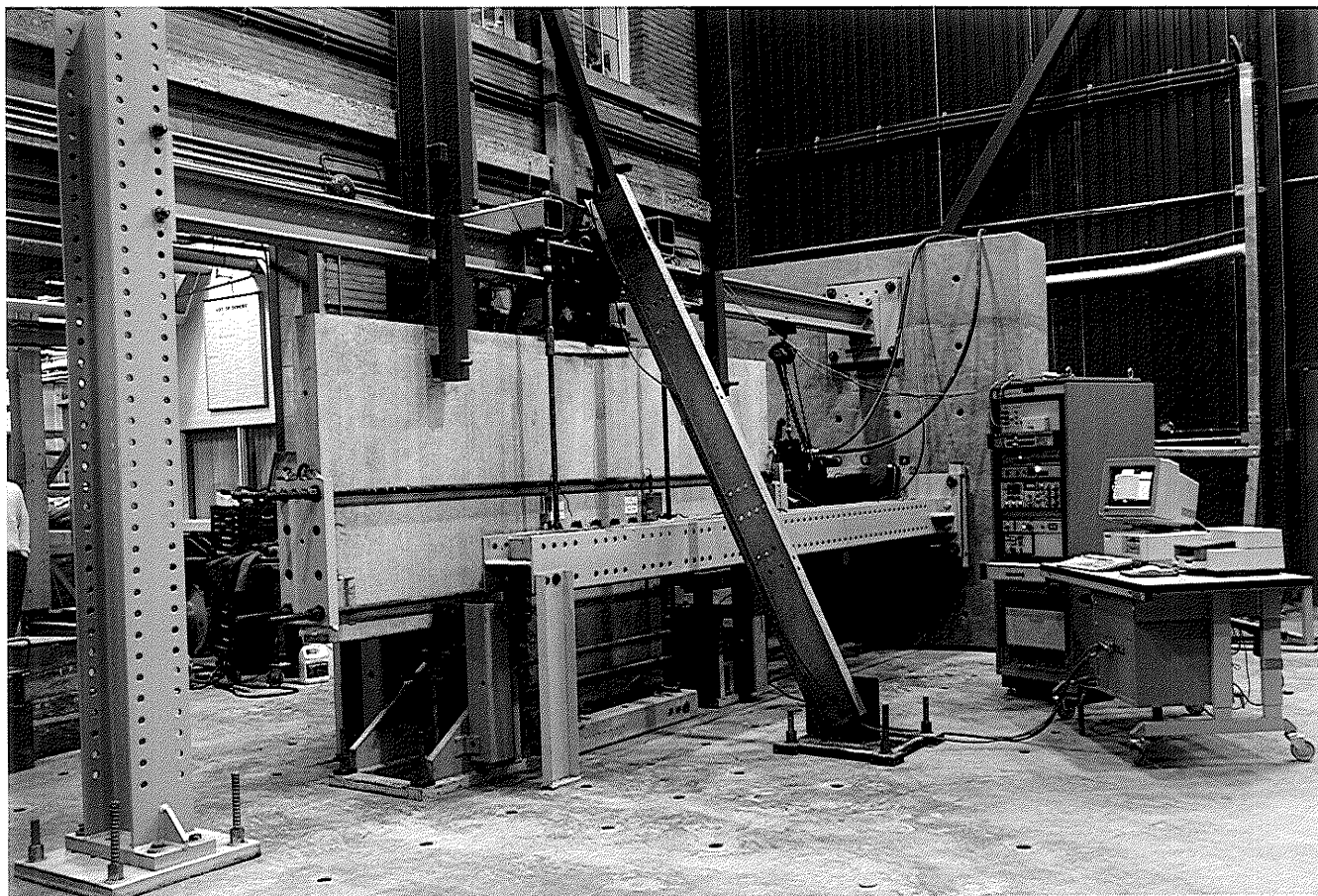
Figure 3.28   Experimental Setup
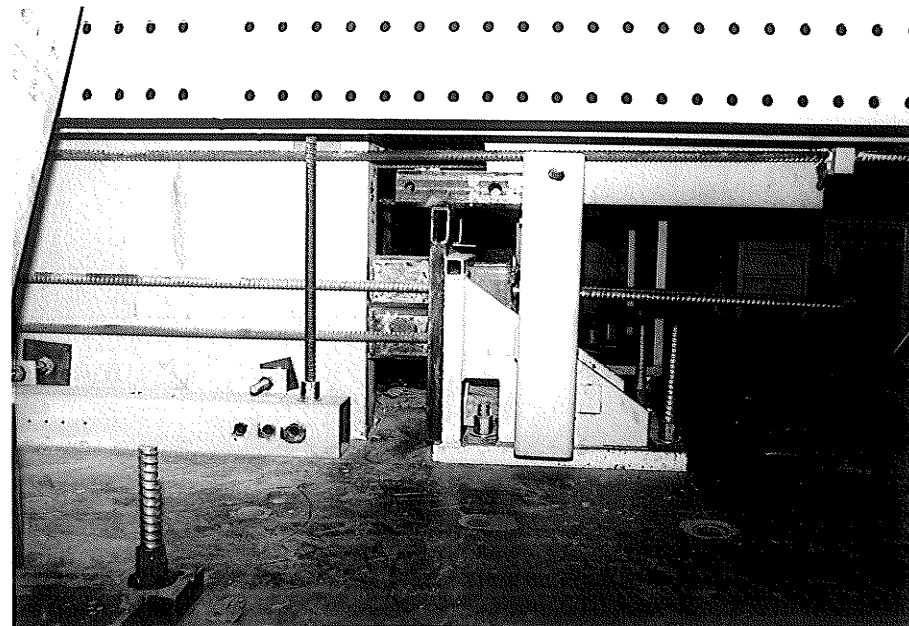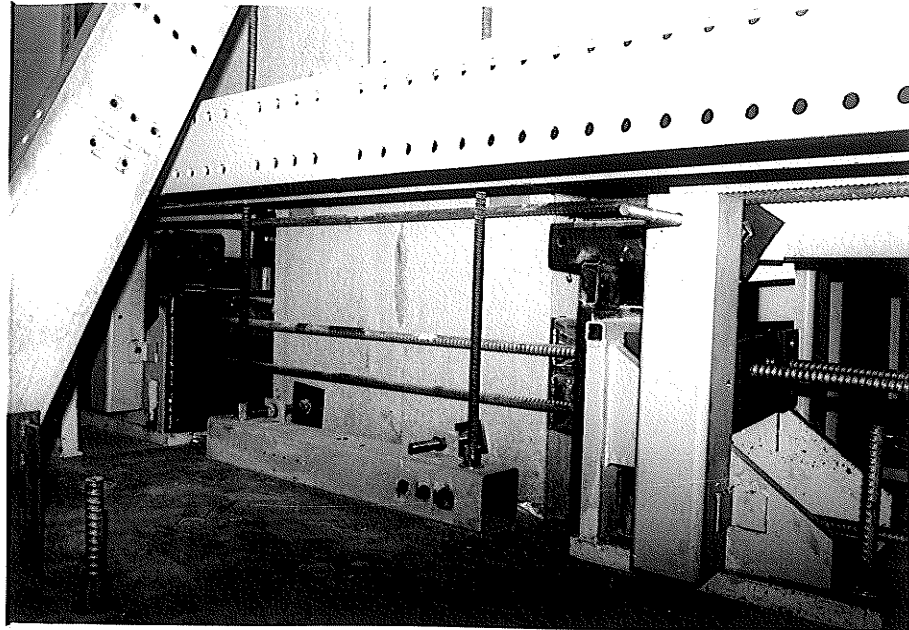
Figure 3.29   Reaction Abutments
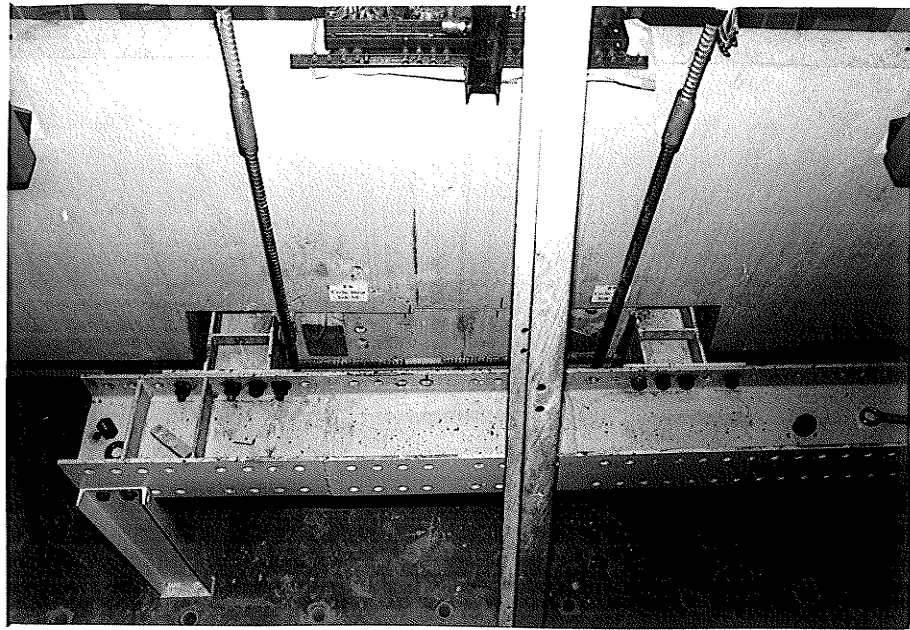
Figure 3.30   Reaction Cross Beams
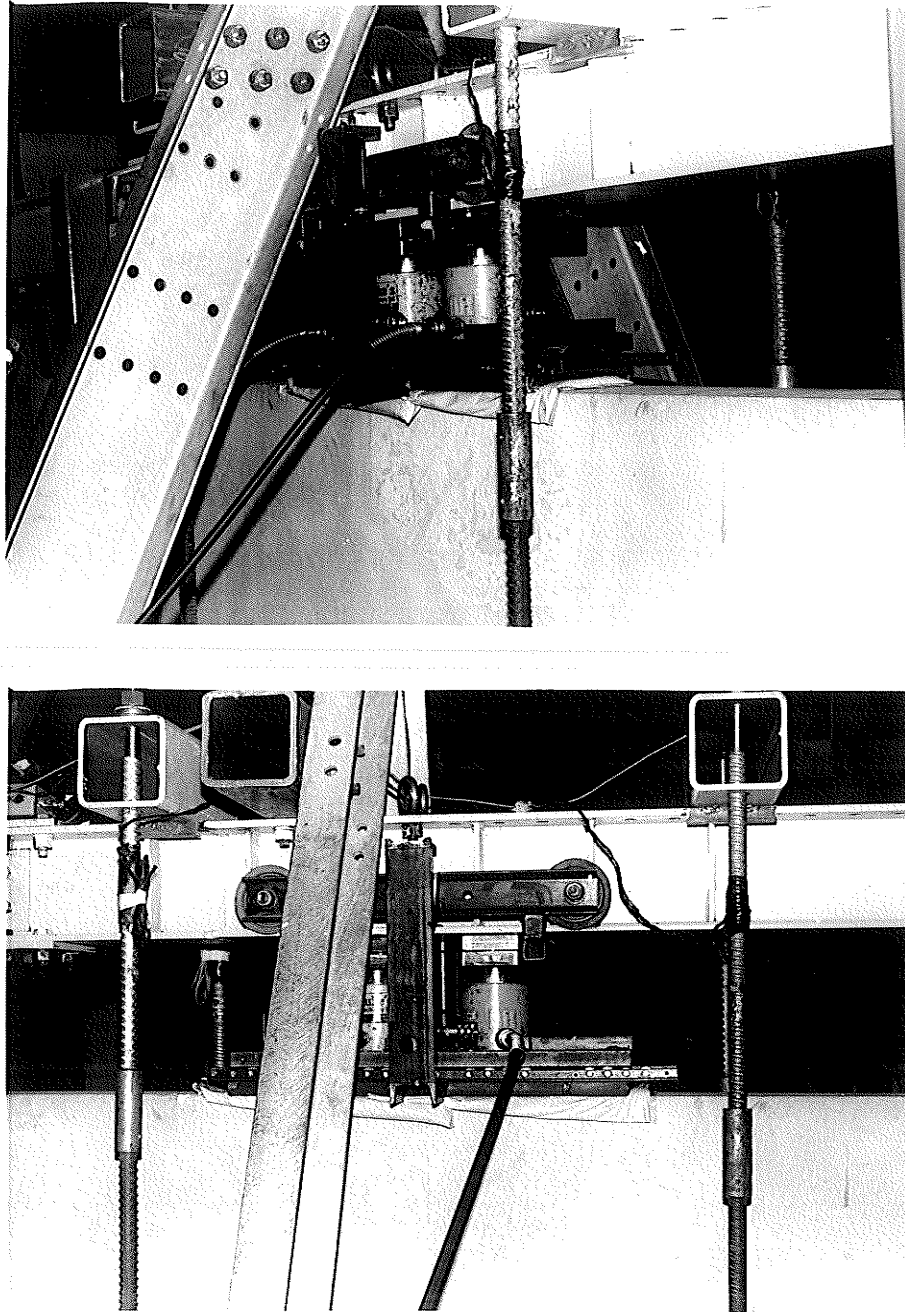
Figure 3.31   Gravity Load Simulator (Vertical Preload System)

DP - Cyclic Shear
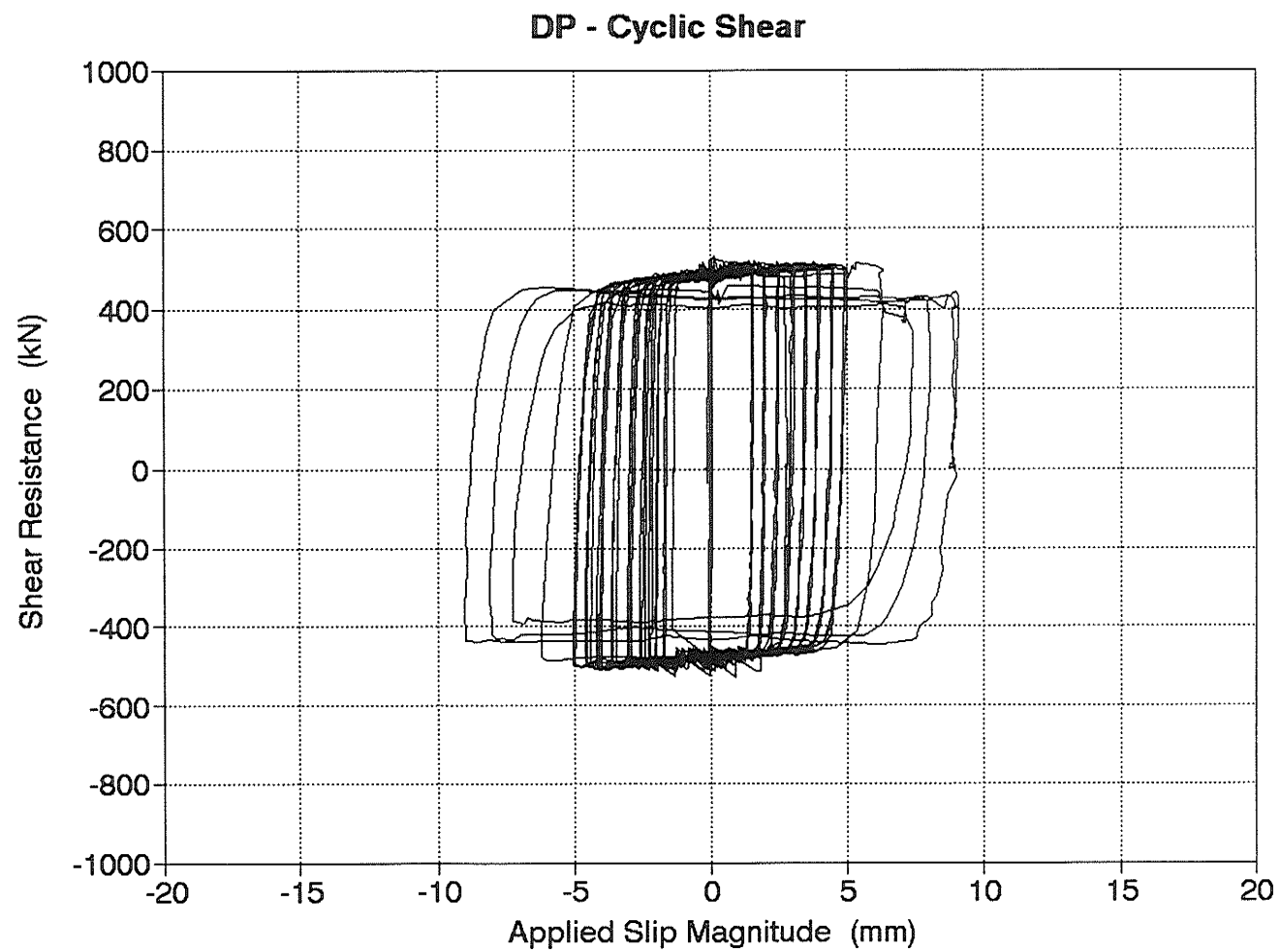
Figure 4.1   Specimen DP - Shear Resistance - Slip Behaviour Over the Duration of the Experiment
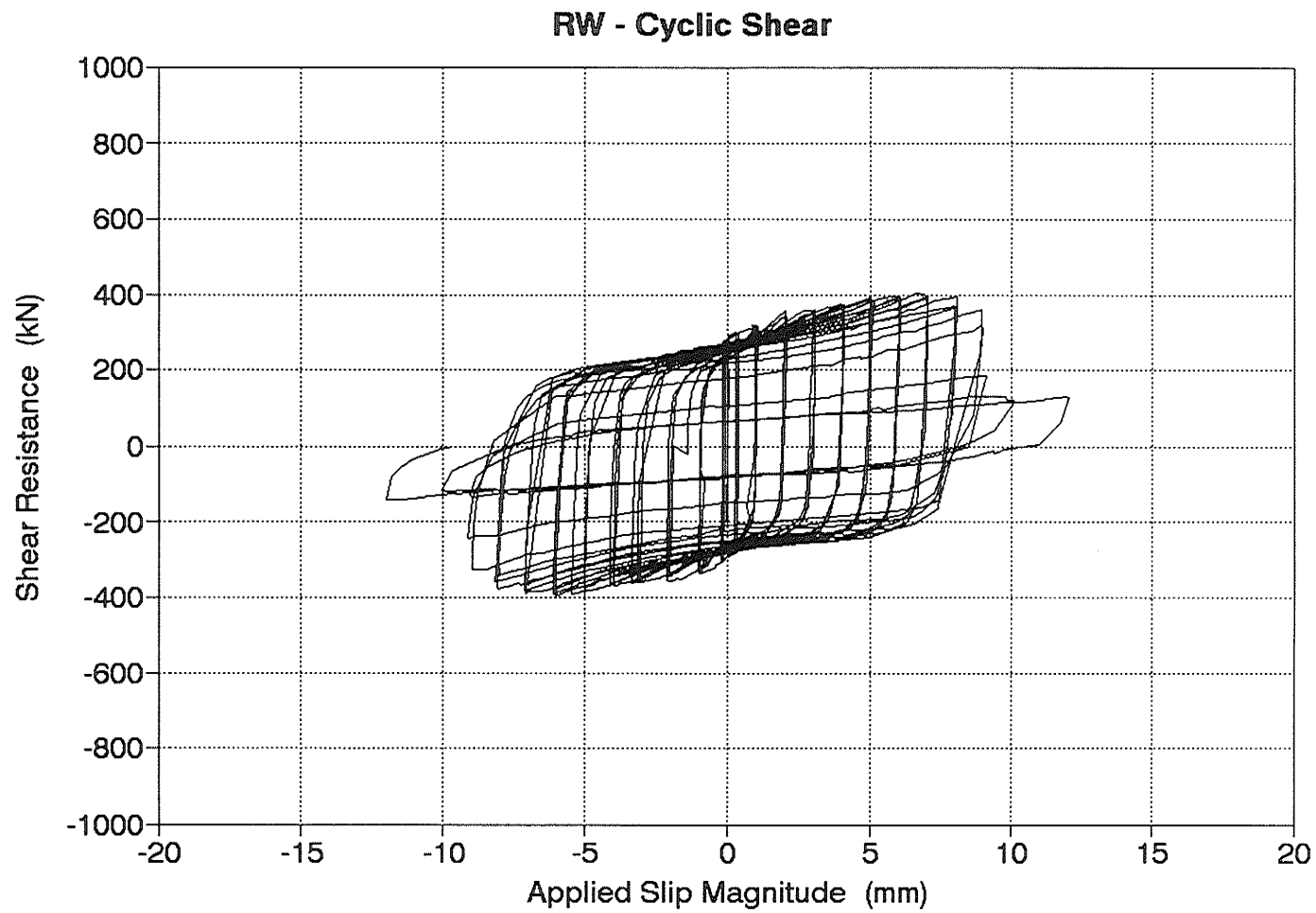
Figure 4.2   Specimen RW - Shear Resistance - Slip Behaviour Over the Duration of the Experiment

PTS - Cyclic Shear
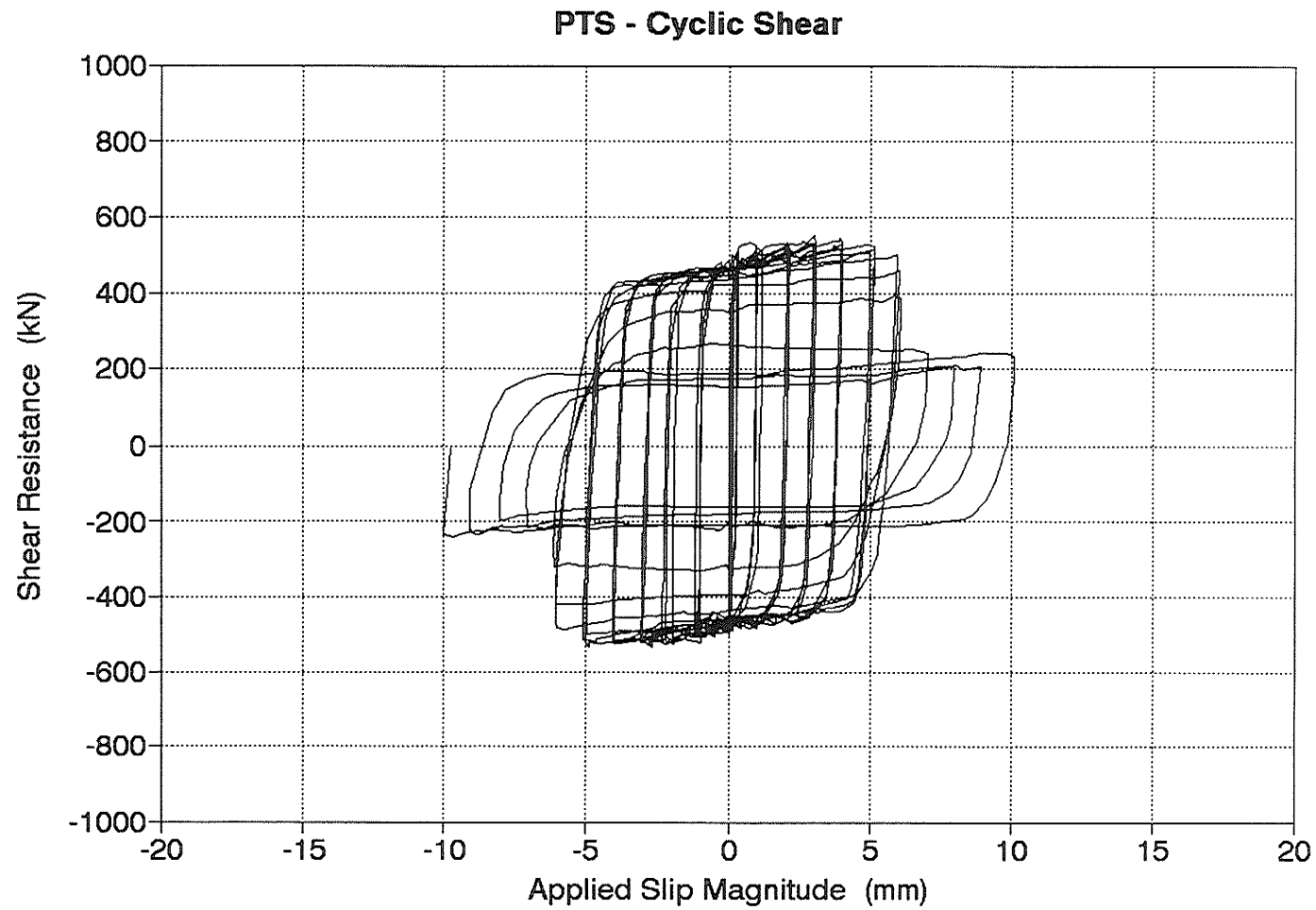
Figure 4.3   Specimen PTS - Shear Resistance - Slip Behaviour Over the Duration of the Experiment
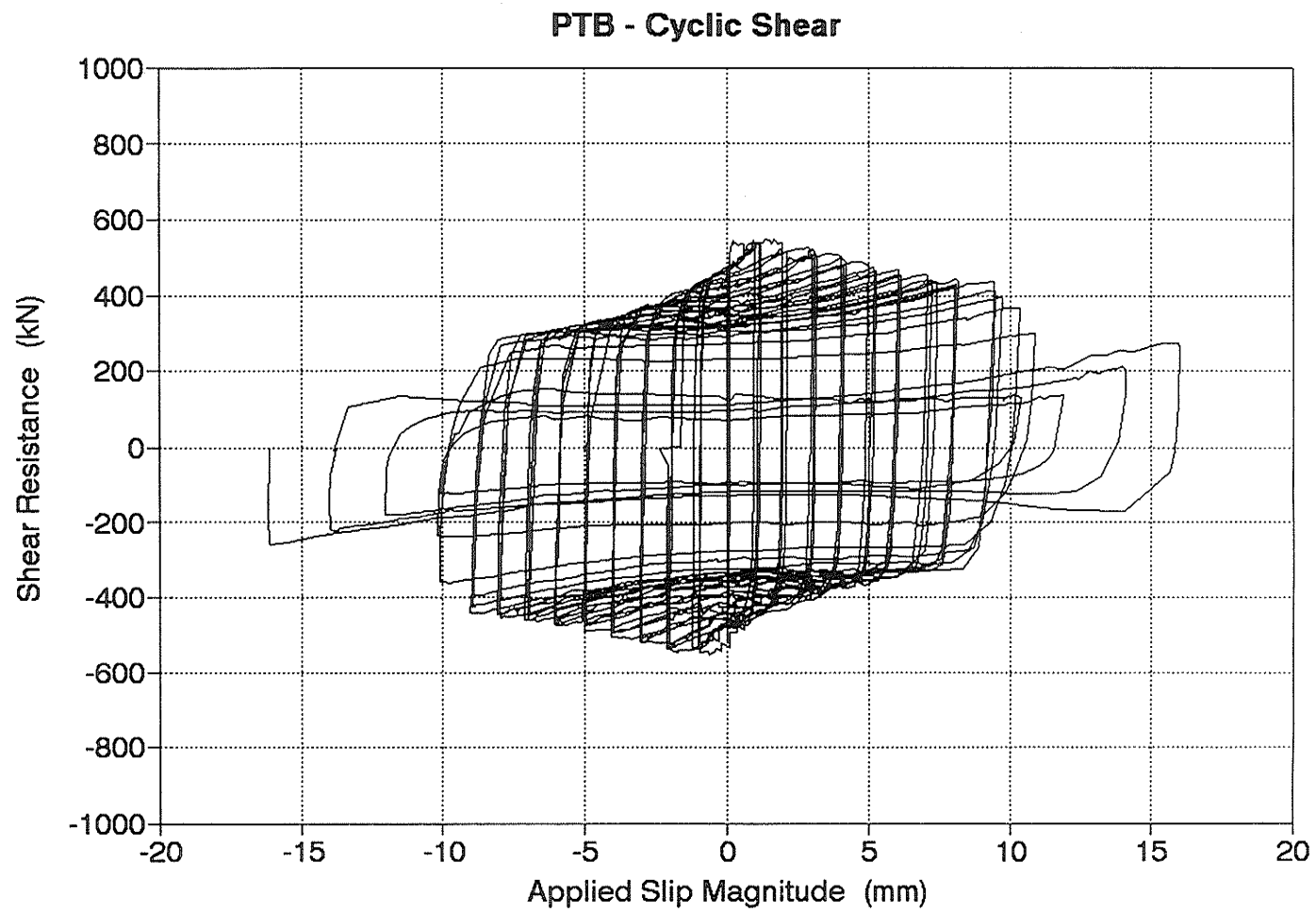
Figure 4.4   Specimen PTB - Shear Resistance - Slip Behaviour Over the Duration of the Experiment

SK - Cyclic Shear
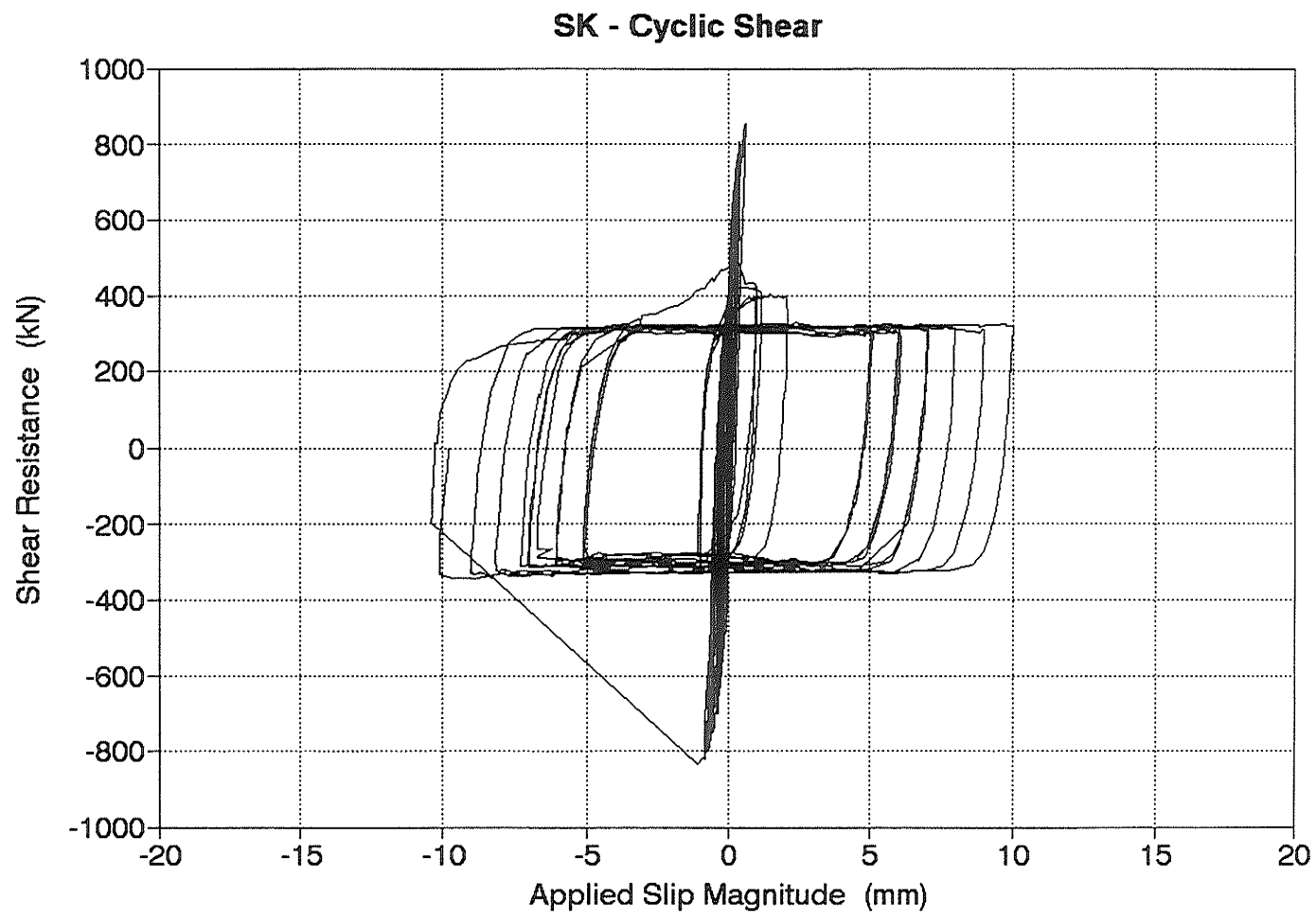
Figure 4.5   Specimen SK - Shear Resistance - Slip Behaviour Over the Duration of the Experiment

PTB - Static Shear

Rupture of East bar
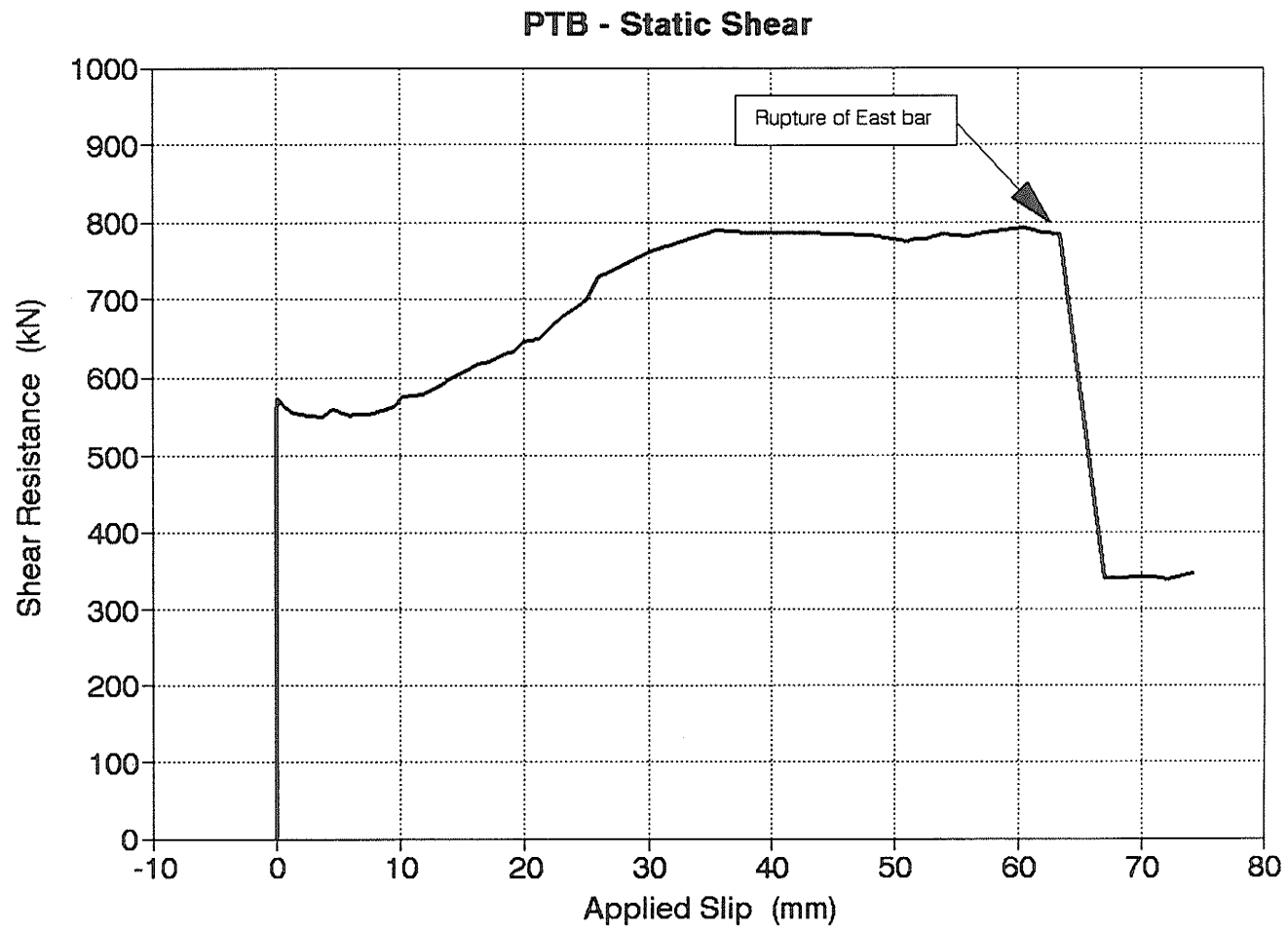
Figure 4.6   Specimen PTB-S - Shear Resistance - Slip Behaviour Over the Duration of the Experiment
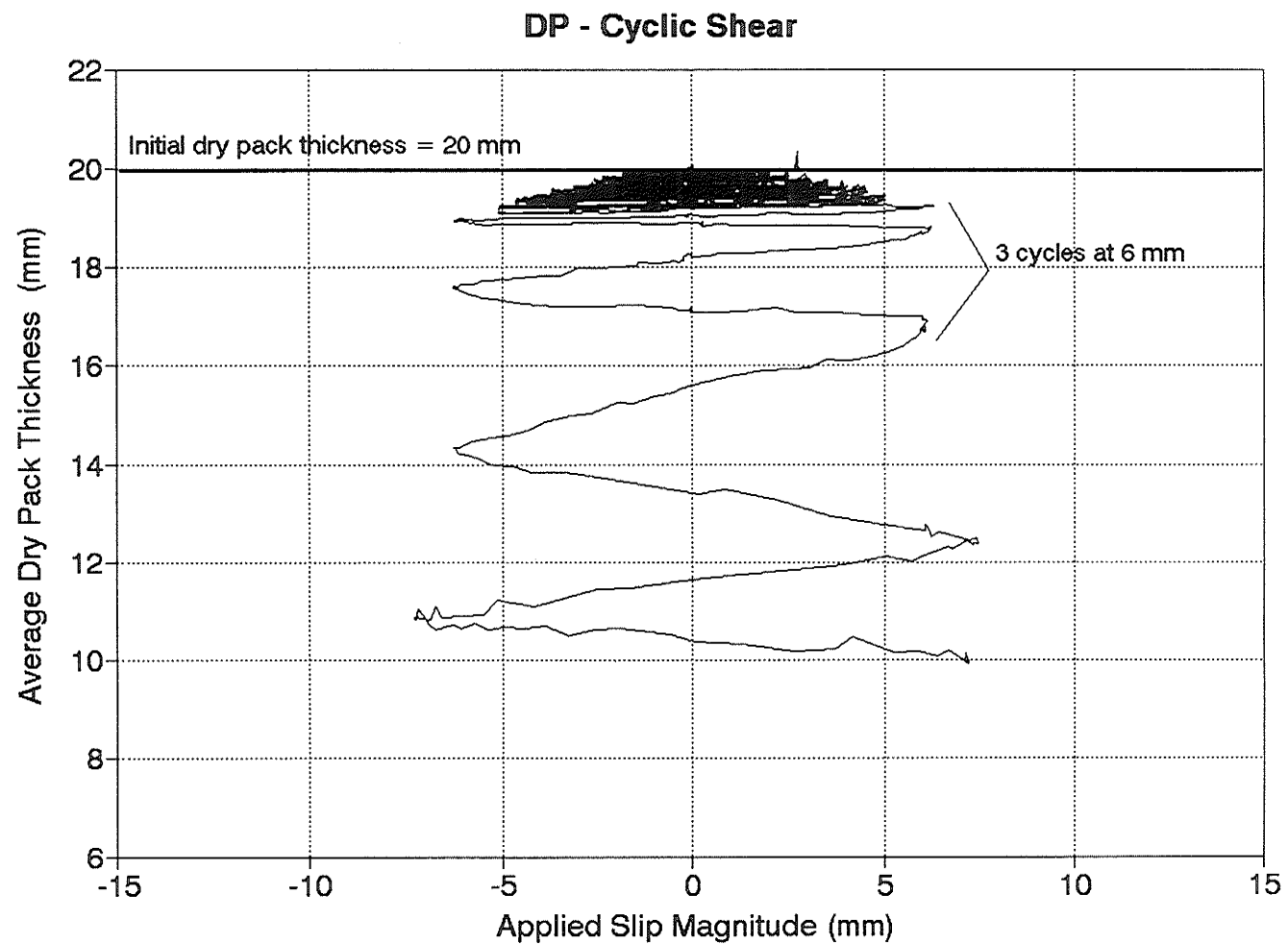
Figure 4.7   Specimen DP - Variation of the Dry Pack Thickness After the Initiation of Slip

RW - Cyclic Shear

Initial Grout Thickness = 20 mm

3 cycles at 9 mm

Average Dry Pack Thickness (mm)

Applied Slip Magnitude (mm)
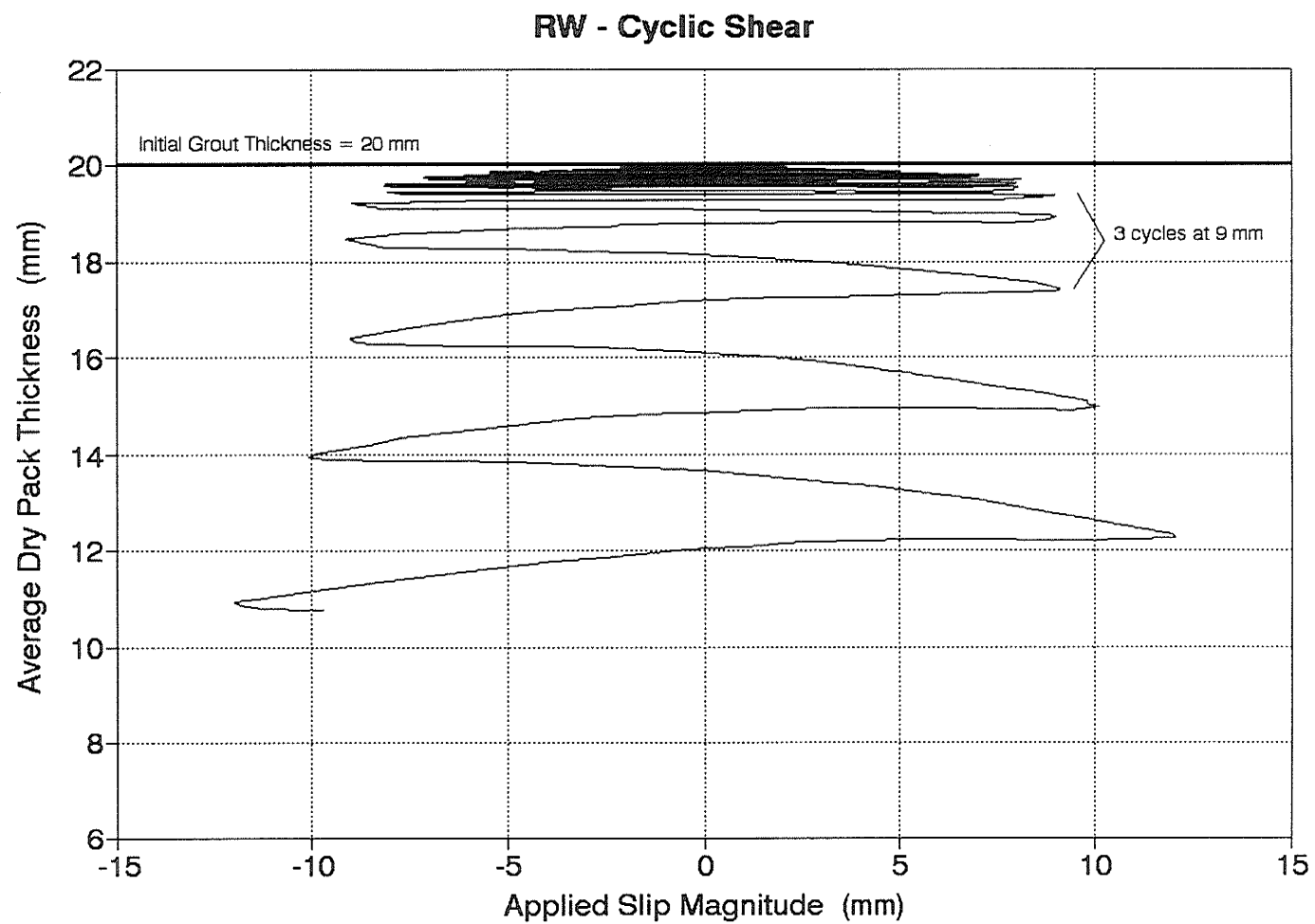
Figure 4.8   Specimen RW - Variation of the Dry Pack Thickness After the Initiation of Slip

Figure 4.9   Specimen PTS - Variation of the Dry Pack Thickness After the Initiation of Slip

PTB - Cyclic Shear
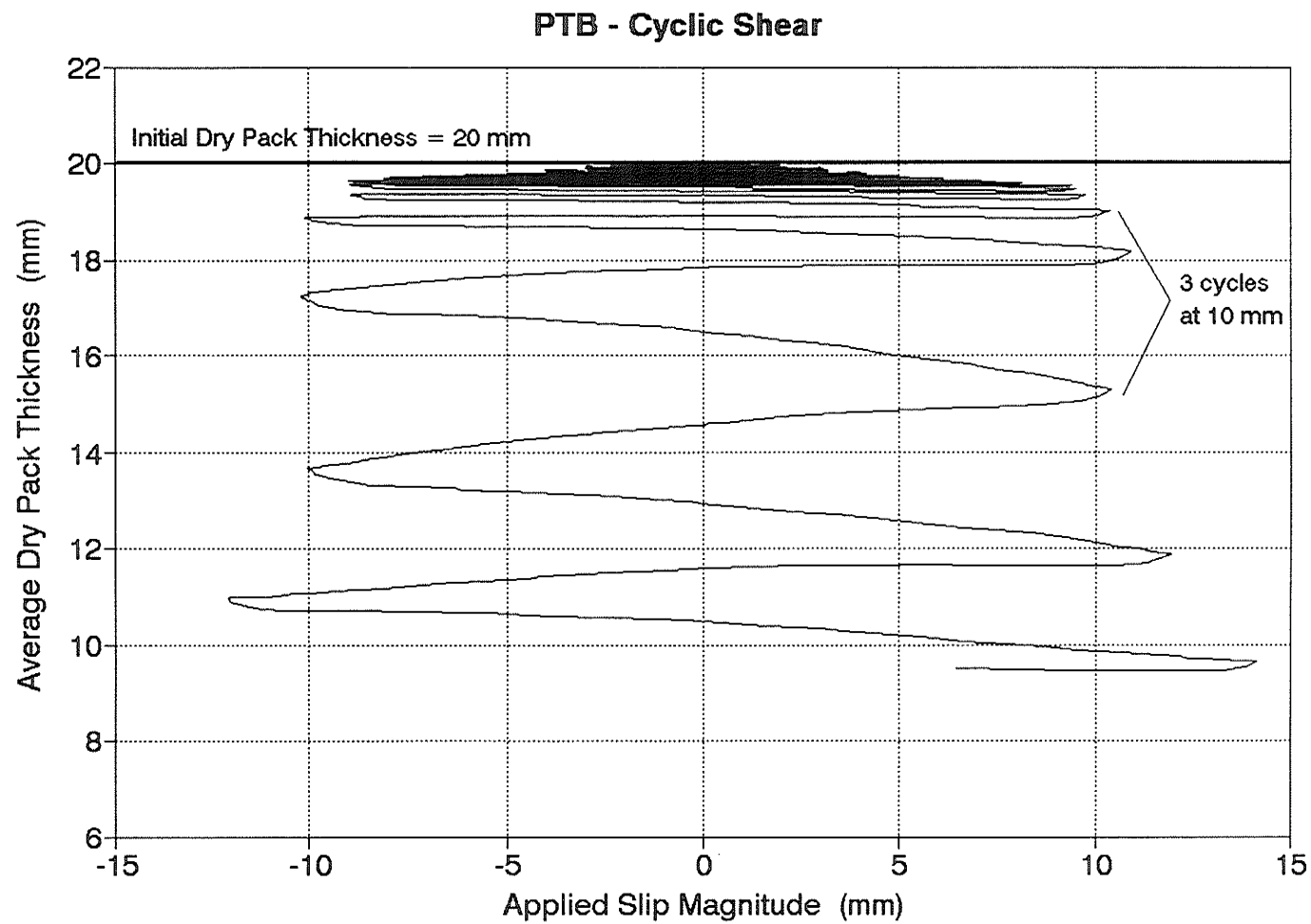
Figure 4.10   Specimen PTB - Variation of the Dry Pack Thickness After the Initiation of Slip

SK - Cyclic Shear

Chart: Average Dry Pack Thickness (mm) vs Applied Slip Magnitude (mm)

Initial Dry Pack Thickness = 20 mm

Manual Reading

240
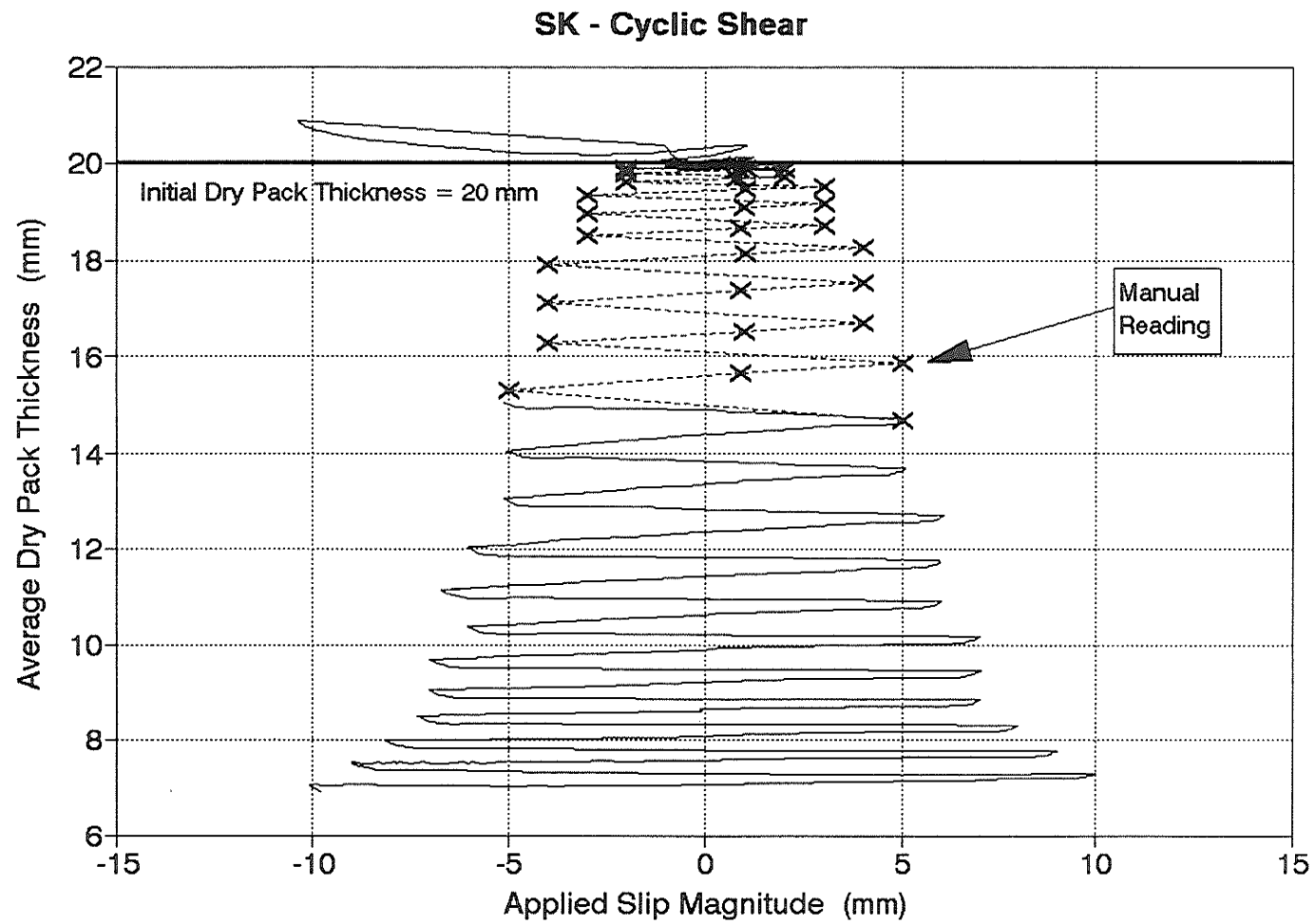
Figure 4.11   Specimen SK - Variation of the Dry Pack Thickness After the Initiation of Slip

PTB - Static Shear
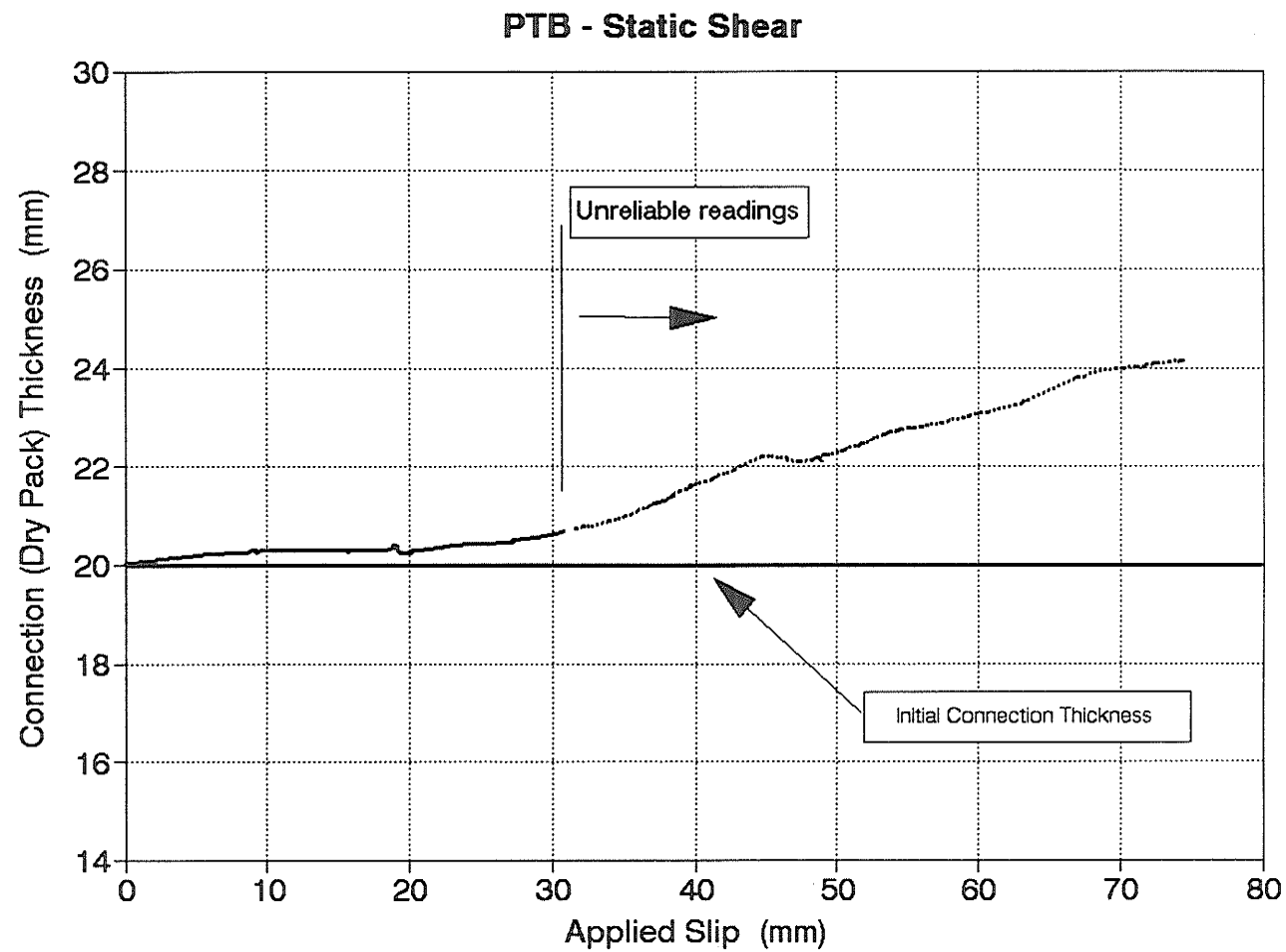
Figure 4.12   Specimen PTB-S - Variation of the Dry Pack Thickness After the Initiation of Slip
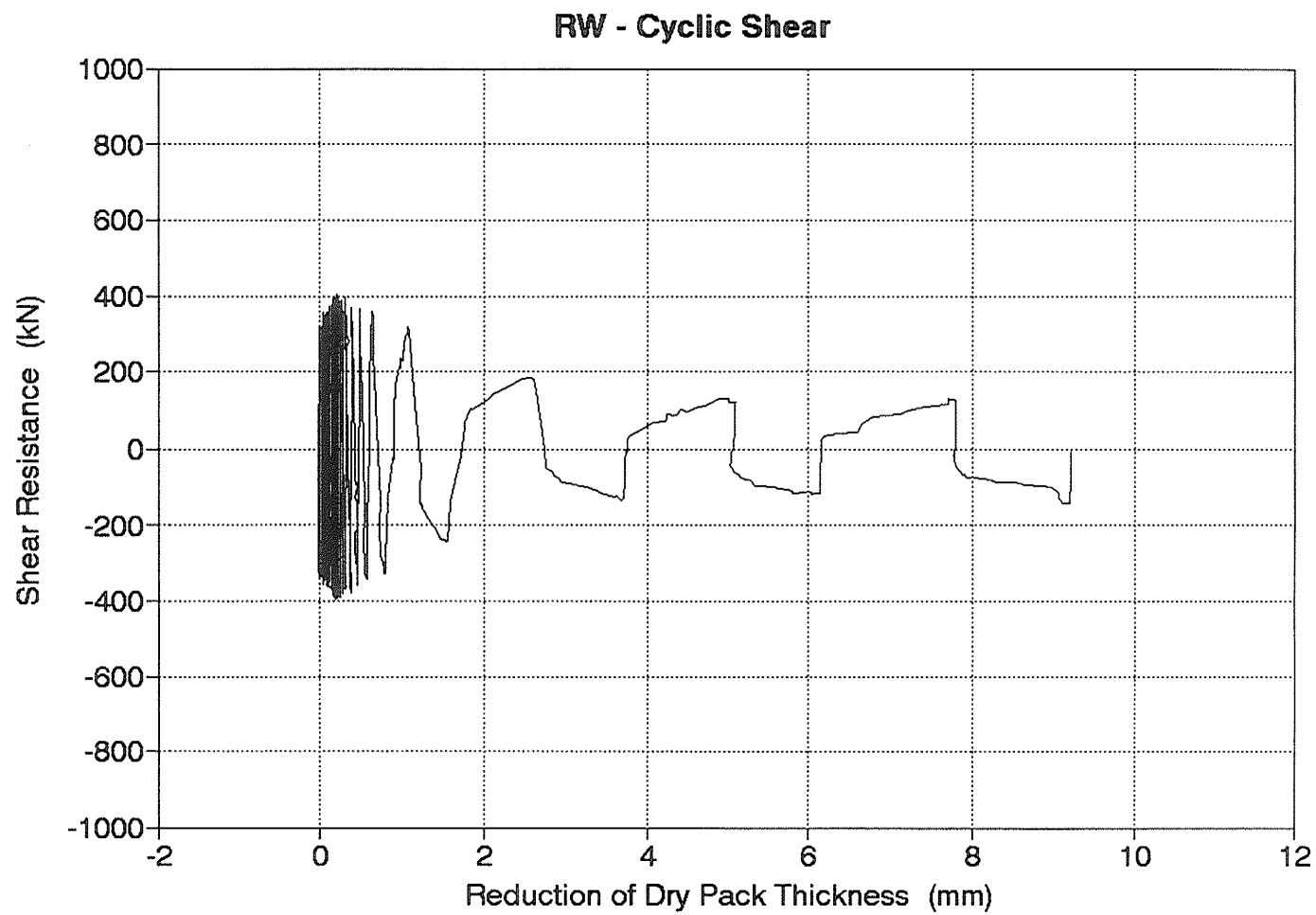
Figure 4.13   Specimen RW - Shear Resistance - Reduction of Dry Pack Thickness Relationship
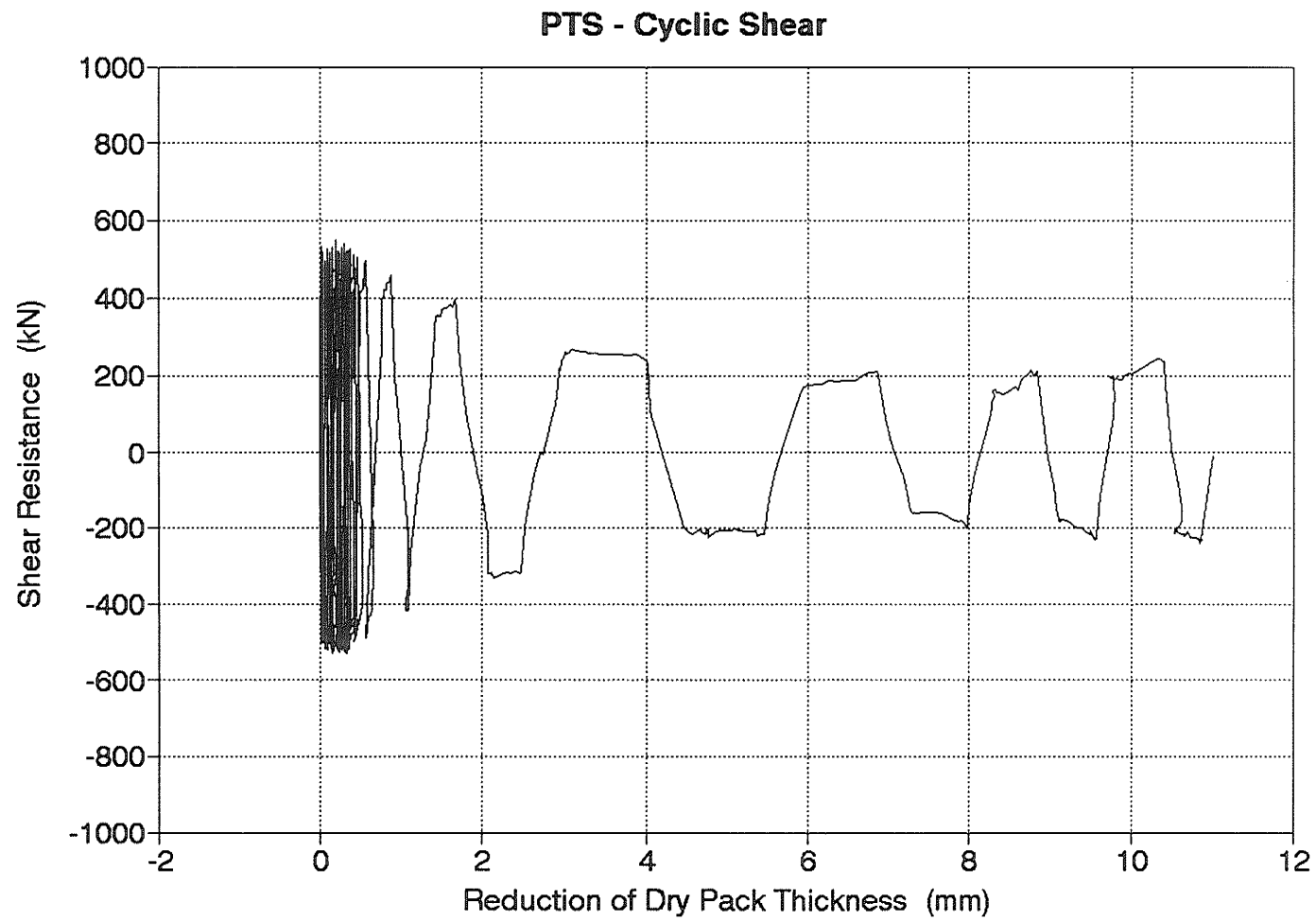
Figure 4.14   Specimen PTS - Shear Resistance - Reduction of Dry Pack Thickness Relationship
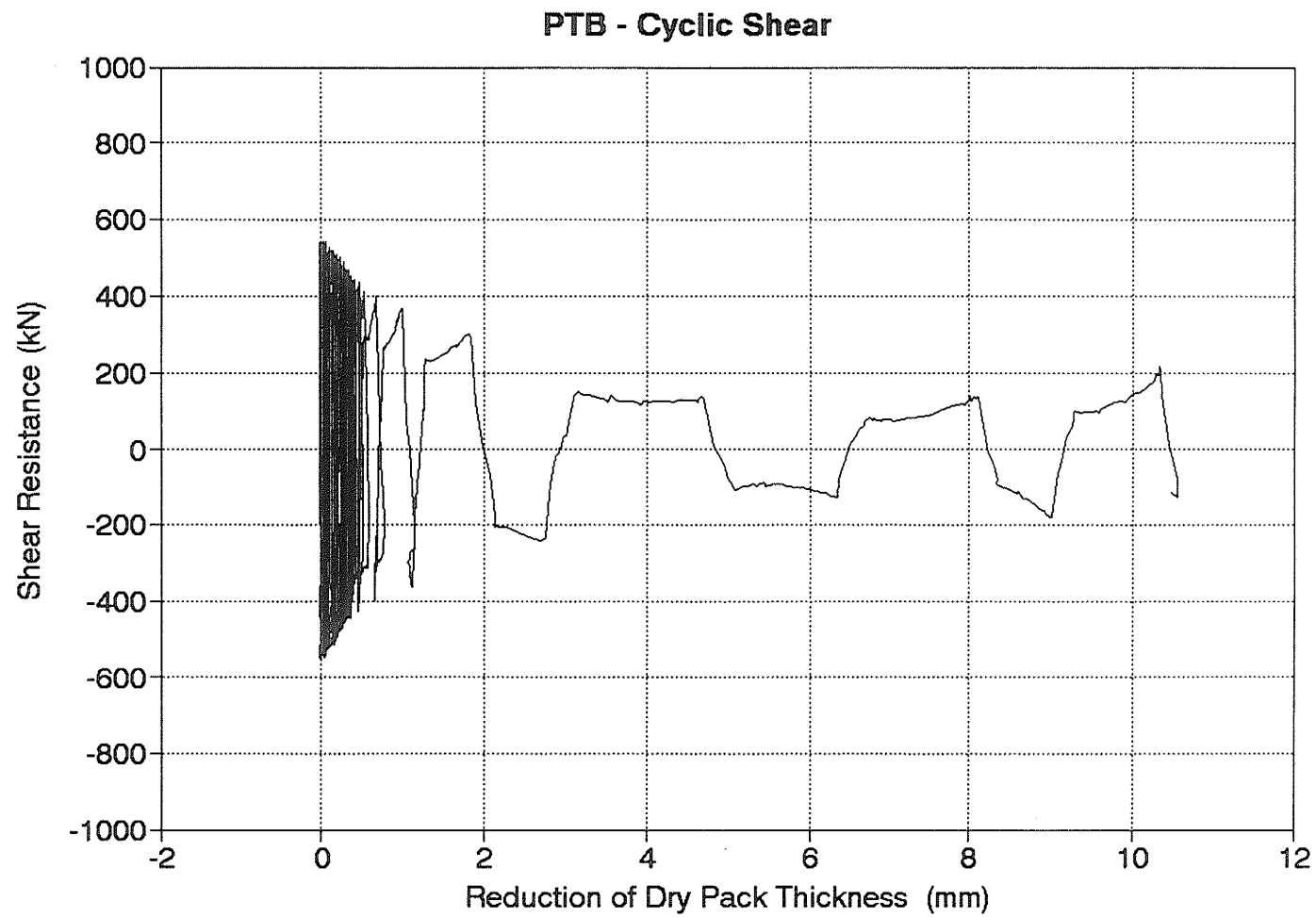
PTB - Cyclic Shear

Figure 4.15   Specimen PTB - Shear Resistance - Reduction of Dry Pack Thickness Relationship
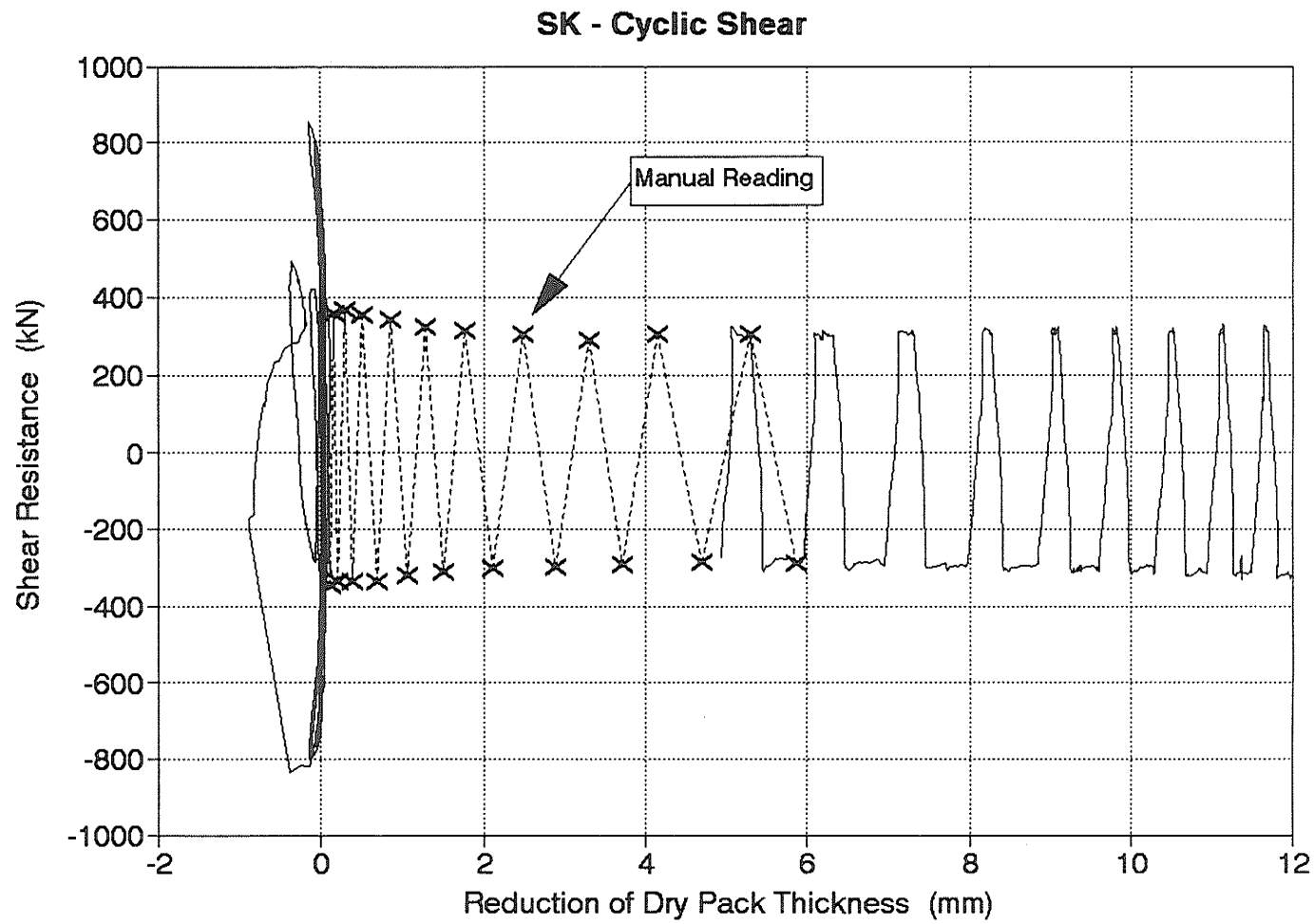
Figure 4.16   Specimen SK - Shear Resistance - Reduction of Dry Pack Thickness Relationship
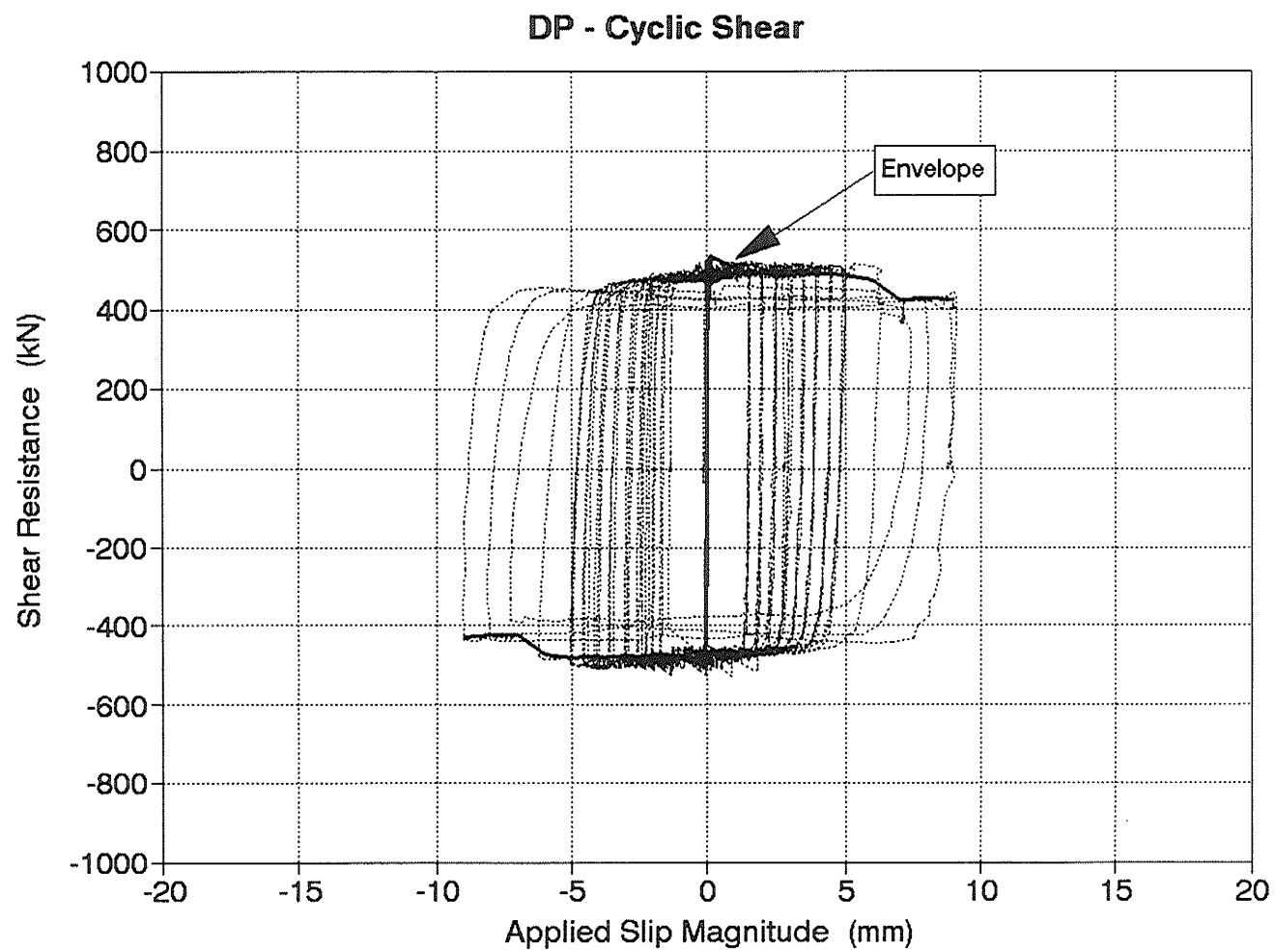
Figure 4.17   Specimen DP - Cyclic Shear Behaviour Envelope
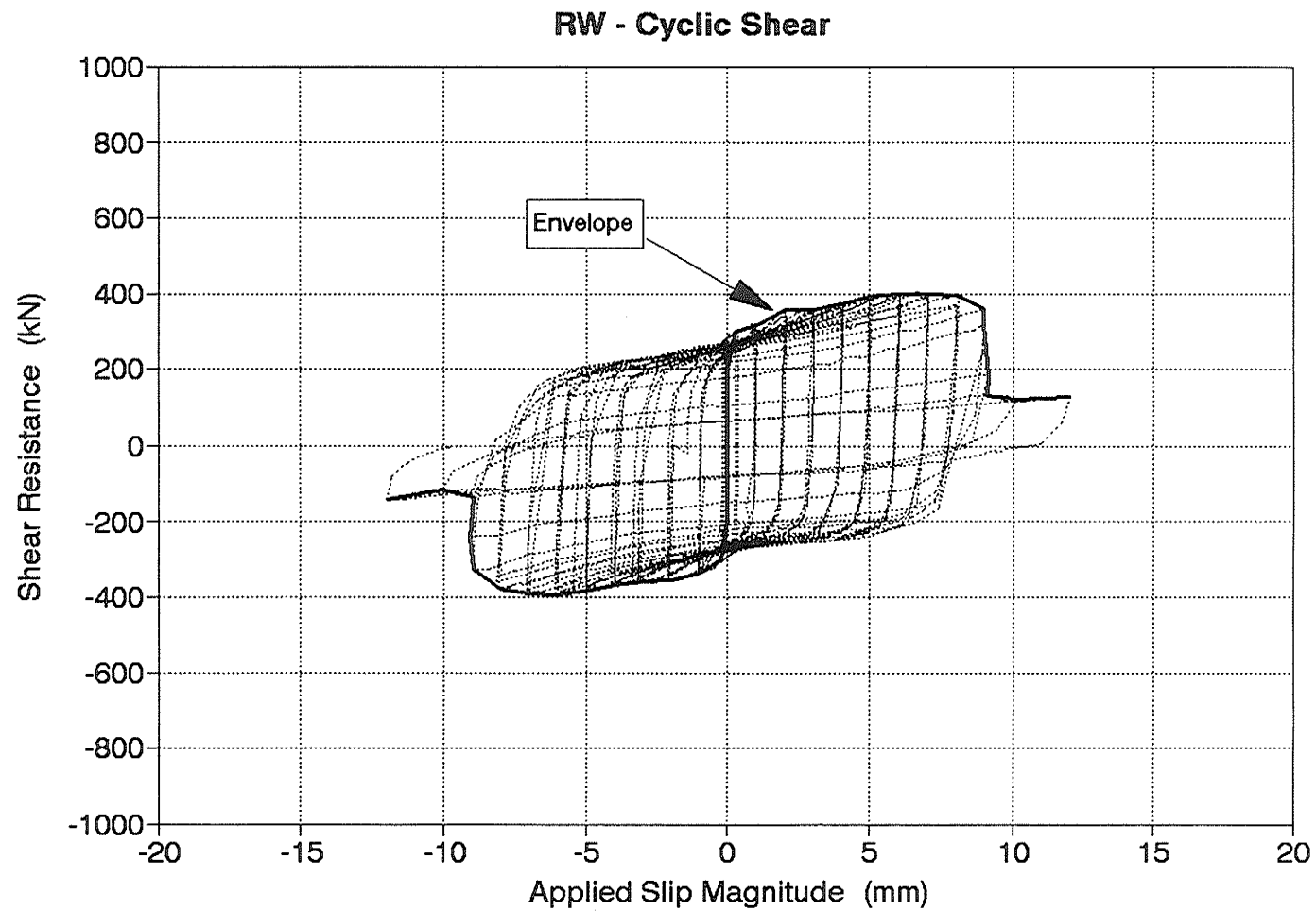
Figure 4.18   Specimen RW - Cyclic Shear Behaviour Envelope
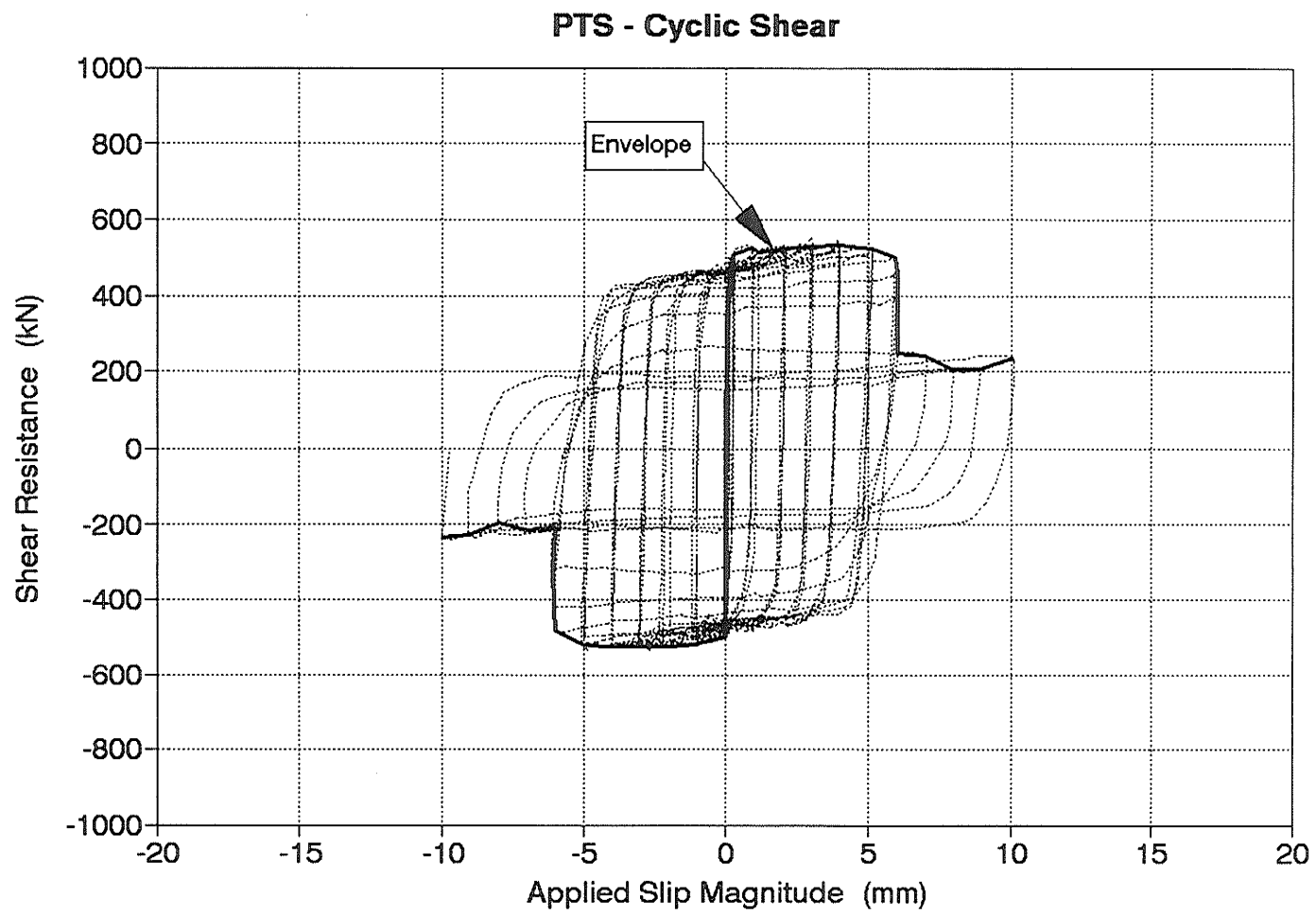
Figure 4.19   Specimen PTS - Cyclic Shear Behaviour Envelope
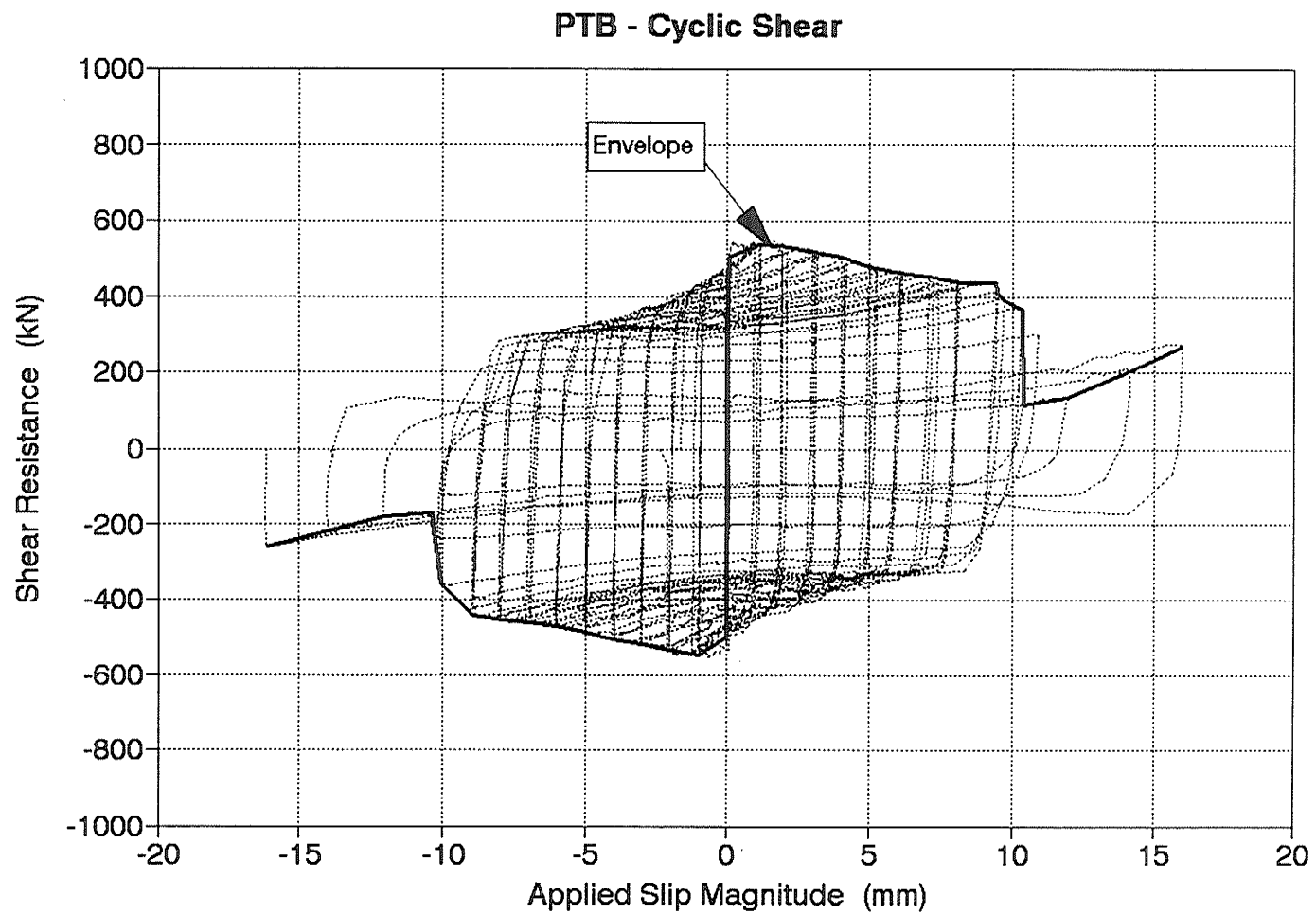
Figure 4.20   Specimen PTB - Cyclic Shear Behaviour Envelope
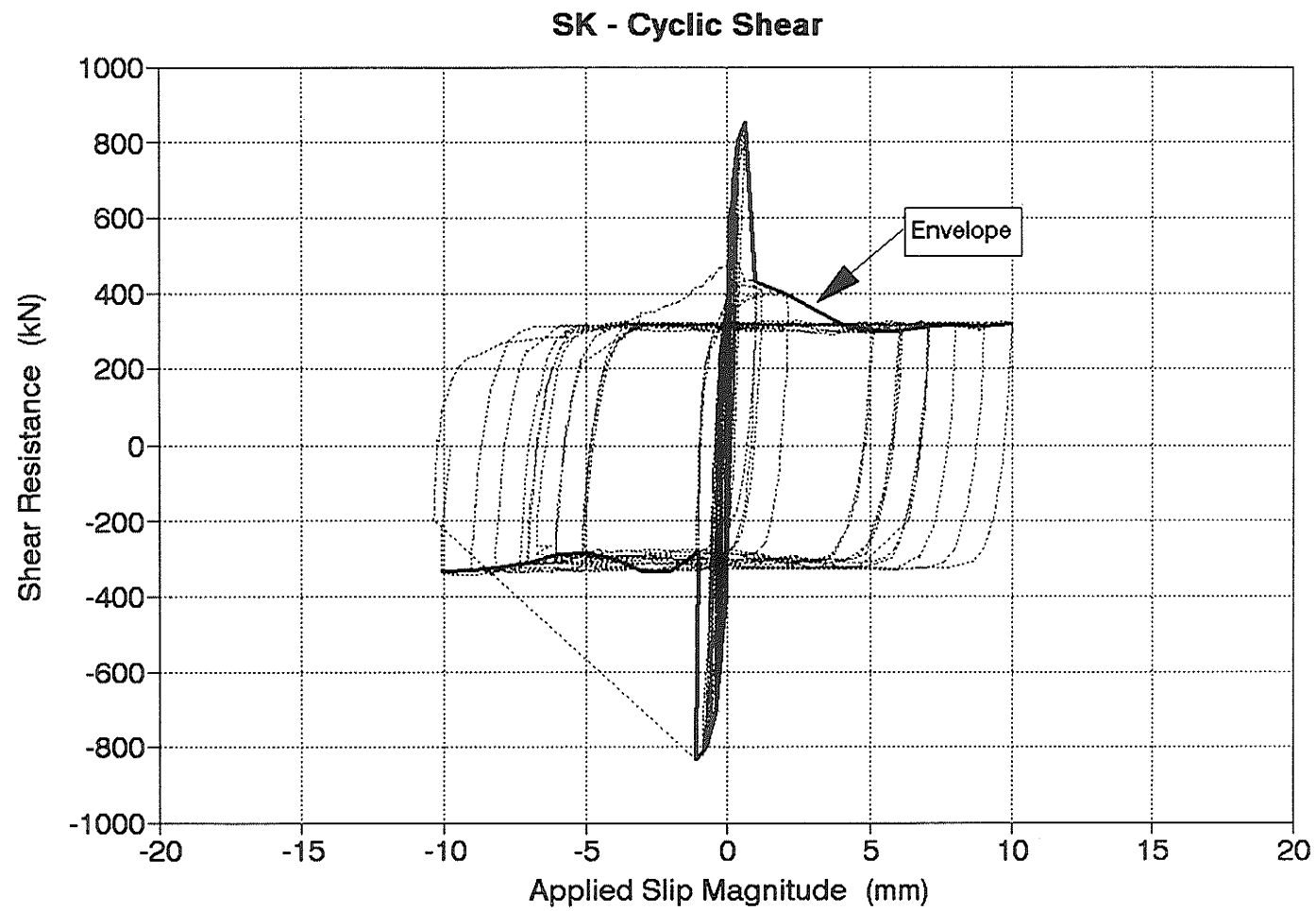
Figure 4.21   Specimen SK - Cyclic Shear Behaviour Envelope

DP - Cyclic Shear
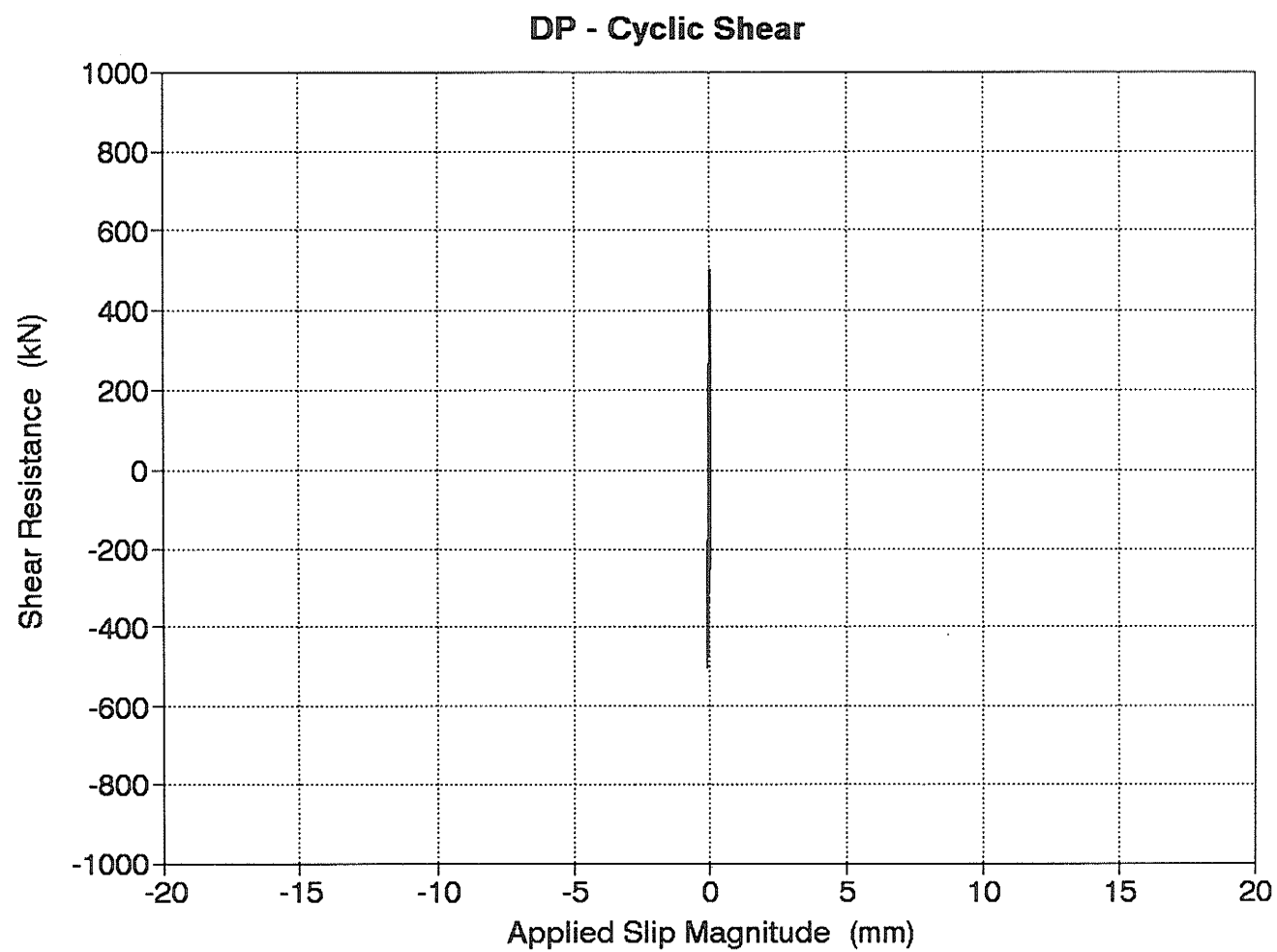
Figure 5.1   Specimen DP - Elastic Connection Behaviour Prior to the Initiation of Slip
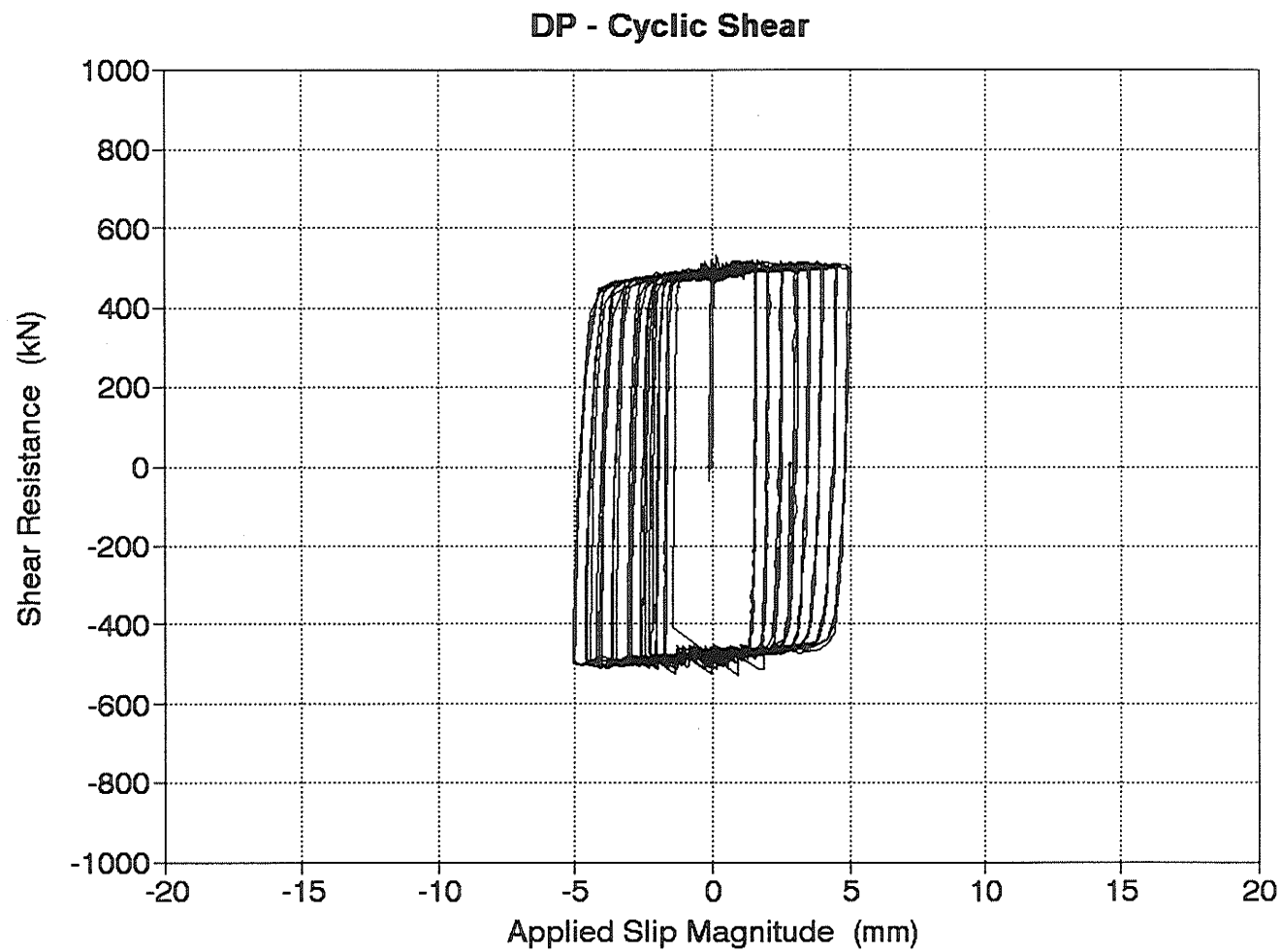
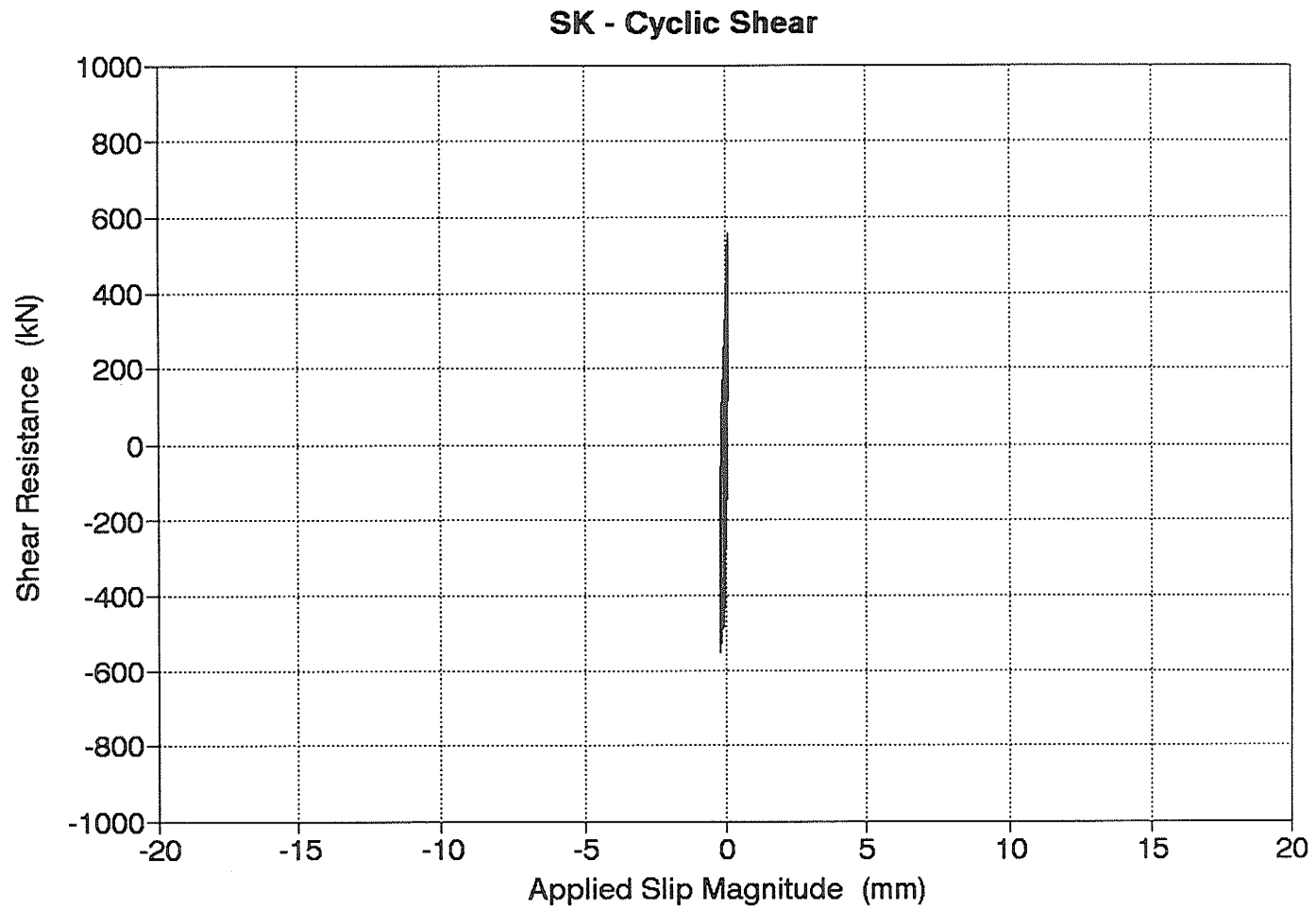Figure 5.2   Specimen DP - Inelastic Connection Behaviour After the Initiation of Slip
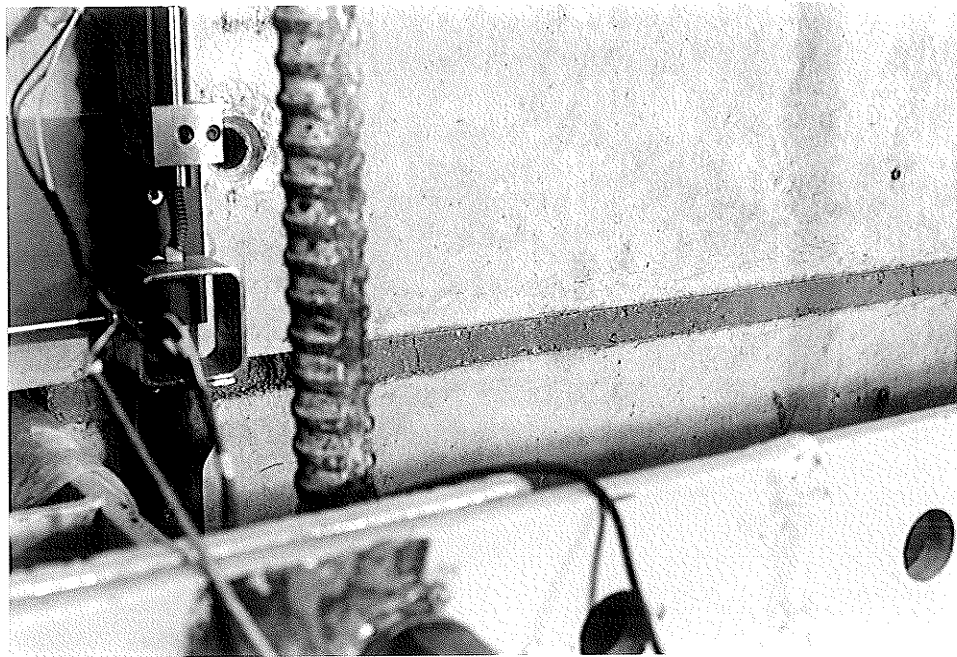
Figure 5.3   Specimen DP - Condition of the Dry Pack at the Start of Testing
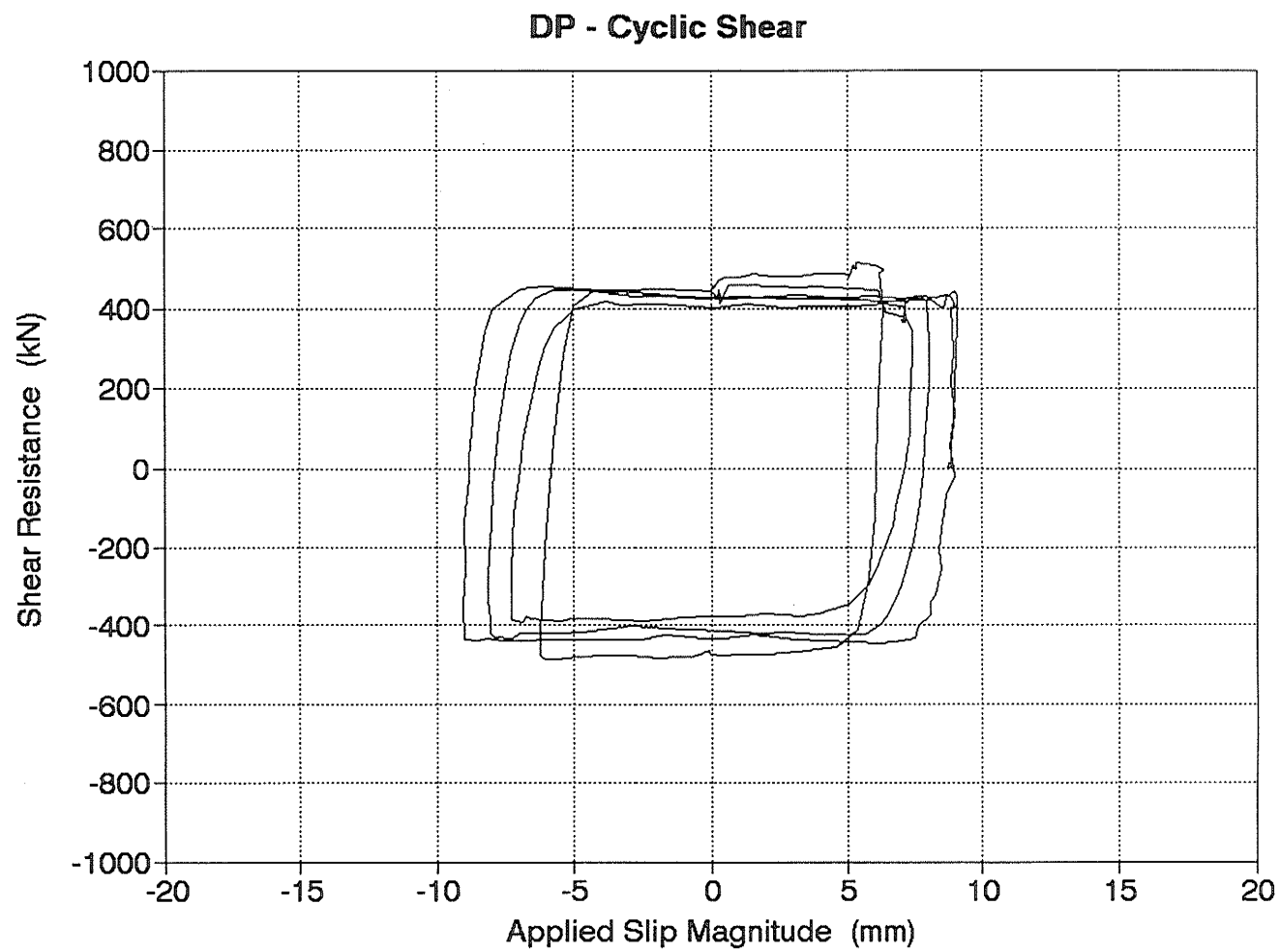
Figure 5.4   Specimen DP - Connection Behaviour After Crushing of the Dry Pack
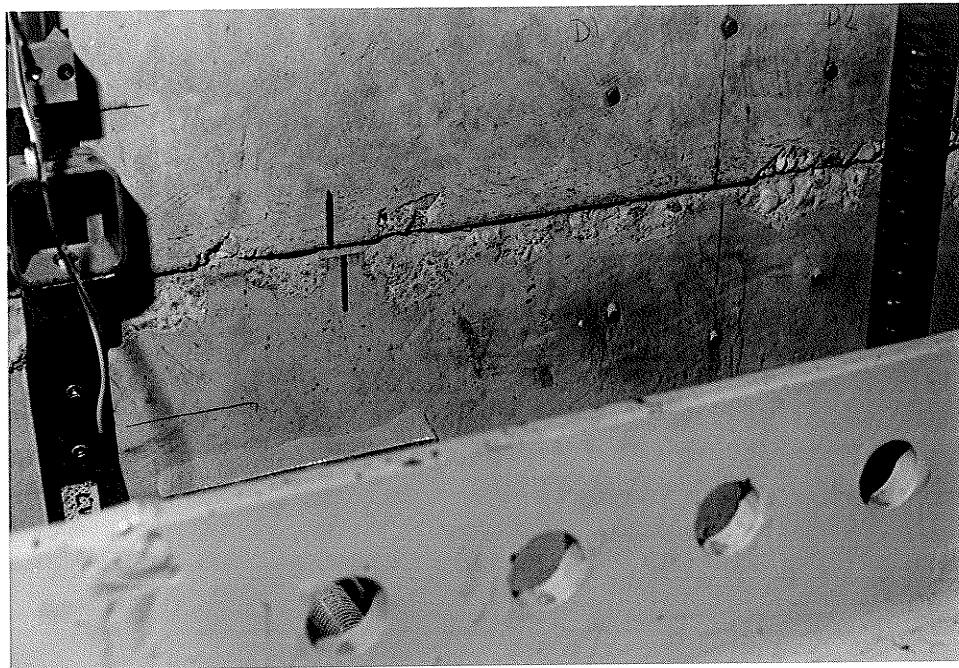
Figure 5.5   Specimen DP - Condition of the Dry Pack After Crushing

RW - Cyclic Shear
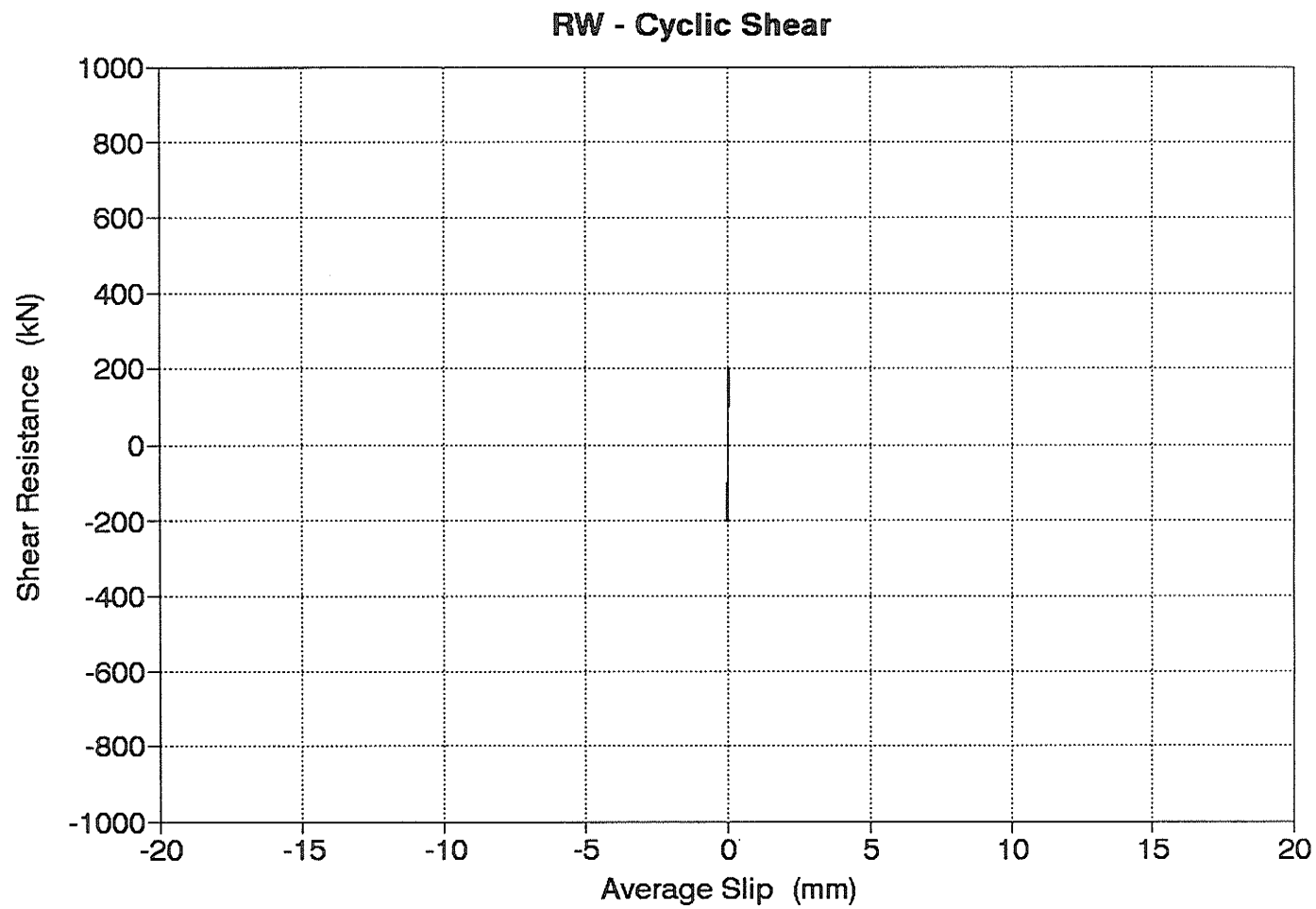
Figure 5.6   Specimen RW - Elastic Connection Behaviour Prior to the Initiation of Slip

RW - Cyclic Shear
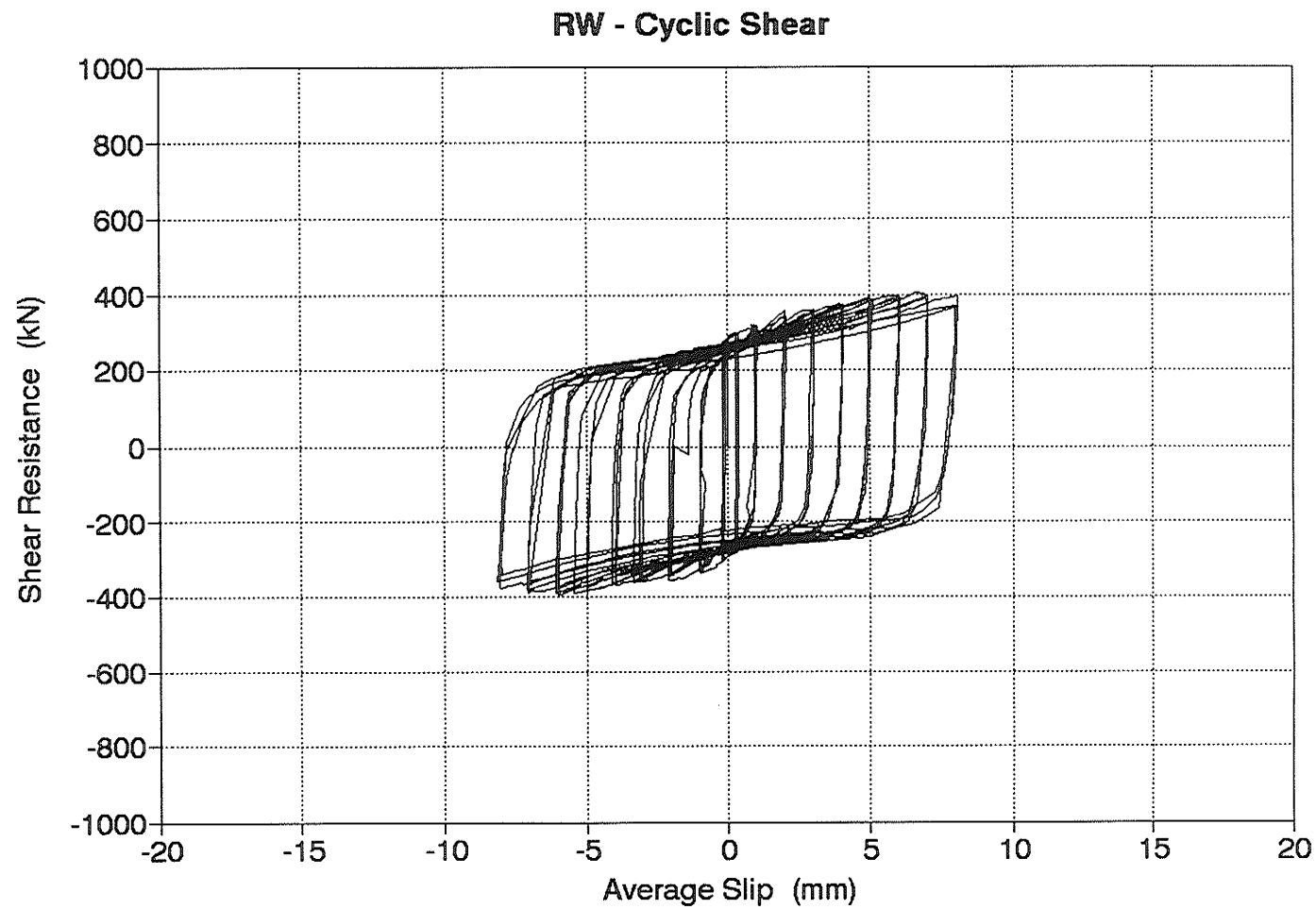
Figure 5.7   Specimen RW - Inelastic Connection Behaviour After the Initiation of Slip

RW - Cyclic Shear
+/- 6.0 mm
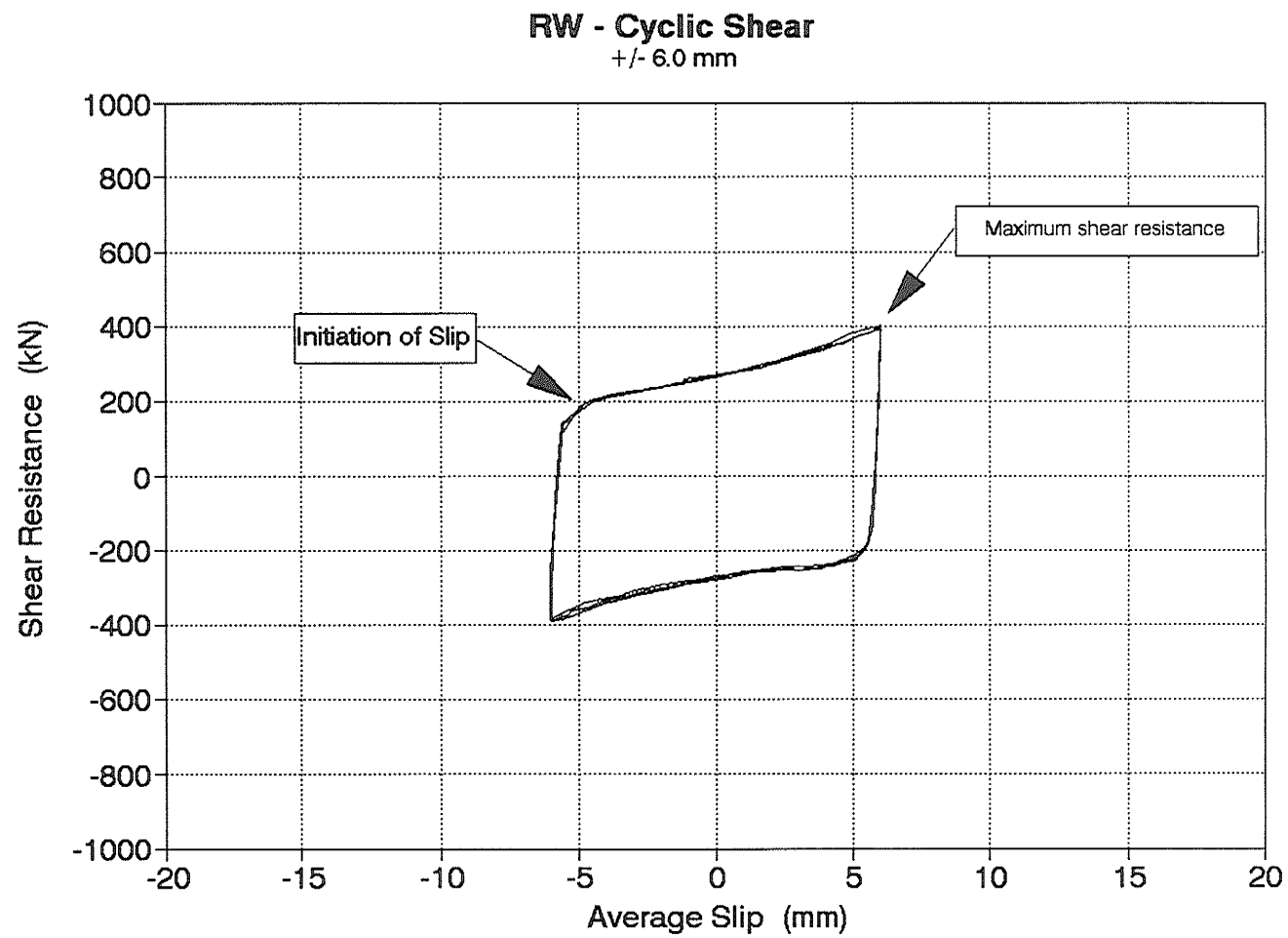
Figure 5.8   Specimen RW - Typical Hysteretic Behaviour After the Initiation of Slip
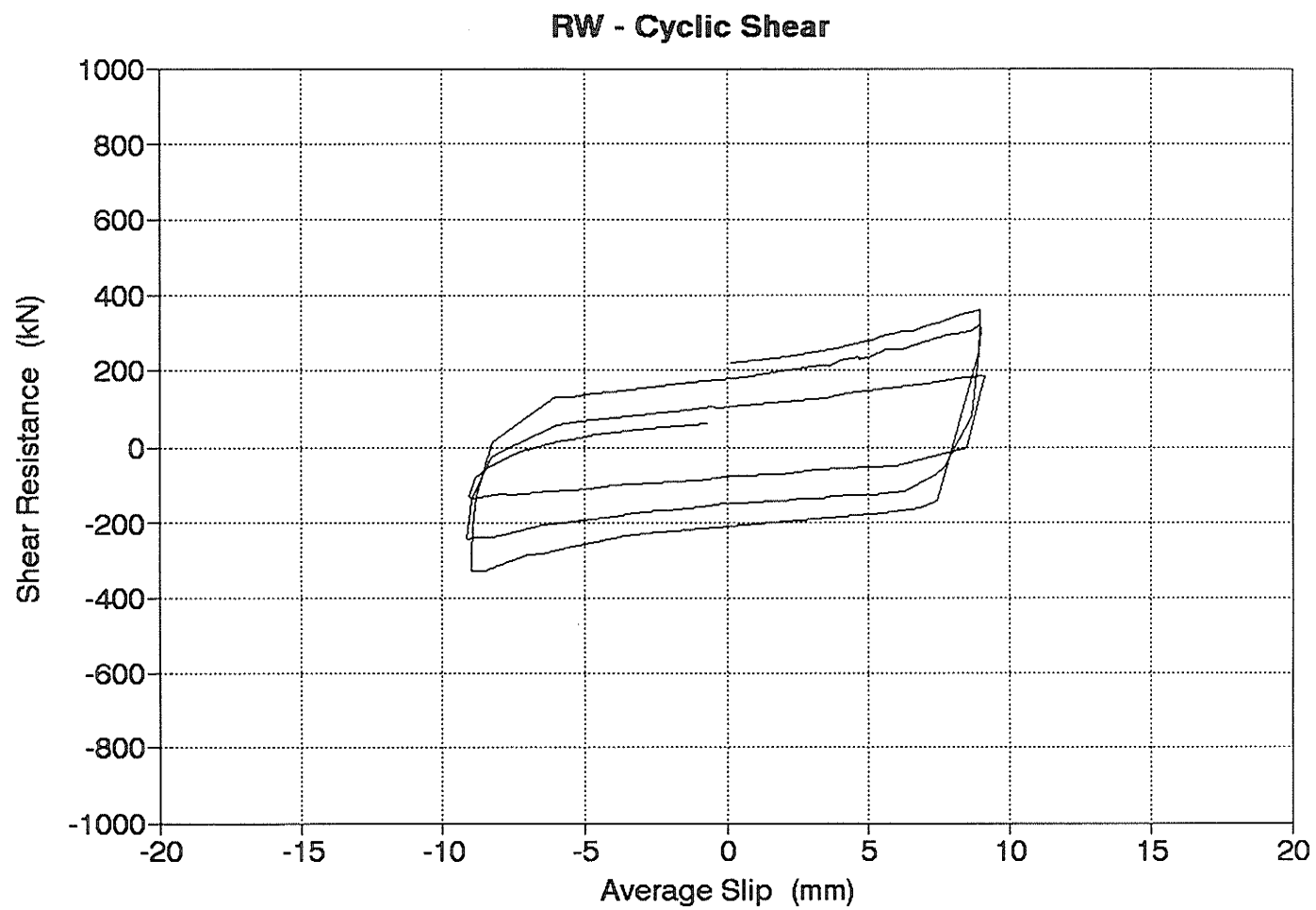
Figure 5.9   Specimen RW - Connection Behaviour at Failure (Slip Magnitude = 9 mm)
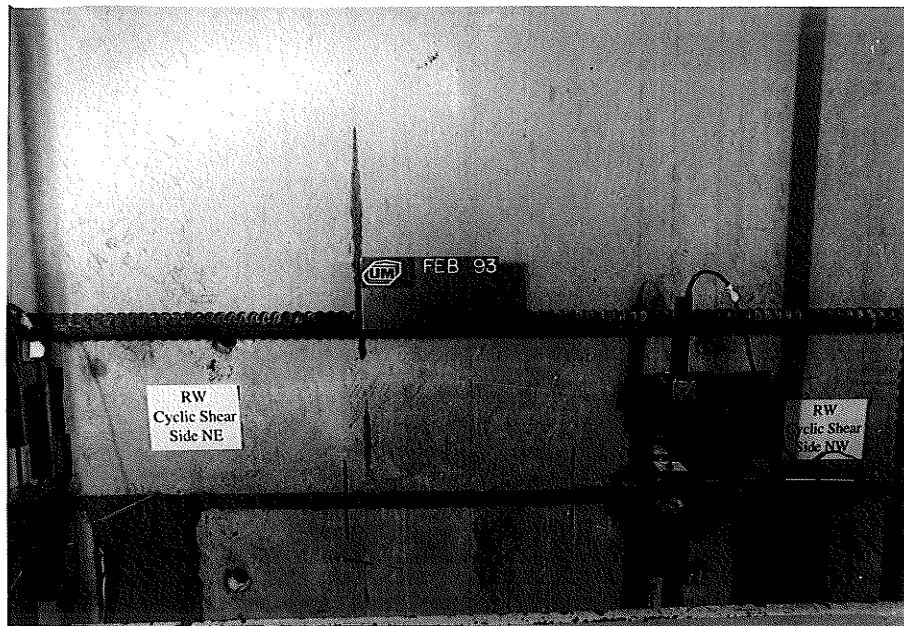
Figure 5.10   Specimen RW - Condition of the Dry Pack at the Start of Testing
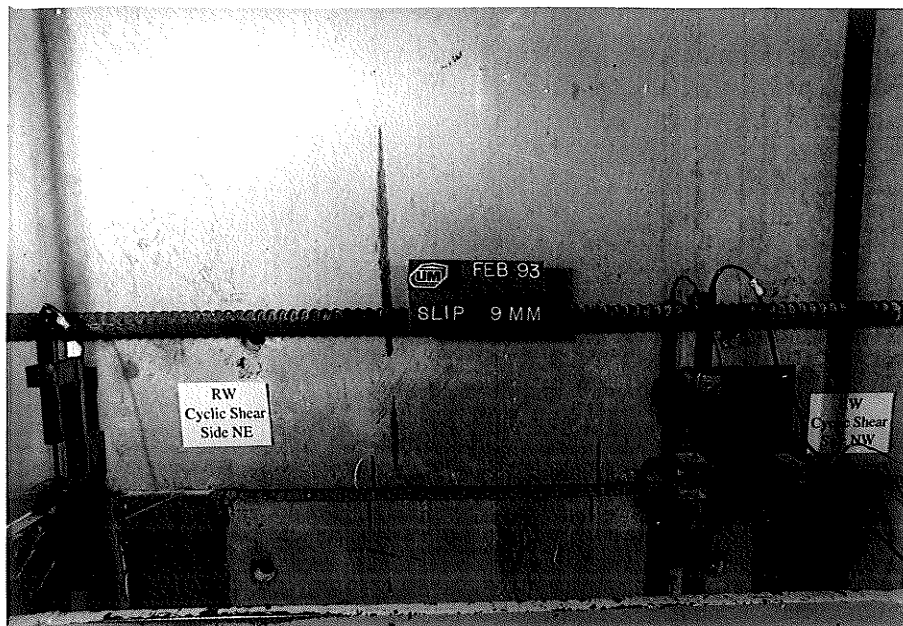
Figure 5.11   Specimen RW - Condition of the Dry Pack After Crushing
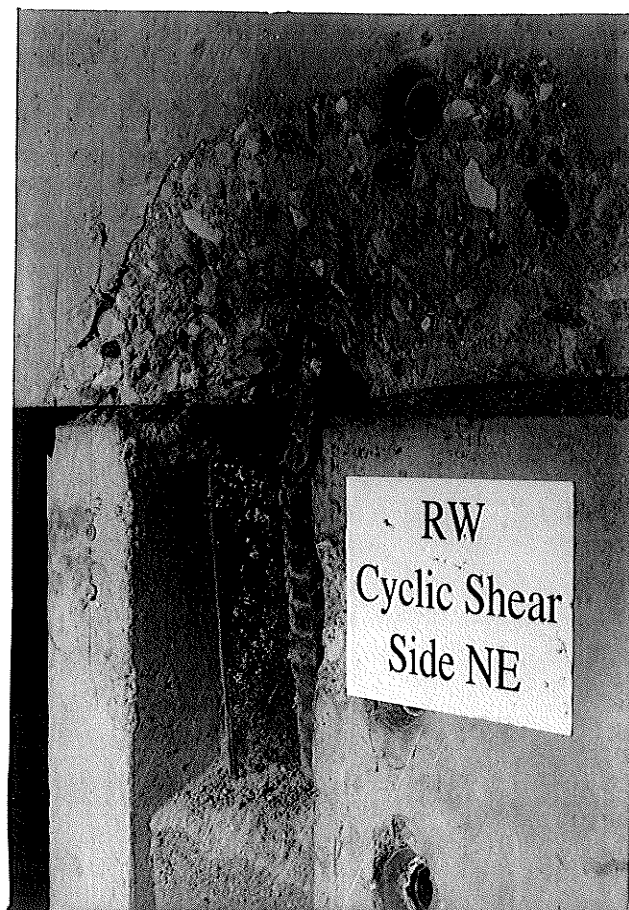
Figure 5.12   Specimen RW - Buckled Continuity Bar After Failure of the Connection

RW - Cyclic Shear
+/- 10.0 mm and 12.0 mm
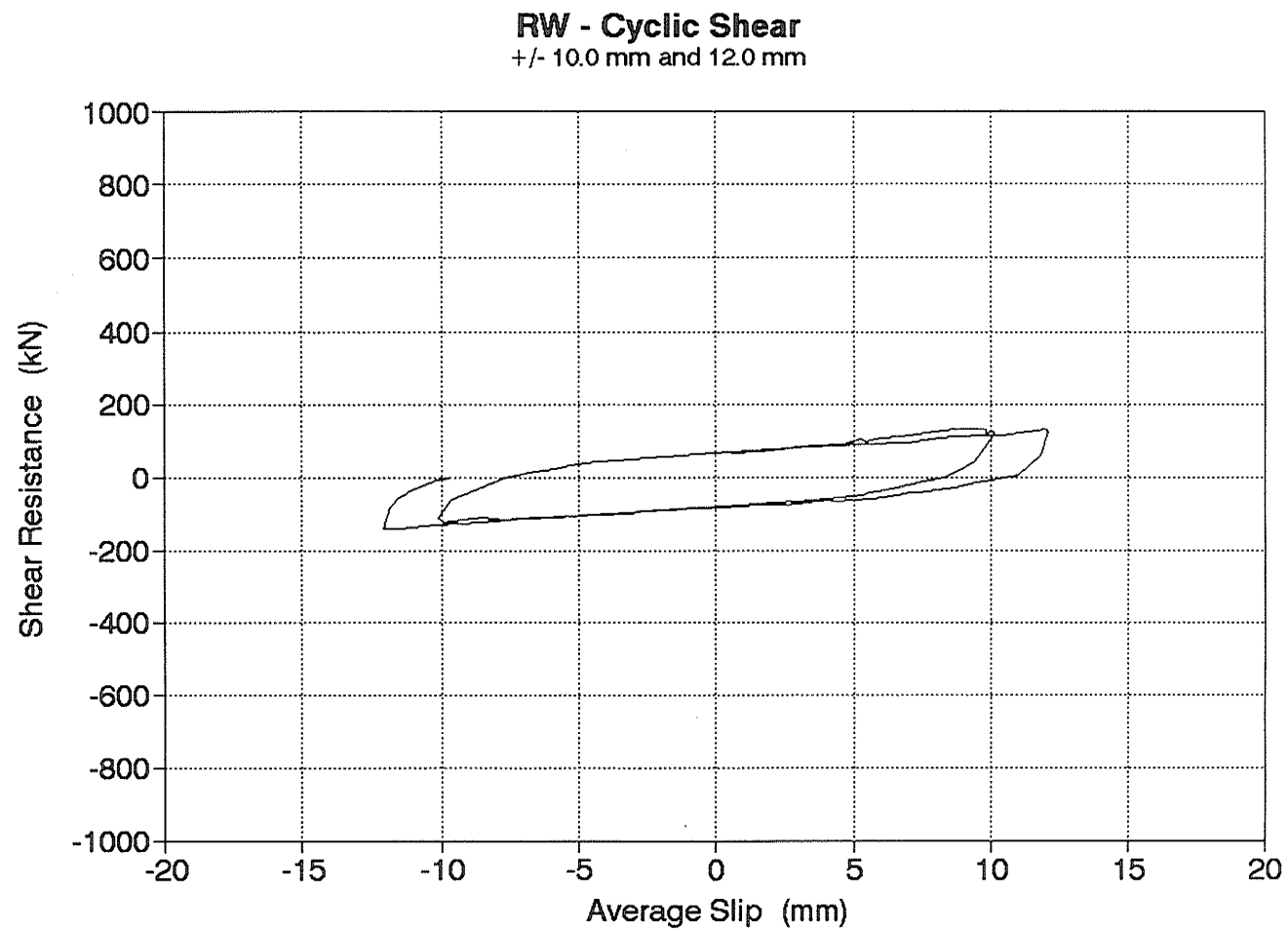
Figure 5.13   Specimen RW - Connection Behaviour After Crushing of the Dry Pack

RW - Cyclic Shear

Legend:
West Bar
East Bar

NOTE: Compressive strains are negative.
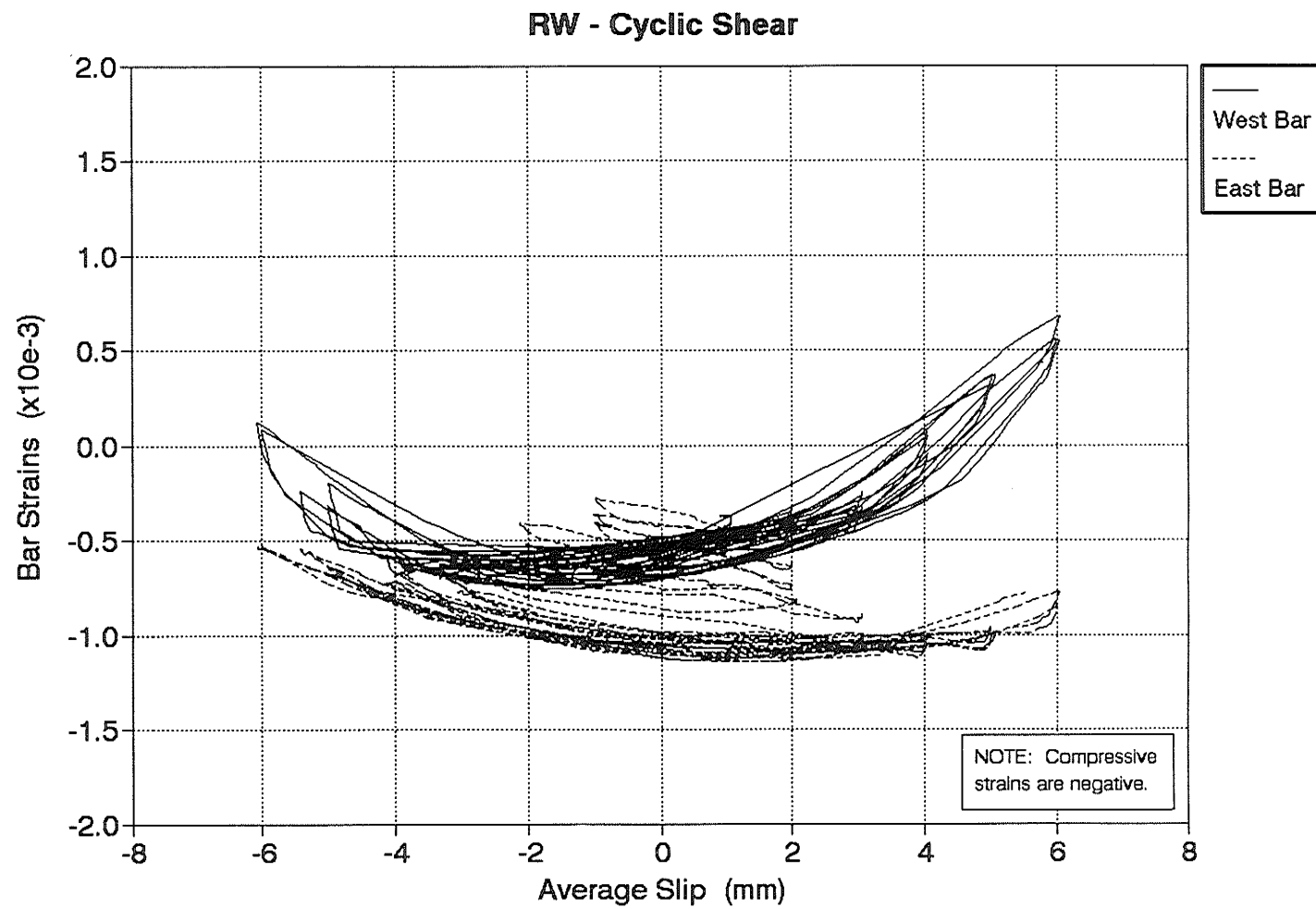
Figure 5.14   Specimen RW - Overall Reinforcement Strain Behaviour
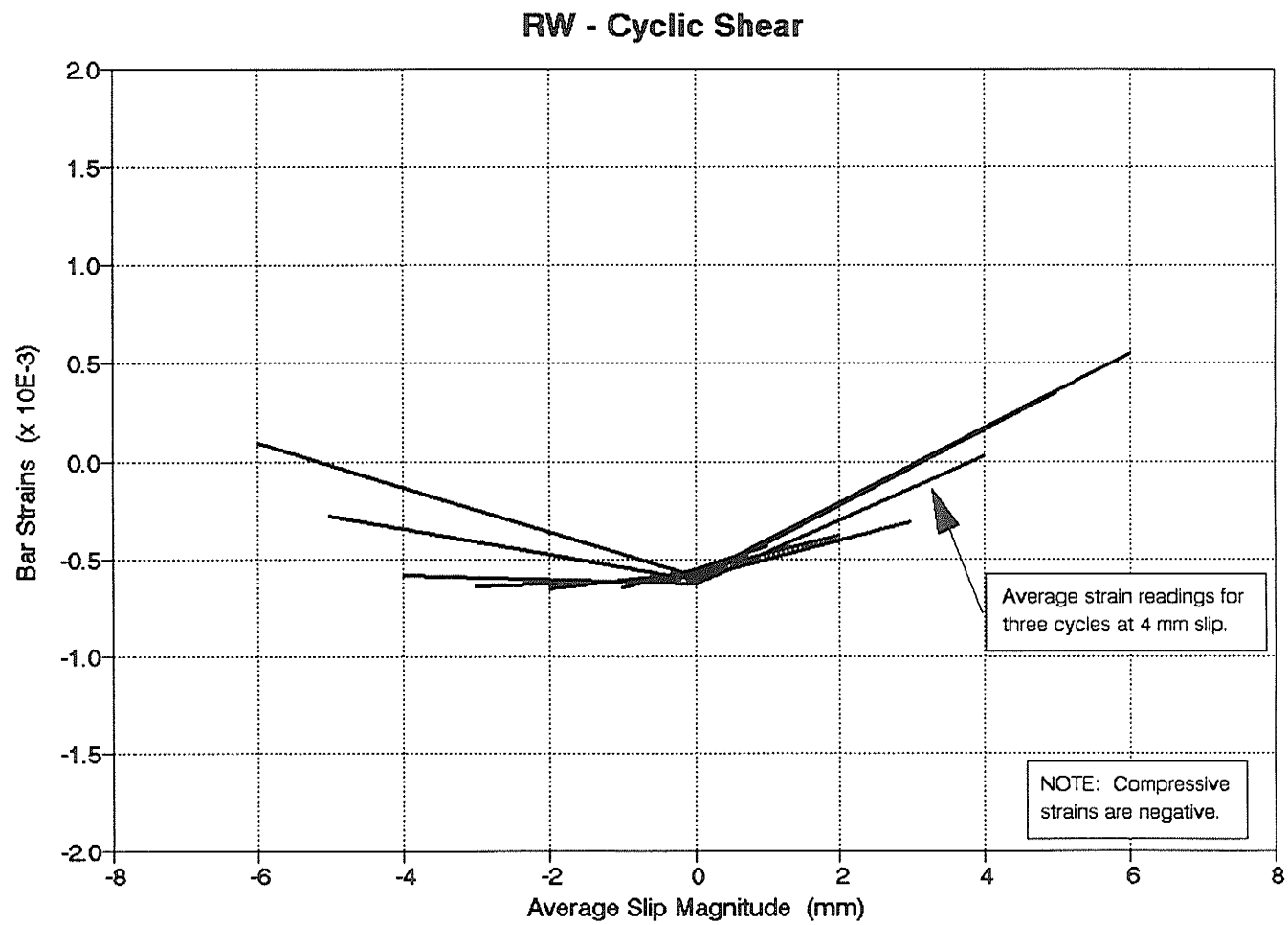
Figure 5.15(a) Specimen RW - Average Maximum Strain Behaviour: West Bar

RW - Cyclic Shear
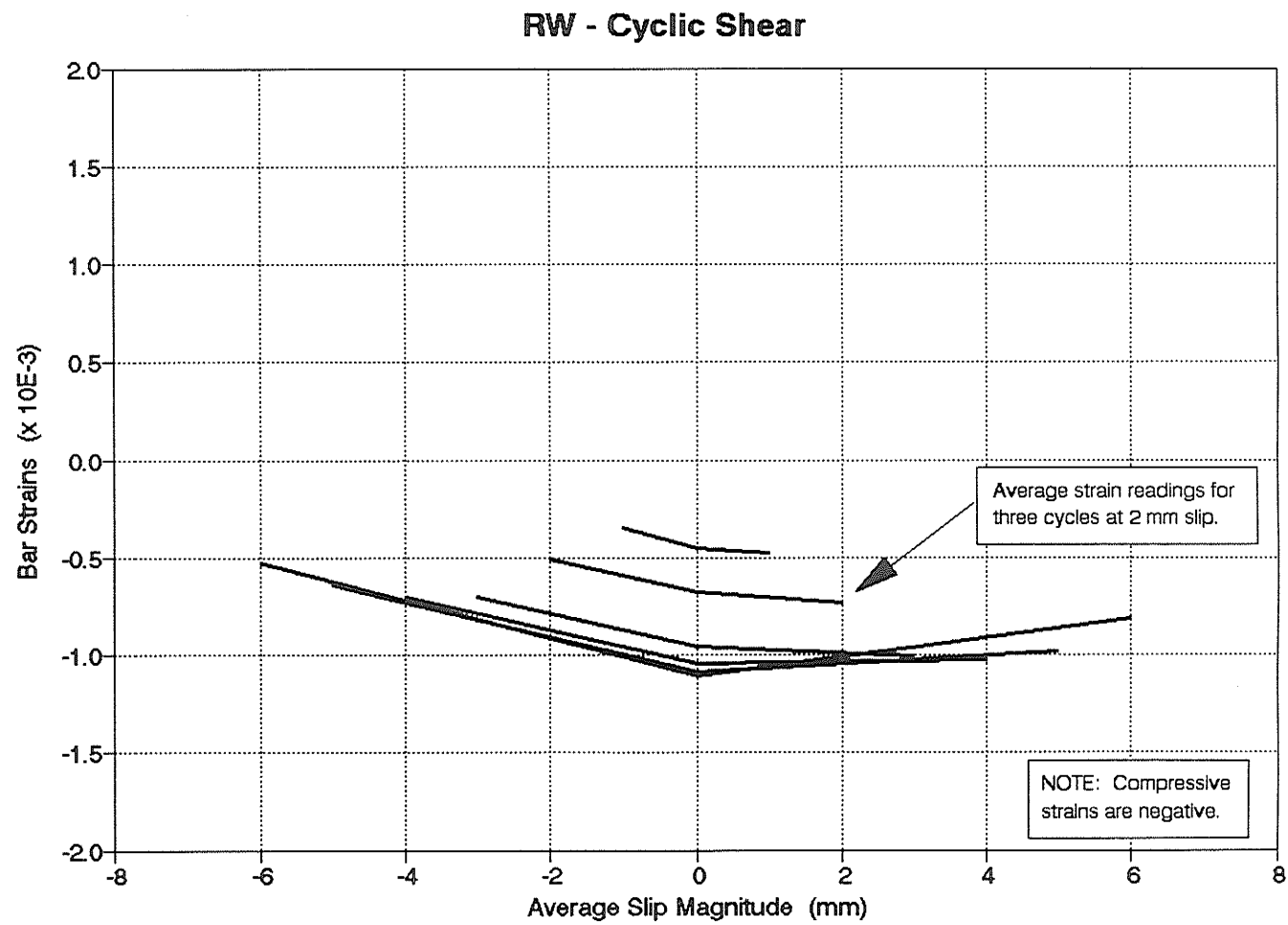
Figure 5.15(b) Specimen RW - Average Maximum Strain Behaviour: East Bar
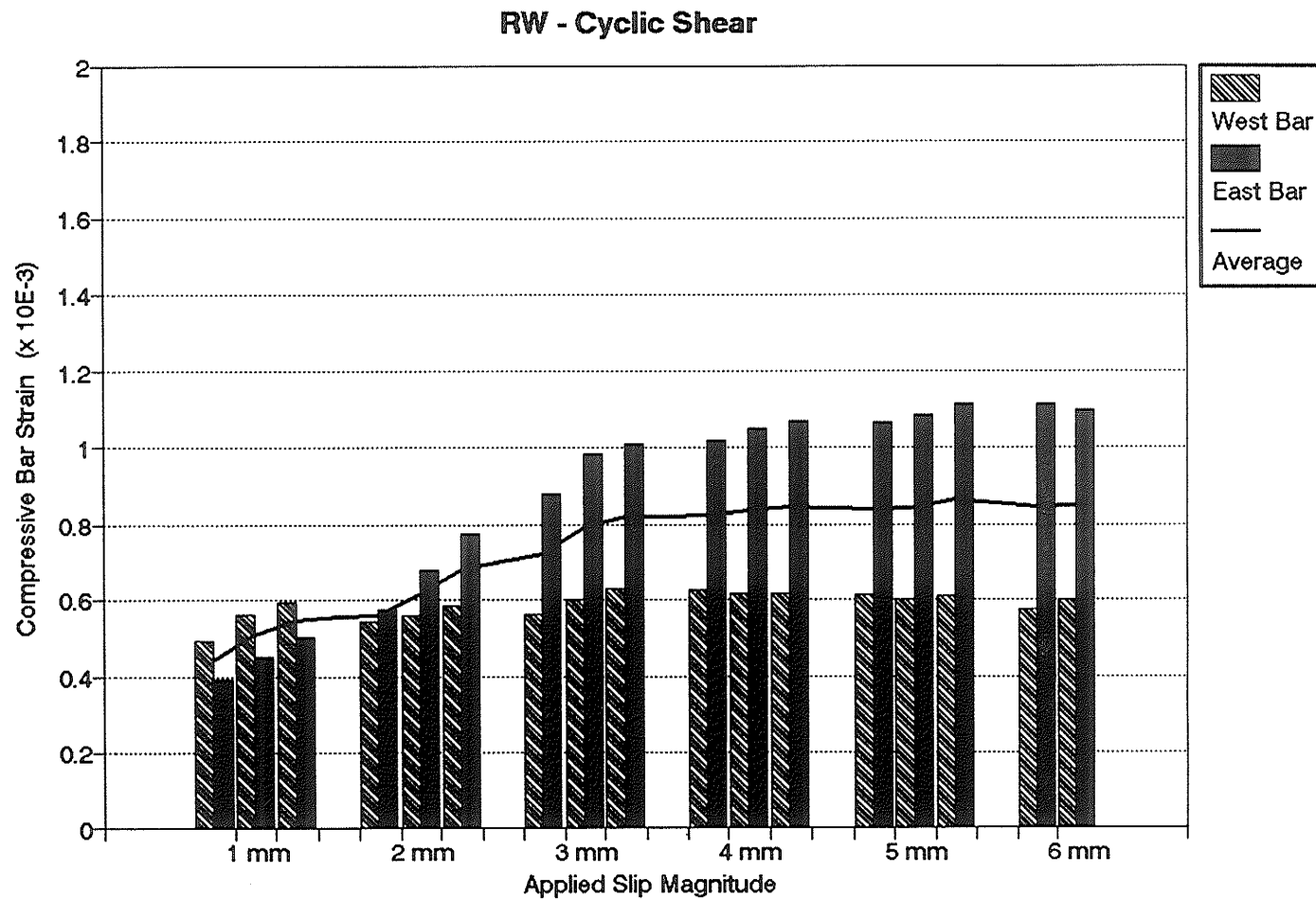
Figure 5.16   Specimen RW - Reinforcing Bar Strains at the Zero Slip Position
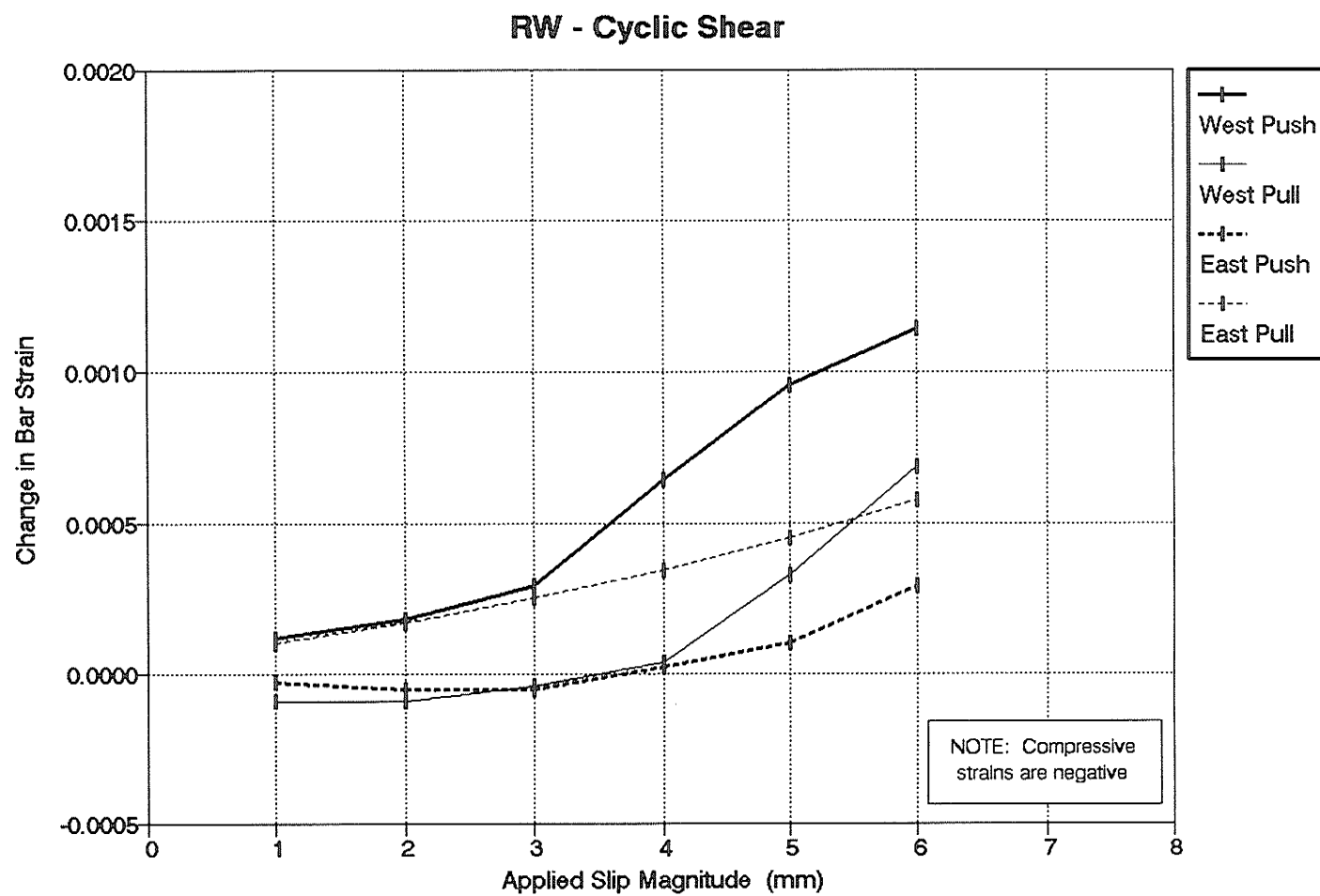
Figure 5.17   Specimen RW - Change of Bar Strains for a Given Slip Magnitude
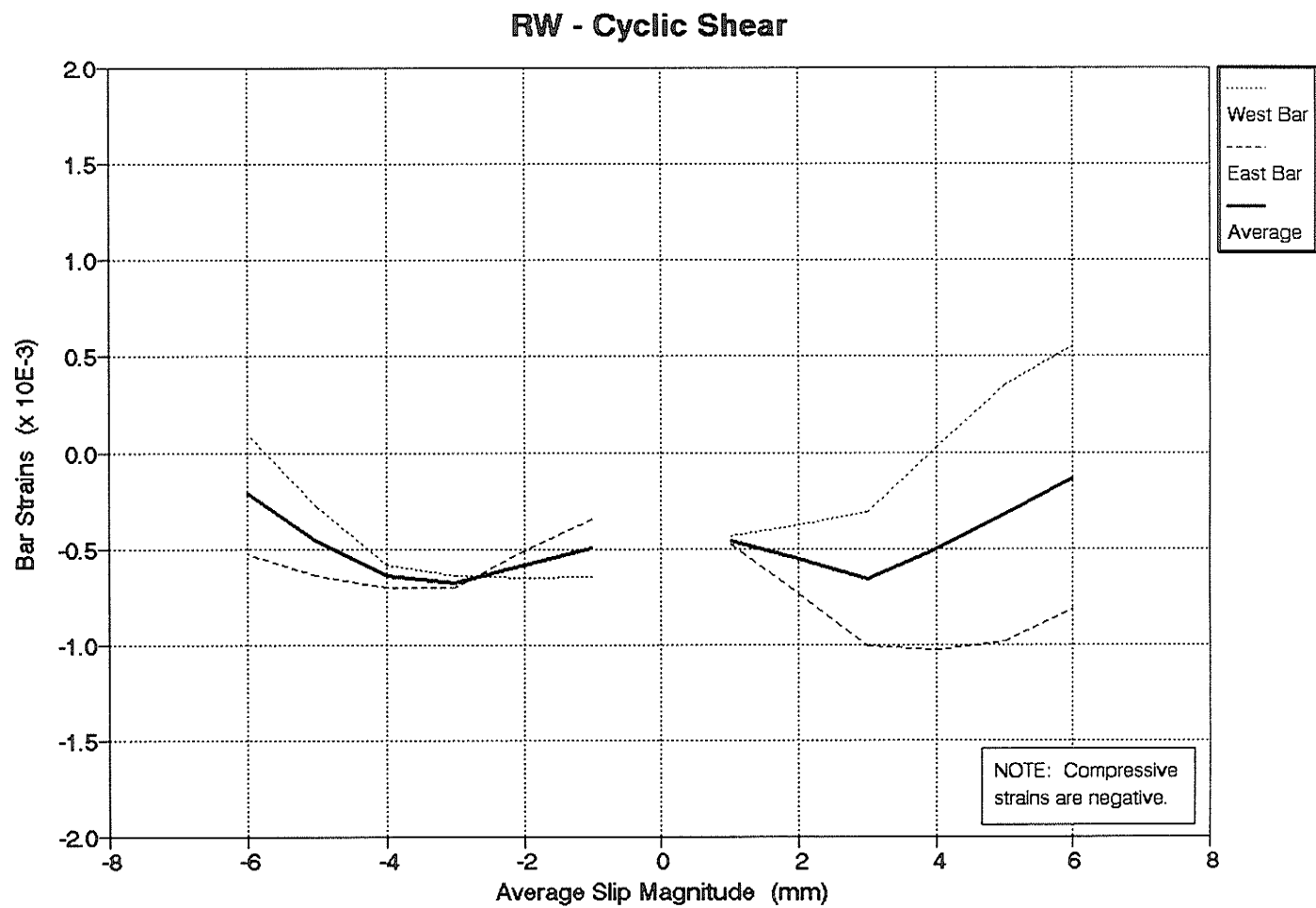
Figure 5.18   Specimen RW - Average Envelope of Reinforcing Bar Strains

PTS - Cyclic Shear
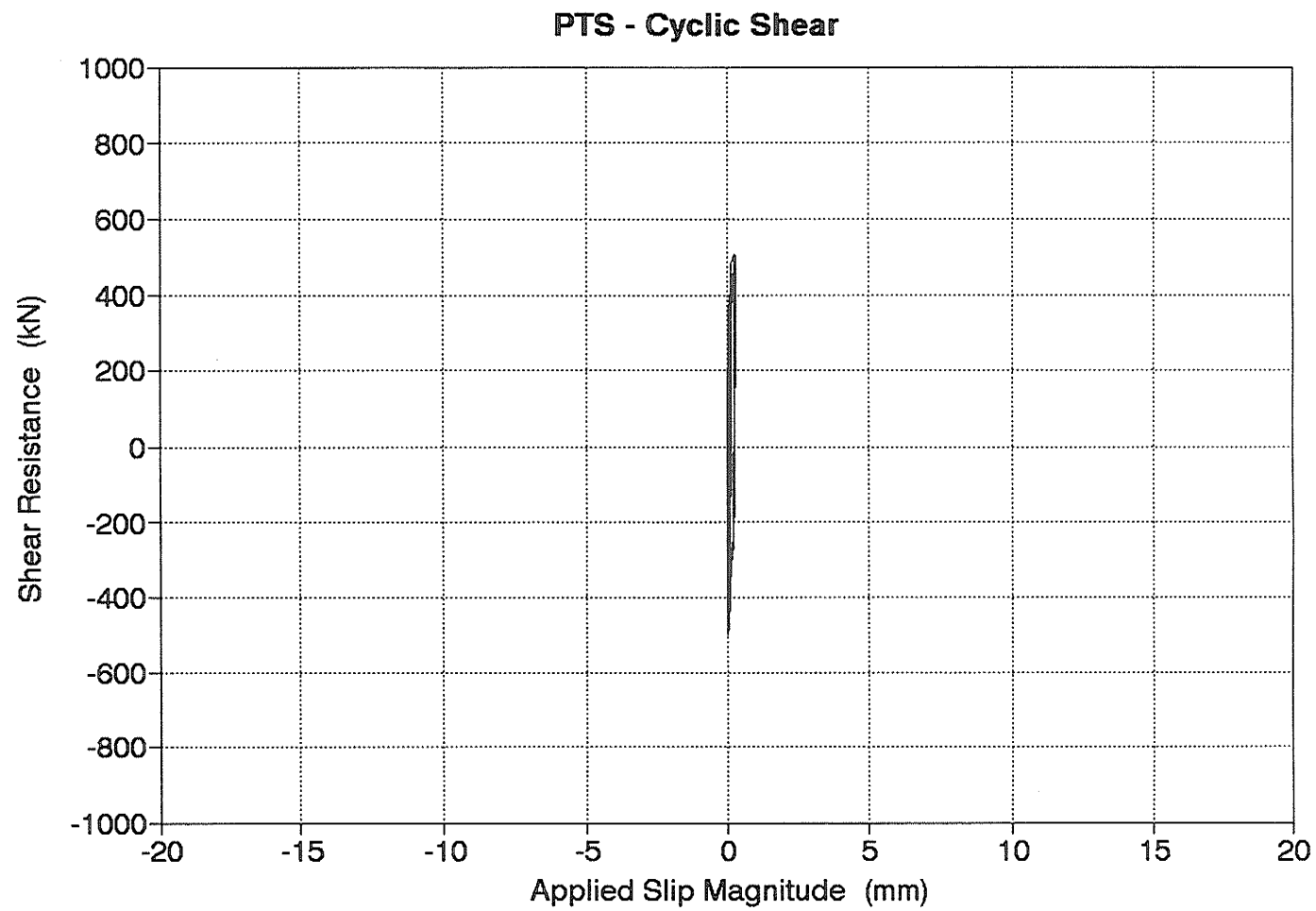
Figure 5.19   Specimen PTS - Elastic Connection Behaviour Prior to the Initiation of Slip

PTS - Cyclic Shear
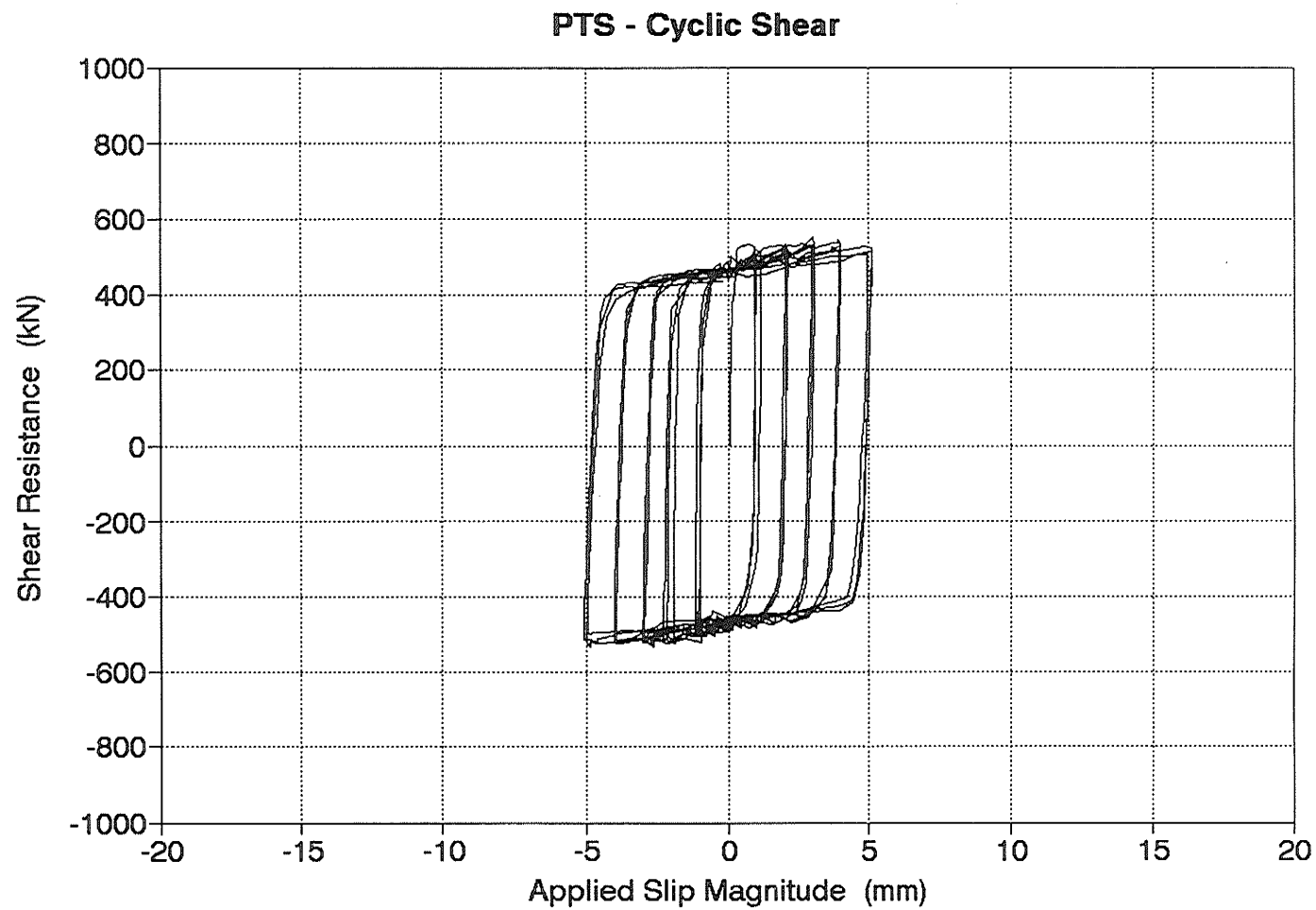
Figure 5.20   Specimen PTS - Inelastic Connection Behaviour After the Initiation of Slip
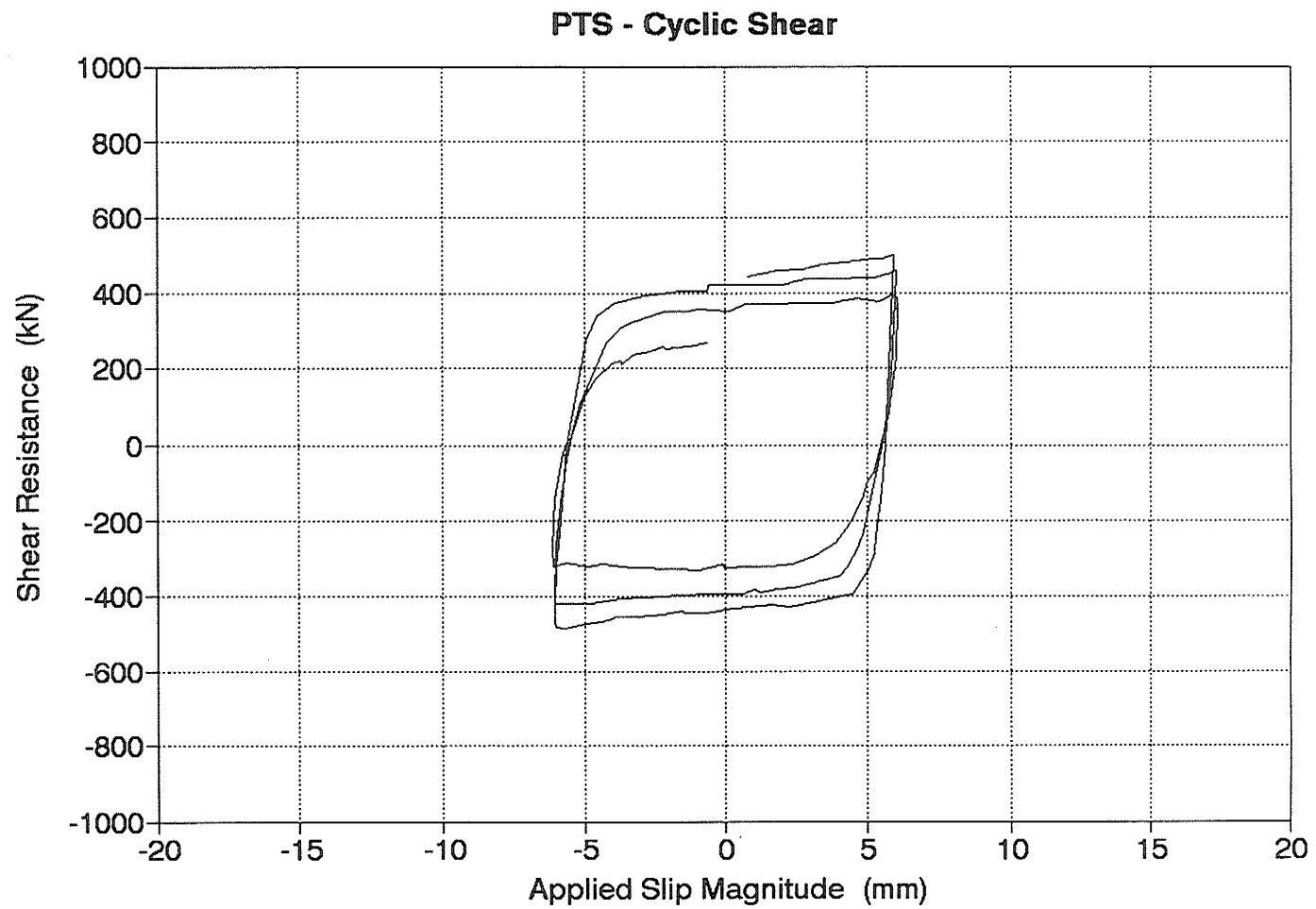
Figure 5.21   Specimen PTS - Connection Behaviour at Failure (Slip Magnitude = 6 mm)
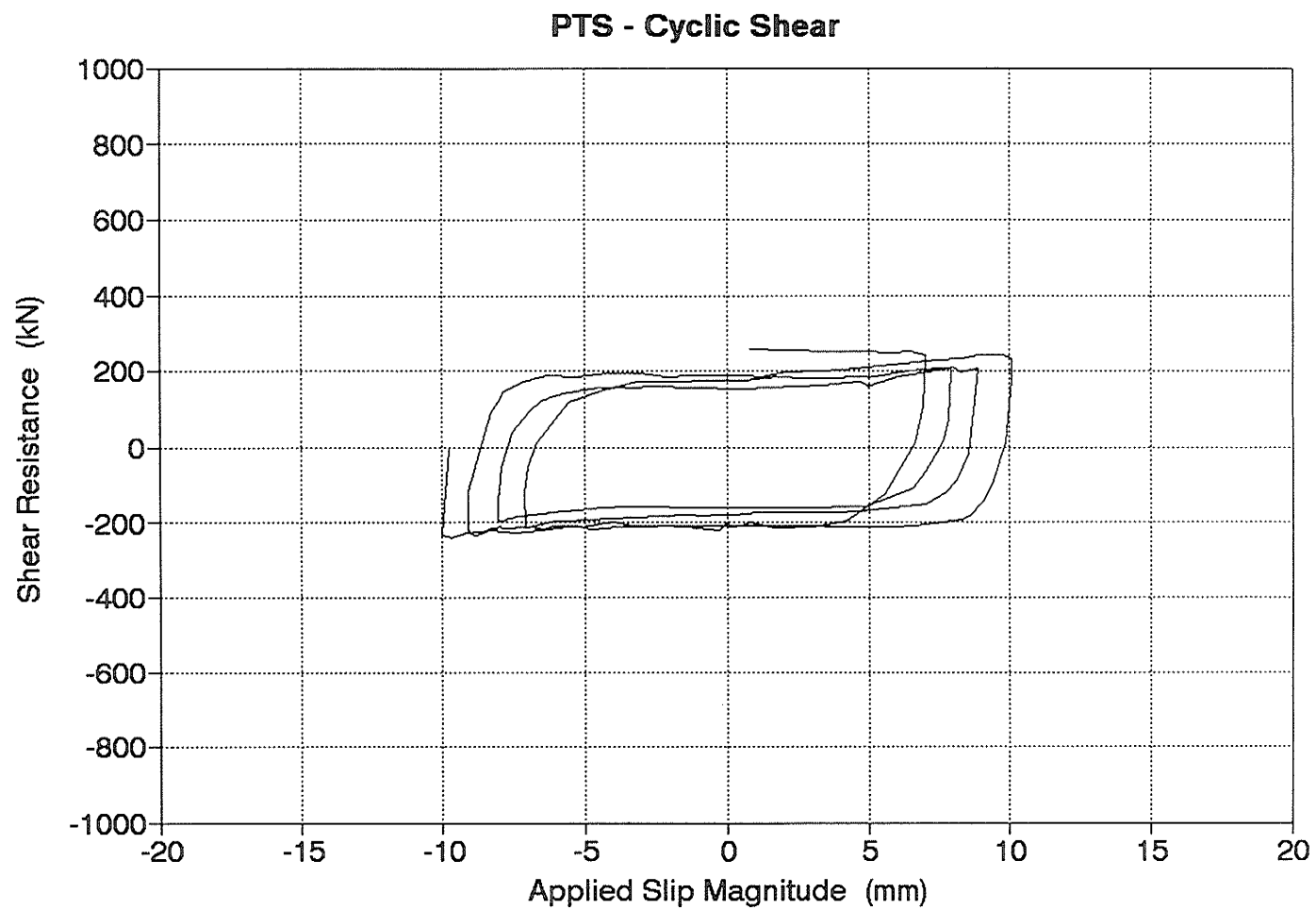
Figure 5.22   Specimen PTS - Connection Behaviour After Crushing of the Dry Pack
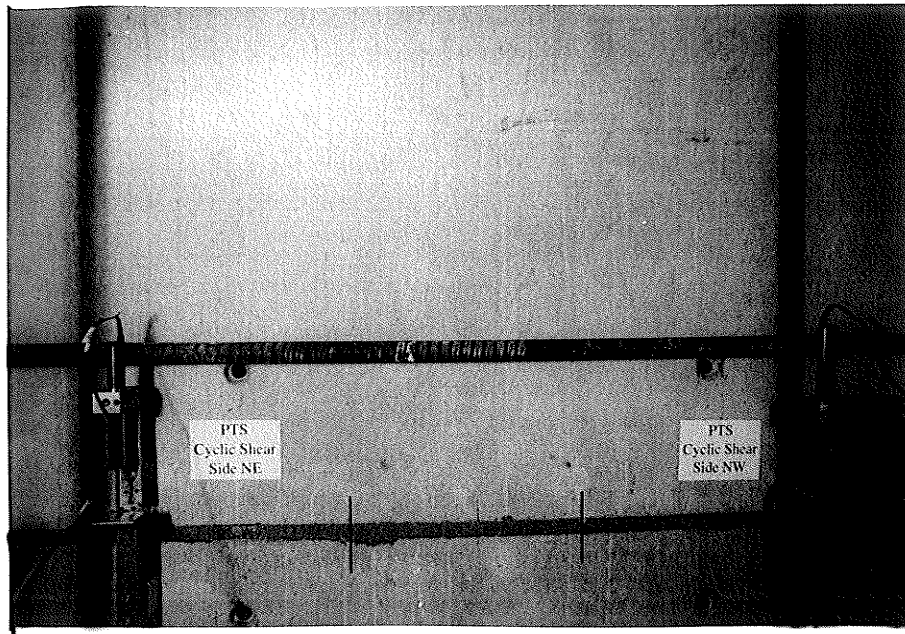
Figure 5.23   Specimen PTS - Condition of the Dry Pack at the Start of Testing
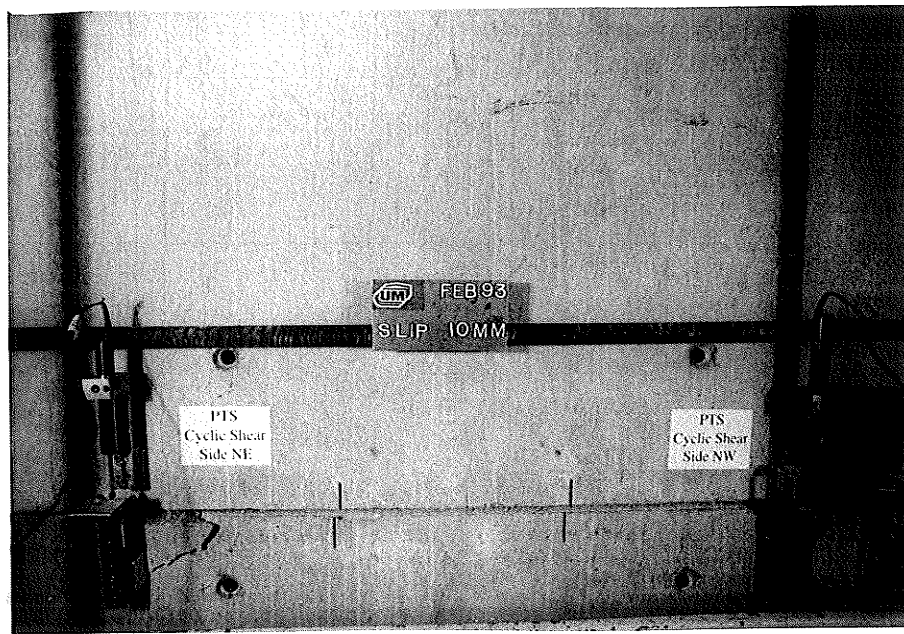
Figure 5.24   Specimen PTS - Condition of the Dry Pack After Crushing
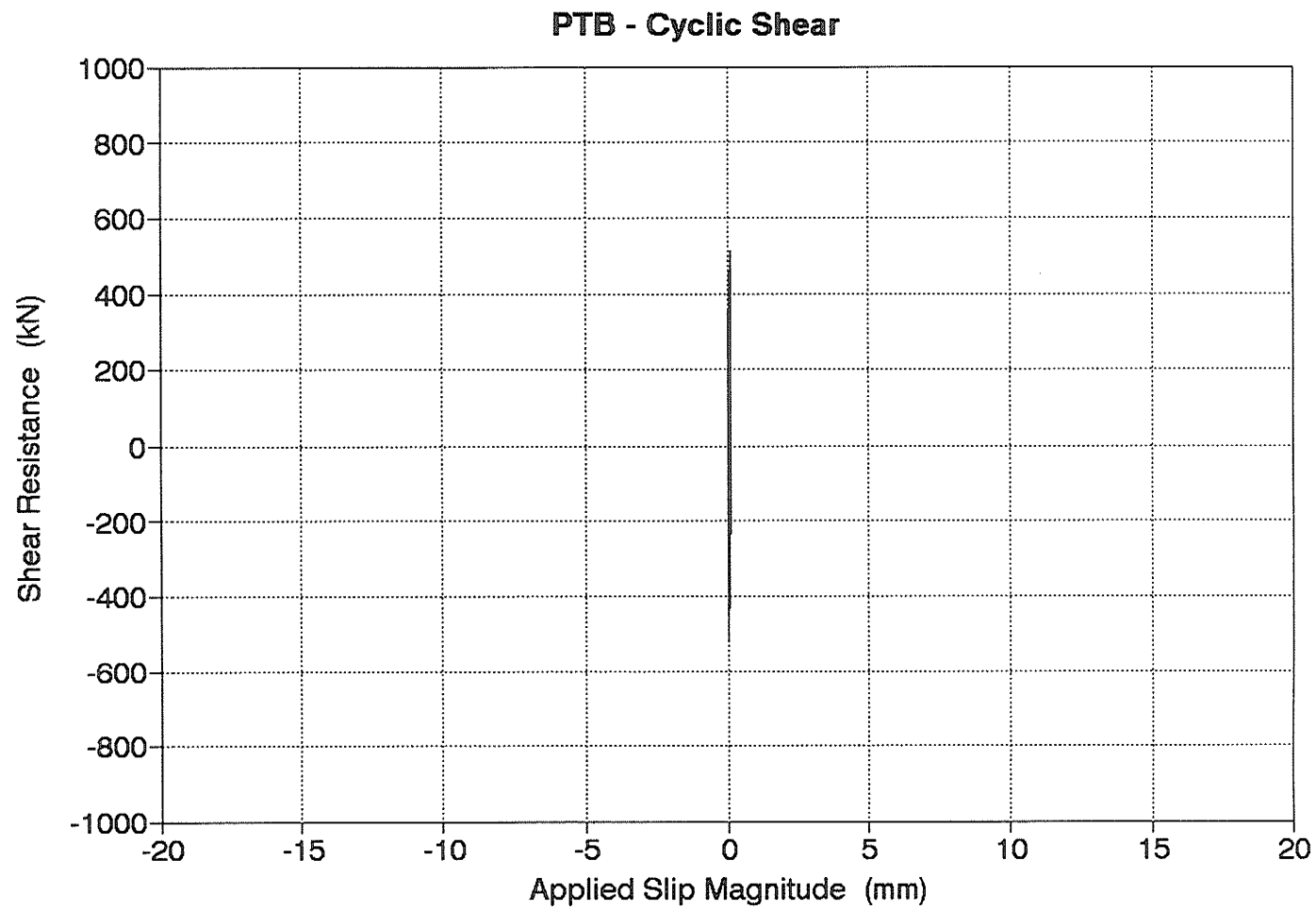
Figure 5.25   Specimen PTB - Elastic Connection Behaviour Prior to the Initiation of Slip

PTB - Cyclic Shear
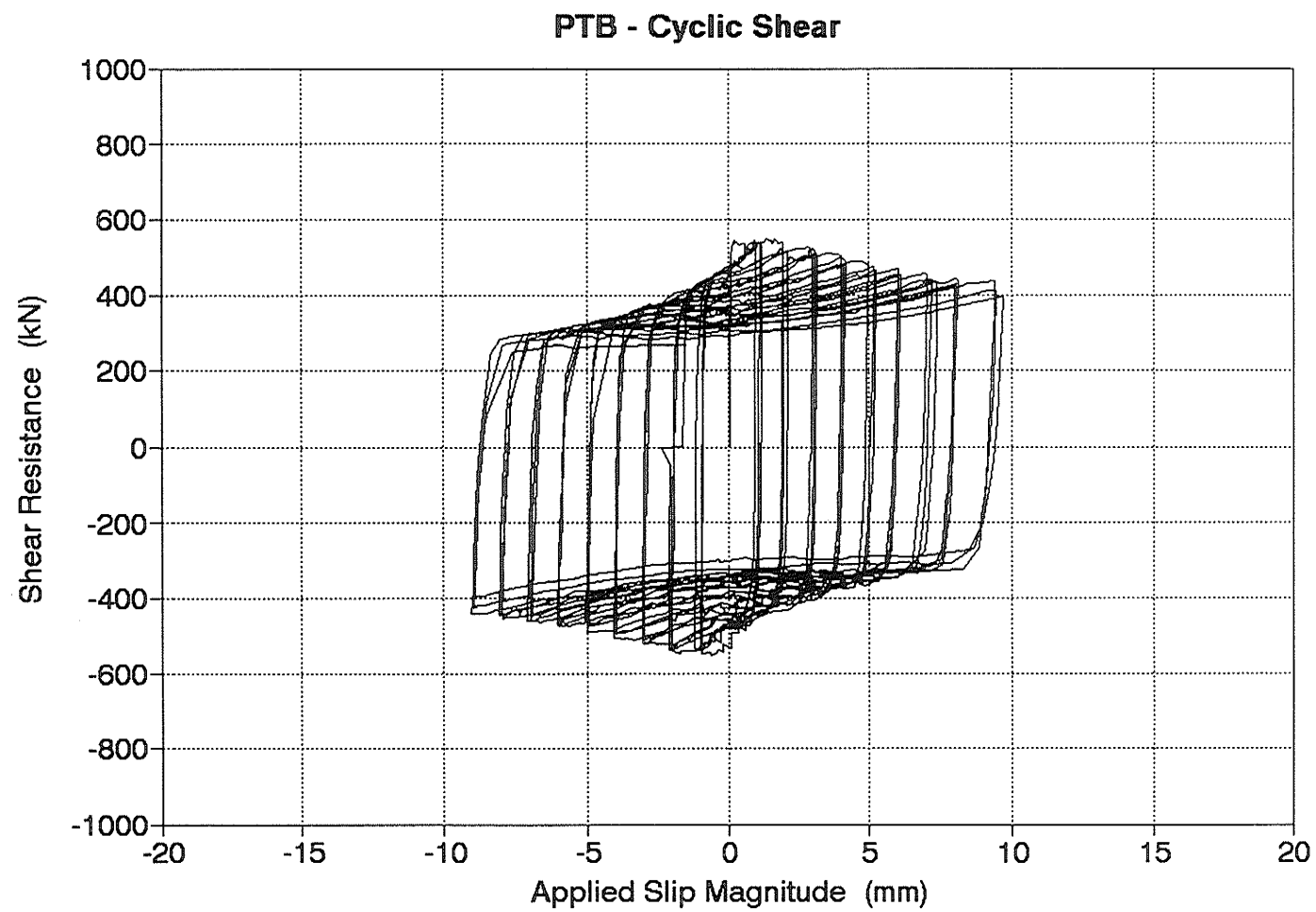
Figure 5.26   Specimen PTB - Inelastic Connection Behaviour After the Initiation of Slip
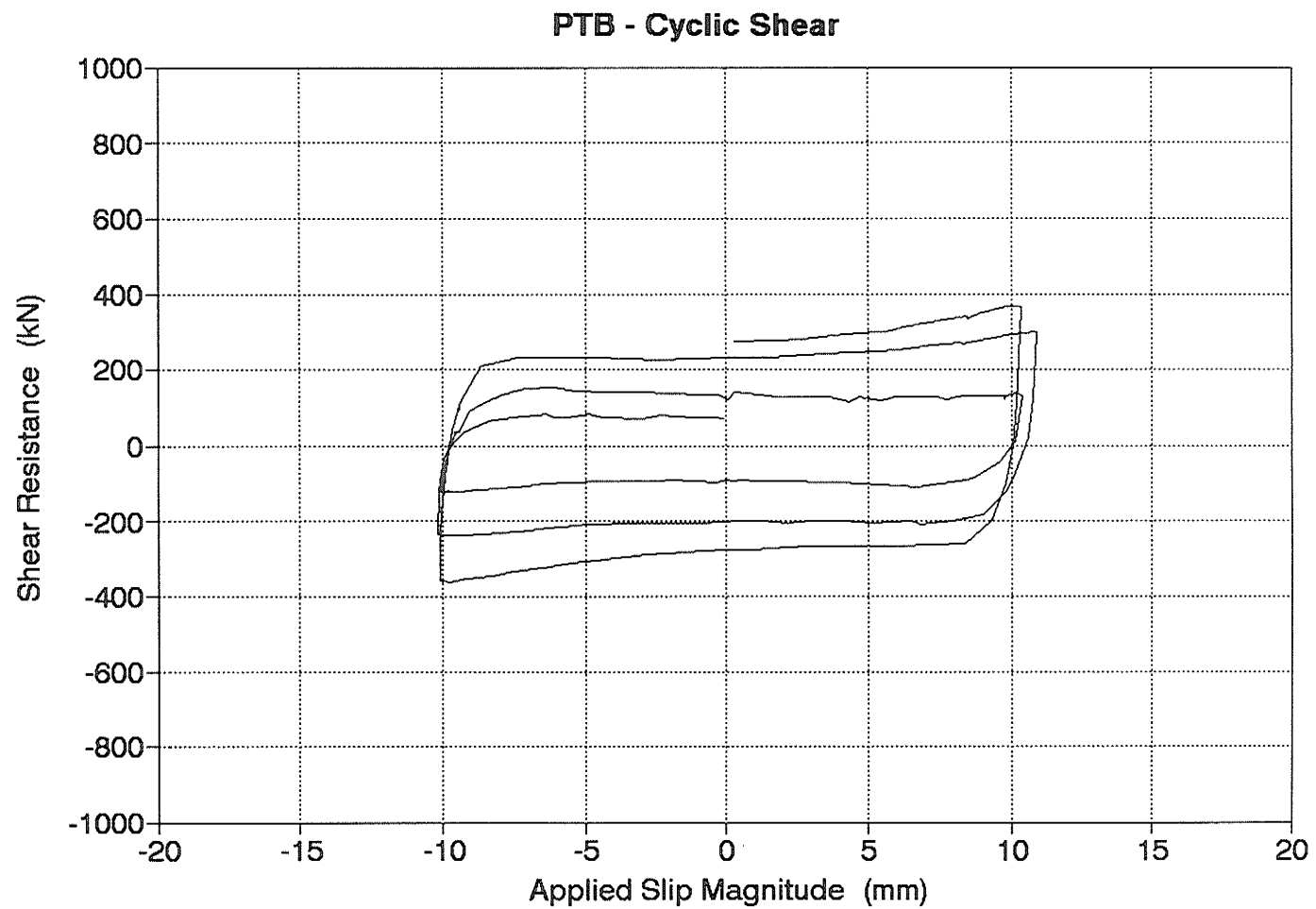
Figure 5.27   Specimen PTB - Connection Behaviour at Failure (Slip Magnitude = 10mm)

PTB - Cyclic Shear
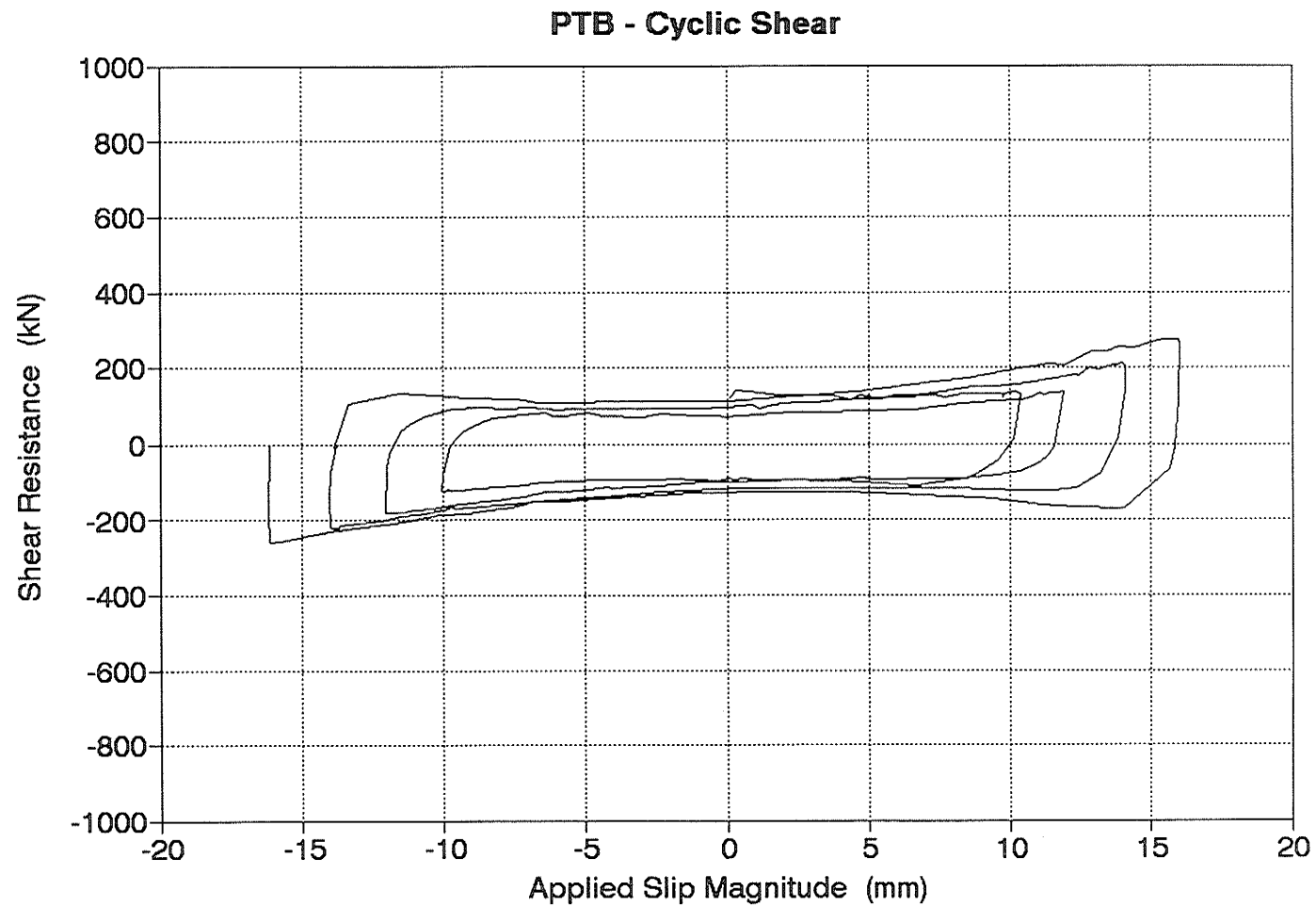
Figure 5.28   Specimen PTB - Connection Behaviour After Crushing of the Dry Pack
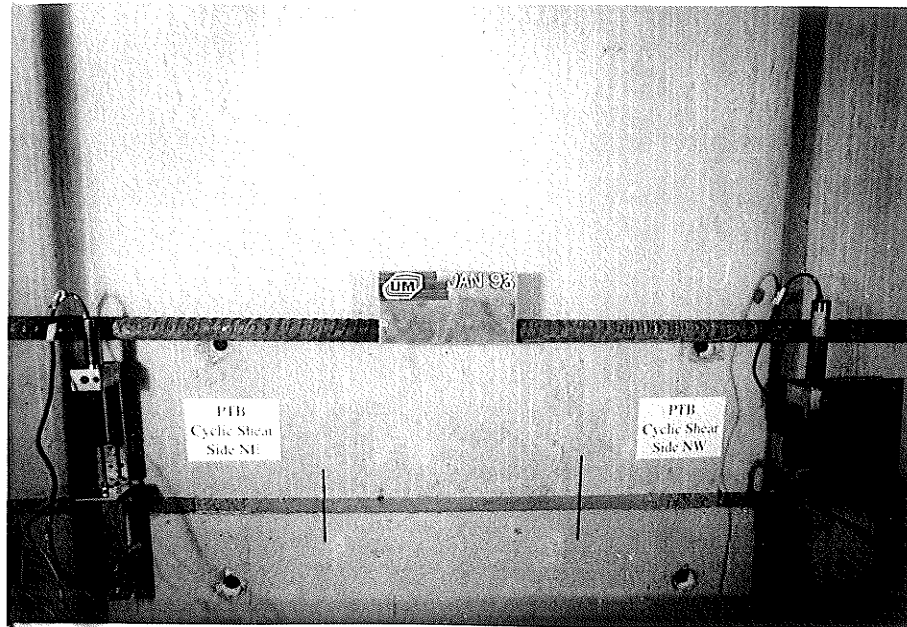
Figure 5.29   Specimen PTB - Condition of the Dry Pack at the Start of Testing
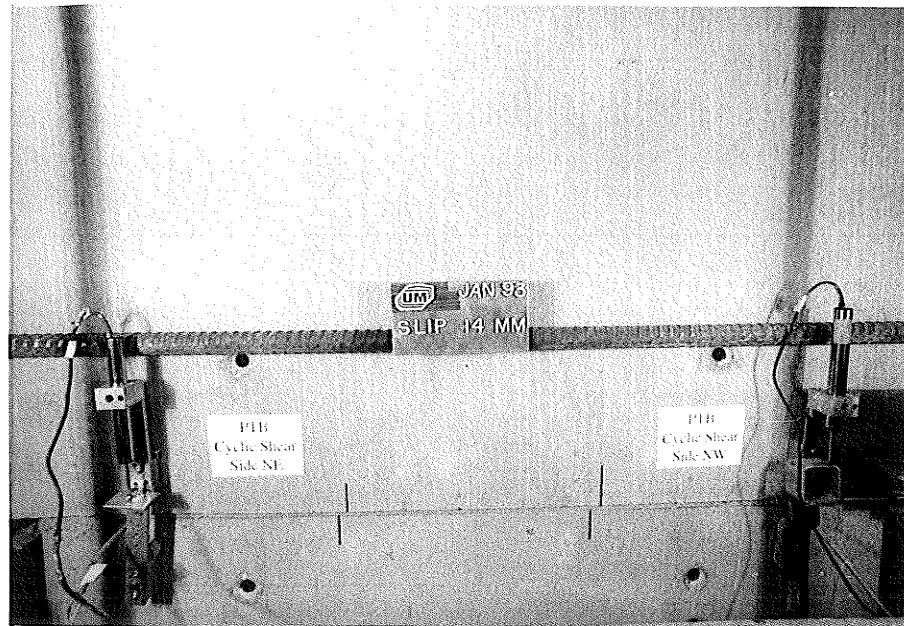
Figure 5.30   Specimen PTB - Condition of the Dry Pack After Crushing

PTB - Cyclic Shear

Legend:
— Outside Gauge
······ Inside Gauge

Initial Effective Strains:
Outside Gauge: 3.09x10e-3
Inside Gauge: 2.95x10e-3

Y-axis: Applied Shear Load (kN)
X-axis: Bar Strain (milli-strain)
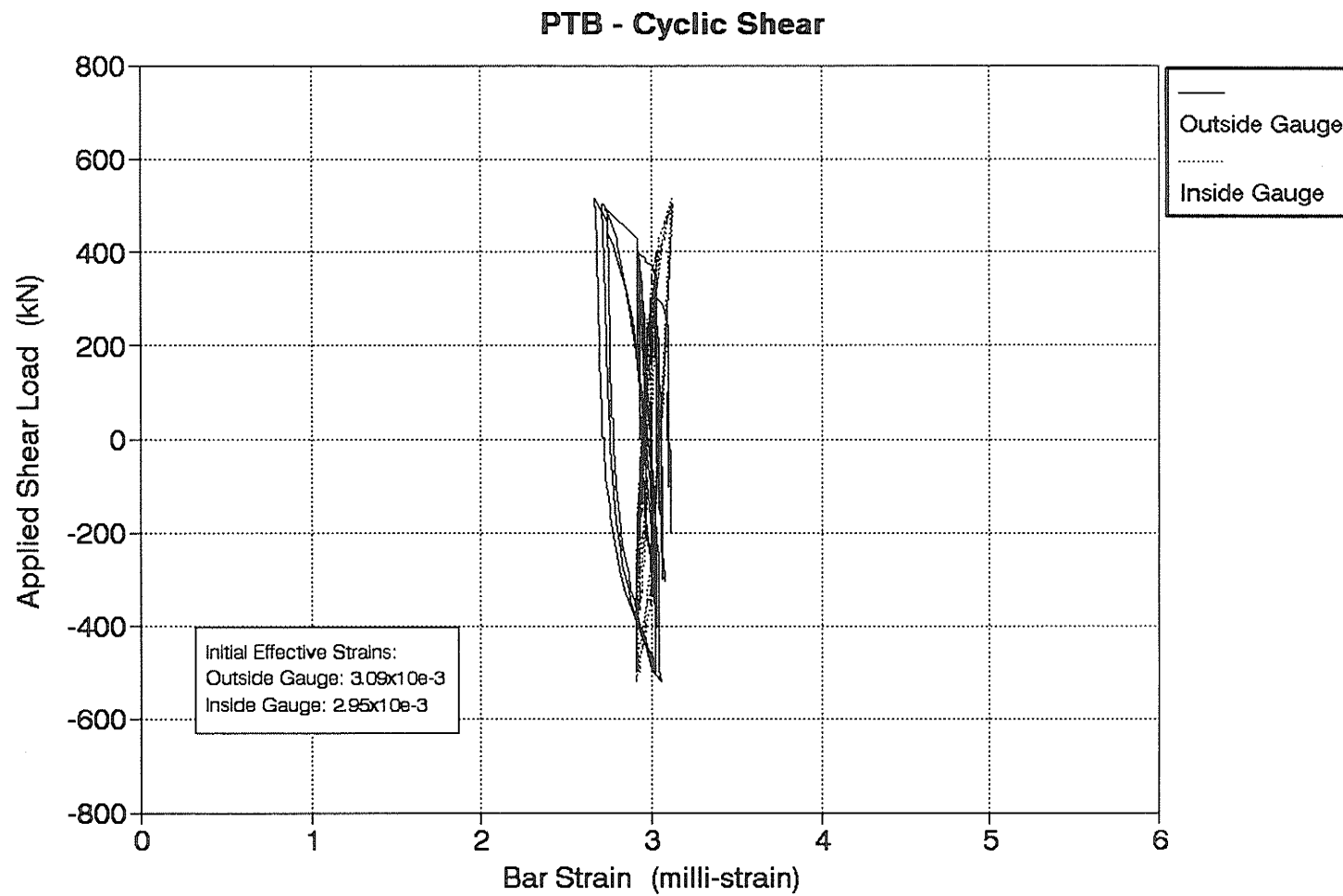
Figure 5.31(a) Specimen PTB - Variation of Bar Strain Prior to the Initiation of Slip: West Bar

PTB - Cyclic Shear

Legend:
— Outside Gauge
...... Inside Gauge

Initial Effective Strains:
Outside Gauge: 2.99x10e-3
Inside Gauge: 3.18x10e-3

Y-axis: Applied Shear Load (kN), from -800 to 800
X-axis: Bar Strain (milli-strain), from 0 to 6
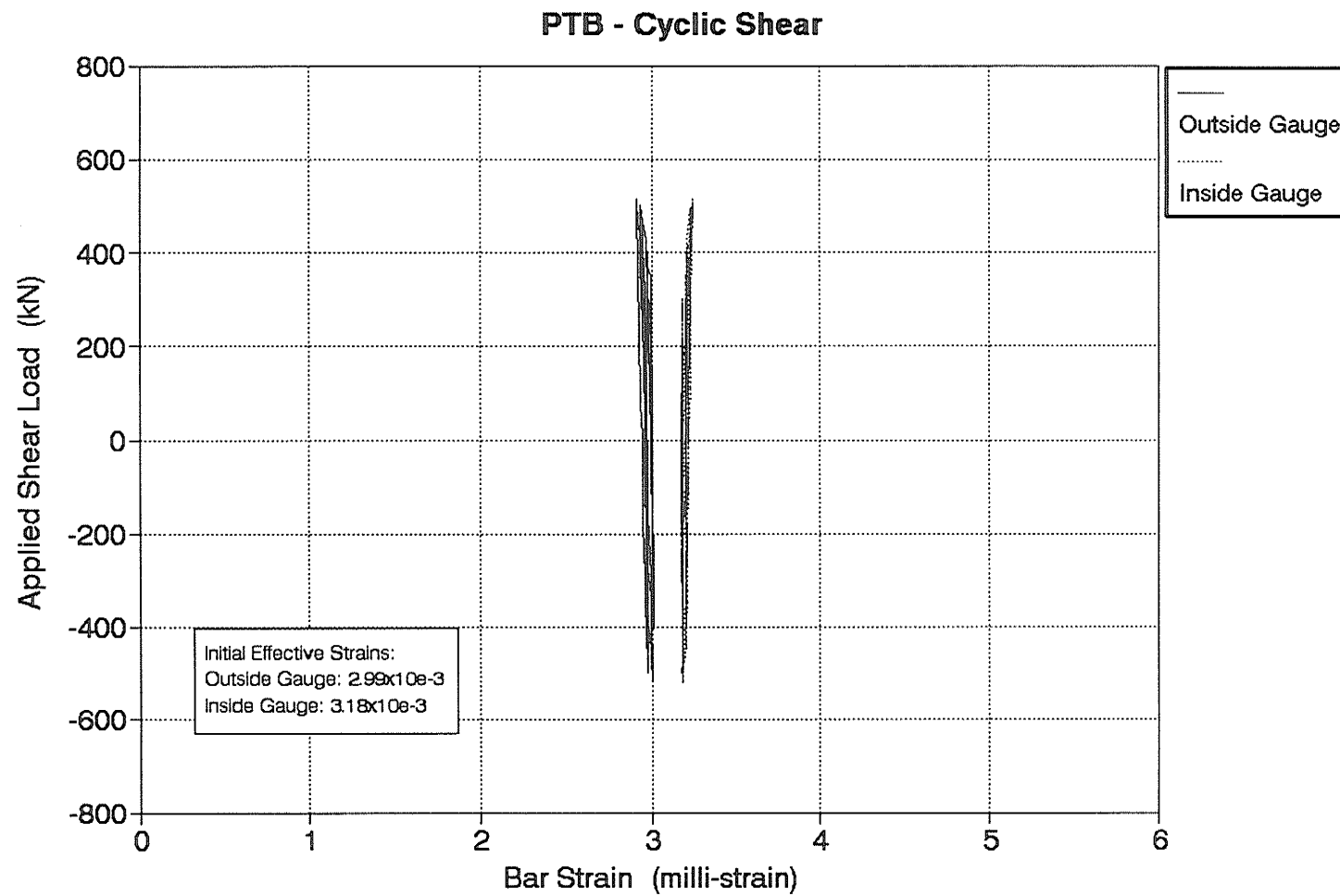
Figure 5.31(b) Specimen PTB - Variation of Bar Strain Prior to the Initiation of Slip: East Bar
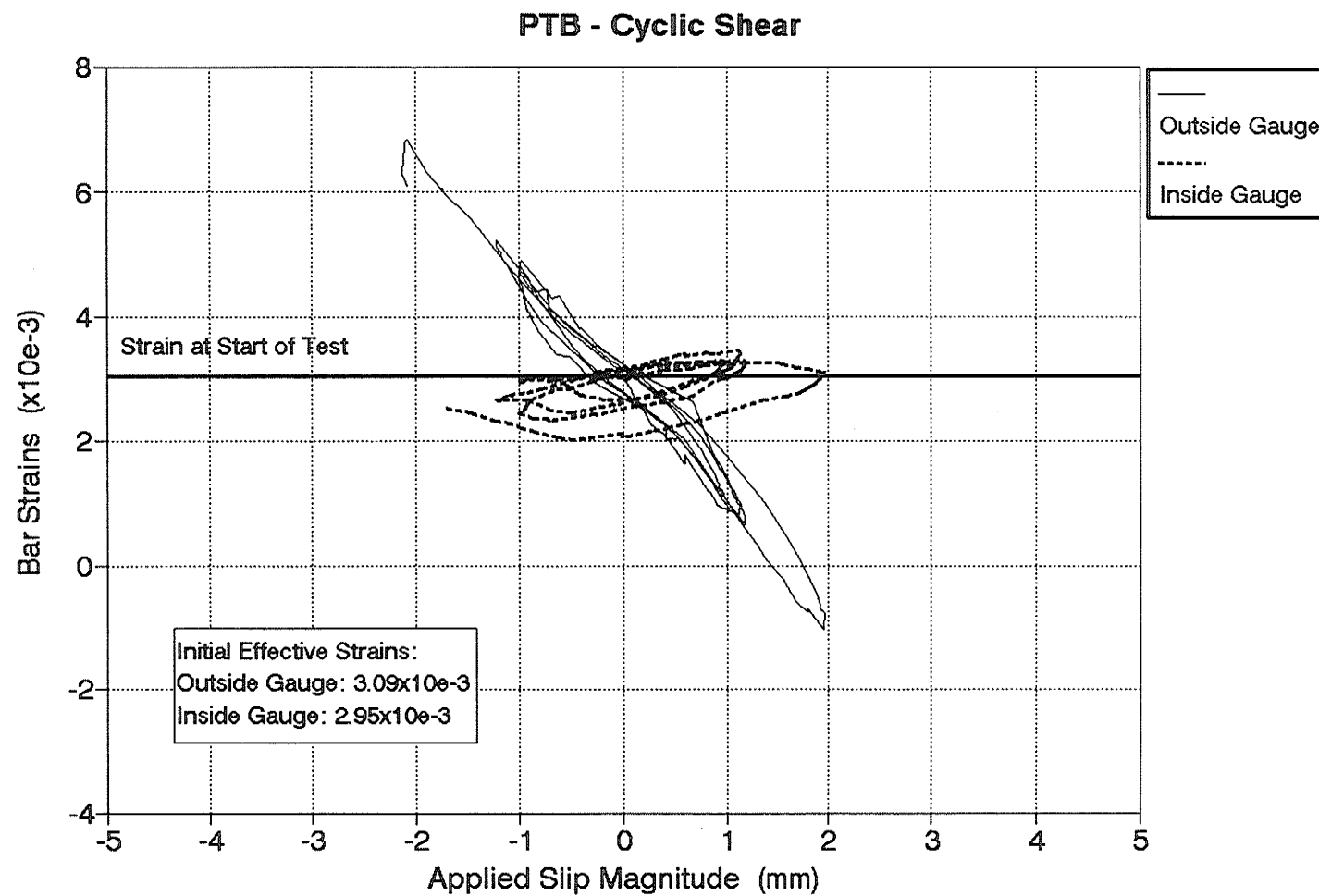
Figure 5.32(a) Specimen PTB - Variation of Bar Strain After the Initiation of Slip: West Bar
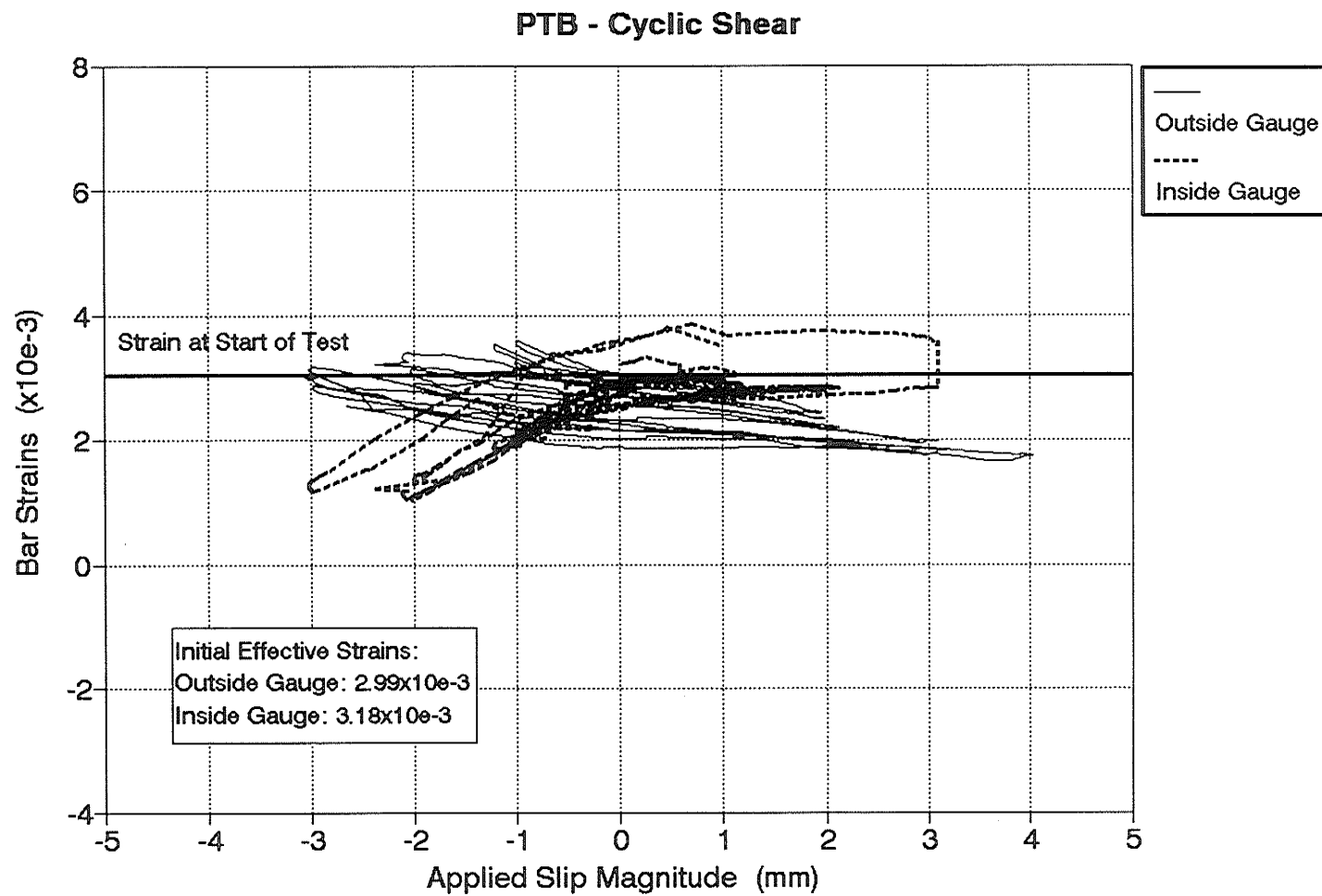
Figure 5.32(b) Specimen PTB - Variation of Bar Strain After the Initiation of Slip: East Bar
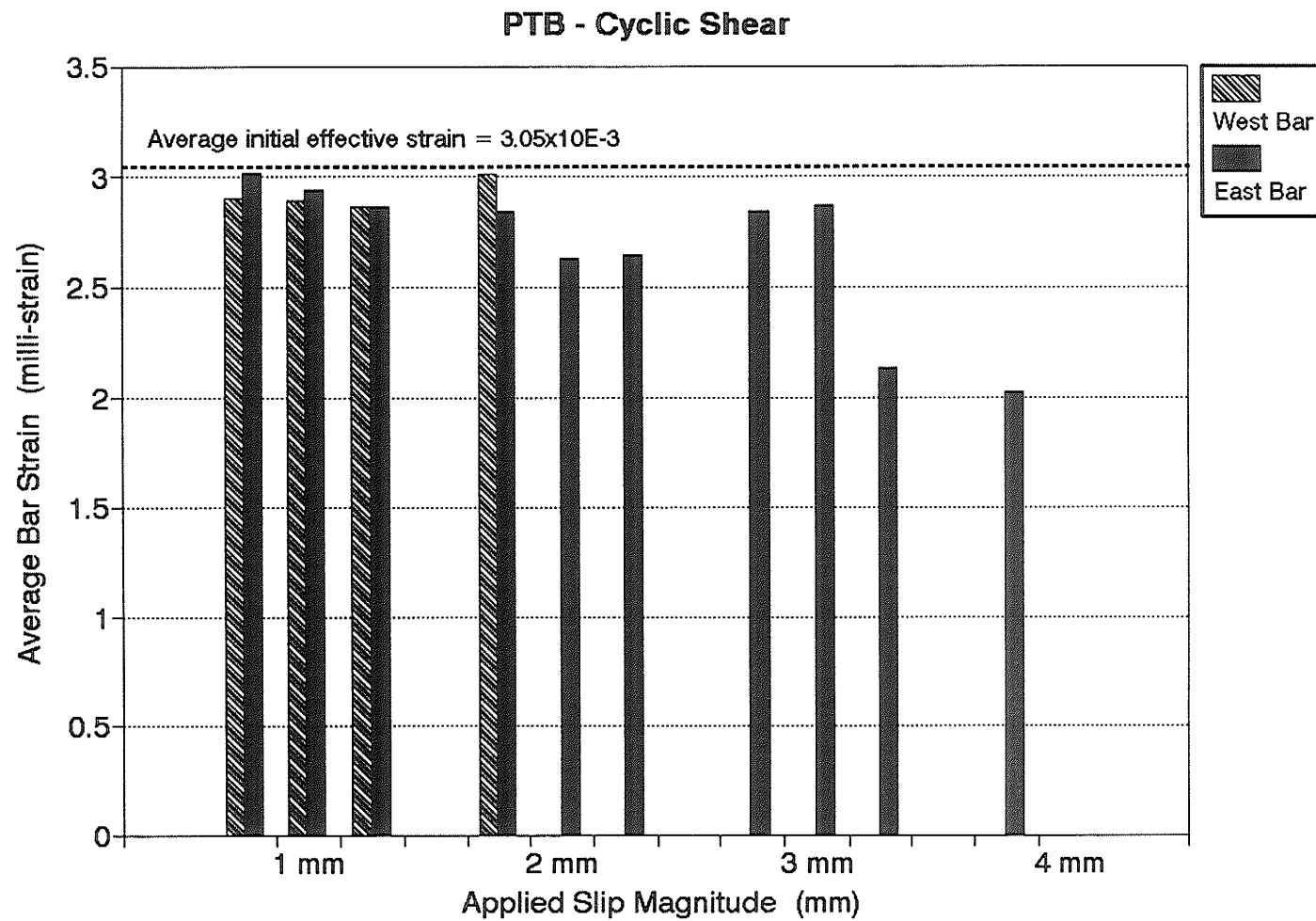
Figure 5.33   Specimen PTB - Prestressing Bar Strains at the Zero Slip Position

SK - Cyclic Shear

Figure 5.34   Specimen SK - Elastic Connection Behaviour Prior to the Initiation of Slip

SK - Cyclic Shear
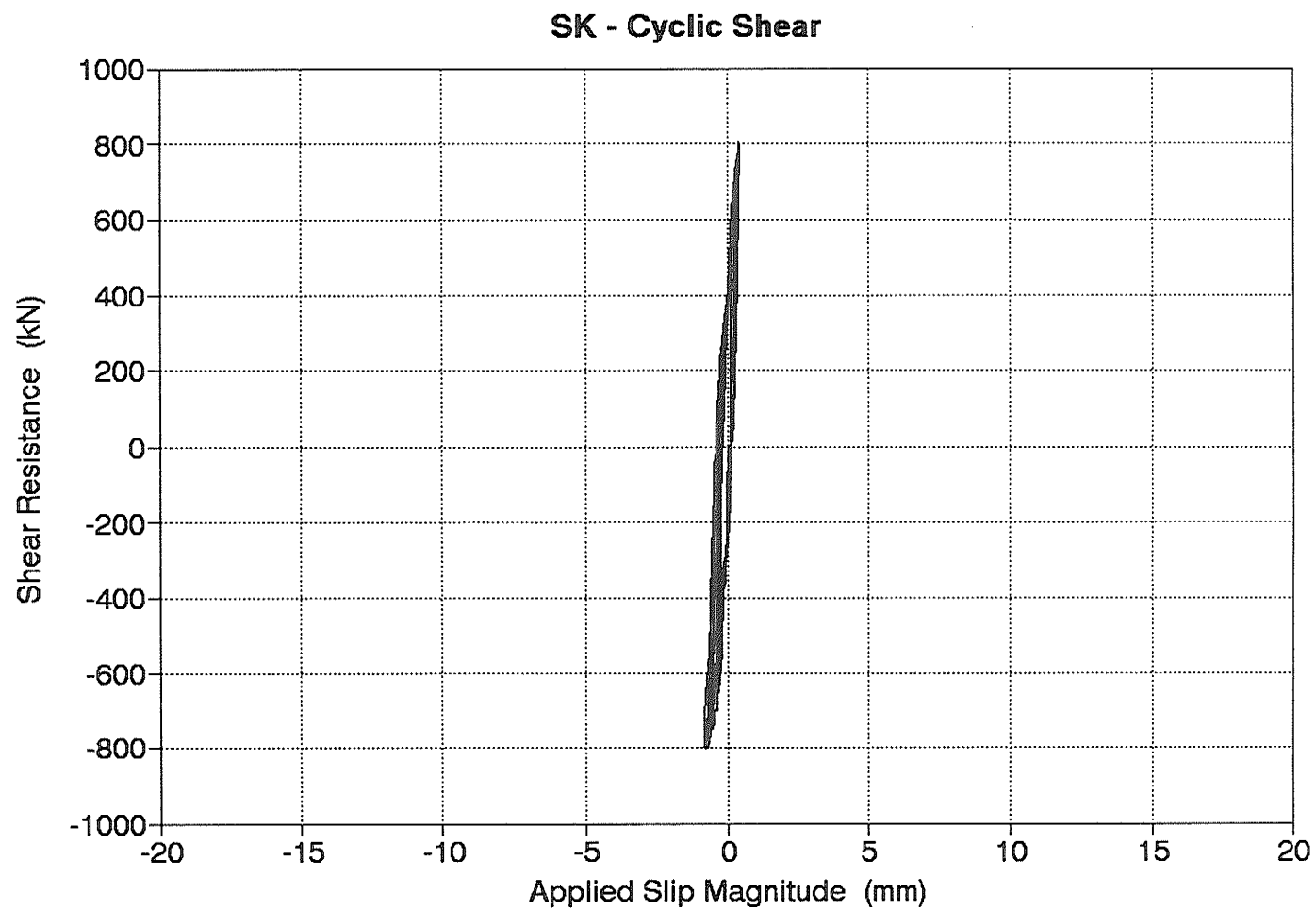
Figure 5.35(a) Specimen SK - Inelastic Connection Behaviour After the Initiation of Slip But Prior to Cracking of the Dry Pack Within the Shear Keys

SK - Cyclic Shear
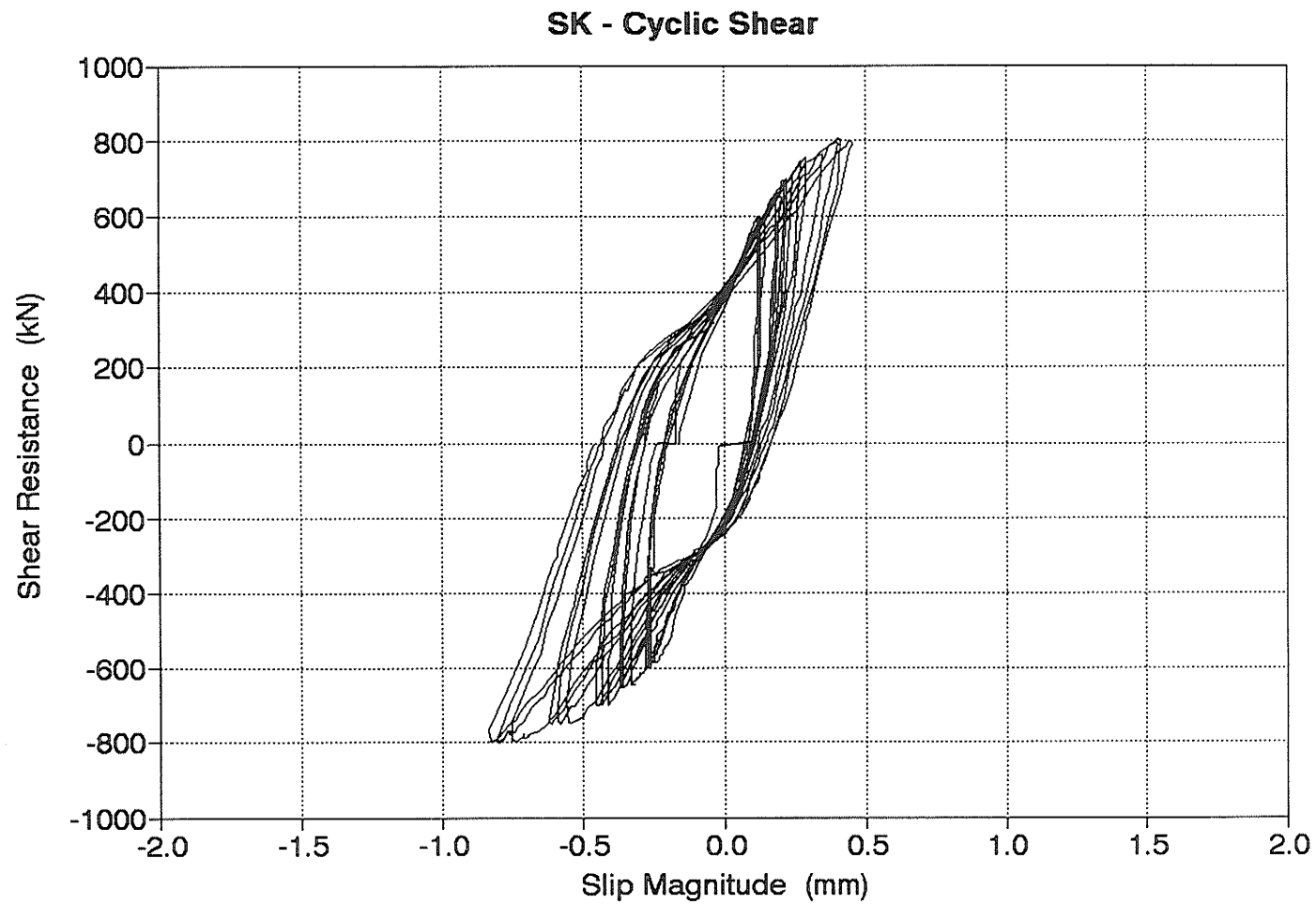
Figure 5.35(b) Specimen SK - Inelastic Connection Behaviour After the Initiation of Slip But Prior to
Cracking of the Dry Pack Within the Shear Keys (Enlarged Scale)
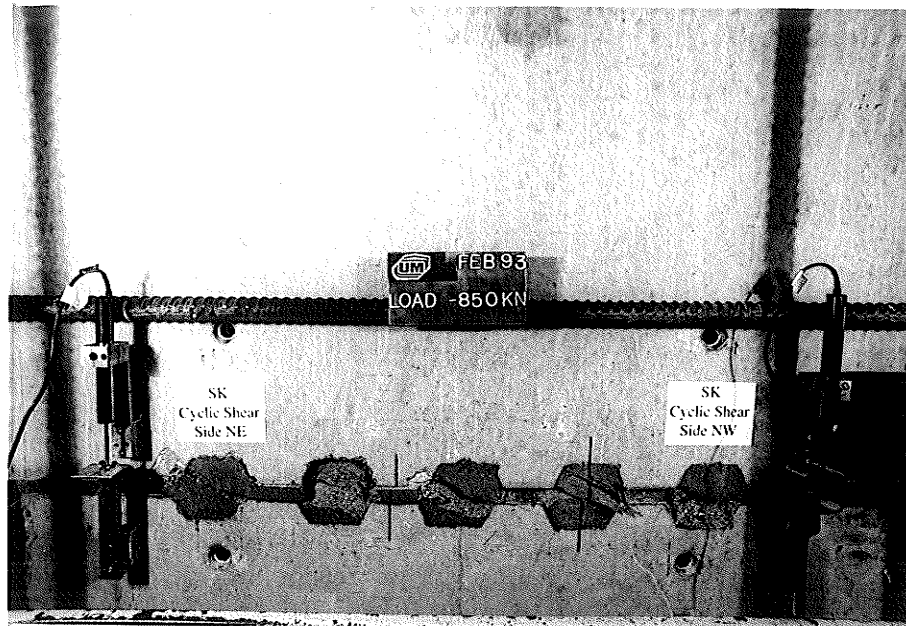
Figure 5.36   Specimen SK - Condition of the Dry Pack Immediately After Cracking
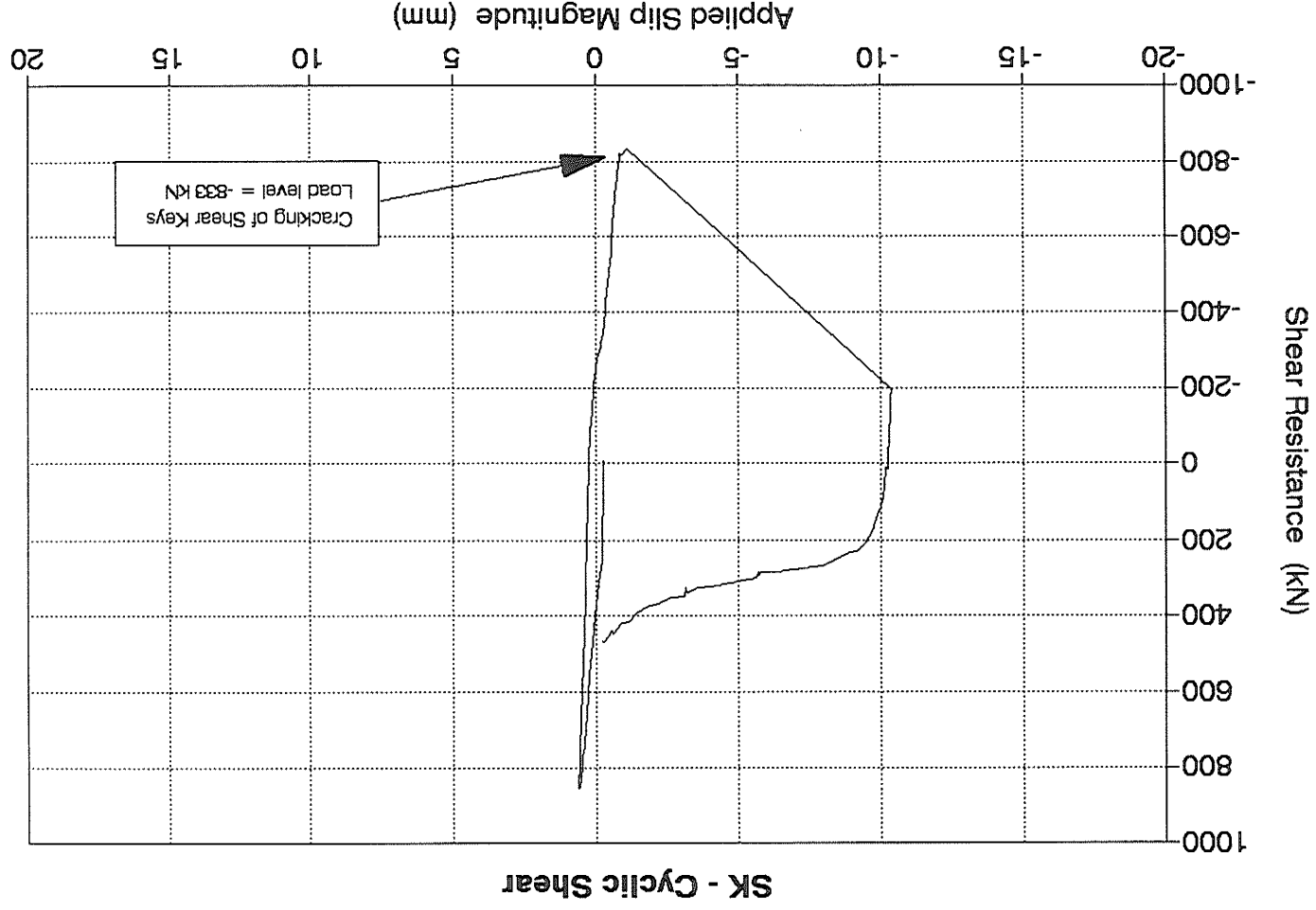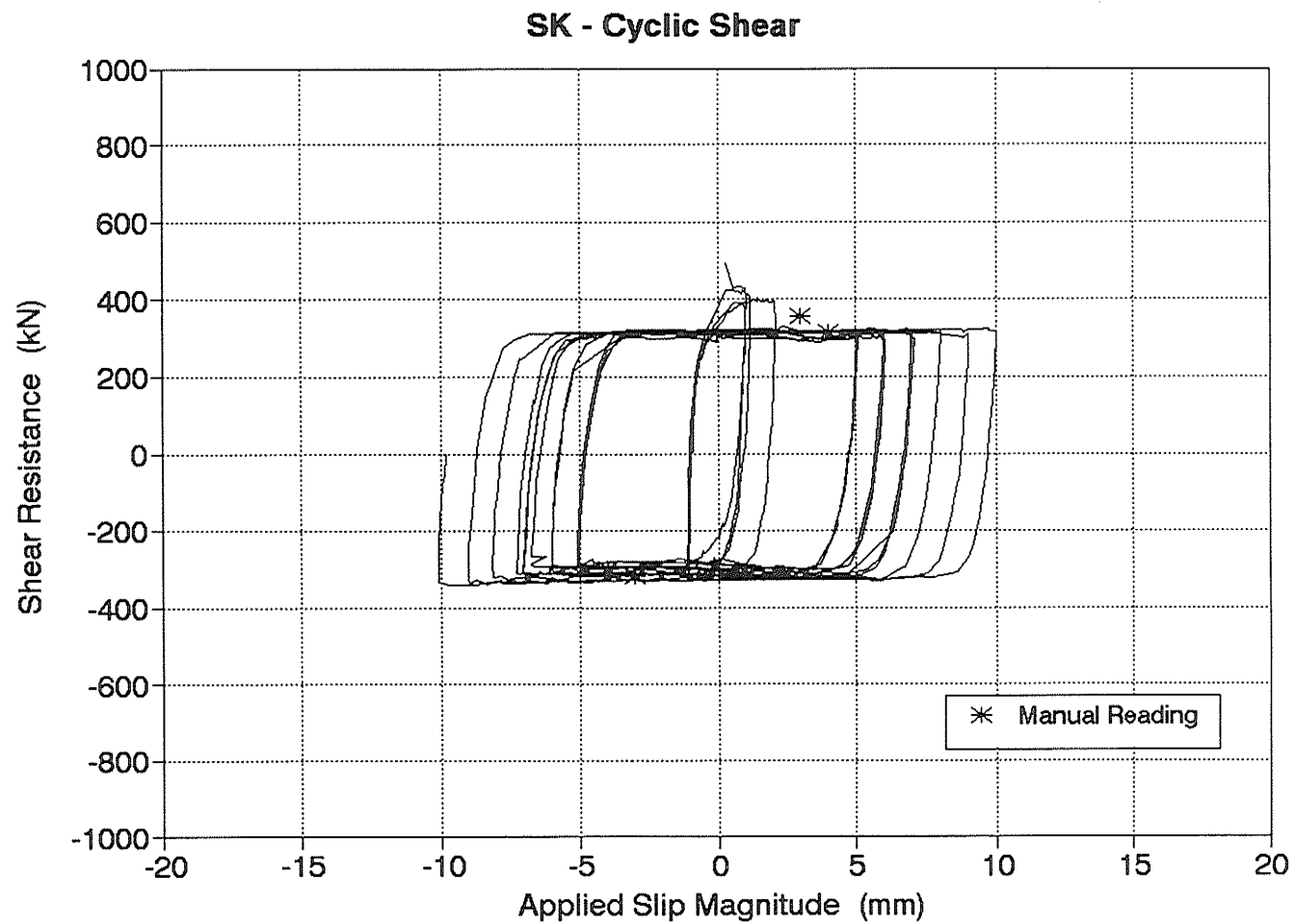
Figure 5.38   Specimen SK - Inelastic Behaviour After Cracking and Gradual Deterioration of the Dry Pack
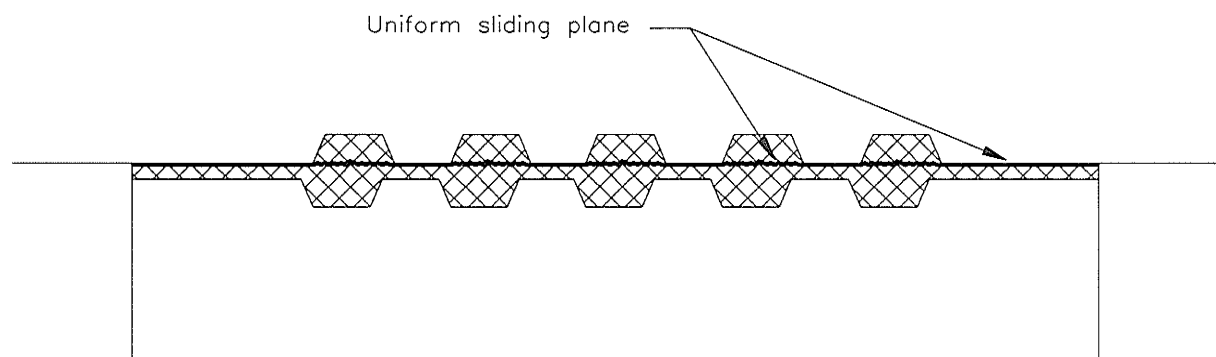
Figure 5.39   Specimen SK - Slip Interface After Cracking of the Shear Keys and Deterioration of the Dry Pack
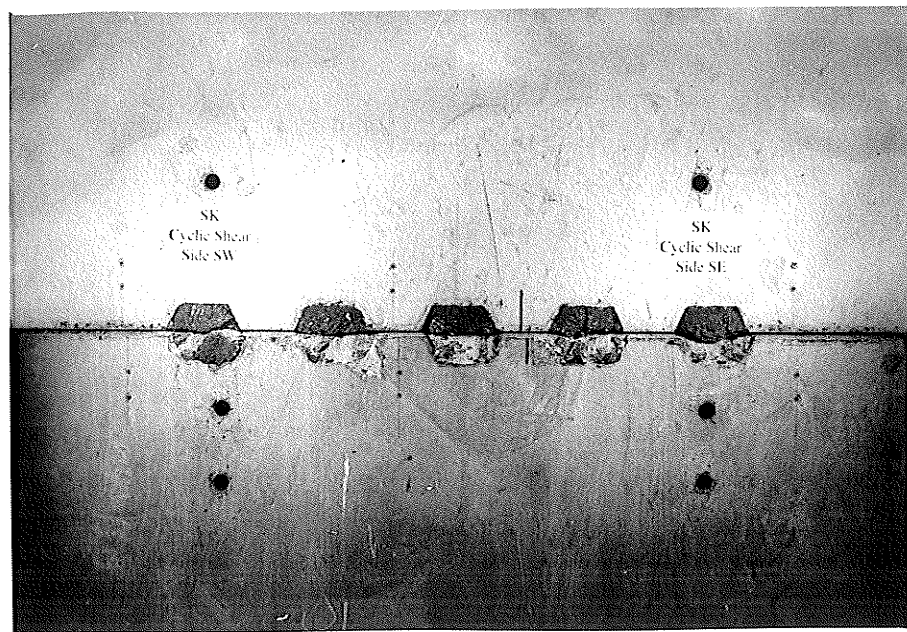
Figure 5.40   Specimen SK - Slip Interface at the End of Testing

SK - Cyclic Shear

Y-axis: Shear Resistance (kN), ranging from -1000 to 1000

X-axis: Reduction of Dry Pack Thickness (mm), ranging from -1.0 to 1.0

Cracking of dry pack within shear keys.

NOTE:
Negative values indicate opening of connection.
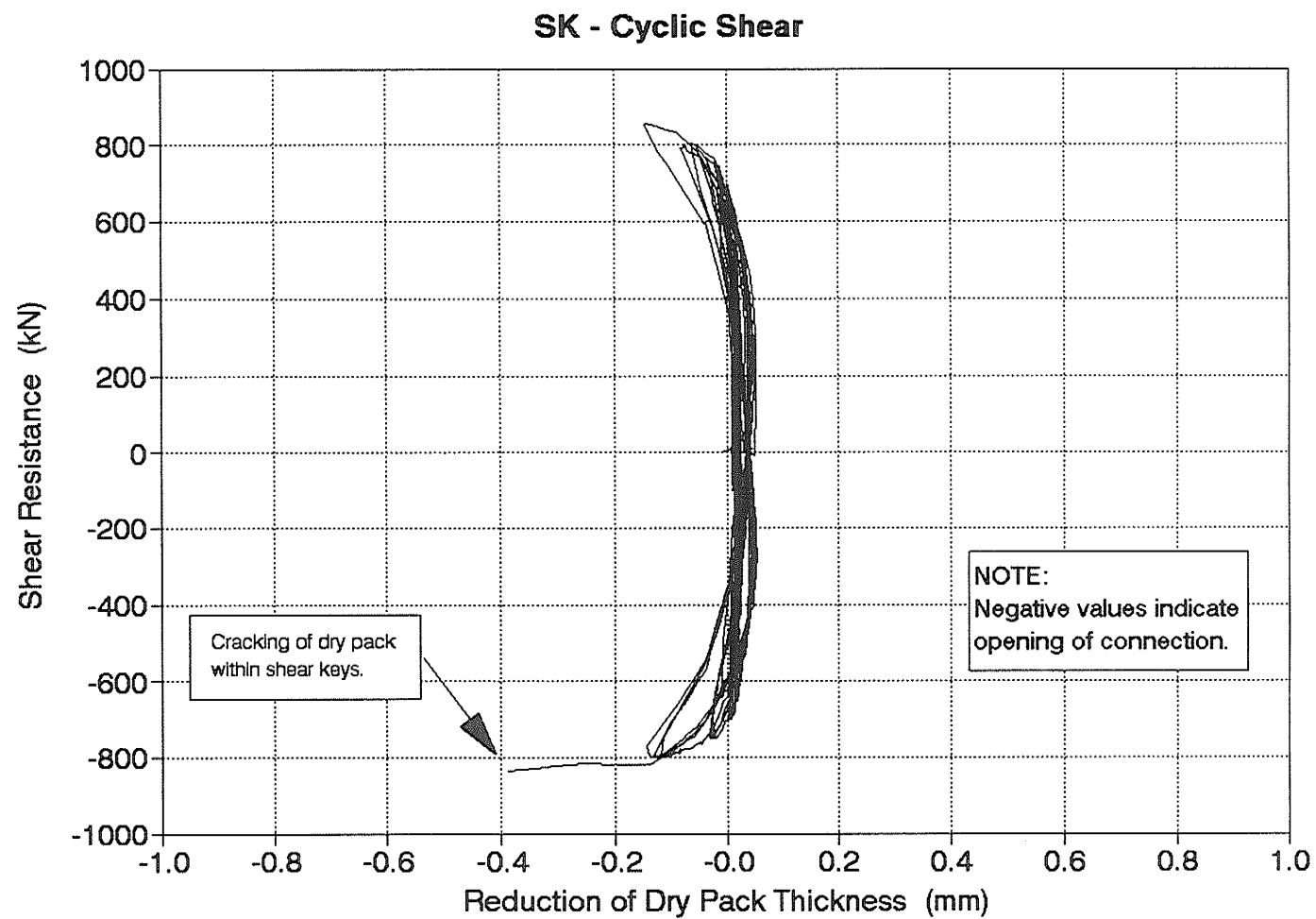
Figure 5.41   Specimen SK - Variation of Dry Pack Thickness Prior to Cracking of the Shear Keys (Enlarged Scale)
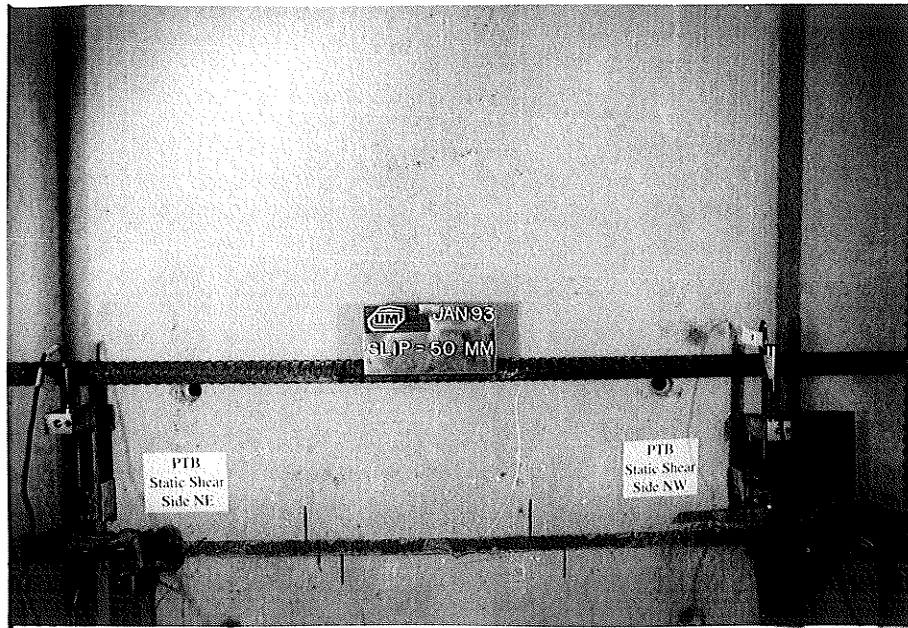
Figure 5.42   Specimen PTB-S - Condition of the Dry Pack After Significant Slip
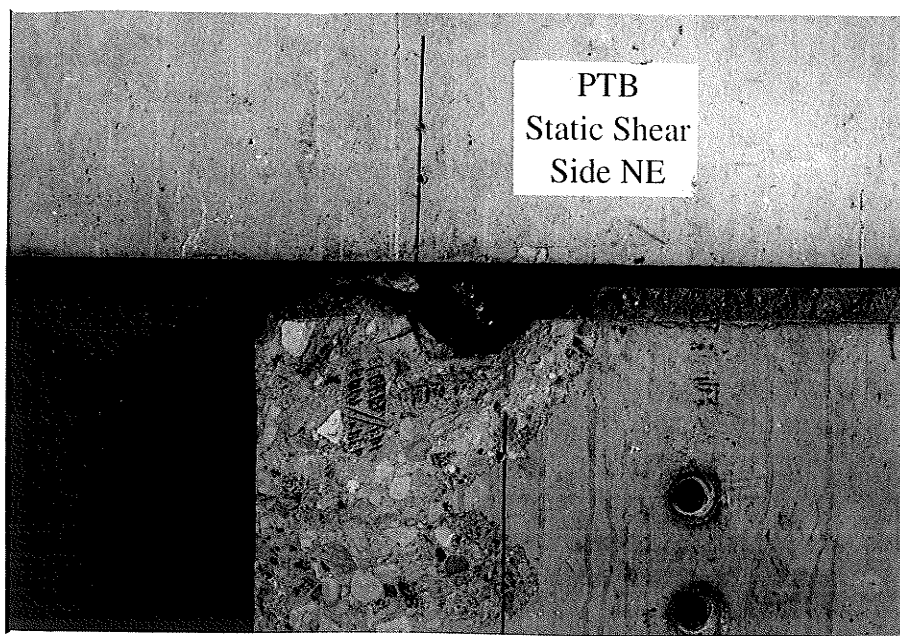
Figure 5.43   Specimen PTB-S - East Bar at the End of Testing

Load Direction

UPPER PANEL

Dry Pack Grout

90 mm

Rupture location

65 mm

LOWER PANEL

Kink Length = 110 mm
Kink Angle = 35 deg.

150 mm
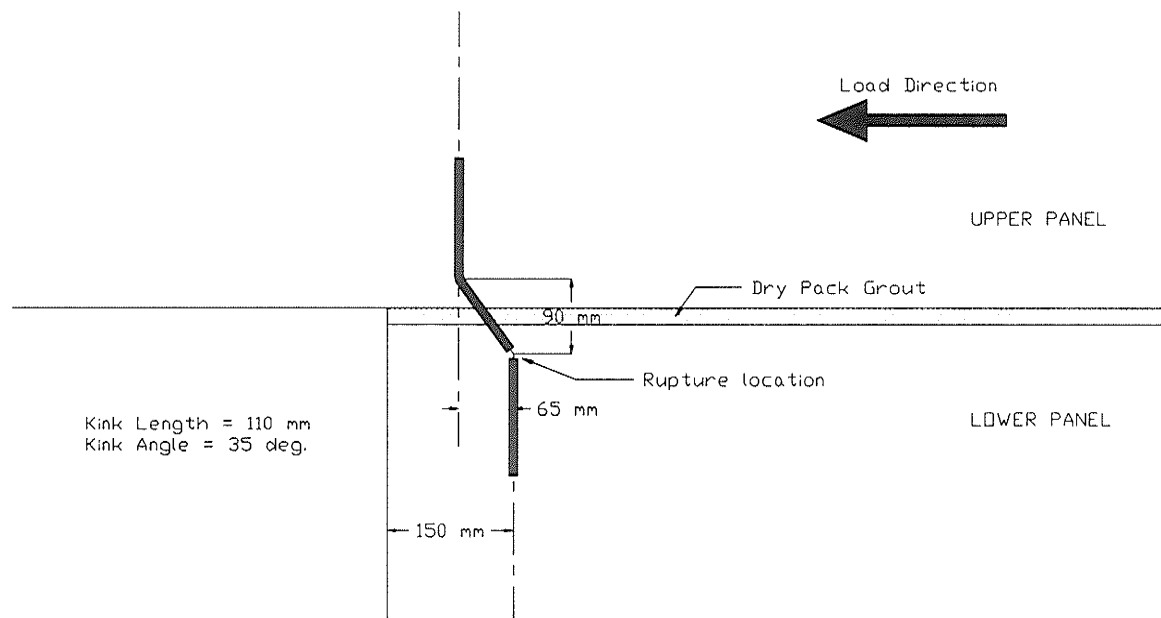
Figure 5.44   Specimen PTB-S - Deformed Shape of the East Bar at Rupture

PTB - Static Shear
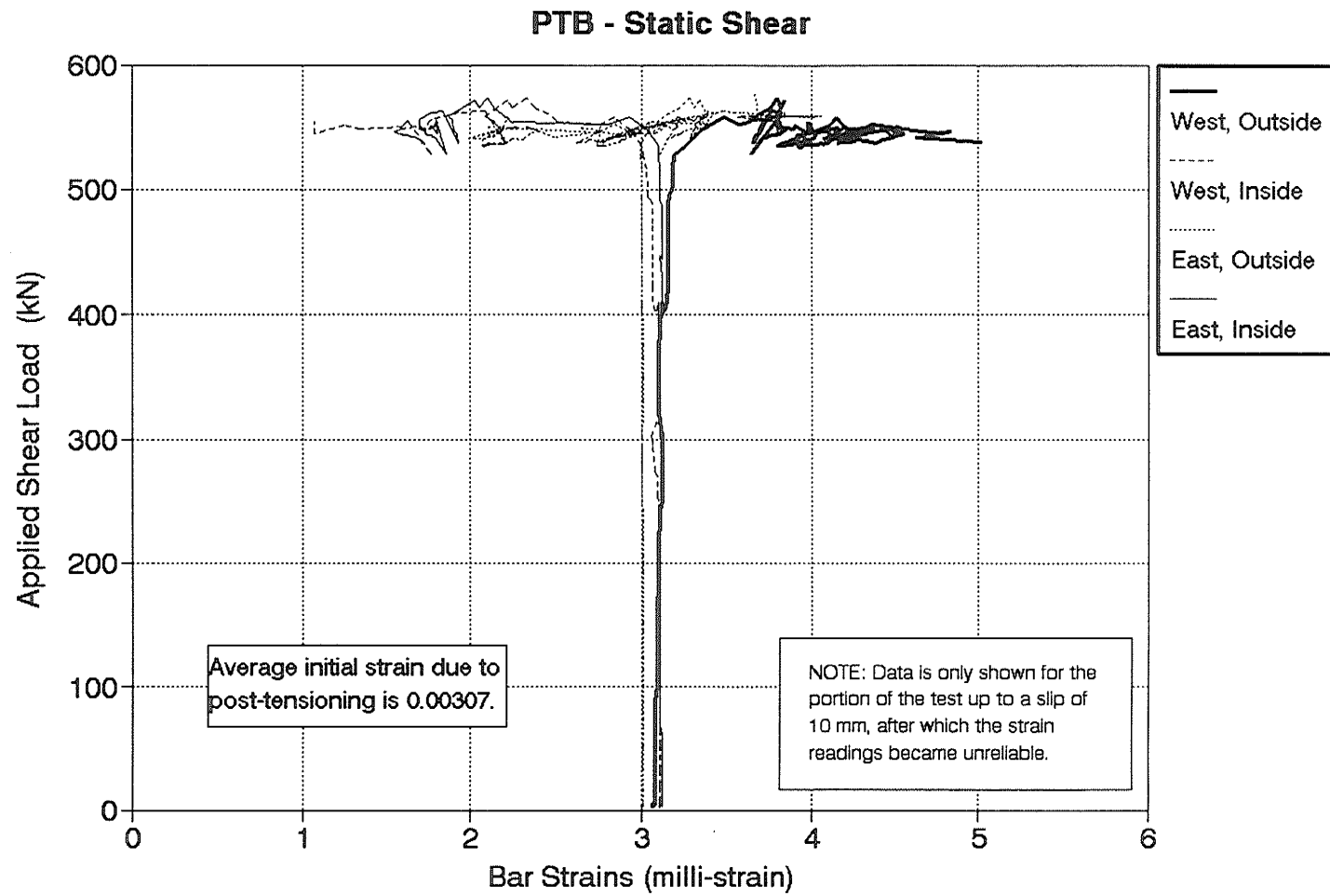
Figure 5.45   Specimen PTB-S - Variation of Bar Strains
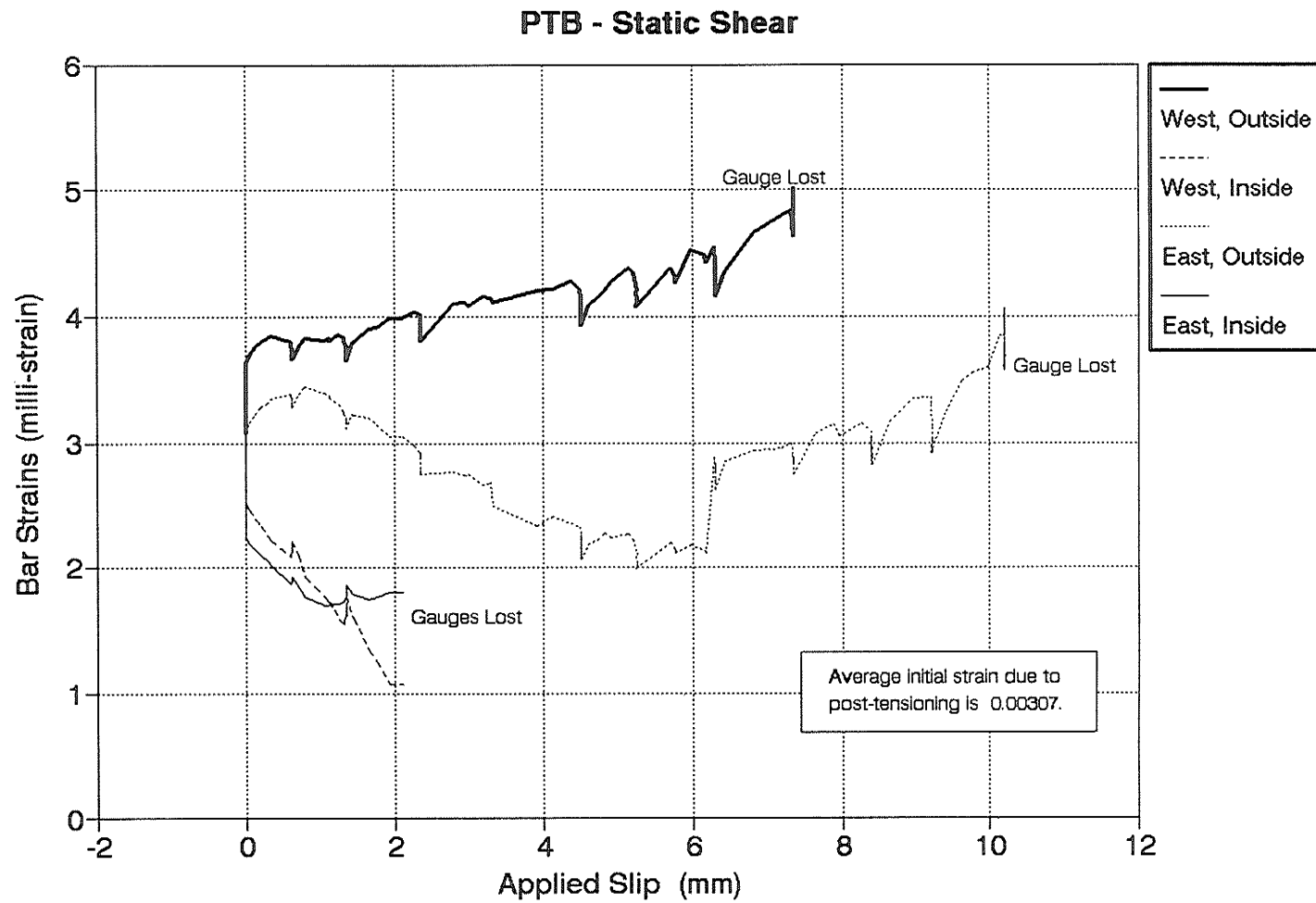
Figure 5.46   Specimen PTB-S - Variation of Bar Strains After the Initiation of Slip

PTS - Cyclic Shear

COMMENTS:

Stage I - Elastic behaviour before initiation of slip.
Stage II - Inelastic behaviour before significant deterioration of dry pack.
Stage III - Inelastic behaviour after significant deterioration of dry pack
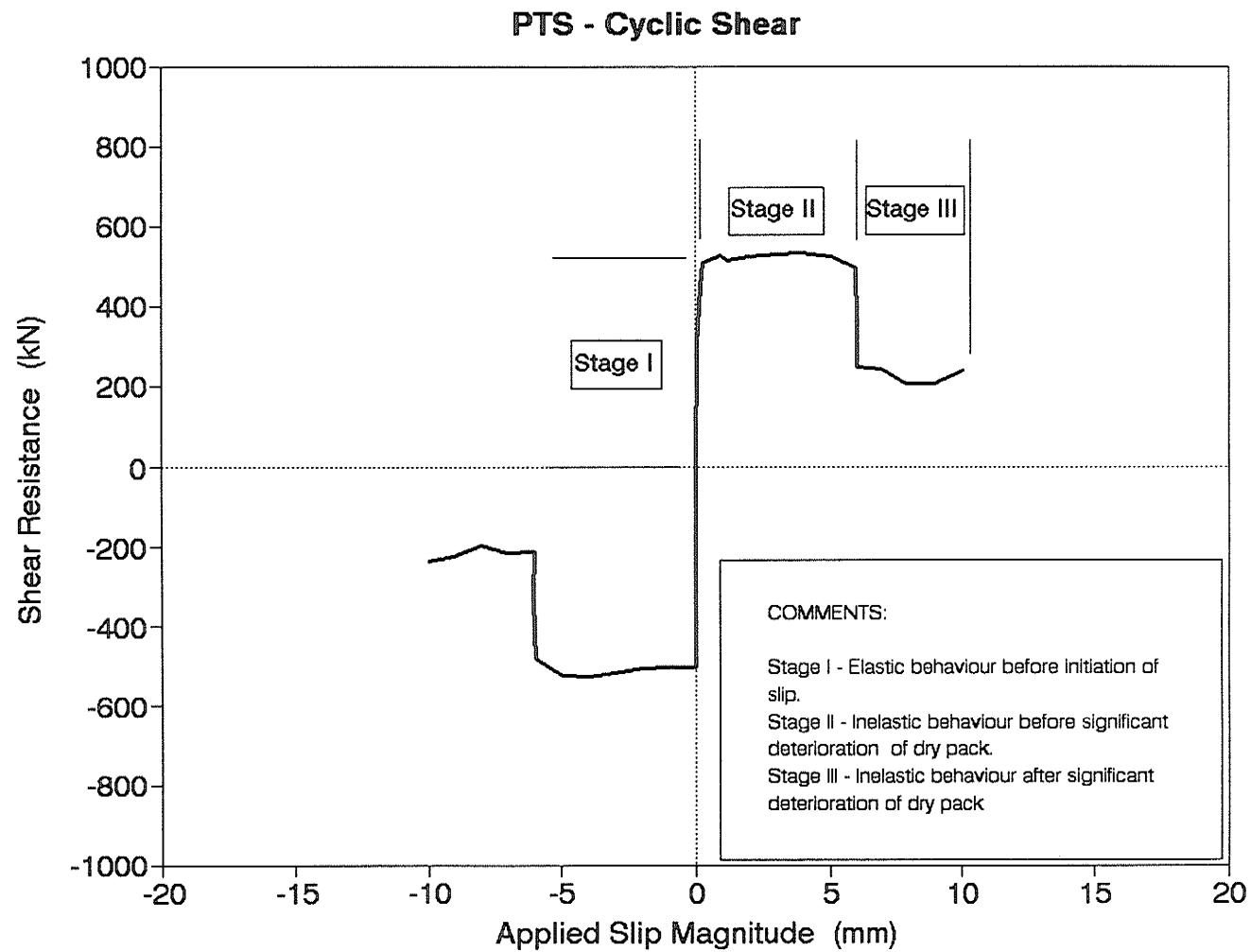
Figure 5.47   Stages of Cyclic Shear Connection Behaviour
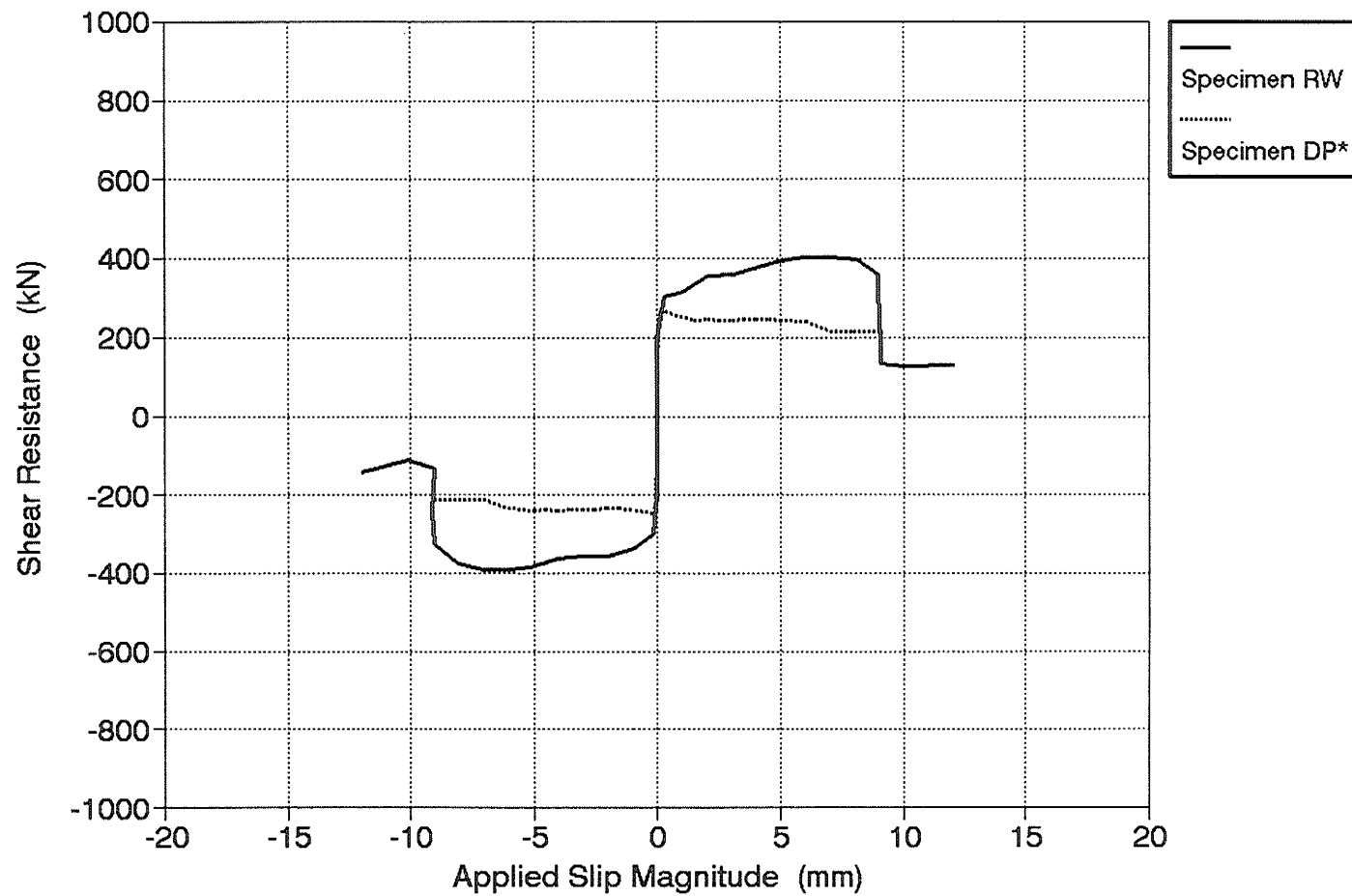
Figure 5.48　Effect of Mild Steel Continuity Bars on Connection Cyclic Shear Behaviour
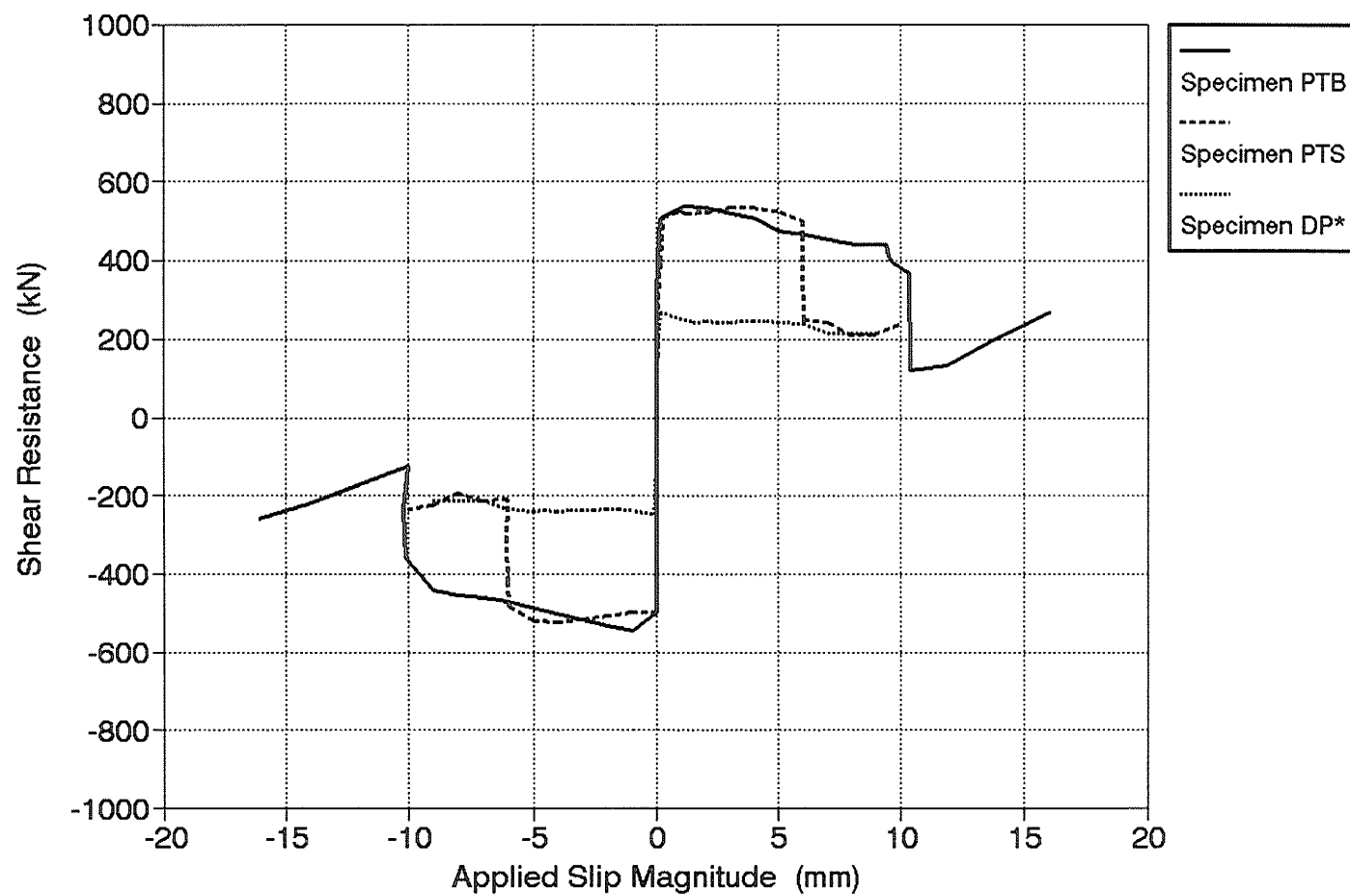
Figure 5.49   Effect of Post-tensioning on Connection Cyclic Shear Behaviour
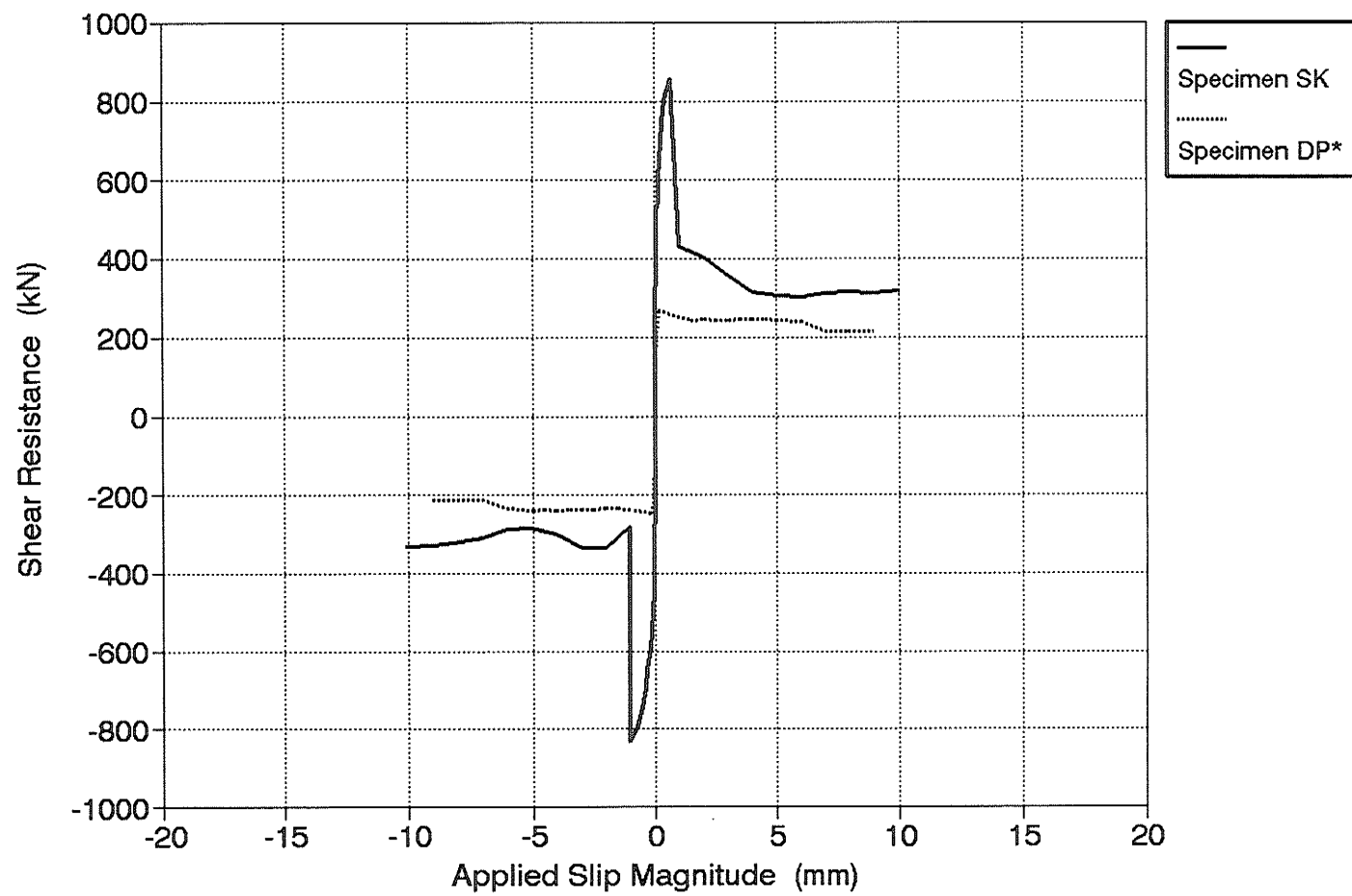
Figure 5.50   Effect of Multiple Shear Keys on Connection Cyclic Shear Behaviour
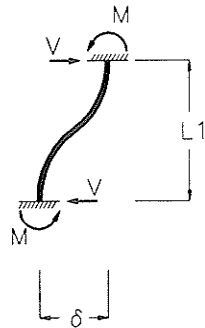
$$V = \frac{2M}{L1}$$

M = end moment in bar determined from moment curvature relationship

ϕ = section curvature at ends of bar

$$= \frac{6\delta}{(L1)^2}$$

L1 = deformed length

δ = applied slip displacement

(a)   Flexural mechanism
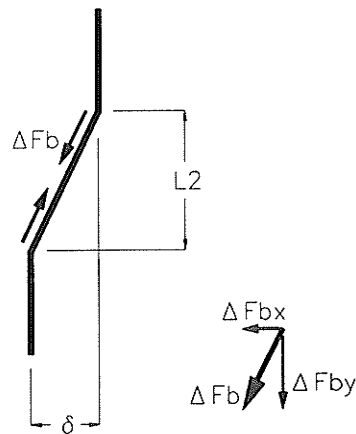
ΔFb = tensile increase in axial bar force

$$= [\, \Delta\varepsilon \; E \,]\; Ab$$

$\Delta\varepsilon$ = increase in axial strain

$$= \sqrt{1 + (\delta/L2)^2} - 1$$

E = elastic modulus of steel

Ab = cross−sectional area of bar

L2 = kink length

δ = applied slip displacement

ΔFbx = horizontal component of ΔFb

$$= \frac{\Delta Fb \; \delta}{L2 + \Delta\varepsilon L2}$$

ΔFby = vertical component of ΔFb

$$= \frac{\Delta Fb \; L2}{L2 + \Delta\varepsilon L2}$$

(b)   Kinking mechanism

Figure 6.1   Shear Resistance Mechanisms Developed In Continuity Bars Due To Applied Slip Displacement Between Precast Concrete Panels

$$Vf1 = \mu(\sigma n)(Ac)$$
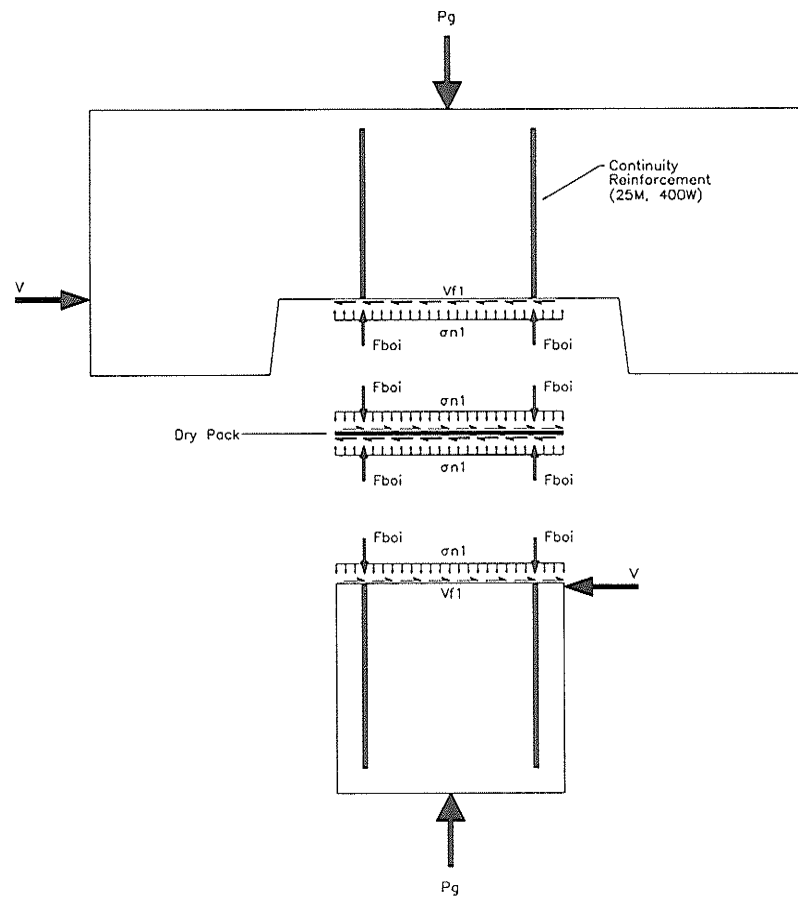
where:

μ = coefficient of friction
= 0.8 (measured from cyclic shear specimen DP)

$\sigma n1$ = vertical stress acting on dry pack due to net gravity load
= $\dfrac{Pg - 2Fboi}{Ac}$

Pg = applied gravity load

$Fboi$ = force in one continuity bar due to applied gravity load when the connection is in the zero slip position at the start of a cycle to slip magnitude i

Ac = cross-sectional area of the connection

303

Figure 6.2 V_{fl}: Frictional Resistance Provided By Net Gravity Load Acting On Dry Pack
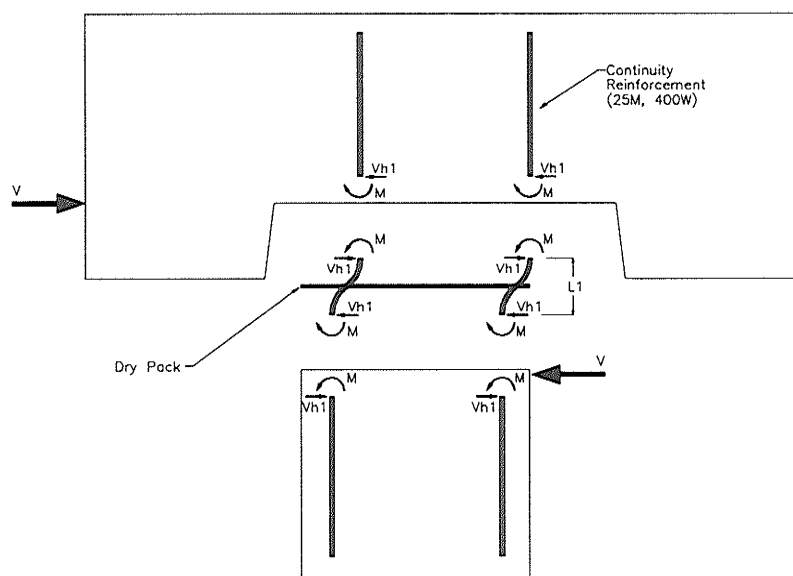
$$Vh1 = \frac{2 \times [\ 2M\ ]}{L1}$$

where:

M = end moment in the bar, limited by the plastic moment capacity, Mp (defined in Figure 2a)

$L1$ = effective deformed length

Figure 6.3 V_{h1}: Direct Shear Resistance Provided By End Shear Forces Resulting From Flexural Deformation of the Continuity Bars
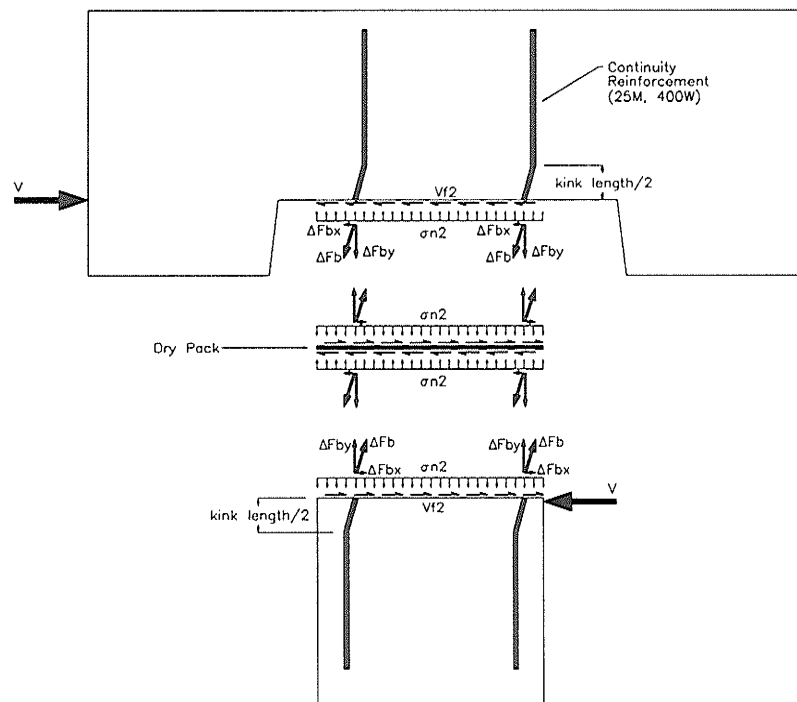
$$Vf2 = \mu (\sigma n2)(Ac)$$

$$Vh2 = 2 [\Delta Fbxi]$$

where:

μ = coefficient of friction
= 0.8 (measured from cyclic shear specimen DP)

$\sigma n2$ = vertical stress acting on dry pack due to clamping action
= $\dfrac{2 [\Delta Fbyi]}{Ac}$

$\Delta Fbyi$ = vertical component of ΔFbi

$\Delta Fbxi$ = horizontal component of ΔFbi

ΔFbi = increase in axial bar force at slip magnitude i, due to kinking mechanism (defined in Figure 2b)

Ac = cross-sectional area of the connection

305

Figure 6.4 V_{f2}: Frictional Resistance Provided By Clamping Action
V_{h2}: Direct Shear Resistance Provided By Kinking Mechanism

RW - Cyclic Shear

Legend:
—— at 0 Slip Position
------ at Applied Slip

Y-axis: Axial Force in Bars (kN)

X-axis: Applied Slip Magnitude (mm)

compression is negative
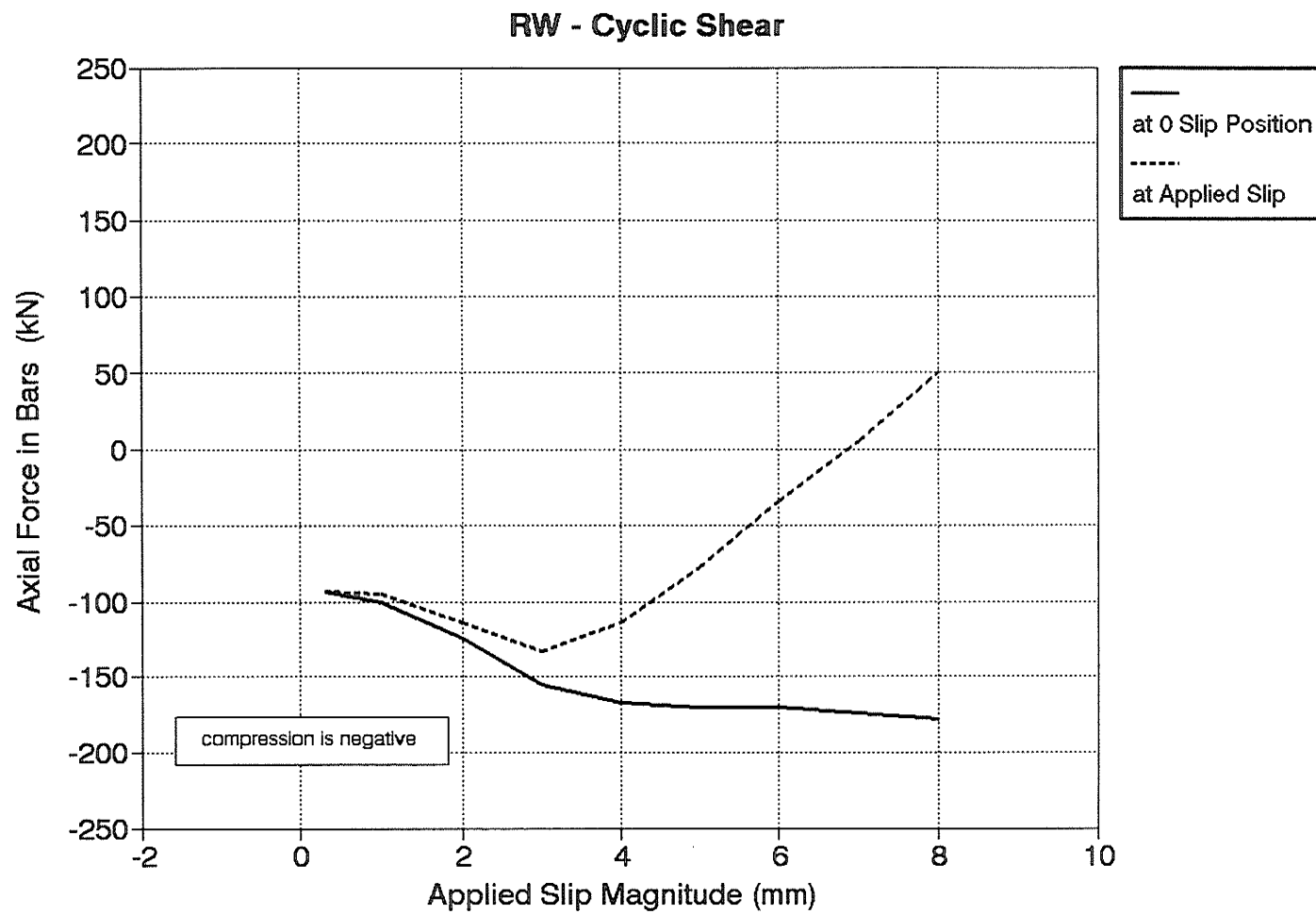
Figure 6.5   Specimen RW - Variation of Axial Bar Force
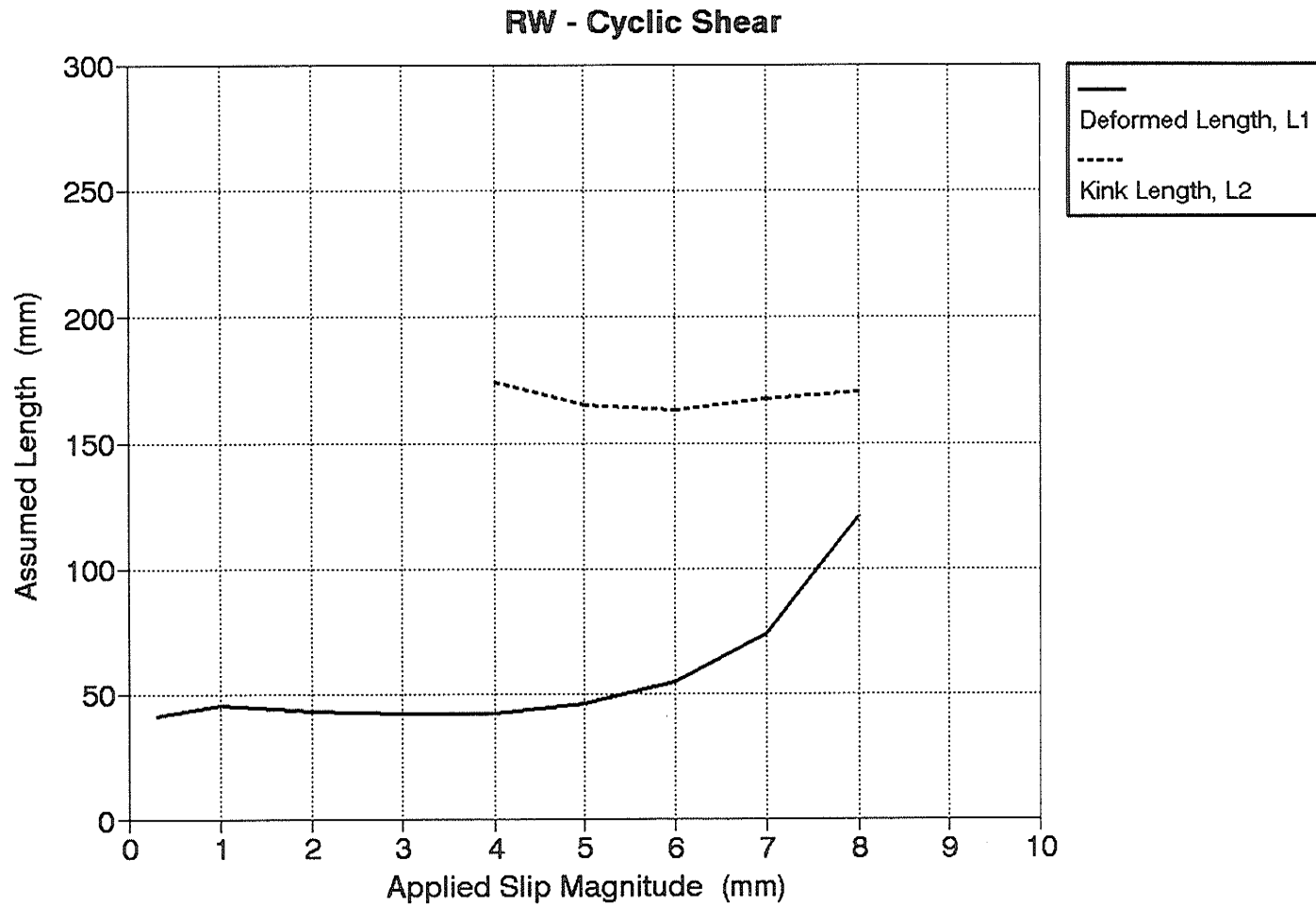
Figure 6.6   Specimen RW - Variation of the Deformed Length, L_1 and the Kink Length, L_2

RW - Cyclic Shear

Legend:
- Measured Vr
- Vf1 **
- Vh1
- Vf2 **
- Vh2 **

** Based on measured data
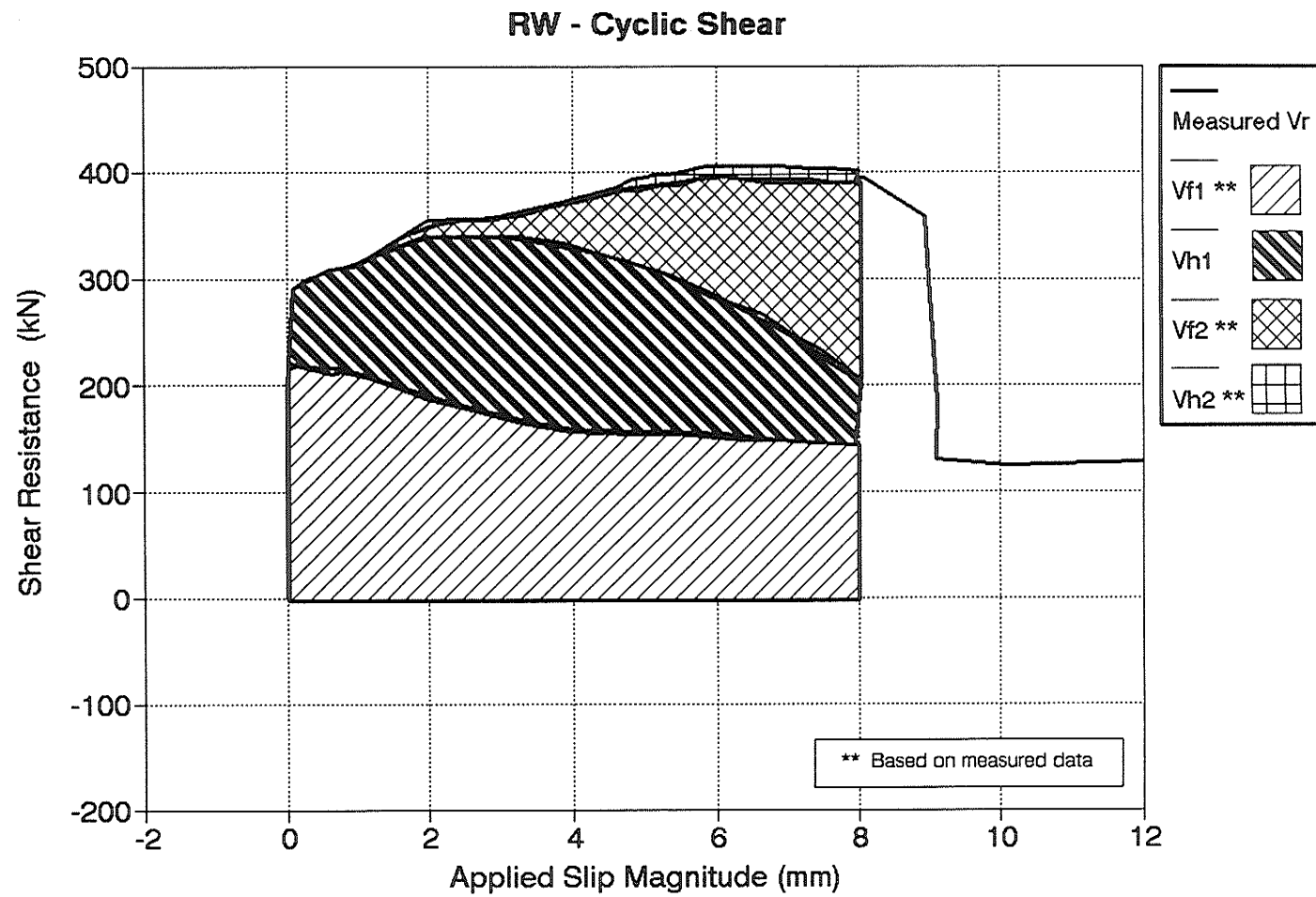
Figure 6.7   Specimen RW - Variation of the Components of Shear Resistance
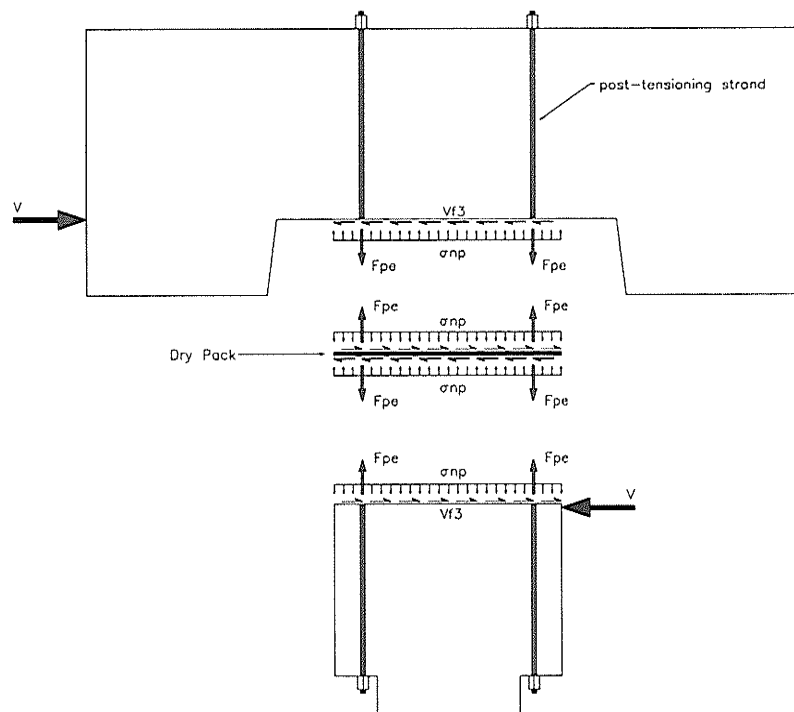
$$Vf3 = \mu(\sigma ng)(Ac)$$

where:

μ = coefficient of friction
= 0.91 (refer to Section 6.3.2)

σng = vertical stress acting on dry pack due to post-tensioning
= $\dfrac{2Fpe}{Ac}$

Fpe = effective prestressing force per strand

Ac = cross-sectional area of the connection

Figure 6.8 V_{f3}: Frictional Resistance Provided By Post-tensioning of the Connection Using Strands

Figure 6.9   Specimen PTS - Variation of the Components of Shear Resistance

Figure 6.10 V_{f4}: Frictional Resistance Provided by the Tensile Force in the Post-tensioning Bars

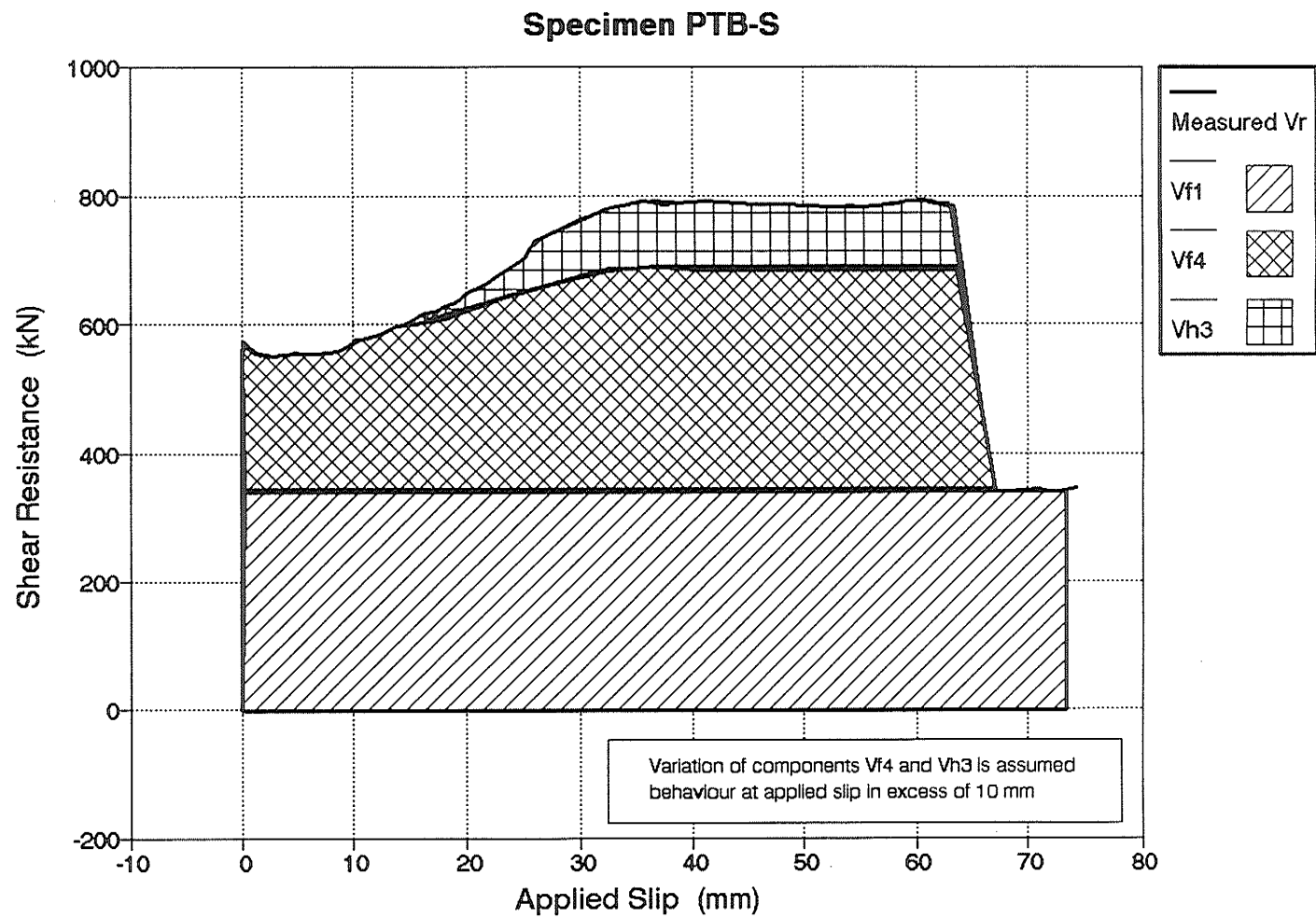V_{h3}: Direct Shear Resistance Provided by the Kinking Mechanism

Specimen PTB-S

Legend:
- Measured Vr
- Vf1
- Vf4
- Vh3

Variation of components Vf4 and Vh3 is assumed behaviour at applied slip in excess of 10 mm

X-axis: Applied Slip (mm)
Y-axis: Shear Resistance (kN)

312

Figure 6.11   Specimen PTB-S - Variation of the Components of Shear Resistance
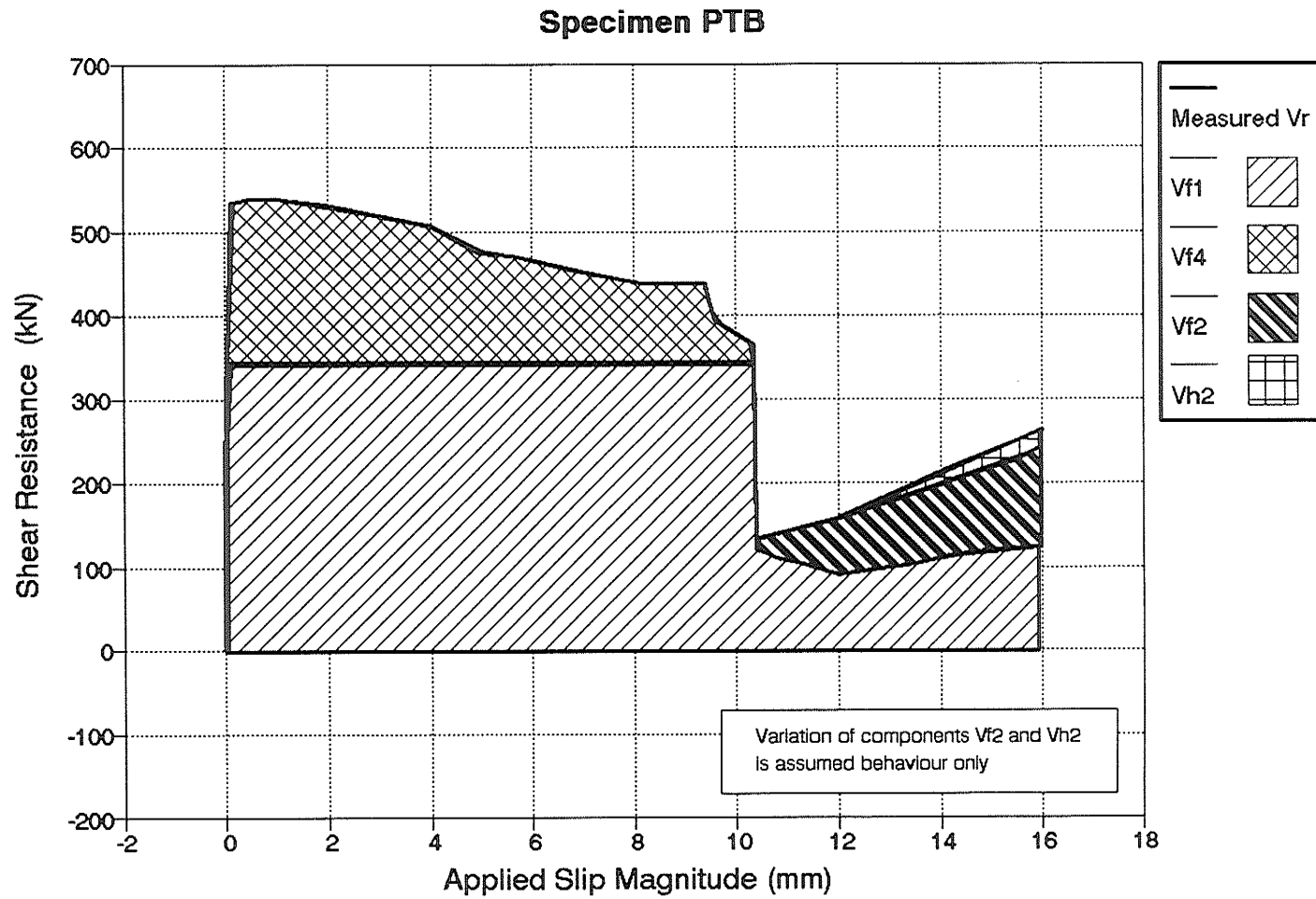
Specimen PTB

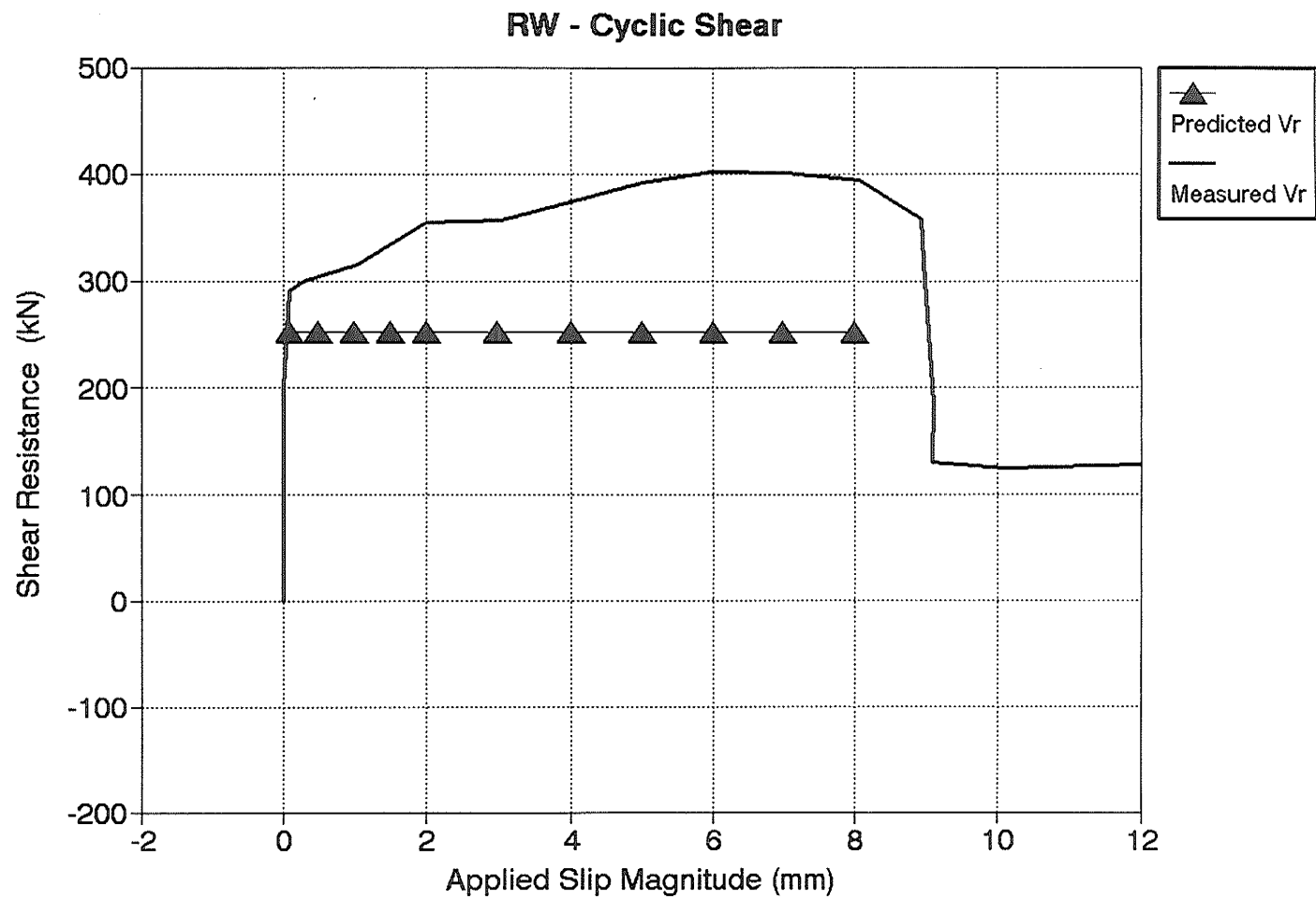Figure 6.12   Specimen PTB - Variation of the Components of Shear Resistance

RW - Cyclic Shear

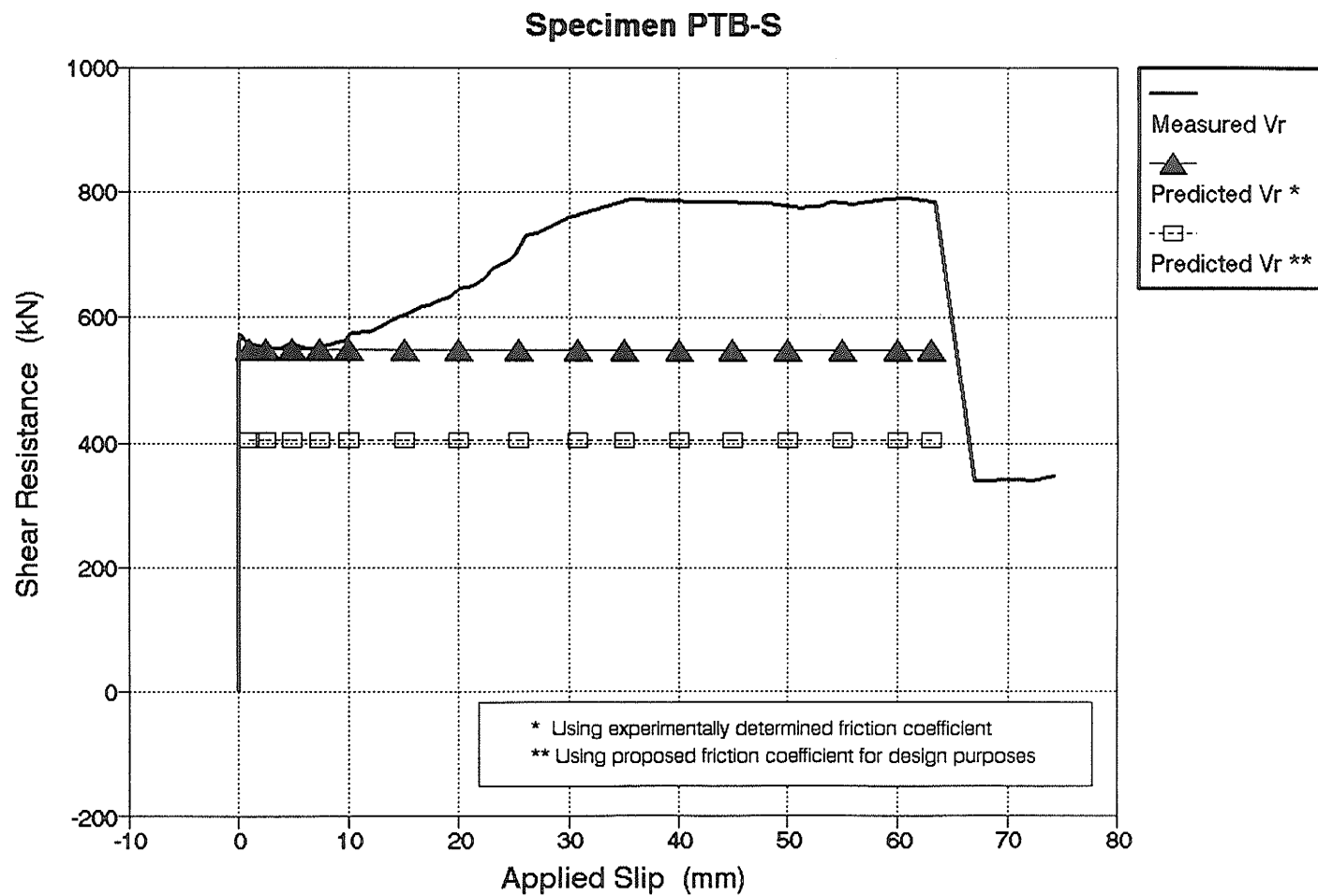Figure 7.1   Specimen RW - Predicted Cyclic Shear Behaviour for Design Purposes

Specimen PTB-S

Legend:
— Measured Vr
▲ Predicted Vr *
-□- Predicted Vr **

* Using experimentally determined friction coefficient
** Using proposed friction coefficient for design purposes

Figure 7.2   Specimen PTB-S - Predicted Shear Resistance - Slip Behaviour (monotonic loading)

Specimen PTB

Legend:
— Measured Vr
····|···· Vf1
--|-- Vf4
▲ Predicted Vr

X-axis: Applied Slip Magnitude (mm)
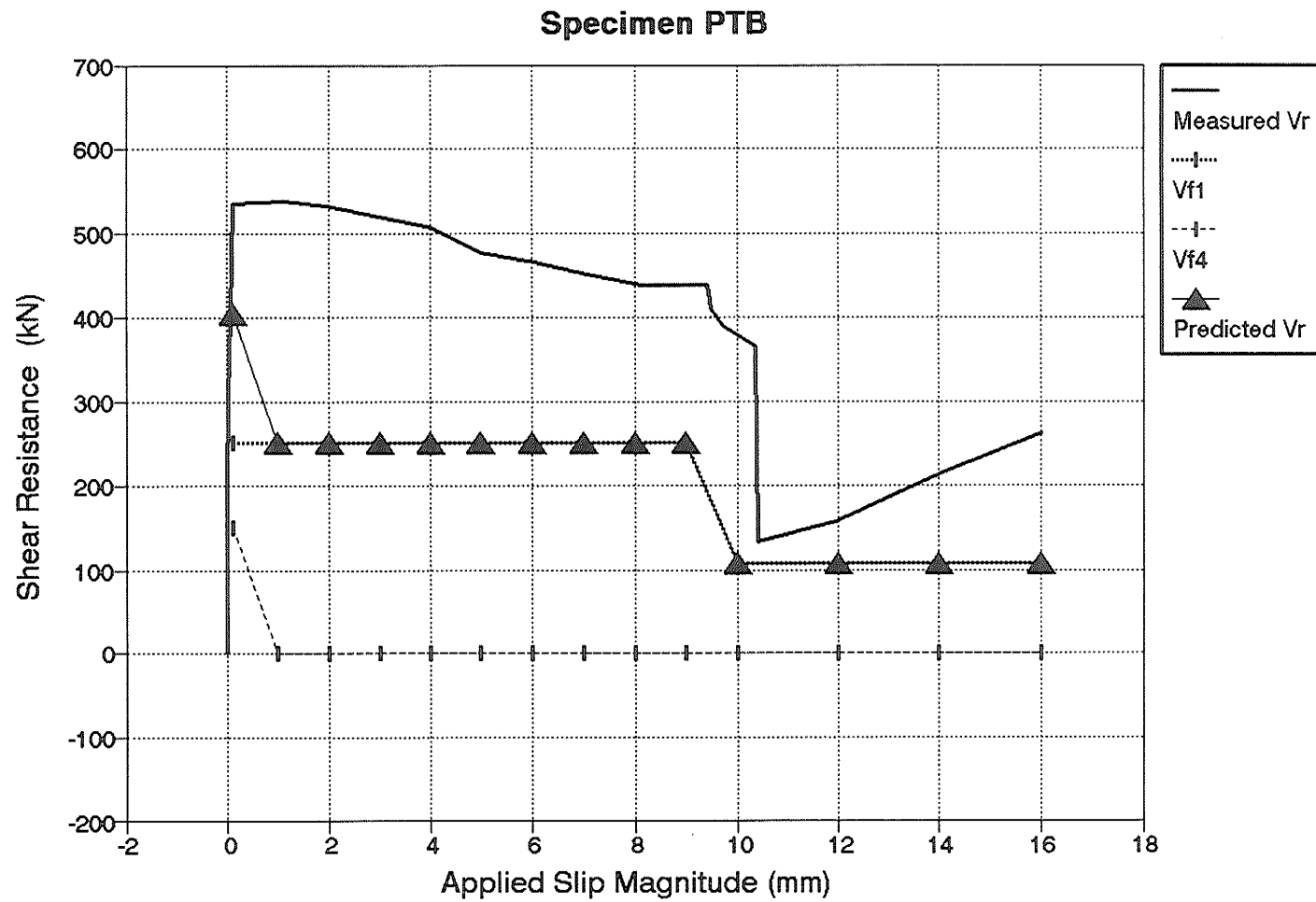Y-axis: Shear Resistance (kN)

Figure 7.3   Specimen PTB - Predicted Cyclic Shear Behaviour For Design Purposes

APPENDIX

APPENDIX

Calculation of Initial Strain in the Continuity Bars

The initial compressive strain in the continuity bars prior to the application of shear loading is based on the distribution of vertical forces at the connection level. The strain in the bars is produced by the applied gravity loads (normal to the connection) with consideration for possible shrinkage strains in the dry pack. The initial compressive strain may be estimated using the following procedure.

Shrinkage Strain

The shrinkage strain in the dry pack may be estimated using the procedure described in the CPCI Metric Design Manual (3). The variables involved in the procedure are defined on page 2-7 of the Metric Design Manual.

$$\varepsilon_{sh} = \varepsilon_{shu} \left(\frac{t}{C_s + t} \right) P_{sh}$$

ε_{sh} = ultimate shrinkage strain
   = 780 x 10^{-6}

P_{sh} = Shrinkage modification factor
   = $P_c P_h P_f P_r P_{sl} P_v$

C_s = shrinkage coefficient
   = 35

t = time in days
   = 35

P_c = 1.00		P_r = 0.783	
P_h = 1.00		P_{sl} = 0.890	
P_f = 1.04		P_v = 1.00	

P_{sh} = 0.725

$$\varepsilon_{sh} = (.000780) \left(\frac{35}{35+35} \right) (0.725)$$

$$\varepsilon_{sh} = 0.000283$$

Strain Due to Applied Gravity Load

The distribution of forces at the connection level may be determined using a transformed section analysis.

Area of dry pack $\quad = A_c$ - As $\qquad\qquad\qquad\qquad$ E_{dp} $\quad$ = 7000 MPa
$\qquad\qquad\qquad\qquad$ = 180,000 - 1000
$\qquad\qquad\qquad\qquad$ = 179,000 mm²

Area of steel $\qquad$ = 1000 mm² $\qquad\qquad\qquad\qquad$ Es $\quad$ = 200,000 MPa

$$P_g = P_{dp} + P_s$$
$$= f_{dp}A_{dp} + f_s A_s$$
$$= \varepsilon_{dp}E_{dp}A_{dp} + \varepsilon_s E_s A_s$$

$$\varepsilon_s = \varepsilon_{dp} = \frac{P_g}{E_{dp}A_{dp} + E_s A_s}$$

$$= \frac{360000N}{(7000MPa)(179000mm^2) + (200000MPa)(1000mm^2)}$$

$$\varepsilon_s = 0.000248$$

Total Initial Strain

$\varepsilon_i \quad = 0.000283 \;+\; 0.000248$
$\varepsilon_i \quad = 0.000531$

Therefore

F_{boi} = 53.1 kN $\qquad\qquad$ (25M bar)